

Development of Friction and Texture Performance Models



NCDOT Project 2022-05
FHWA/NC/2022-05
August 2023



B. Shane Underwood, Ph.D., et al.
Department of Civil, Construction, and
Environmental Engineering
North Carolina State University



**RESEARCH &
DEVELOPMENT**

This page is intentionally blank

Technical Documentation Page

1. Report No. FHWA/NC/2022-05	2. Government Accession No.	3. Recipient's Catalog No.	
4. Title and Subtitle Development of Friction Performance Models		5. Report Date August 31, 2023	
		6. Performing Organization Code	
7. Author(s) B. Shane Underwood, Ph.D., Cassie Castorena, Ph.D., Boris Goenaga, Ph.D., Benson Munywoki, and Paul Rogers, P.E.		8. Performing Organization Report No.	
9. Performing Organization Name and Address Civil, Construction, and Environmental Engineering, North Carolina State University 915 Partners Way Raleigh NC 27606		10. Work Unit No. (TRAIS)	
		11. Contract or Grant No.	
12. Sponsoring Agency Name and Address North Carolina Department of Transportation Research and Development Unit 1020 Birch Ridge Drive Raleigh, North Carolina 27610		13. Type of Report and Period Covered Final Report August 1, 2021 – July 31, 2023	
		14. Sponsoring Agency Code RP2022-05	
Supplementary Notes:			
16. Abstract <p>NCDOT manages the annual Highway Safety Improvement Program to address crashes in the following emphasis areas: lane departure, frontal impact/intersection, and pedestrian and bicycle crashes in an effort to reduce crashes by the installation of safety improvement countermeasures at locations with patterns of correctable crashes. Lane departure crash patterns can be identified in various ways with one of the methodologies being an increased frequency of lane departure crashes and/or crash rates during wet road conditions. Lane departure crashes and crash rates may increase when the surface is wet because skid resistance can be affected and reduced under these conditions. Recent studies have shown that friction and, more notably macrotexture, are negatively affected when the pavements are newly overlaid, but did not provide the NCDOT with a pavement friction and macrotexture performance model or performance thresholds. This research study has used a combination of field experiments, laboratory experiments, and statistical analysis to achieve three objectives; 1) characterize friction and texture performance models for North Carolina roadways, 2) propose friction and texture performance thresholds, and 3) identify asphalt mixture compositional factors that affect the as-constructed macrotexture and friction. The objectives were met using a combination of field and laboratory friction and texture experiments. The performance models developed in this research were shown to accurately predict in-service friction and texture and were validated using completely independent measurements. To define thresholds, pavement segments were grouped according to their available friction or texture and then the relationship between the aggregated crash rates and texture/friction were used to identify values where crash rates showed a marked increase. On the basis of this analysis, the research team recommends the following investigatory and intervention thresholds: macrotexture investigatory level: 0.80 mm, macrotexture intervention level: 0.6 mm, friction investigatory level: 0.57 for non-interchanges and 0.65 for interchanges, and friction intervention level (specific to Moventor BV-11 equipment at 60-mph): 0.43 for non-interchanges and 0.49 for interchanges. These thresholds are specific for the devices used; in the case of texture the AMES AccuTexture 100 and for friction the Moventor BV-11 at 60-mph. The sites in this research were primarily high speed, controlled access roadways and so these recommendations are most applicable to similar types of roadways. Data from the North Carolina highway network was combined with these threshold values and predictions from the friction and texture performance models to evaluate the benefit-cost implications from deploying a set of maintenance and rehabilitation strategies to address friction and texture problems. While the precise cost implications varied by the maintenance scenario evaluated or the interest rate used, all the combinations showed a benefit-cost ratio greater than one.</p>			
17. Key Words Pavement friction, macrotexture, highway safety, flexible pavements		18. Distribution Statement	
19. Security Classif. (of this report) Unclassified	20. Security Classif. (of this page) Unclassified	21. No. of Pages 230	22. Price

Disclaimer

The contents of this report reflect the views of the author who is responsible for the facts and the accuracy of the data presented herein. The contents of the report do not reflect the official views or policies of the North Carolina Department of Transportation. This report does not constitute a standard, specification, or regulation.

Acknowledgments

The research team would like to express their gratitude and appreciation to the North Carolina Department of Transportation (NCDOT) for the provided funding needed to conclude this research study.

TABLE OF CONTENTS

List of Figures	iii
List of Tables	viii
Executive Summary	1
1. Introduction.....	5
1.1. Overview.....	5
1.2. Connection of Research to Previous Effort	5
1.3. Status of the Literature.....	6
1.3.1. Friction and Texture Performance	6
1.3.2. Establishing Investigatory and Intervention Thresholds.....	8
1.3.3. Knowledge Gaps and Applications.....	9
1.4. Report Organization.....	10
2. Data Processing.....	11
2.1. Overview.....	11
2.2. Continuous Pavement Friction Measurements (CFME).....	13
2.3. High-Speed Texture Measurements.....	14
2.4. Field Core Observations	14
2.5. Crash Records	16
2.6. Supplementary Information	16
2.6.1. Traffic	16
2.6.2. Road Geometry	17
3. Pavement Friction and Texture Performance Modeling.....	21
3.1. Overview.....	21
3.2. Updates to FHWA/NC 2020-11 Mix Composition Models	21
3.3. Performance Model Development	22
3.3.1. Modeling Seasonality.....	23
3.3.2. Friction Performance	24
3.3.3. Texture Performance.....	24
3.4. Results.....	24
3.4.1. Friction Performance	25
3.4.2. Texture Performance.....	28
3.5. Summary	31
4. Definition and Evaluation of Friction and Texture Thresholds	33
4.1. Overview.....	33
4.2. Methodology	33
4.2.1. Establishing Friction-Texture Demand Categories for North Carolina	33
4.2.2. Representative Friction and Texture Values.....	35
4.2.3. Crash Rates Estimation Procedure.....	36
4.2.4. Estimating the Investigatory and Intervention Thresholds	37
4.3. Results.....	40
4.3.1. GPF Method 3.....	41
4.3.2. Sequential Logit Regression	44
4.4. Recommended Friction and Texture Thresholds.....	48
4.5. Cost-Benefit Analysis	50
4.6. Summary	51
5. Conclusions and Recommendations	53

5.1. Conclusions.....	53
5.2. Recommendations.....	54
5.2.1. PFMP Recommendations.....	54
5.2.2. Future Research Recommendations.....	54
6. Implementation and Technology Transfer Plan.....	57
7. References.....	59
Appendix A. Detailed Literature Review	67
Appendix B. Mixture Volumetrics of Tested Sites.....	123
Appendix C. Device Comparison	127
Appendix D. Friction and Texture Testing Dates.....	138
Appendix E. Additional Considerations for representative friction values	144
Appendix F. Friction and Texture Prediction After an Asphalt Overlay.....	146
Appendix G. Friction and Texture Performance Model Technical Details	162
Appendix H. Evaluation of the Effect of Asphalt Overlays on Highway Safety	184
Appendix I. Investigatory and Intervention Thresholds	197
Appendix J. Cost-Benefit Analysis.....	203

LIST OF FIGURES

Figure 1. Skid resistance variation with time or traffic.	6
Figure 2. Macrotexture variation with time or traffic.	7
Figure 3. Concept of site and homogeneous road segment, Site 113.	12
Figure 4. Data collected for the PFMP framework.	13
Figure 5. Core extraction and height adjustment.	15
Figure 6. Images of laboratory test equipment used in this study: (a) BPT and support base and (b) AMES 9500-line texture scanner.	15
Figure 7. (a) Location of counting stations and (b) StreetLight sites.	17
Figure 8. Elements of the ROCA toolbox.	18
Figure 9. Distribution of the training set and the 160 sites.	18
Figure 10. Distribution of interchanges along the primary road network of North Carolina.	19
Figure 11. Methodology followed to calibrate the performance models.	23
Figure 12. Example of the friction prediction process for: (a) Site 4.1 and (b) Site 14.	26
Figure 13. Friction model verification plot for: (a) Site 4.1, (b) Site 8, (c) Site 131, and (d) Site 155.	26
Figure 14. Friction prediction check for: (a) Site 142 (dense mix), (b) Site 134.1 (OGFC), and (c) Site 111.3 (UTBWC).	27
Figure 15. Example of the <i>MPD</i> prediction process for: (a) Site 4.1 and (b) Site 14.	29
Figure 16. Texture model verification plot for: (a) Site 4.1, (b) Site 8, (c) Site 131, and (d) Site 155.	30
Figure 17. <i>MPD</i> prediction check for: (a) Site 142 (dense mix), (b) Site 134.1 (OGFC), and Site 111.3 (UTBWC).	31
Figure 18. Example of the friction demand category definition.	34
Figure 19. Total number of miles with friction and texture observations on each friction demand category.	35
Figure 20. Back-cast prediction process.	36
Figure 21. Total number of miles available for threshold determination after combining the observed friction and texture with the back-casted values.	36
Figure 22. Graphical representation of the elements for GPF Method 3.	38
Figure 23. Sequential Logit model structure.	40
Figure 24. Observations available to determine thresholds for: (a) <i>MPD</i> and (b) friction.	41
Figure 25. Wet lane departure crash rate variation as a function of Friction for Category-1.	42
Figure 26. Wet lane departure crash rate variation as a function of Friction for Category-1 at 65-70 mph.	42
Figure 27. Wet lane departure crash rate variation as a function of <i>MPD</i> for Category-1.	43
Figure 28. Wet lane departure crash rate variation as a function of <i>MPD</i> for Category-1 using only segments with a speed limit of 65-70 mph.	43
Figure 29. Probability $P(L_k \leq R_k < U_k)$ as a function of texture and a fixed friction of 0.4, for Category-1 at: (a) 55-mph, (b) 60-mph, (c) 65-mph, and (d) 70-mph.	45
Figure 30. Probability $P(L_k \leq R_k < U_k)$ for: (a) friction = 0.4 and (b) friction = 0.8.	46
Figure 31. $P(R < 10)$ envelope for a speed limit of 55-mph (left panel) and 70-mph (right panel).	46
Figure 32. Investigatory Thresholds for the different demand categories for (a) Friction and (b) <i>MPD</i>	48

Figure 33. Friction demand categories definition for Site 101.	49
Figure A.1. Friction concept schematic.	68
Figure A.2. Friction variation during a braking maneuver.	68
Figure A.3. Three-dimensional representation of the friction surface.	69
Figure A.4. Two-dimensional representation of the friction surface.	70
Figure A.5. Illustrative example of the friction variation as a function of the slip speed for two pavements with different macrotexture characteristics.	71
Figure A.6. (a) Friction values collected with the BV-11 Moventor Skiddometer, and (b) Rado Model development.	73
Figure A.7. Skid resistance variation with time or traffic.	74
Figure A.8. Data collection plan used by the British Highway Agency (BHA).	75
Figure A.9. Mean Summer SCRIM coefficient (MSSC) variation: (a) with constant heavy traffic volume, (b) with changing heavy traffic volume (35).	76
Figure A.10. Macrotexture variation with time or traffic.	76
Figure A.11. (a) Circular casting mold, (b) capping mold, and (c) square sample holder (49).	84
Figure A.12. Finished specimen (49).	85
Figure A.13. Bonding agent ingredients for aggregate specimen preparation: (a) AASHTO PP 103-20 bonding agent formula, and (b) new bonding agent formula of Saghafi et al. (45).	86
Figure A.14. Comparing the aggregate arrangement in the specimen preparation.	86
Figure A.15. Technician pouring a batch into the partitioned compaction mold.	88
Figure A.16. DFT placed into a guide template.	89
Figure A.17. Properly positioned specimen in the TWPD.	89
Figure A.18. Asphalt mixture volumetrics.	90
Figure A.19. Asphalt mixture phase diagram (63).	92
Figure A.20. Cross section of HFS and illustration showing the typical dimensions of epoxy and calcinated bauxite (5).	95
Figure A.21. Evolution of friction of a HFS surface (5).	95
Figure A.22. (a) Abbott curve and the volume parameters and (b) projected area (5).	96
Figure A.23. Application of the SMA method to predict the variation in the expected number of crashes.	101
Figure A.24. Elements of a pavement friction management program.	107
Figure A.25. LWST friction versus pavement age for divided, non-event friction demand segments (Method 1) (18).	109
Figure A.26. Graph LWST friction versus pavement age for divided, non-event friction demand segments (method 2) (18).	109
Figure A.27. LWST friction distribution and wet/(wet+dry) crash ratio for divided non-event friction demand segments (Method 3) (18).	110
Figure A.28. Investigatory levels determined with CLS regression (18).	111
Figure A.29. Setting the investigatory level (86).	113
Figure A.30. Initial investigation scheme (86).	114
Figure A.31. Data collection and computational framework and data items for network-level curve safety assessment using mobile devices (92).	120
Figure A.32. Conceptual relationship between friction demand, speed, and friction availability (7).	121
Figure C.1. Distribution of friction values measured with (a) BV-11 and (b) SCRIM.	129
Figure C.2. Distribution of <i>MPD</i> values measured with (a) AMES HSTP and (b) SCRIM.	129

Figure C.3. (a) Scatter plot of the <i>MPD</i> comparisons and (b) Box plot of the <i>MPD</i> mean differences.....	131
Figure C.4. (a) <i>MPD</i> values on Site 139.1 and (b) Portion of the dataset selected to compute the mean.....	131
Figure C.5. (a) <i>MPD</i> values on Site 111.4 and (b) Portion of the dataset selected to compute the average <i>MPD</i>	132
Figure C.6. (a) Scatter plot of the friction comparisons and (b) Box plot of the friction means differences.....	133
Figure C.7. (a) Friction values on Site 111.4 and (b) Portion of the dataset selected to compute the mean.....	133
Figure C.8. Scatter plot for friction comparisons after removing outliers.....	134
Figure C.9. Friction regression model proposed for: (a) all sites combined, (b) dense-graded, (c) UTBWC, and (d) OGFC.....	135
Figure C.10. Scatter plot for <i>MPD</i> comparisons after removing outliers.....	136
Figure C.11. <i>MPD</i> regression model proposed for: (a) all sites combined, (b) dense-graded, (c) UTBWC, and (d) OGFC.....	136
Figure E.1. Representative friction value for Site 111.3 NB.....	144
Figure E.2. Comparison of the average 0.1-mile 2.5 th friction percentile against site statistics: (a) 2.5 th friction percentile of the entire site, (b) 10 th friction percentile of the entire site, (c) 25 th percentile of the entire site, and (d) 50 th percentile of the entire site.....	145
Figure F.1. Pavement construction quality program.....	148
Figure F.2. Evaluating the effect of the pavement construction process.....	149
Figure F.3. Illustration of the terms “surface” and estimated mean texture depth (<i>EMTD</i>) (Taken from ISO-13473).....	151
Figure F.4. Field measurements and core locations for Site 23: (a) <i>MPD</i> and (b) Friction value.....	151
Figure F.5. Comparison of the representative friction before and after the overlay.....	153
Figure F.6. Comparison of the representative <i>MPD</i> before and after the overlay.....	154
Figure F.7. Comparison of laboratory measurements with field friction: (a) <i>BPN</i> , (b) <i>MPD</i> , (c) <i>BPN</i> without pre-construction observations, and (d) <i>MPD</i> without pre-construction observations.....	157
Figure F.8. Comparison of laboratory measurements with field <i>MPD</i> : (a) lab <i>MPD</i> , (b) average peak, (c) lab <i>BPN</i> without pre-construction observations, and (d) average peak without pre-construction observations.....	158
Figure F.9. Model prediction plot for: (a) texture and (b) friction.....	160
Figure G.1. Proposed friction performance curve.....	164
Figure G.2. Friction performance model calibration procedure.....	164
Figure G.3. Friction values variation by the day of the year for measurements in the: (a) CL and (b) RWP.....	166
Figure G.4. Texture <i>MPD</i> values variation with the day of the year for measurements in the: (a) CL and (b) RWP.....	167
Figure G.5. Prediction checks of the seasonal friction model.....	168
Figure G.6. Prediction check for Site 111.3 (UTBWC): (a) model fit and (b) fitted values along line of equality.....	169
Figure G.7. Prediction check for Site 134.1 (OGFC): (a) model fit and (b) fitted values along line of equality.....	169

Figure G.8. Prediction check for Site 142 (Dense Mix): (a) model fit and (b) fitted values along line of equality.	169
Figure G.9. Friction variation with respect to: (a) cumulative traffic and (b) cumulative truck traffic.	170
Figure G.10. Histogram of the site-specific parameters; (a) parameter and (b) parameter b.	171
Figure G.11. Friction model evaluation: (a) individual Phase 1 friction performance curves and (b) prediction check.	172
Figure G.12. Prediction plot for Phase 2 model.	173
Figure G.13. Prediction plot for Group-2 sites in Phase 1 of friction performance.	174
Figure G.14. Example of entire friction performance model for sites used in Phase 1 calibration.	174
Figure G.15. Friction prediction checks for all data sets.	177
Figure G.16. <i>MPD</i> variation with respect to: (a) cumulative traffic and (b) cumulative truck traffic.	178
Figure G.17. <i>MPD</i> model assessment: (a) prediction check, (b) initial <i>MPD</i> variation across sites (Parameter <i>a</i>), and (c) <i>MPD</i> rate of change across families (Parameter <i>b</i>).	179
Figure G.19. AADT distribution across the texture performance model calibration set.	182
Figure H.1. Geometry and speed limit distribution across the study sites.	186
Figure H.2. AADT distribution across the study sites.	187
Figure H.3. Surface type distribution across the study sites.	187
Figure H.4. Monthly variation in the number of crashes for Site R1.	188
Figure H.5. Distribution of site for ‘before’ and ‘after’ periods.	188
Figure H.6. Rolling average for the total number of crashes in Site R1.	189
Figure H.7. Rolling average for sites with different traffic levels.	190
Figure H.8. Combinations of ‘before’ and ‘after’ periods.	191
Figure H.9. Ratio of total crashes, θ_e , for each site in Scenario 1.	193
Figure H.10. Proportion of divided and undivided sites, for each crash type, where $\theta_e > 0.8$. (a) Total crashes, (b) Total wet crashes, (c) Lane departure crashes, and (d) Lane departure wet crashes.	195
Figure H.11. Proportion of sites with a dense-mix and UTWBC/OGFC surface, for each crash type, where $\theta_e > 0.8$. (a) Total crashes, (b) Total wet crashes, (c) Lane departure crashes, and (d) Lane departure wet crashes.	195
Figure I.1. Wet lane departure crash rate variation as a function of <i>MPD</i> for Category-1.	197
Figure I.2. Wet lane departure crash rate variation as a function of <i>MPD</i> for Category-1 at 65-70 mph.	197
Figure I.3. Wet lane departure crash rate variation as a function of <i>MPD</i> for Category-1 at 55-60 mph.	198
Figure I.4. Wet lane departure crash rate variation as a function of <i>MPD</i> for Category-2 (tangents).	198
Figure I.5. Wet lane departure crash rate variation as a function of <i>MPD</i> for Category-3 (curves).	199
Figure I.6. Wet lane departure crash rate variation as a function of <i>MPD</i> for Category-4 (interchanges).	199
Figure I.7. Wet lane departure crash rate variation as a function of friction for Category-1.	200
Figure I.8. Wet lane departure crash rate variation as a function of friction for Category-1 at 65-70 mph.	200

Figure I.9. Wet lane departure crash rate variation as a function of friction for Category-1 at 55-60 mph.	201
Figure I.10. Wet lane departure crash rate variation as a function of friction for Category-2 (tangents).....	201
Figure I.11. Wet lane departure crash rate variation as a function of friction for Category-3 (curves).	202
Figure I.12. Wet lane departure crash rate variation as a function of friction for Category-4 (interchanges).....	202
Figure J.1. North Carolina primary road network across the different climate regions.	203
Figure J.2. (a) Proportion of the network in each surface type and (b) Distribution of pavement age for each surface type.....	204
Figure J.3. Distribution of SCRIM measurements: (a) MPD_{SCRIM} and (b) SC	205
Figure J.4. Example of the MPD_{SCRIM} performance curve for Scenario 1: (a) Section ID: 1, and (b) Section ID: 343.....	210
Figure J.5. Example of the friction performance curve for Scenario 1: (a) Section ID: 1, and (b) Section ID: 343.	211
Figure J.6. Treatment selection decision tree for Scenario 2.....	212
Figure J.7. Distribution of the probabilities (a) $P(R<10)$ and (b) $P(R<30)$ in year 2022.	213
Figure J.8. Treatment selection decision tree for Scenario 3.....	214

LIST OF TABLES

Table 1. Distribution of Group-1 sites across North Carolina division units.	11
Table 2. Distribution of Group-2 sites across North Carolina’s division units.	11
Table 3. Summary of original and modified friction and <i>MPD</i> models.	21
Table 4. Number of sites per family.	23
Table 5. Sites with new observations used for friction model validation.	27
Table 6. Summary of the root mean square errors on the friction validation sites.	28
Table 7. ANOVA table for texture model.	28
Table 8. Random effect coefficients for the rate of deterioration.	28
Table 9. Summary of the root mean square errors on the <i>MPD</i> validation sites.	31
Table 10. Distribution of site mileage by speed limit and road functional class.	34
Table 11. Nomenclature used for the proposed thresholds.	38
Table 12. Lane departure wet crash rate, in 100-Mvmt ₁₃ , percentile distribution across the different observations.	41
Table 13. Investigatory and intervention Friction Thresholds estimated with the GPF-Pivot method.	42
Table 14. Investigatory and intervention <i>MPD</i> thresholds estimated with the GPF-Pivot method.	44
Table 15. Coefficients of the sequential Logit model.	44
Table 16. Relative risk based on $P(R < 10)$ for different speed limits.	47
Table 17. Recommended investigatory thresholds.	49
Table 18. Assigning the investigatory and intervention levels for the segments of Site 101.	50
Table 19. Recommended investigatory thresholds.	54
Table A.1. Fitting coefficients of the logarithmic model for MTD (14).	80
Table A.2. Devices used for friction measurement in the laboratory (7, 45).	83
Table A.3. Device used to simulate traffic polishing in the laboratory (7, 45).	83
Table A.4. Generated crash data to illustrate the Bootstrap method.	105
Table A.5. Bootstrap samples generated with the observations of Table A.4.	106
Table A.6. Illustrative state ILs of friction for different friction demand categories (18).	111
Table A.7. Typical skid resistance value ranges measured with a LWST (67).	112
Table A.8. Site categories and investigatory levels from HD28 (86).	112
Table A.9. T10:2002 Skid Resistance Investigatory Levels in New Zealand (87).	115
Table A.10. SCRIM Friction Thresholds Using GPF Method 3 (1).	115
Table A.11. Requirements for Initial Texture Depth for Trunk Roads Including Motorways, U.K. (1).	116
Table A.12. Minimum Macrottexture Requirements for New Zealand (87).	116
Table A.13. FAA recommended friction survey frequency (29).	116
Table A.14. FAA recommended friction level classification for runway pavement surfaces (29).	117
Table A.15. Typical reduction in skid resistance experienced by traffic compared with SCRIM machines measurements (86).	118
Table A.16. Friction coefficients and crash rate (88).	118
Table B.1. Group-1 sites selected for friction and texture measurements.	123
Table B.2. Group-2 sites selected for friction and texture measurements.	124
Table D.1. Friction Measurements.	138

Table D.2. Texture Measurement Dates.	141
Table F.1. Summary of the observations from the field cores.	152
Table F.2. Coefficients of the initial representative <i>MPD</i> models.	154
Table F.3. Coefficients of the average friction models.	155
Table F.4. Coefficients of the <i>MPD</i> models derived with the ALL sites using the surface scanned with the AMES 9500 laser.	159
Table F.5. Coefficients of the friction models derived with ALL sites using the surface scanned with the AMES 9500 laser.	159
Table G.1. Parameters of the seasonal model.	168
Table G.2. Friction percent changes on Group-2 sites.	171
Table G.3. ANOVA table for Phase-1 friction model.	171
Table G.4. ANOVA table for Phase-2 friction model.	172
Table G.5. Average values of the parameters of the friction model for the different mix types.	175
Table G.6. New sites used for friction model validation.	177
Table G.7. Summary of the root mean square errors on the completely new sites for friction model validation.	177
Table G.8. <i>MPD</i> percent changes on Group-2 sites.	178
Table G.9. ANOVA table for texture model.	179
Table G.10. Average value Δa_{site} of the texture model for the different mix types.	180
Table G.11. Summary of the root mean square errors on the completely new sites for <i>MPD</i> model validation.	182
Table G.12. Average <i>MPD</i> values one month after construction for each surface type.	182
Table G.13. Prediction of the expected <i>MPD</i> at different number of days after construction. ...	183
Table G.14. Average <i>MPD</i> values at different number of days after construction.	183
Table H.1. Summary of results based on the parametric method.	194
Table J.1. Inputs defined on each scenario.	207
Table J.2. Cost per crash – Lane Departure Crashes ¹	208
Table J.3. Summary of the cost-benefit analysis (discount rate of 3%).	217
Table J.4. Summary of the cost-benefit analysis (discount rate of 5%).	218
Table J.5. Summary of the cost-benefit analysis (discount rate of 7%).	219

This page is intentionally blank

EXECUTIVE SUMMARY

NCDOT manages the annual Highway Safety Improvement Program to address crashes in the following emphasis areas: lane departure, frontal impact/intersection, and pedestrian and bicycle crashes in an effort to reduce crashes by the installation of safety improvement countermeasures at locations with patterns of correctable crashes. Lane departure crash patterns can be identified in various ways with one of the methodologies being an increased frequency of lane departure crashes and/or crash rates during wet road conditions. Lane departure crashes and crash rates may increase when the surface is wet because skid resistance can be affected and reduced under these conditions. The precise loss in skid resistance is dependent on many factors, but the consensus among experts is that pavement friction and macrotexture are important factors. Although the NCDOT actively addresses skid resistance issues as they are identified, recent studies have shown that friction and, more notably macrotexture, are negatively affected when the pavements are newly overlaid. While the current studies have successfully identified the potential for issues in recently overlaid projects, they have not yet provided the DOT with pavement friction and macrotexture performance models. That is a function or set of functions capable of capturing and quantifying the magnitude of the change due to an overlay and the longer-term temporal changes in friction and macrotexture over the lifetime of the pavement surface. Without these performance curves it is difficult to impossible to identify performance thresholds, limits on friction and macrotexture that warrant investigation or intervention, and subsequently manage friction performance across the roadway network.

With respect to this need, three specific objectives were set for this research; 1) characterize friction and texture performance models, 2) propose friction and texture performance thresholds, and 3) identify asphalt mixture compositional factors that affect the as-constructed macrotexture and friction.

To develop friction and texture performance models, observations from FHWA/NC 2020-11 and data collected in the current effort were combined and organized in two main groups. Thirty-six sites in Group-1 were primarily used to describe the early friction and texture development. These sites had received a surface overlay at some point between the end of 2019 and middle of 2022 and were evaluated around that same time. One-hundred seventeen sites in Group-2 were used to describe the long-term friction and texture development; therefore, these sites were rehabilitated prior to 2018 and were more than three years old. Continuous friction measurement equipment and a high-speed texture profiler were used to characterize friction and texture, respectively. These observations were collected in the outermost lane, both in the right wheel path and in the center of the lane. All the observations were collected after construction in both site groups, but in 13 Group-1 sites a measurement was collected before the asphalt overlay was placed. Also, a set of field cores were extracted from 13 Group-1 sites and transported to the laboratory to get static friction using a British Pendulum Tester and texture scans using an AMES 9500 rapid laser texture scanner.

The comparison of the laboratory and the field observations collected before and after the overlay has shown, at least in the case of North Carolina's mixtures, that there is strong evidence that texture reduces after an asphalt overlay. This reduction was 55% on average and observed to be as high as 73%. On the other hand, the effect of asphalt overlays on friction is not clear because half of the sites evaluated showed an average reduction of 17%, whereas the other half showed an increase of 19%.

Two sets of models were developed to predict the initial friction and texture as a function of mixture composition. The first set can be used to predict the average representative friction and texture in the field based on the as-designed mixture composition. It was found that the Mean Profile Depth (*MPD*) can be estimated using the gradation coefficient of curvature and the voids filled with asphalt. In the case of friction, the proposed model indicates that friction is affected by the skewness of the texture profile and the interaction of asphalt content and the proportion of fines in the mix.

To model friction/texture performance, the measurements collected in the center of the lane (CL) and right wheel path (RWP) were compared to evaluate if they were statistically different. The statistical comparison indicated that overall, the mean friction values recorded in the CL were different than those collected in the RWP. The analysis showed that CL values were higher than the RWP values in 70% of the 251 comparisons evaluated. For texture, the statistical comparison suggested the *MPD* there was no qualitative or statistical evidence that indicated the *MPD* observations from the RWP were lower than the CL. Hence, seasonal models were calibrated only for friction and these models were used to remove seasonality from RWP records. Once seasonality is removed from the RWP records these were used to calibrate the performance models.

Mixed effect (random/fixed) models were used to account for the unobserved random heterogeneity in friction and texture. These random parameters were coupled with fixed parameters that capture consistent deterioration patterns as a function of the traffic levels, climate, and surface type. Randomness was assumed to manifest in the initial friction and texture and occur due to variability that results from different mixture volumetrics and construction quality of pavements in the same family.

The model validation showed that the proposed performance models can capture individual deterioration trends. The random effect in the intercept seemed to capture the majority of the deterioration trend at each site. The proposed expressions to predict from mixture composition the initial friction and texture after an overlay can be used to approximate the random effect in the intercept. The friction performance model suggested the same friction rate of deterioration should be used across families, whereas different rates must be considered for texture, with the faster deterioration observed in the pavements located in the coastal areas and slower deterioration observed for pavements located in the mountains.

The general methodology to determine the friction and texture investigatory threshold included the following steps: 1) characterizing friction and texture at a network level, 2) identifying the safety measure to compare against friction and texture, 3) modeling friction and texture performance, 4) applying Method 3 of the NCHRP 108 Guide for Pavement Friction, and 5) evaluating the economic implications of setting an investigatory threshold.

In Step 1, the 10th friction percentile and the 50th mean profile depth percentile were used as the values that represent the available skid resistance on a given pavement. In Step 2, the safety measure selected was the lane departure wet crash rate in a period of 13-months. Next, in Step 3, the proposed performance models were used to predict friction and texture values to complement the available observations. Later in Step 4, friction and texture histograms were estimated and the aggregate crash rate for each bin was computed. The crash rate variation was used to set the investigatory values. Finally in Step 5, the North Carolina highway network, the friction and texture performance models, and a set of maintenance and rehabilitation strategies were used to estimate the cost/benefit ratio of including safety requirements in the pavement maintenance

planning and execution. Two main surface treatments were analyzed, Open Graded Friction Courses (OGFC) and Ultra-Thin Bounded Wearing Course (UTBWC).

While the precise cost implications varied by the maintenance scenario evaluated or the interest rate used, all the combinations showed a benefit-cost ratio from using the OGFC and UTBWC greater than one. A minimum benefit-cost ratio of 4.5 was obtained and the maximum observed was 12. It must be noted that the economic analysis conducted in this project focused on the primary economic implications of implementing a pavement friction management program (PFMP), secondary and tertiary implications (e.g., long-term administrative costs, environmental impact, budget allocation, etc.) were not evaluated.

On the basis of these conclusions, the research team recommends the following with respect to the State's pavement friction management program:

- For new pavements, it is recommended to collect four equally spaced measurements during the first year of construction. Then, subsequent measurements should be conducted in the summer.
- Avoid collecting friction or texture measurements in sites with more than 20 consecutive dry days. In this situation, there is a greater chance that dust and contaminants could affect friction observations.
- The highest friction and texture measurement frequencies should be used in interstates, US-routes, curves, ramps, and intersections.
- Friction should be measured at 40-mph and 60-mph. The 40-mph is relevant in ramps and intersections. The thresholds proposed here were set based on friction at 60-mph.
- For quality control, define a section in North Carolina for friction and texture device calibration/verification.

With respect to pavement investigatory and intervention thresholds, the research conducted herein recommends the following:

- Macrotexture investigatory level: 0.80 mm (specific to AMES AccuTexture 100),
- Macrotexture intervention level: 0.60 mm (specific to AMES AccuTexture 100),
- Friction investigatory level (specific to Moventor BV-11 at 60-mph): 0.57 for non-interchanges and 0.65 for interchanges, and
- Friction intervention level (specific to Moventor BV-11 equipment at 60-mph): 0.43 for non-interchanges and 0.49 for interchanges.

The research team also suggests that future work be conducted to characterize friction and texture for other surface treatments, such as microsurfacing, chip seals, diamond grinding, grooving, stone matrix asphalt mixtures, etc. The information gained from these surfaces should be used to evaluate the efficacy of other mitigation strategies.

This page is intentionally blank

1. INTRODUCTION

1.1. Overview

The available skid resistance during wet conditions is one of the major safety concerns for the North Carolina Department of Transportation (NCDOT). Skid resistance is relevant because it is a critical factor affecting highway safety during wet conditions. Skid resistance is the force that develops when a tire that is prevented from rotating (for example when brakes are applied to avoid a collision) slides along a pavement surface. When skid resistance is higher, the overall stopping distance decreases, which can help to reduce vehicle collisions. However, since many factors contribute to any single collision, increasing skid resistance does not guarantee a reduction in collisions. Wet conditions have a negative effect on skid resistance because the water serves to lubricate the driving surface and thereby reduces the sliding forces. This lubricating effect is dependent on many factors including the surface micro- and macro-texture, surface texture connectivity, tire characteristics, speed, and others. Historically, the NCDOT has taken an active role in identifying and correcting problematic areas by using locked-wheel skid tests and other standard and best practice methods.

Although the NCDOT has been actively addressing skid resistance issues as they are identified, FHWA/NC 2017-02 (1) and previous FHWA/NC 2020-11 (2) have found that pavement friction is affected by overlays and that pavement macrotexture is reduced when a new surface layer is placed on a roadway. The FHWA/NC 2020-11 project quantified the precise magnitude of this change and highlighted factors that are contributing to its longevity but was not able to definitively identify causative factors, nor was it within the scope of that project to characterize friction/macrotexture performance functions. These functions are necessary to develop a fully functioning pavement friction management program. Likewise, the FHWA/NC 2020-11 did not collect sufficient data to make recommendations with respect to the material factors that may contribute to greater or less impact to friction/macrotexture and thus positively impact roadway safety. To address this issue, research is needed to characterize friction and macrotexture performance models and to identify preliminary thresholds that allow the NCDOT to identify potential problematic sites.

Based on this need, the specific objectives of the research study described in this report are to;

1. Characterize friction and texture performance models,
2. Develop friction and texture performance investigatory thresholds, and
3. Identify asphalt mixture compositional factors (gradation, asphalt content, presence of modified versus non-modified asphalt, etc.) that affect the as-constructed macrotexture and friction.

1.2. Connection of Research to Previous Effort

This research has built upon but does not duplicate the work conducted under FHWA/NC 2020-11. Under that project the research team; 1) evaluated the effect of surface overlays on friction and macrotexture to confirm the findings from FHWA/NC 2017-02, 2) estimated the traffic repetitions needed to reach friction equilibrium (T_1), and 3) developed a strategy for how to best monitor the friction and surface characteristics of North Carolina roadways. Some of the models presented in FHWA/NC 2020-11 have been updated based on the new observations collected in this project and based on the new modeling techniques that are discussed in this document. Where relevant in the results section of this report, the original and modified models are shown together so that it is

clearly understood which models from the FHWA/NC 2020-11 project have been supplemented by the findings in this study.

1.3. Status of the Literature

A summary review of the literature pertaining to this project is presented in Appendix A, but a summary of the most relevant components of this review is presented below.

1.3.1. Friction and Texture Performance

Figure 1 shows the general model that is internationally accepted to represent skid resistance performance over time or traffic for a new pavement surface, which includes three distinct phases (3–9). In the initial phase, the skid resistance increases as the binder film covering the aggregate is removed. After the bituminous film is worn away, the aggregate microtexture is exposed to traffic and, hence, skid resistance increases. Then, once exposed, aggregates suffer from a normal polishing process and their friction level reduces. This friction reduction is associated with two possible mechanisms; one is a reduction in the microtexture friction component because aggregates are polished, and the other is that aggregates might lose angularity and become rounder. This rounding reduces macrotexture as well and contributes to the loss of friction. The loss of angularity and polishing might occur simultaneously. These processes continue until an equilibrium phase is achieved where the skid resistance tends towards an asymptotic value.

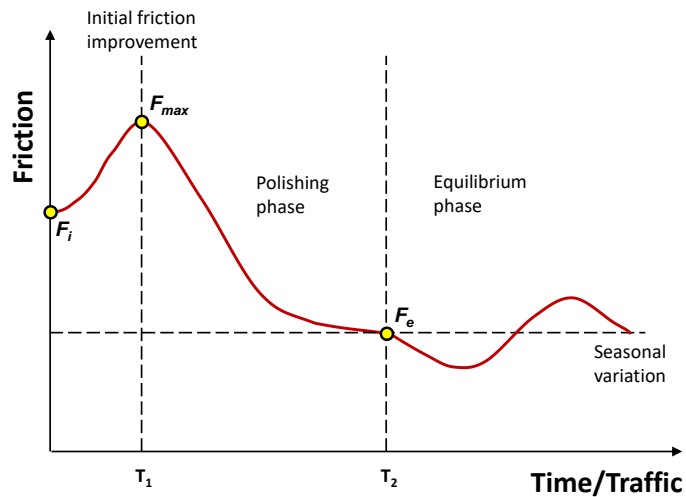


Figure 1. Skid resistance variation with time or traffic.

Once the equilibrium phase is reached (i.e., after T_2), the only variation in friction is attributed to the seasonal fluctuation of temperature and precipitation at the pavement location (if traffic levels remain constant). This fluctuation is denoted as the seasonal effect.

No consensus exists about the duration of each phase. The time span over which the binder cover of the aggregates is removed (age $< T_1$) depends on the binder type and truck traffic characteristics. For example, T_1 has been observed to occur at two or three months for dense-graded asphalt mixes, but the first phase may extend throughout the entire life of a Stone Mastic Asphalt (SMA) mix surface (10).

Different regression equations have been proposed over the years to describe the traffic-induced polishing effect (i.e., the phase between T_1 and T_2). A detailed discussion of these models is included in Appendix A. These expressions use aggregate polishing resistance properties, usually

expressed in terms of the Polished Stone Value (PSV) and the cumulative traffic. Some expressions use mixed traffic volumes others focus on truck traffic. Likewise, authors like Jayawickrama and Thomas (11) and Cenek et al. (12) have developed some expressions to describe friction seasonality that use as input variables of air (or pavement temperature) and the amount of precipitation.

The general macrotexture performance model is depicted in Figure 2, which includes four components (1, 2, 4, 8, 9, 13): initial macrotexture (M_i), equilibrium macrotexture (M_e), time to equilibrium (T_1), and the harmonic characteristics of the seasonal effect. The general model suggests that macrotexture is maximum immediately after construction and decreases because of a densification of the surface due to the traffic repetitions (13).

It is generally accepted and proven that texture values do not vary substantially due to traffic polishing. It is important to note that other factors may contribute to an increase in macrotexture during a pavement's service life. For example, age-induced raveling and the loss of surface fines may increase the surface texture (4). This process is represented by the line with the positive slope in Figure 2. Most of the texture performance models presented in the literature are based on laboratory observations. Raveling and the loss of surface fines may not be replicated in the laboratory, so these effects have not been fully described.

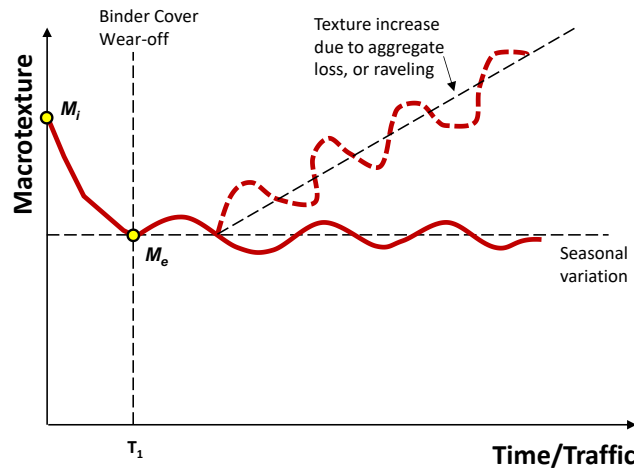


Figure 2. Macrotexture variation with time or traffic.

Texture changes induced by traffic were studied by Miao et al. (13, 14) who evaluated the degradation of mean texture depth (MTD) with traffic volume and developed the model structure indicated in Equation (1). To develop this model, field tests were conducted seven times in a period of two years. Two highway sections were included in the field test, covering four surface types. Macrotexture was characterized using the Sand Patch Test (SPT).

$$MTD = a \cdot \text{Log}(\text{Traffic}) + b \quad (1)$$

where;

a and b = regression coefficients presented in (14).

MTD = mean texture depth measured with a SPT, in mm.

A similar model suggesting that *MTD* decays with repeated traffic loading was evaluated by Wu and Abadie (13) who characterized friction and texture in the laboratory and then validated their results with field observations.

The raveling process, described in Figure 2, has been observed by different researchers (15). This process starts once the binder has been peeled off from the aggregates, then due to a combined effect of weather and traffic coarse and fine aggregates are lost. This aggregate loss generates more voids in the mix and thus increases the texture profile irregularities, which translates into higher texture parameters. Several field texture observations have been reported as part of the Phase VII (2018-2021) of the National Center of Asphalt Technology (NCAT) Test Track findings (15). In these experiments, a power growth in texture values with respect to traffic was initially observed after which the texture stabilizes at a roughly constant value. Interestingly though, in some locations, truck traffic seems to be the causative factor for raveling whereas in other locations, the best descriptor is pavement age.

1.3.2. Establishing Investigatory and Intervention Thresholds

Two forms of minimum skid resistance thresholds are commonly used by highway agencies for pavement friction management, namely the investigatory level and the intervention level. The investigatory threshold value is the higher, and less serious of the two thresholds. When the surface texture and/or friction is at the investigatory level(s) there exists some evidence that crash rates may be negatively affected by the surface characteristics of the pavement. However, since there are many interacting factors that contribute to crashes, the criticality of the surface characteristics being at the investigatory level for any given site cannot be estimated. Hence, there is a need to investigate the site more closely to determine whether maintenance or restorative treatments are needed. Even if it is determined that such treatments are not immediately necessary, pavements at the investigatory level should be continually monitored because they are at a point where continued decreases in surface texture and/or friction may lead to higher crash rates. In contrast, the intervention level is the more serious of the two thresholds and represents the condition where an agency should consider immediate corrective action, such as maintenance or restorative treatment. At this level, there exists more substantive evidence that crash rates are affected by the surface texture and friction values and so the safety risk can increase rapidly when surface texture and/or friction fall below the intervention level (16).

Typically, the common criteria for establishing the skid resistance thresholds are (7, 16, 17):

- Engineering judgment
- Deterioration trend of the skid resistance
- Crash history
- Other agencies practice similar site characteristics.

In the NCHRP 108 Guide for Pavement Friction (GPF), Hall et al. (7) recommended using three methods to establish skid resistance thresholds:

- Method 1: Set the threshold based on historical skid resistance trends. The big challenge with this method is to identify the point at which friction starts to decrease rapidly.
- Method 2: Set the threshold based on a combination of historical skid resistance and crash data. The problem with this method is that is hard to identify the exact conditions where friction and crash trends start to decrease or increase, rendering the assessment subjective.

- Method 3: Identify the skid resistance probability mass function (pmf) and calculate the expected crash rate for each value of the pmf. The thresholds are set based on expected values of crash rates. Consequently, safety is underestimated on some sites and overestimated in others.

The methodology proposed in the NCHRP 108 GPF was developed based on a friction monitoring program that uses the locked-wheel skid tester (LWST). A similar attempt was made by de Leon Izeppi et al. (18) who proposed a methodology for determining investigatory levels using a continuous friction measurement equipment (CFME). This new methodology is discussed in Appendix A. Finally, the intervention threshold is typically set as a percentage of the investigatory value.

1.3.3. Knowledge Gaps and Applications

Based on the literature discussed above and in Appendix A, there are some important knowledge gaps:

Friction and Texture Performance

- New testing technologies, such as the CFME for friction and high-speed texture profiler (HSTP) for texture, can capture more precise friction and texture values and provide more precise representations of the available skid resistance. However, these new technologies lack historical observations to get reliable representations of skid resistance performance.
- There are different technologies available to measure friction and each has its own pros and cons. The choice of a friction-measuring device will depend on the specific problem. The U.S. does not currently have an established protocol for measuring friction, including the optimal speed or the location along the pavement. Consequently, some agencies have started monitoring friction based on previous experience with a LWST or based on the device available for monitoring the network to inform the development of a protocol. However, a direct comparison of the measurements collected with devices from different manufacturers and/or technologies is not possible.
- Though a good correlation between devices has been reported, this correlation depends highly on the tire and speed used for measurements. Most of the comparisons presented in the literature focused on evaluating a possible correlation at a specific condition; however, there are no references about the effect of climate on devices from different manufacturers, or with different measurement mechanisms.
- Texture parameters, such as the *MPD* or *MTD*, are sensitive to the measurement location within the pavement (e.g., the center of the lane versus wheel paths), the technology used (laser resolution and frequency), and the processing algorithm applied (filtering techniques). Hence, measurements collected by different operators, with different testing technologies, at different locations on the pavement surface may not be directly comparable.

Pavement Friction Management Program (PFMP)

- Road geometry information is needed to accurately establish friction demand categories. In the case of North Carolina, information related to highway alignment is not easily available at a network level, in particular the super elevation and curve radius. Surrogates of this information, such as the Ball Bank Indicator (BBI) index can be used, but it is necessary to evaluate the relationship of this index with crash risk and friction.

- Though both the investigatory and intervention thresholds proposed by the federal aviation administration (FAA) serve as a reference, it is important to notice these values were envisioned for airports. To set investigatory levels for a highway network it is necessary to consider crash risks, which can be estimated by any of the statistical methods discussed in Appendix A.
- Although there are some references in the U.S. for friction and texture thresholds, most of these references are based on a LWST.
- Texture is easier to measure at a network level than friction. However, most agencies do not have a measurement protocol for texture. Moreover, the attempts to use texture information as a predictor in a safety performance function (SPF) are quite limited.
- In the PFMP structures available in the literature, the analysis module that relates friction and texture in the field has not been explored. While the U.K. and New Zealand have PFMPs, their programs do not include references for the quality control process of friction and texture in the field. It is imperative that such protocol becomes available among practitioners.
- Also, as with any other network-level asset management, PFMPs are susceptible to data variability due to changes in the data collection process, either by a change in vendor or technology used. This is the current situation faced by many agencies that are migrating from friction collected with an LWST to values measured with a CFME. This data variability poses a challenge for data processing and forecasting future conditions.

1.4. Report Organization

This report is composed of seven primary sections and ten appendices. Chapter 1 presents the needs, objectives, and summarizes the most relevant literature on friction and texture performance and thresholds (see Appendix A for the full literature review). Chapter 2 describes the primary data collected, i.e., friction and texture values, the secondary information, pertaining road geometry and characteristics and the crash records for each of the tested sites. Chapter 3 presents the different elements of the friction and texture performance models; it shows the modeling techniques selected to represent each of these elements and includes the considerations needed for making predictions. Chapter 4 presents the steps followed to establish a set of preliminary friction and texture thresholds, where three evaluation methods are discussed. Subsequently, Chapter 5 presents the conclusions of this research and corresponding recommendations. Chapter 6 provides the implementation and technology transfer plan, respectively. Chapter 7 lists the references cited in the main body of the report. Appendices A – J provide detailed literature review and detailed analysis and results for those who are interested.

2. DATA PROCESSING

2.1. Overview

In this research, two groups of sites were evaluated; Group-1 and Group-2. The sites in Group-1 were primarily used to describe the early friction and texture development. These sites had received a surface overlay at some point between the end of 2019 and middle of 2022 and were evaluated around that same time. Group-2 sites were used to describe the long-term friction and texture development; therefore, these sites were rehabilitated prior to 2018 and are more than three years old. Table 1 and Table 2 show the distribution of the sites in Group-1, and Group-2, respectively.

Table 1. Distribution of Group-1 sites across North Carolina division units.

Surface Type	Division														Total
	1	2	3	4	6	5	7	8	9	10	11	12	13	14	
	CO					PI						MO			
JCP															0
S9.5B			1			1		2							4
S9.5C		1	6	4	3			8				1		1	24
S9.5D				1	2	1			1						5
UTBWC													3		3
OGFC															0
Total	0	1	7	5	5	2	0	10	1	0	0	1	3	1	36
	18					14						4			

CO: Coastal region; PI: Piedmont region; MO: Mountain region; JCP: Joint-Concrete Pavement; S9.5B, C, D: Superpave mixes designed for low, moderate, and high traffic; UTBWC: Ultra-Thin Bounded Wearing Course; OGFC: Open-Graded Friction Course.

Table 2. Distribution of Group-2 sites across North Carolina's division units.

Surface Type	Division														Total
	1	2	3	4	6	5	7	8	9	10	11	12	13	14	
	CO					PI						MO			
JCP						1			2						3
S9.5B		1		1	2	1	1					1	1		8
S9.5C		3	1		6	7	1	10	8	1	6	6	2	6	57
S9.5D				3		1	1					1	2		8
UTBWC	1			1		1	3	1	6	1		2	6		22
OGFC			1	9		2			2					5	19
Total	1	4	2	14	8	13	7	11	17	2	6	10	11	11	117
	29					66						22			

CO: Coastal region; PI: Piedmont region; MO: Mountain region; JCP: Joint-Concrete Pavement; S9.5B, C, D: Superpave mixes designed for low, moderate, and high traffic; UTBWC: Ultra-Thin Bounded Wearing Course; OGFC: Open-Graded Friction Course.

As shown, the sites were selected to represent the three predominant climate regions in North Carolina, coastal, piedmont, and mountains. The spatial distribution of the sites is tracked within the report by using the administrative division number where the project was placed, i.e., one of the 14 divisions used by the NCDOT. The highest proportion of sites are located in the piedmont region and most of the sites are surfaced with a S9.5C mix surface. However, collectively this data does cover all three regions and all surface types. The mixture composition for both site groups is

included in Appendix B. Group-1 includes 10 Interstates, 16 US-Routes, and 10 NC-Routes. Eleven of the Group-1 sites also received a measurement before the overlay was placed. The number of observations collected after the construction of the overlay varied from one to nine observations. Each observation consisted of a measurement of friction and texture; typically, both measurements were collected on the same date. If not, they were collected one day apart. For the Group-2 sites, 54 are Interstates, 60 are US-Routes, and the remaining 3 are NC-Routes.

For each site, the research team consulted the Highway Construction And Materials System (HiCAMS) and the NCDOT – Connect website to obtain the Job Mix Formula (JMF) (for mixture composition and as-designed volumetrics) and the construction dates. For some of these sites, it was also possible to locate the as-produced volumetrics from the North Carolina quality control plan database. Also, for each site, the annual traffic survey of 2019 was consulted to identify the annual average traffic volumes. Finally, it is noted that additional field cores from quality assurance operations in Division 1, 5, 6, 7, 10, and 13 were evaluated using the static laser to complemented measurements taken on Group-1 sites.

For the purposes of this report, a ‘site’ is a roadway that is being studied while a ‘segment’ refers to a subset of a site that is homogeneous with respect to geometry type (e.g., tangent, curves, tangents with an intersection, etc.) and average annual daily traffic (AADT). Most sites consist of multiple segments. An example of one study site (Site 113) is shown in Figure 3 to illustrate the meaning of these definitions. For the site shown, there are five homogeneous road segments with AADTs equal to 25,000, 21,500, 21,000, 20,500, and 21,500 vehicles per day (vpd).

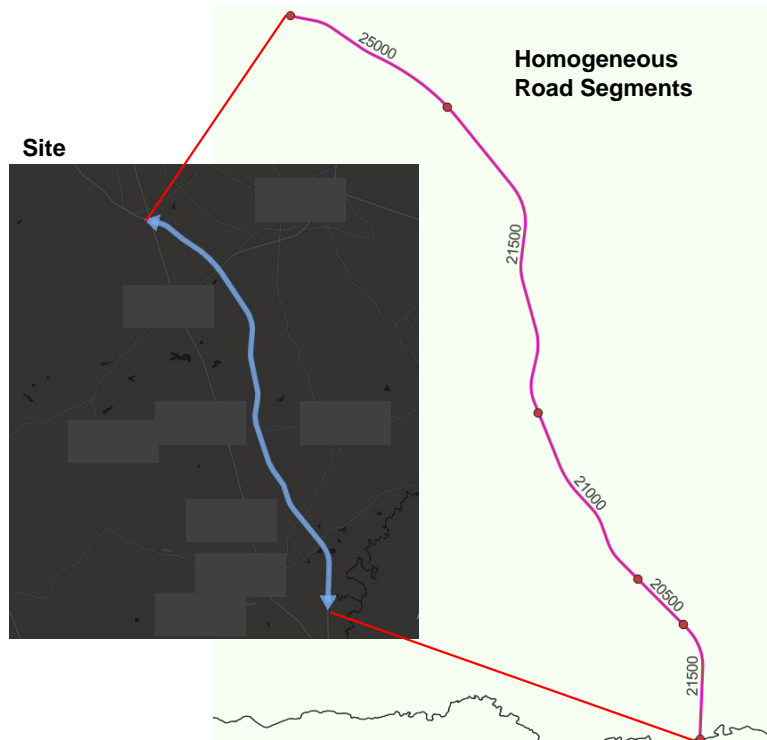


Figure 3. Concept of site and homogeneous road segment, Site 113.

The field friction and texture measurements performed in both groups of sites were collected by KPR engineering in collaboration with the North Carolina Department of Transportation (NCDOT). A subset of pavements in the second group received an additional friction and texture

measurement using the Sideway-Force coefficient Routing Investigation Machine (SCRIM). This extra measurement was carried out by WDM USA, and the values were used to compare the two different testing devices and to assess the implications of using different testing technologies to characterize the skid resistance at a network level. These measurements were part of two NCDOT research projects, FHWA/NC 2020-11 “Evolution of Pavement Friction and Macrotexture after Asphalt Overlay” and the present research effort. Figure 4 provides an overview of the data elements that were captured in this research. These data elements are the same for both groups of sites. As indicated in Figure 4, the data collected from these sites included field core measurements, field measurements of friction and macrotexture, crash inventory before and after the overlay, and supplementary information.

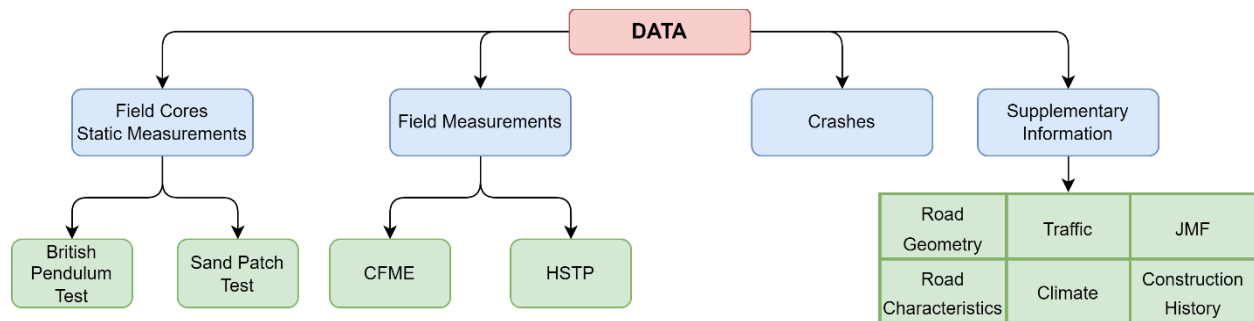


Figure 4. Data collected for the PFMP framework.

2.2. Continuous Pavement Friction Measurements (CFME)

Most of the friction measurements used in this study were conducted by KPR Engineering and were complemented by a set of measurements made by WDM USA. The device used by KPR was the CFME Moventor Skiddometer BV-11. This device was the same one used in the previous research project FHWA/NC 2020-11 and the reader is referred to that report for more specific details on the specification of the device. In brief, the Moventor device measures at a continuous slip ratio of 17% and reports measurements every 10 ft (3 m). KPR friction data was collected in the outermost lane, and within that lane the measurements were conducted in the right wheel path (RWP) and in the center of the lane (CL), at 60-mph (96 km/h). Some sites also received an extra measurement at 40-mph (60 km/h).

WDM USA used the Sideway-force Coefficient Routine Investigation Machine (SCRIM) for friction measurements. This device uses dynamic vertical load measurements with a free rolling test wheel oriented at a 20-degree angle relative to the travel direction. It reports friction values every 26.4 ft (8 m). Friction was measured at operating speeds and values were later standardized to a speed of 50 mph (80 km/h). All the observations were collected in the left wheel path (LWP) of the outer most lane. A comparison of the technical details of two devices is presented in Appendix C along with a comparison of measurements with the two instruments on the same sites.

The friction measurements made by KPR were the ones used for performance model calibration and for the definition of investigatory thresholds. WDM USA observations were used only to compare measurement technologies and to illustrate the concept of a PFMP. The friction measurement dates made by KPR in each site are indicated in Table D.1 of Appendix D. For each site, the target date for the first measurement was within the first 15 to 30 days of the overlay construction. For each site, friction measurements were processed following the same statistical process described in the previous research project FHWA/NC 2020-11, i.e., the research team

decided to use the 2.5th percentile calculated in 0.1-mile increments and then the average of these 0.1-mile values was defined as the representative friction value (2).

This metric was used whenever possible; however, as discussed in Chapter 4, when a site is divided into friction demand categories, it is possible to end up with short segments of roads less than 0.5-miles long. Splitting these short sections into 0.1-mile segments to compute the 2.5th percentile and then taking the average does not provide any statistical benefit given the small sample size. For this reason, the representative friction for each of these short segments is set as the 10th percentile of the entire site. The reader can refer to Appendix E for more details about the selection process of the 10th percentile.

2.3. High-Speed Texture Measurements

The equipment used for macrotexture measurements was the Ames Engineering High Speed Texture Profiler (HSTP) and was operated by KPR engineering. This device was the same one used in the previous research project FHWA/NC 2020-11 and the reader can refer to that report for further details on the testing technology (2). Like for friction, the measurements made by KPR were complemented with observations made by WDM USA in a subset of the Group-2 sites.

KPR measured texture in the CL and RWP of the outermost lane in the traffic flow direction at the posted speed limit. Once collected, the software that accompanies the Ames HSTP applies the filters indicated by ISO-13473 to remove potential outliers and then compute the following texture parameters: mean profile depth (*MPD*), estimated mean texture depth (*EMTD*), root mean square depth (*RMSD*), mean elevation (*Ra*), elevation mean square root (*Rq*), kurtosis (*Rku*), and skewness (*Rsk*). These metrics are reported every 10 ft (3 m).

Texture measurements were processed following the statistical procedure established in the previous research project FHWA/NC 2020-11. Accordingly, each site is divided into 0.1-mile segments, the 50th percentile of the texture parameters are computed on each segment and the representative value of the site is defined as the average of the 50th percentiles computed on the 0.1-mile segments. The texture measurement dates made by KPR in each site are indicated in Table D.2 of Appendix D.

In the case of WDM USA, texture was reported in terms of *MPD*, which was measured using a single spot laser mounted in the SCRIM machine. Because in this report, in particular in the analysis presented in Appendix C, the *MPD* was the parameter selected to compare the measurements made by WDM and KPR, it was decided to use superscripts to differentiate the parameter resulting from the data of each vendor, i.e., *MPD* without superscript was used to denote the values collected by KPR and *MPD_{SCRIM}* was used to indicate the *MPD* obtained from WDM data. The reader can refer to Appendix C for a comparison of the two testing technologies. The *MPD* measurements made by KPR were the ones used for performance model calibration and for the definition of investigatory thresholds. WDM USA observations were used to compare measurement technologies and to illustrate the concept of Pavement Friction Management Program (PFMP).

2.4. Field Core Observations

The lab measurements on field cores were carried out for 16 of the 34 sites in Group-1 using cores taken a few days after the overlay. Also, in three of these Group-1 sites, a set of pre-construction cores were acquired to compare the long-term conditions with the recently overlaid ones. The core acquisition process was coordinated with the division engineers. The average height and diameter

of the cores was 8-10 in. (20-25 cm) and 6-8 in. (15-20 cm), respectively. In the field, the cores were collected in the center of the RWP, and their location was estimated using a GPS receiver. The NCDOT personnel tried to evenly separate the cores along the section surveyed with the CFME device and the Ames laser scanner. Three cores were extracted from each site, except for Site 24 where four cores were extracted, and for sites 34/35, 37, and 39 in addition to the three after construction cores another three pre-construction cores were obtained.

Once the cores were pulled from the field, they were transported to the lab to obtain the laboratory friction and texture measurements. The cores were cut to an approximate height of 4 in. (10 cm), as indicated in Figure 5, so that they would fit beneath the laser profiler and inside the BPT testing jig. In the case of friction, BPT measurements were carried according to ASTM E303-93. To facilitate the measurement process, the research team developed a device that serves as a support base for the BPT and that also holds steady the field cores and keep the surface leveled, as shown in Figure 6 (a).



Figure 5. Core extraction and height adjustment.

Two different techniques were used to measure the texture of the field cores. First, an SPT was conducted on each core following the ASTM E965-15 specification. The result of this test is the mean texture depth (*MTD*). Second, the AMES 9500 rapid laser texture scanner (rLTS) was used to scan the surface of the cores and obtain the *MPD*. The devices are shown in Figure 6. The measurements made with the AMES 9500 rLTS were used to replace the measurements made with the custom laser used in the previous research project because this device produce surface scans with higher resolution.

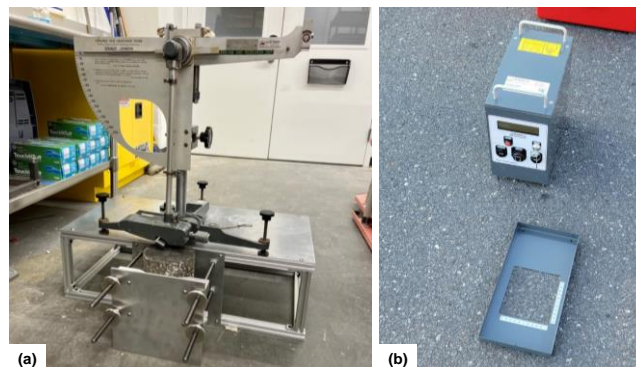


Figure 6. Images of laboratory test equipment used in this study: (a) BPT and support base and (b) AMES 9500-line texture scanner.

The specifications for the AMES 9500 laser are as follows: scan area of 4 in. by 4 in. (100 by 100 mm); vertical resolution of 0.01 mm; length resolution of 2048 points in 4 in. (spacing = 0.0496 mm); width resolution of 2448 points in 4 in. (spacing = 0.0415 mm); scan time for full scan of 90 seconds; and elevation height data and scan intensity image are collected.

The output of the laser measurements were processed according to the ISO 13473. Three parameters were manually computed using the 3D scanned surface, the *EMTD*, the average peak height and the average valley depth. The peak height is the positive difference between the surface elevation and the mean plane, while the valley depth is the negative difference between the surface elevation and the surface mean plane. In addition to three parameters mentioned above, the following indices were obtained: *MPD*, *RMS*, *Ra*, *Rq*, *Rsk*, and *Rku*.

2.5. Crash Records

For each Group-1 and Group-2 site, the crash history was extracted from the NCDOT Traffic Safety Systems (TSS). In the NCDOT-TSS, each crash event is inventoried by completing a collision report form, which contains all the information required to describe the severity of the crash (property damage only, injury type A, B, or C, and fatal). These severity levels are equivalent to those defined in the Model Minimum Uniform Crash Criteria (MMUCC) (19). It also describes the events that led to the collision and the location of the crash. Based on the description of the event, four crash types were evaluated: total, total wet, lane departure, and lane departure wet crashes. These records correspond to the period of January 1 of 2010 to April 30 of 2023.

2.6. Supplementary Information

2.6.1. Traffic

Traffic was characterized by three different sources of information, i) Set-1 consists of a set of continuous traffic counting stations, ii) Set-2 consists of traffic predictions extracted from the StreetLight database, and iii) Set-3 consists of annual average daily traffic (AADT) from the NCDOT traffic survey. StreetLight is a company that uses information from mobile devices and ground counting stations to make a continuous characterization of the different modes of transportation across the USA and Canada.

Set-1 Traffic Dataset (ST1)

The NCDOT has 113 continuous counting stations distributed across the state. These stations report hourly and daily vehicle counts. Due to various reasons, such as maintenance, weather, or malfunction, the stations do not operate the entire year. Though the specific type of sensors varied across the network, all generally involve embedded loop-piezo-loop sensor arrays.

Prior to analysis, the vehicle counts from 2015-2021 from all 113 stations were reviewed to remove outliers and to verify that at least 200 days of data were available in each year for each station. Additionally, only stations that have been operating for at least three consecutive years prior to 2020 were considered for the analysis, i.e., the minimum period before 2020 was set as 2017-2019. After applying these two filters, the numbers of continuous counting stations reduced from the original 113 to 65, and the data was cleansed by removing outliers following the same procedure employed in Goenaga et al. (20). Afterwards, daily counts were totaled by month for each station and used to calculate the Monthly Average Daily Traffic (*MADT*) according to Equation (2).

$$MADT_{Station\ i,j} = \frac{Monthly\ Sum\ Daily\ Counts\ Station\ i}{\#days\ Month\ j} \quad (2)$$

The 65 stations are presented in Figure 7 (a) and are distributed as follows across the road functional classes; 17 are placed on Interstates, 26 on US-Routes, seven on NC-routes, 14 on secondary routes, and one on a local road. These stations are diverse with respect to baseline traffic and varied from an approximately 500 average vehicles per day (vpd) to 142,600 vpd.

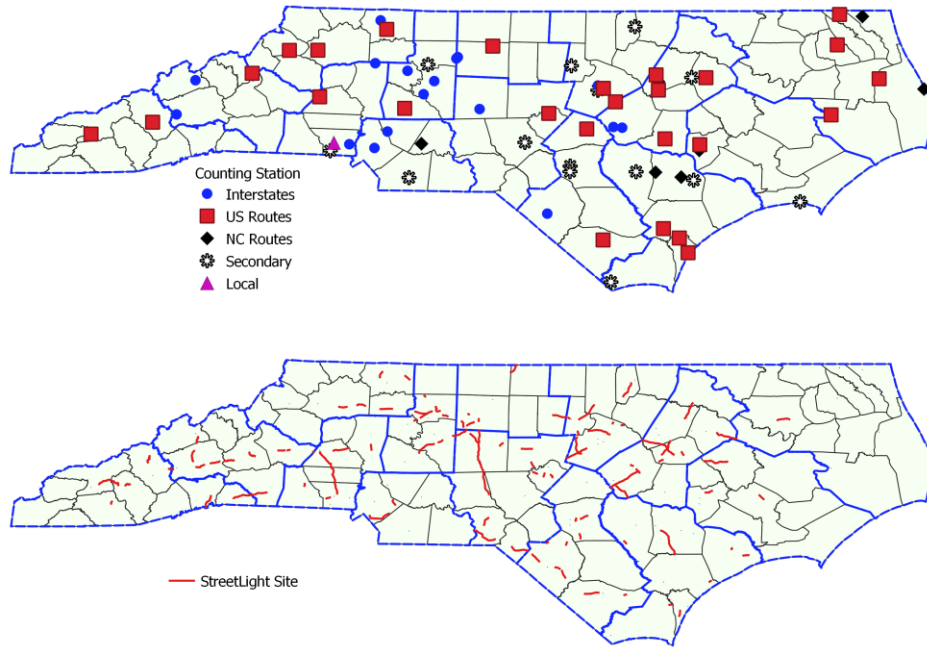


Figure 7. (a) Location of counting stations and (b) StreetLight sites.

Set-2 Traffic Dataset (ST2)

The second source of traffic data was the Streetlight database. This platform provided estimates of the MADT for a set of road sites that were selected based on their construction history and surface type. Traffic predictions were extracted for 147 sites, selected based on their construction history, and 49 segments placed adjacent to a continuous counting station from ST1, yielding a total 196 locations (sites and segments, shown in Figure 7 (b)) analyzed using the StreetLight platform. The observations in the 49 segments adjacent to the ST1 counting stations sections were used to compare and validate the StreetLight predictions. These observations were extracted for the years 2017-2021.

Set-3 Traffic Dataset (ST3)

Finally, the third dataset consisted of the AADT, reported by the NCDOT traffic survey unit for years 2017-2019. This information is publicly available on the NCDOT website in the form of a shapefile. GIS tools were used to match the locations of the counting stations with the line layers of the shapefile. In this way, the AADT was extracted for the road segments adjacent to each counting station in ST1 and the segments of the 147 sites in ST2. Therefore, the ST3 AADT values are reported by segments.

2.6.2. Road Geometry

Curve Identification

Because curves are not differentiated from tangents in the NCDOT GIS system, it was necessary to find a methodology that could successfully identify curves and their corresponding radius of

curvature from roadway shapefile. Therefore, the tool developed by Bil et al. (21), the Road Curve Analyzer (ROCA), which is an ArcGIS toolbox for road alignment identification and curve radii computation, was used to differentiate between curves and tangents. This toolbox requires the information presented in Figure 8. As shown, it is necessary to define a training data set, then this information is used to conduct an empirical Bayes categorization where the probability of being a straight segment, or a curve is computed. After categorizing each element, the toolbox used a set of predefined rules to compute the radius of curvature.

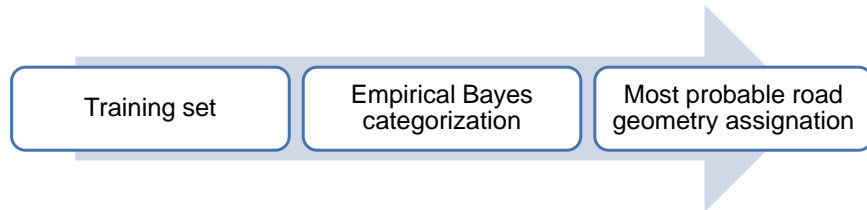


Figure 8. Elements of the ROCA toolbox.

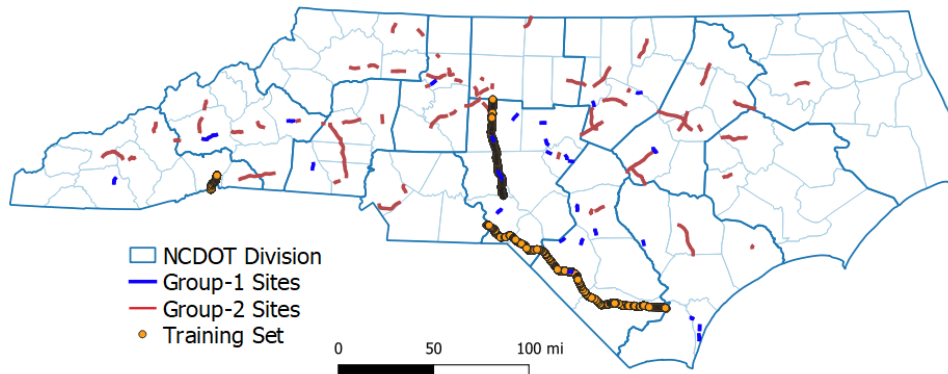


Figure 9. Distribution of the training set and the 160 sites.

In this research, 193 road-miles were selected and manually classified into curves or tangent segments. These 193 road-miles were used as the training sets in the ROCA toolbox. Then all sites in the dataset were classified using the trained model, for a total of 1,111.5 miles. The results were randomly checked for correctness using Group-1 sites. Each section of these sites was found to be correctly identified, verifying the calibrated ROCA toolbox. The distribution of the training set and the evaluated sites is depicted in Figure 9.

Ramp and Intersection Identification

The location of the interchanges along the routes was determined using a shapefile provided by the NCDOT. This shapefile contains the geometry that delimits the area of influence, entry and exits of a given interchange. Once the sites were categorized either into a tangent or into a curve, the resulting entities were intersected with the geometry of the interchanges and the length of the total site inside an interchange was computed. The interchange distribution across the primary road network of North Carolina is presented in Figure 10.

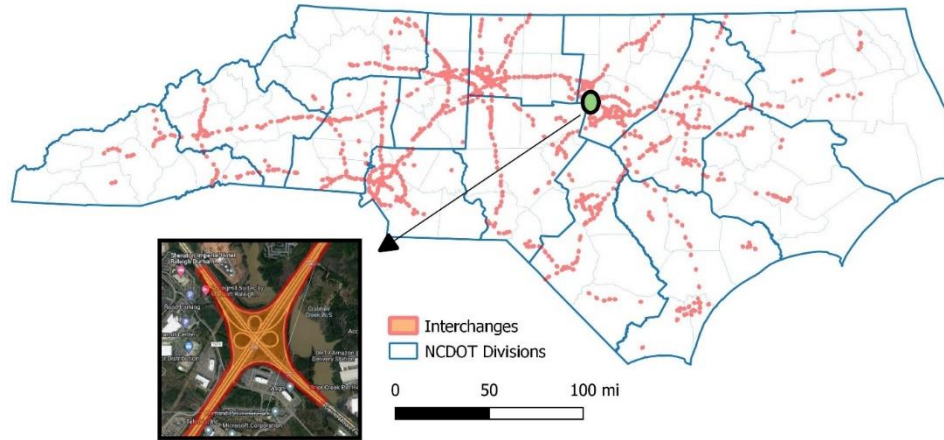


Figure 10. Distribution of interchanges along the primary road network of North Carolina.

Road Characteristics

The road characteristics of each site, including the number of lanes, type of facility (divided vs undivided), speed limit, design speed, and functional class were extracted from the NCDOT road characteristics shapefile, accessed through the connect website of the NCDOT. There are seven possible functional classes, including: interstates, freeways, principal arterials, minor arterials, major collector, minor collector, and local.

As will be discussed in Chapter 4, to define a set of investigatory and intervention friction and texture thresholds, those sites that were rehabilitated during the period of analysis, or for which the surface type is portland cement concrete were removed from the database. Also, the geometry of the sites was intersected with the milepost extension of the crash dataset to get accurate estimates of the crash rate.

This page is intentionally blank

3. PAVEMENT FRICTION AND TEXTURE PERFORMANCE MODELING

3.1. Overview

This chapter details two main model development tasks; 1) updates to the FHWA/NC 2020-11 mixture composition-to-friction/texture models and 2) extension of the friction and texture performance models to cover a larger temporal span. The first modeling task is important in order to better understand how mixture composition factors affect texture and friction. The second model development is important because, for a PFMP it is important to be able to estimate the available friction and texture throughout a pavement's life. These measurements are critical because research suggests that a reduction in the available friction and texture of a pavement surface could contribute to increases in collisions (22, 23) when other factors that affect crash rates, such as changes in traffic patterns, roadway geometry, vehicle speeds etc., are constant.

3.2. Updates to FHWA/NC 2020-11 Mix Composition Models

In FHWA/NC 2020-11, a set of expressions were calibrated to predict the expected friction and texture as a function of mixture composition. Two types of models were proposed, one that relied on mixture composition and another that included field cores to represent the construction quality. These cores were used to obtain a 3D representation of the pavement surface in the field. In the current research effort, these models were updated by incorporating the observations collected in the news sites that were evaluated in this project. These additional observations increased the number of field cores from 10 to 13 and added ten new observations to the field friction and texture site measurements after construction (one additional UTBWC, two OGFC, and seven dense graded mixes).

Appendix F provides a detailed description of the models and the data used for their calibration, but Table 3 summarizes the original and modified models. The models shown in Equations (8) and (10) are of particular interest to other parts of the research project. In addition to estimating the effect of mixture composition on texture and mixture composition and as-constructed surface texture on friction, these expressions can be used to approximate the random effects in the intercept of the proposed performance models for a pavement that has not been used during the calibration process, i.e., to make predictions for new pavements. This process is discussed in detail in the validation procedure presented later in this chapter.

Table 3. Summary of original and modified friction and MPD models.

Model ¹	Version	Equation
1	Original	$Friction_{field} = 0.645 + 0.141 \times (Cc + Pk + Vy) - 0.00548 \times (\% AC \times P_{200})$ (3)
	Modified	$Friction_{field} = 0.619 + 0.172 \times (Cc + Pk + Vy) - 0.0060 \times (\% AC \times P_{200})$ (4)
2	Original	$MPD_{field} = 0.243 + 0.331 \times EMTD_{lab}$ (5)
	Modified	$MPD_{field} = 0.433 + 0.310 \times MPD_{lab} - 0.025 \times \% AC$ (6)
3	Original	No significant expression was found (7)
	Modified	$Friction_{representative} = 0.786 - 0.065 \times Rsk - 0.580 \times (\% AC \times P_{200})$ (8)
4	Original	$MPD = 0.674 + 0.150 \times Cc - 0.00088 \times P_{200} \times VFA$ (9)
	Modified	$MPD_{representative} = 1.22 - 0.009 \times VFA + 0.087 \times Cc - 0.046 \times (\% AC \cdot Dense)$ (10)

¹Model 1-Friction prediction based on field cores and mixture volumetrics; Model 2-MPD prediction based on field cores and mixture volumetrics; Model 3-Friction prediction based on as-designed mixture volumetrics; Model 4-MPD prediction based on as-designed mixture volumetrics

where;

$Friction_{field}$	= 250-ft average, centered in a field core location, of the continuous friction,
MPD_{field}	= 250-ft average, centered in a field core location, of the continuous MPD ,
$Friction_{representative}$	= average of the 2.5 th friction percentile estimated every 0.1-miles,
$MPD_{representative}$	= average of the 50 th MPD percentile estimated every 0.1-miles, in mm,
Cc	= gradation coefficient of curvature, computed with Equation (105),
$\%AC$	= mix designed asphalt content,
P_{200}	= aggregate gradation percent passing Sieve No. 200 (0.075 mm),
Pk	= average peak elevation of the texture surface, in mm,
Vy	= average valley depth of the texture surface, in mm,
Rsk	= texture profile skewness (mm ³ /mm ³),
VFA	= as-designed asphalt mix voids filled with asphalt, and
$Dense$	= binary variable; 1 = Dense mix and 0 = otherwise.

3.3. Performance Model Development

Mixed effect (random/fixed) models were used to describe friction and texture evolution while accounting for the unobserved random heterogeneity. The random parameters in these models account for individual friction/texture deterioration rates and/or initial friction/texture values (24). These random parameters are coupled with fixed parameters that capture consistent deterioration patterns as a function of the traffic levels, climate, and surface type. Randomness is assumed to manifest in the initial friction and texture and occur due to variability that results from different mixture volumetrics and construction quality of pavements in the same family.

Group-1 and Group-2 sites were combined to calibrate the performance models and the observations were processed as indicated in Chapter 2. The representative friction (at 60-mph) and texture in 0.1-mile increments was defined as the 2.5th friction percentile and 50th MPD percentile, respectively. The variation of the mean friction and texture was computed in this way across the sequential set of measurements in each site. Trends with respect to time, climatic conditions, and traffic were used to evaluate seasonality, early evolution, and long-term performance.

StreetLight $MADT$ predictions for each site were used to estimate the cumulative traffic until the moment of the friction/texture measurement, as indicated in Equation (11). These traffic predictions were used in all sites except for Sites 8, 9, and 15, because these have an AADT lower than 6,000 vpd. For these sites, cumulative traffic was estimated by assuming a constant AADT equal to that observed in 2019.

$$Cumulative\ Traffic = \sum_{i=1}^{Meas.\ date-Overlay\ Date} (MADT_i) \quad (11)$$

For the long-term performance predictions, sites were grouped into families defined by the combination of climate region and surface type. In this sense, there are three climate regions, piedmont, coastal, and mountains, and two distinct surface types, dense mixes (S9.5B, S9.5C, and S9.5D) and high-friction courses (UTBWC and OGFC). It must be noted that in this research, the term high friction course (HFC) is used to refer UTWBC or OGFC as surfaces that provide either high-friction and/or high-texture. In the literature the term is used to refer to any of these surface types (5, 7, 9, 14, 22). Hence, a total of six different families were defined, and the number of sites in each family is summarized in Table 4.

The methodology followed for the modeling effort is depicted in Figure 11. As shown, the friction and texture collected in the center of the lane (CL) and right wheel path (RWP) were compared to evaluate if they are statistically different. This evaluation is important because the performance models rely on the hypothesis that the CL experiences lesser traffic repetitions than the RWP; hence, the CL can be used to calibrate a seasonal model to remove the seasonal effect from the RWP observations. Once seasonality is removed from the RWP records these were used to calibrate the performance models.

Table 4. Number of sites per family.

Family	Surface	Climate Region	Number of Sites
1		Blue Ridge	26
2	Dense	Piedmont	40
3		Coastal Plains	32
4		Blue Ridge	15
5	High-Friction Courses (HFC)	Piedmont	17
6		Coastal Plains	13

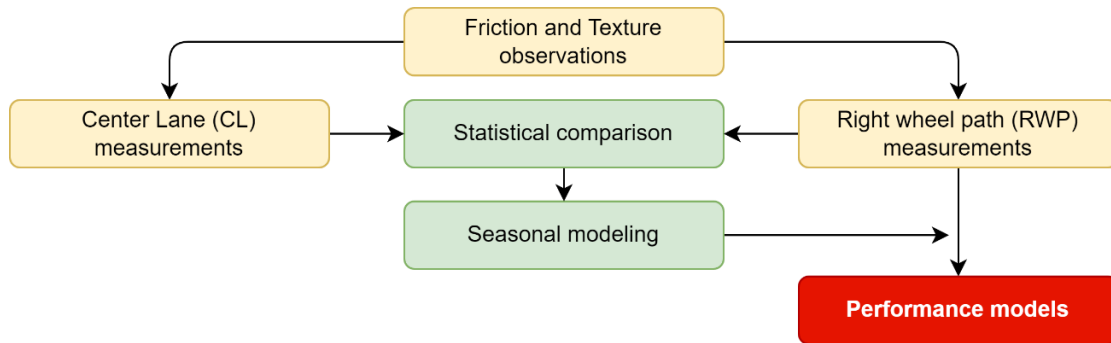


Figure 11. Methodology followed to calibrate the performance models.

3.3.1. Modeling Seasonality

The functional form shown in Equation (12) was used to describe seasonality. This model was calibrated in the FHWA/NC 2020-11 using CL measurements and is updated here by including new observations. For the model calibration, only observations from sites with at least three measurements after the overlay were included, i.e., a total of 33 sites.

$$SF = \frac{Obs_{Seasonal}}{Obs_{Mean}} = a_0 + a_1 \times \sin\left(\frac{2\pi \times DoY}{365} + a_2\right) + a_3 \times Temp + a_4 \times DD \quad (12)$$

where;

- SF = seasonal factor,
- $Obs_{seasonal}$ = observed value at any given day of the year,
- Obs_{Mean} = mean value of friction or texture without seasonal effect,
- a_0 to a_4 = coefficients to be calibrated,
- DoY = Julian calendar days,
- $Temp$ = average 7-day mean temperature, Celsius degrees, and
- DD = number of dry days.

3.3.2. Friction Performance

Based on the finding of the FHWA/NC 2020-11 and the research presented by Goenaga et al. (28), the functional form of the friction performance model is given in Equation (13). This model uses cumulative traffic (T) as the independent variable and has two parts, the first part describes the early friction evolution when $T \leq T_{max}$ and the long-term performance when $T > T_{max}$. The traffic repetitions required to reach the maximum friction (F_{max}) is estimated from the Phase-1 functional form shown in Equation (14). The details on the selection of the functional form and the calibration process to obtain the model coefficients are provided in Appendix G.

$$FN(T) = \begin{cases} (a + \Delta a_{site}) + (b + \Delta b_{site}) \cdot T + c \cdot T^2 & \rightarrow T \leq T_{max} \\ (A + \Delta A_{site}) \cdot \exp[(B + \Delta b_{family}) \cdot T] & \rightarrow T > T_{max} \end{cases} \quad (13)$$

where;

- a = fixed effect of Phase-1 *Friction* intercept,
- Δa_{site} = random effect of Phase-1 *Friction* intercept, one value per site,
- b = fixed effect of Phase-1 *Friction* rate of change,
- Δb_{site} = random effect of Phase-1 *Friction* rate of change, one value per site,
- c = fixed effect of the second order curvature,
- A = fixed effect of Phase-2 *Friction* intercept,
- ΔA_{site} = random effect of Phase-2 *Friction* intercept, one value per site,
- B = fixed effect of Phase-2 *Friction* rate of change,
- ΔB_{family} = random effect of Phase-2 *Friction* rate of change, one value per family, and
- T = cumulative traffic.

$$T_{max} = \frac{-b + \Delta b_{site}}{2c} \quad (14)$$

3.3.3. Texture Performance

Similarly, based on the finding of the FHWA/NC 2020-11 and the research presented by Goenaga et al. (28), the proposed texture performance model is shown in Equation (15). The main update from the model proposed in the previous research effort is the inclusion of the random effects terms and the use of traffic instead of time as the independent variable.

$$MPD = (a + \Delta a_{site}) \cdot T^{(b + \Delta b_{family})} \quad (15)$$

where;

- a = fixed effect of *MPD* intercept,
- Δa_{site} = random effect of *MPD* intercept, one value per site,
- T = cumulative traffic,
- b = fixed effect of the *MPD* rate of change, and
- Δb_{family} = random effect of *MPD* rate of change, one value per family.

3.4. Results

The statistical comparison indicated that overall, the friction values recorded in the CL were statistically different than those collected in the RWP. The analysis showed that CL values were higher than the RWP values in 70% of the 251 comparisons evaluated. For texture, the statistical comparison suggested the *MPD* measured in the CL is statistically different than the value

recorded in the RWP. However, there was no qualitative or statistical evidence suggesting the *MPD* observations from the RWP are lower than the CL.

3.4.1. Friction Performance

As a result of the statistical comparison, Equation (12) was only calibrated for friction. The proposed model is presented in Equation (16). Appendix G provides details on the model calibration and verification process.

$$\frac{Friction_{Seasonal}}{Friction_{Mean}} = 1.10 - 0.028 \times \sin\left(\frac{2\pi \times DoY}{365} + 1.59\right) - 0.0065 \times Temp - 0.0002 \times DD \quad (16)$$

This seasonal model was first used to remove the seasonal effect from the RWP observations and then these corrected values were used to calibrate Equation (13) using the MATLAB ‘fitglm’ function. The statistical analysis of the model coefficients of the two phases of Equation (13) are presented in Appendix G. It is noted that neither the random effect term nor the fixed effect term used to represent the exponential decay was statistically significant. Nevertheless, the form shown in Equation (13) was retained for this model because it is the most widely used expression in literature. The final form of the model is shown in Equation (17).

$$FN(T) = \begin{cases} (0.54 + \Delta a_{site}) + (0.0051 + \Delta b_{site}) \cdot T - 7.3 \times 10^{-5} \cdot T^2 \rightarrow \left[T \leq \frac{-0.0051 + \Delta b_{site}}{-14.6 \times 10^{-5}} \right] \\ (-0.44 + \Delta A_{site}) \cdot \exp[-3.7 \times 10^{-4} \cdot T] \rightarrow \left[T > \frac{-0.0051 + \Delta b_{site}}{-14.6 \times 10^{-5}} \right] \end{cases} \quad (17)$$

Model Predictions

Two sites are used as examples to illustrate the process of making predictions with Equation (17), Site 4.1 shown in Figure 12 (a) and Site 14 shown in Figure 12 (b). In both graphs, the friction observations are represented by the blue dots, the fixed effect model predictions for Phase-1 and Phase-2 are represented by the blue dashed lines and the red dotted lines, respectively. In a random effects model, the fixed effect model describes the average value of the deterioration curve. The average performance curve is obtained using Equation (17) when Δa_{site} , Δb_{site} , and ΔA_{site} are equal to zero. If only the fixed effects are used, the model predictions are close to the observations for Site 4.1 but deviate substantially from the measured data for Site 14. By using Equation (14), with $\Delta b_{site} = 0$, the traffic repetitions needed to reach the maximum friction for Sites 4.1 and 14 is estimated as $T_{max} = 35.1$ million repetitions. The second order polynomial (blue dashed line) and the exponential decay (red dotted line) intersect when $T = T_{max}$.

The random effects in the initial frictions estimated during the calibration process for Sites 4.1 and 14 are $\Delta a_{4.1} = 0.03$ and $\Delta a_{14} = -0.06$. The random effect in the initial deterioration rate is $\Delta b_{4.1} = -2.33 \times 10^{-4}$ and $\Delta b_{14} = 3.38 \times 10^{-4}$ for Site 4.1 and 104, respectively. By substituting these Δb values in Equation (17), the T_{max} is estimated to be 33.5 and 37.4 million traffic repetitions for Sites 4.1 and 14, respectively. The predictions using the random effect terms are represented by the black continuous lines. For the purposes of the threshold analysis presented in Chapter 4 the site specific parameters are known through the model calibration process. However, in the future, it may be useful to also use the models with new sites, for which the site specific parameters are not known. Since it is not directly applicable to the threshold analysis presented later, a detailed explanation of the method to estimate these site specific values is only included in Appendix G.

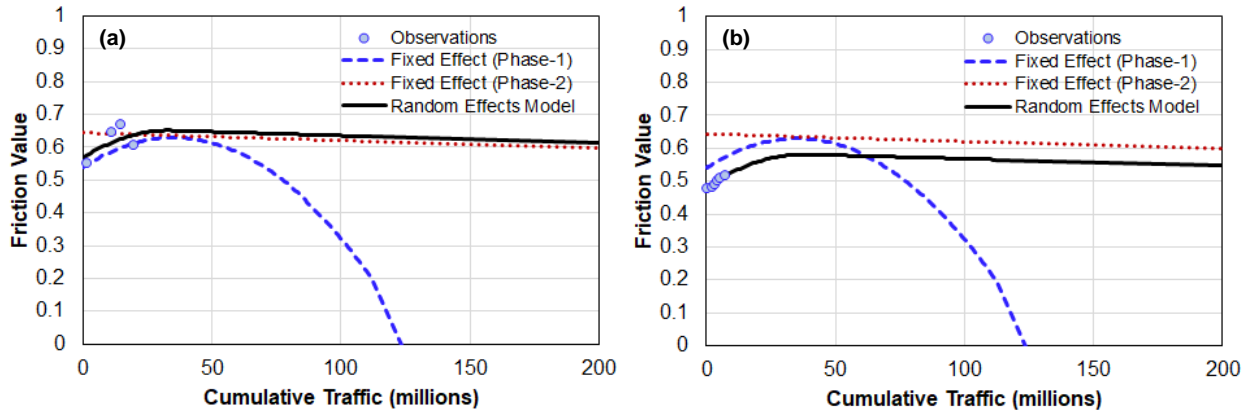


Figure 12. Example of the friction prediction process for: (a) Site 4.1 and (b) Site 14.

Model Verification

Figure 13 shows model verification for individual sites that were used as part of the calibration process. Figure 13 (a) shows the predictions made for a UTBWC site that is less than one year old and Figure 13 (c) shows the predictions made for a UTBWC site greater than 4 years old. Similarly, Figure 13 (b) and Figure 13 (d) show the verifications for dense mixtures at different ages.

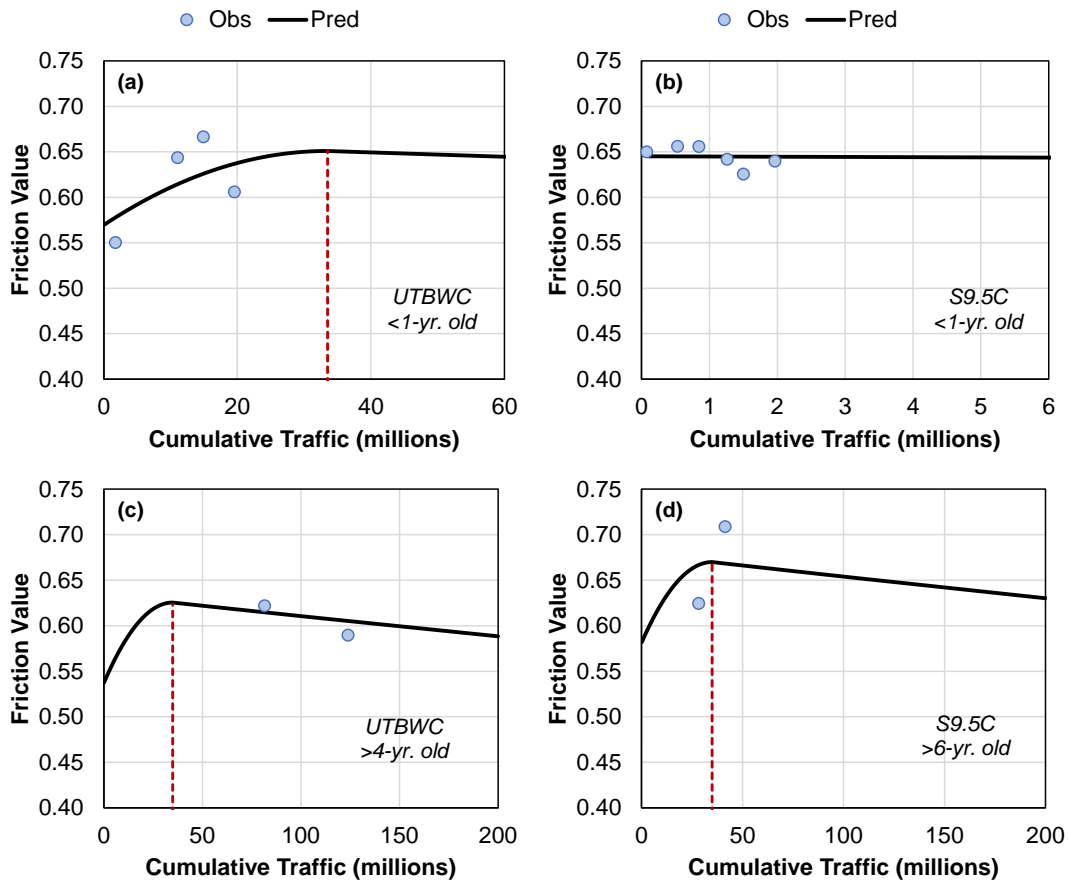


Figure 13. Friction model verification plot for: (a) Site 4.1, (b) Site 8, (c) Site 131, and (d) Site 155.

For both surface types and ages, the model shows a good prediction of friction values. However, as presented in Figure 13, the accuracy of the model reduces for older pavements, like the one in Figure 13 (d). At older ages, the friction deterioration rate tends to deviate from that of the family. As discussed in Appendix G, during Step 3 of the calibration process, most of the pavements with a cumulative traffic higher than T_{max} exhibited a decreasing trend, but a few (mostly the oldest pavements) showed a friction increase.

Model Validation

To validate the model, new observations collected on nine sites that are part of the calibration set were employed to check the prediction of unobserved data using site-specific random effects (see Table 5). The individual coefficients of the friction performance curve for the sites listed in Table 5 were used to predict friction for each of the observations, including the new measurements. Example results are shown in Figure 14.

Table 5. Sites with new observations used for friction model validation.

Site	Surface	Observations Used for Calibration	New Observations
142	S9.5C	A-1, A-2	A-3, A-4, A-5, A-6
146	S9.5D	A-1, A-2	A-3, A-4, A-5
134.1	OGFC	A-1, A-2	A-3, A-4, A-5, A-6
165.4	OGFC	A-1, A-2	A-3, A-4
111.3	UTBWC	A-1, A-2	A-3, A-4, A-5, A-6
5	UTBWC	A-1, A-2, A-3, A-4, A-5	A-6
6	S9.5D	A-1, A-2, A-3, A-4, A-5, A-6, A-7	A-8
18	S9.5C	A-1, A-2, A-3, A-4, A-5, A-6	A-7
33	S9.5C	A-1, A-2, A-3, A-4, A-5, A-6	A-7, A-8, A-9

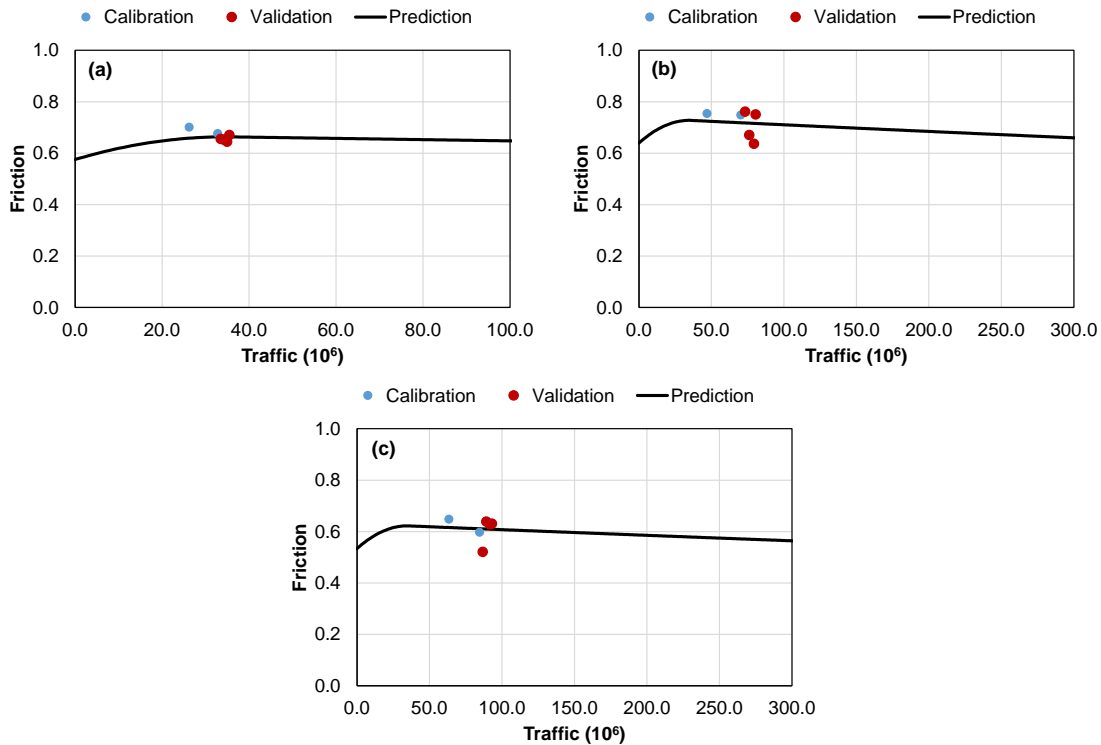


Figure 14. Friction prediction check for: (a) Site 142 (dense mix), (b) Site 134.1 (OGFC), and (c) Site 111.3 (UTBWC).

In these figures, the observations used for calibration are represented by the blue dots, whereas the ones used for validation are shown with red dots. The continuous data series is the model prediction. Table 6 shows a summary of the root mean square errors (RMSE) for the sites listed in Table 5. In general, both the calibration and validation data points are centered on the model prediction and the accuracy of the calibration and validation data sets are comparable as indicated in Table 6. Note that the model was also validated with respect to predictions for completely new sites. This validation was not needed for the threshold analysis, performed in Chapter 4, but does have implications for the use of this model in a PFMP.

Table 6. Summary of the root mean square errors on the friction validation sites.

Site	RMSE	
	Calibration	Validation
142	0.021	0.027
146	0.005	0.024
134.1	0.018	0.045
165.4	0.028	0.074
111.3	0.024	0.068
5	0.064	0.056
6	0.032	0.041
18	0.038	0.011
33	0.051	0.080

3.4.2. Texture Performance

The reader can refer to Appendix G for a detailed description of the calibration process of the texture performance model. The calibrated coefficients in Equation (15) are shown in Table 7. The rate of deterioration random effect coefficients for the six pavement families are shown in Table 8. The final form of the texture performance model is presented in Equation (18).

Table 7. ANOVA table for texture model.

Parameter	Estimate	SE	t-statistic	DF	p-Value	Lower*	Upper*	Std Δa_{site}	Std Δb_{family}
<i>a</i>	-0.74	0.04	-20.6	264	0.0	-0.81	-0.67	0.24	0.06
<i>b</i>	0.13	0.03	4.7	264	0.0	0.08	0.18		

*95% confidence interval

Table 8. Random effect coefficients for the rate of deterioration.

Family	Parameter Δb_{family}	Surface Type	Climate Region
1	-0.070	Dense	Mountains
2	-0.055	Dense	Piedmont
3	-0.029	Dense	Coastal
4	-0.010	HFC	Mountains
5	0.070	HFC	Piedmont
6	0.095	HFC	Coastal

$$MPD(T) = (0.48 + \Delta a_{site}) \cdot T^{(0.13 + \Delta b_{family})} \quad (18)$$

Model predictions

To use Equation (18), it is necessary to have the random effects Δa_{site} and Δb_{family} . These parameters are site-specific and represent the deviation of the initial texture and rate of change from the average values across all sites. Both Δa_{site} and Δb_{family} are estimated during the calibration process for each site; hence, to make predictions for the calibration set it is only necessary to input the

random effect terms and the cumulative traffic into Equation (18). As with the friction model, this model can also be used to predict texture performance over time for completely new sites. In that case the site specific parameter would need to be estimated. Since completely new sites were not used for the threshold analysis, the details and validation of the approach needed for completely new sites are described in detail in Appendix G.

Two examples are presented to illustrate the prediction process. Figure 15 (a) shows Site 4.1 and Figure 15 (b) shows the results for Site 14. Site 4.1 has an UTBWC and belongs to Family 4, whereas Site 14 has a dense surface type and belongs to Family 1. In Figure 15, the predictions made using the fixed effect coefficients only (i.e., setting Δa_{site} and Δb_{family} are equal to zero) are represented by the blue dashed lines. As shown, using the fixed effect alone produces inaccurate predictions.

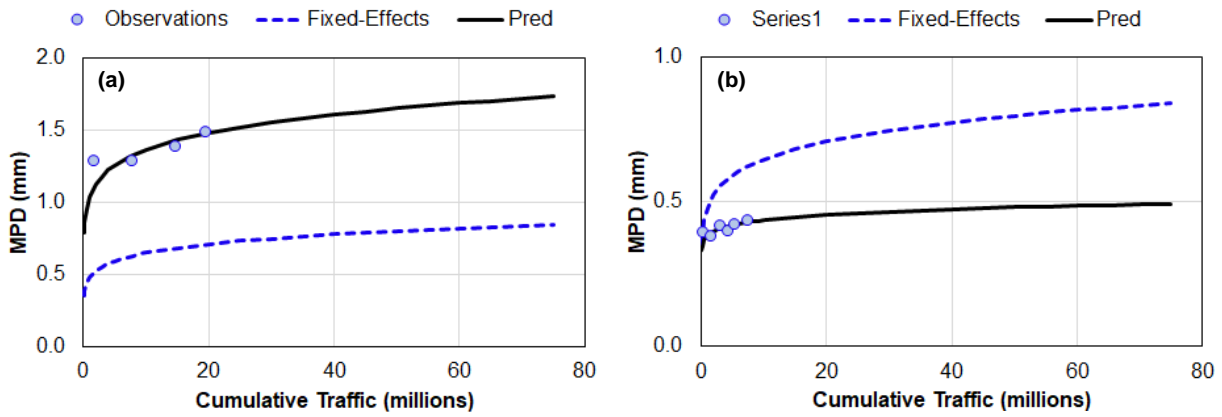


Figure 15. Example of the *MPD* prediction process for: (a) Site 4.1 and (b) Site 14.

The model calibration resulted in $\Delta a_{4.1} = 0.56$ and $\Delta a_{14} = -0.097$ for the intercept of Site 4.1 and Site 14, respectively. Given the family associated with each site, the random effect in the deterioration rate is $\Delta b_{4.1} = -0.010$ and $\Delta b_{14} = -0.070$. Therefore, using these random effect values in Equation (18) the predictions represented by the continuous black lines are obtained. As shown, by including the random effects the model accuracy increases making the predictions to align with the observed data.

Model Verification

Figure 16 shows verification plots for individual sites used in the model calibration. Figure 16 (a) shows the predictions made for a UTBWC site less than 1-year old and Figure 16 (c) depicts the predictions made for a site more than 4-years old. Similarly, Figure 16 (b) and (d) show the verifications for dense mix sites that are 1- and more than 6-years old, respectively. As illustrated, the model has a good prediction capability producing accurate estimations of texture values, for different surface types of different ages.

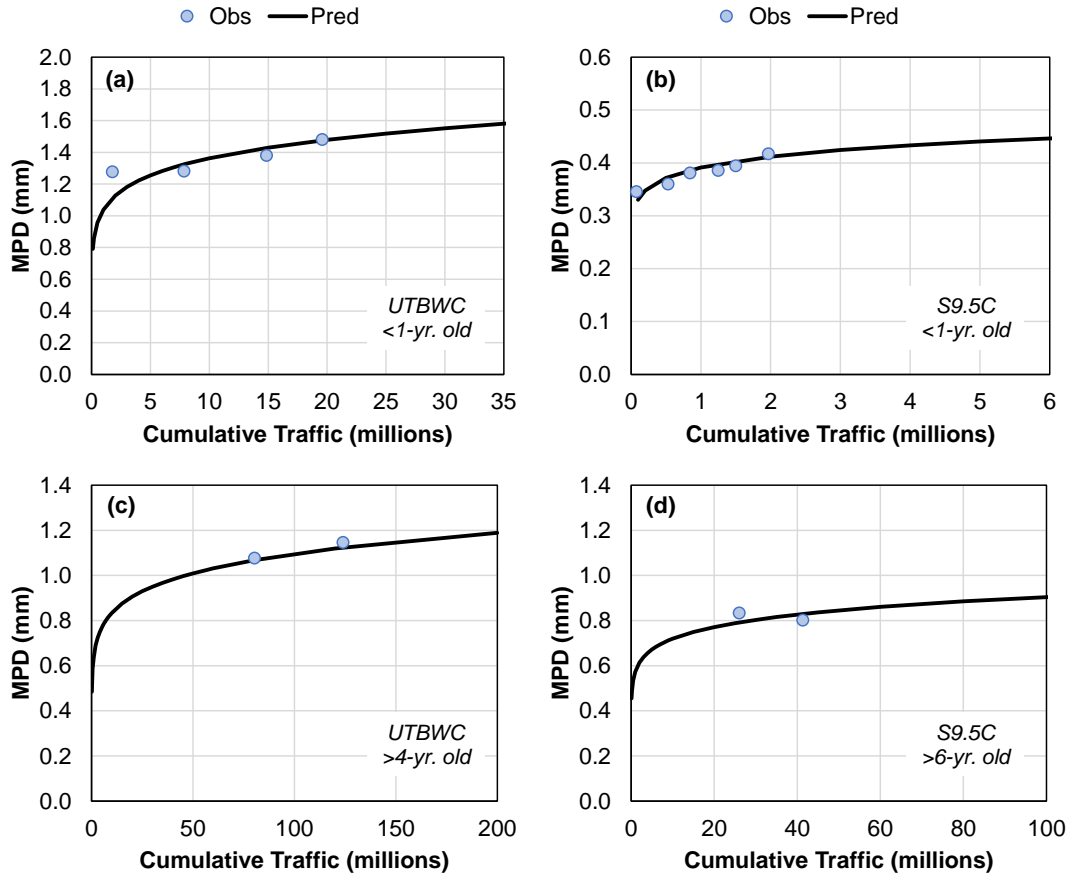


Figure 16. Texture model verification plot for: (a) Site 4.1, (b) Site 8, (c) Site 131, and (d) Site 155.

Model Validation

The procedure used to validate the texture model was the same as the one for friction. The same sites listed in Table 5 were used to validate the texture model. The individual coefficients of the texture performance curves for the sites listed in Table 5 were used to predict *MPD* for each of the observations, including the new measurements. Example results are shown in Figure 17. In these figures, the observations used for calibration are represented by the blue dots, whereas the ones used for validation are shown with red dots. The continuous data series is the model prediction.

Table 9 shows a summary of the root mean square errors (RMSE) for the sites listed in Table 5 and Table G.6. In general, both the calibration and validation data points are centered on the model prediction and the accuracy of the calibration and validation data sets are comparable as indicated in Table 9. Note that the model was also validated with respect to predictions for completely new sites. This application was not needed for the threshold analysis, performed in Chapter 4, but does have implications for the use of this model in a PFMP.

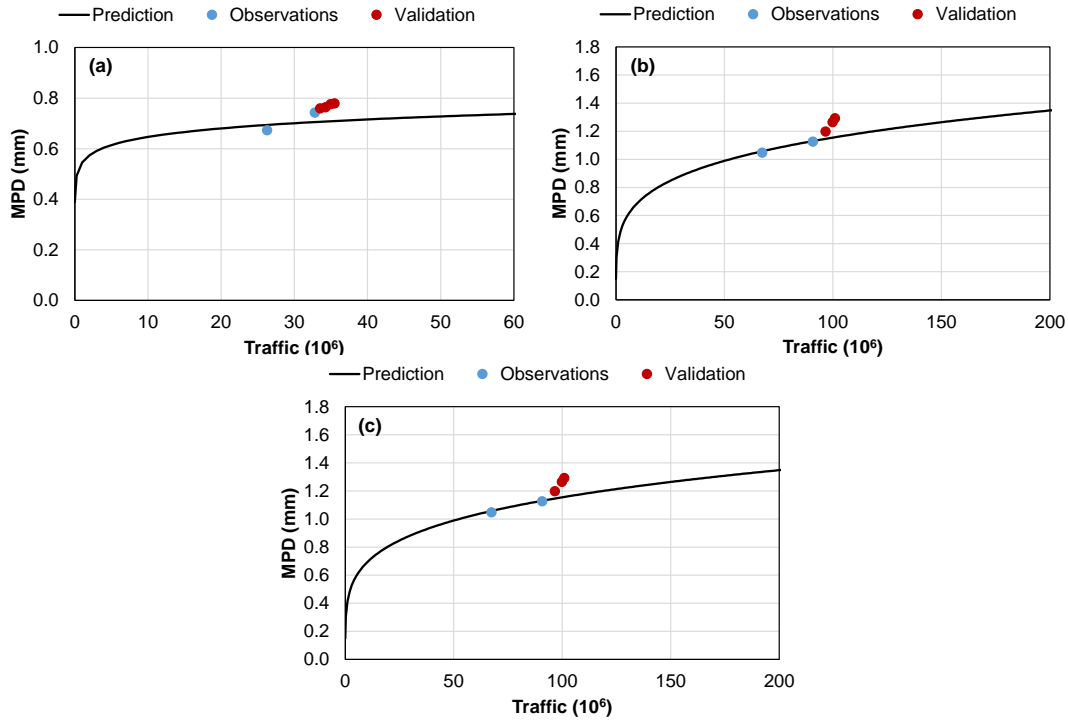


Figure 17. MPD prediction check for: (a) Site 142 (dense mix), (b) Site 134.1 (OGFC), and Site 111.3 (UTBWC).

Table 9. Summary of the root mean square errors on the MPD validation sites.

Site	RMSE	
	Calibration	Validation
142	0.030	0.062
146	0.031	0.039
134.1	0.007	0.106
165.4	0.083	0.132
111.3	0.021	0.067
5	0.101	0.067
6	0.035	0.094
18	0.027	0.057
33	0.038	0.002

3.5. Summary

To model friction and texture performance, a model structure that includes random effects was used. The main results were:

- Pavement families were defined as the combination of surface type and climate region. Two surface types were considered; dense and HFC, which is the combination of UTBWC and OGFC surfaces. Three climate regions were defined, coastal, piedmont, and mountains.
- The model validation showed that the proposed performance models can capture individual deterioration trends. The random effect in the intercept seems to capture the majority of the deterioration trend at each site; but, as shown in the validation procedure in some sites the rate of deterioration may deviate from that of the family. As a solution, when more

observations per site become available it might be possible to incorporate a site-specific deterioration rate.

- The models indicated that the *MPD* has different deterioration rates per family, with the lowest variation observed in dense mixes in the mountains, and the highest variation is associated with HFCs in the coast. For friction, the model indicated the same deterioration rate should be used across families.
- Texture performance models have higher accuracy than friction models. This is attributed to the more stable variation in *MPD* among the successive measurements, whereas friction is more susceptible to seasonal variability due to temperature changes and precipitation.
- Friction decreases due to cumulative effect of traffic repetitions that cause aggregate polishing after an initial phase where friction may increase. It is possible that friction increases due to a moderate to severe raveling process. More research is needed to identify the role of raveling in the friction and texture performance. If raveling occurs, new aggregate faces will be exposed increasing the microtexture friction component.

4. DEFINITION AND EVALUATION OF FRICTION AND TEXTURE THRESHOLDS

4.1. Overview

This chapter evaluates the relationships between crash rates and both friction and texture. This chapter is supported by the findings presented in Chapter 3, Appendix G, and Appendix H. Friction and texture observations have been contrasted against the crash history of Group-1 and Group-2 sites, detailed in Table 1 and Table 2 of Chapter 2. For this analysis, each site has been categorized depending on its geometry, which is used to set the basis for defining friction demand categories. The friction and texture observations used in this chapter were the ones collected by KPR engineering on the dates specified in Appendix D.

Afterwards, friction and texture measurements on the sections that belong to the same demand category were processed according to the methodology discussed in Chapter 2. Finally, crash records were associated with each friction and texture measurement following the method discussed in Appendix H. These records were combined with the information on traffic volumes to compute representative crash rates. Also, to increase the dataset available to calibrate the models, random effect models for friction and texture performance were used to back-cast both indices to gain additional values to compare to the available crash records.

The literature that supports the methodology proposed here is presented in Appendix A. The chapter is organized as follows; first, friction demand categories are presented, then the methods followed to establish and evaluate a set of candidate friction and texture threshold are presented. The chapter ends with the results and conclusions derived from the analysis.

4.2. Methodology

The general methodology to determine investigatory friction and texture thresholds starts by characterizing friction and texture at a network level. A discussion of this process for the North Carolina highway network is presented in Chapter 2. The second step consists of identifying the safety measure that will be compared to friction and texture. The third step focuses on characterizing friction and texture performance. The elements of the friction and texture performance models are fully described in Chapter 3. The last step evaluates the primary economic factors of setting an investigatory threshold at a network level.

4.2.1. Establishing Friction-Texture Demand Categories for North Carolina

The total mileage available for analysis is summarized in Table 10. As shown, most of the data was collected on interstates and freeways, with a small fraction on arterials. In terms of speed, most of the sites are high-speed facilities with speed limits greater than or equal to 55-mph. For a few sites, measurements were collected at 35 and 45-mph but none were acquired at 50-mph. The observations from Group-1 and Group-2 sites were combined to obtain a first approximation to the effect of skid resistance on highway safety.

As indicated in Chapter 2, Section 2.6.2, the ArcMap ROCA toolbox was used to identify curves at a network level. For the threshold determination, a filter was applied to remove sites that met one or more of three criteria; 1) sites that were rehabilitated during the period of analysis, 2) sites with a PCC surface, or 3) sites where the crash record was not available during the analysis period. Finally, based on the reliability of the geolocation records of the crash dataset, the NCDOT highway safety unit recommended to use evaluation lengths greater than 0.3 miles. Hence, the total number of miles shown in Table 10 reduced from 731.3 miles to 507.1 miles.

Table 10. Distribution of site mileage by speed limit and road functional class.

Speed Limit	Functional Class					Total
	Interstate	Freeways	Principal Arterials	Minor Arterials	Major Collector	
35	5.6	0.1	1.0	0.0	0.2	6.9
45	0.0	0.0	5.6	0.0	0.0	5.6
50	0.0	0.0	0.0	0.0	0.0	0.0
55	12.1	27.8	45.3	9.9	5.1	100.2
60	20.4	21.6	8.2	0.0	0.0	50.1
65	150.7	82.8	0.0	0.0	0.0	233.5
70	190.3	131.8	12.8	0.0	0.0	335.0
Total	379.1	264.1	72.9	10.0	5.2	731.3

Consequently, friction demand was defined based on the road geometry (curves vs. tangents) and presence of interchanges. Based on this categorization, four groups were defined as illustrated in Figure 18:

- Category 1: All demands combined (without any friction demand consideration),
- Category 2: Tangents,
- Category 3: Curves, and
- Category 4: Interchanges

It must be noted that these categories are not mutually exclusive, e.g., when one evaluates the tangent geometry, it includes some portion of the segment in the interchange area of influence. Similar effects may occur with the curves. By defining the friction demand categories in this way, it was possible to reduce the number of road segments shorter than 0.3 miles. After the demand categorization, the geometry of the sites was intersected with the milepost extension of the crash dataset to get accurate estimates of the crash rate at the sites. The total number of miles per friction demand category available for the threshold definition is summarized in Figure 19.

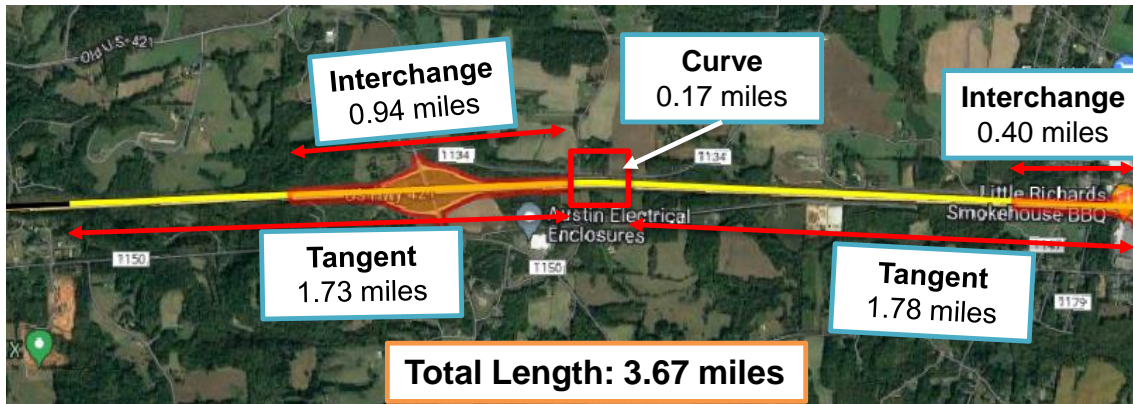


Figure 18. Example of the friction demand category definition.

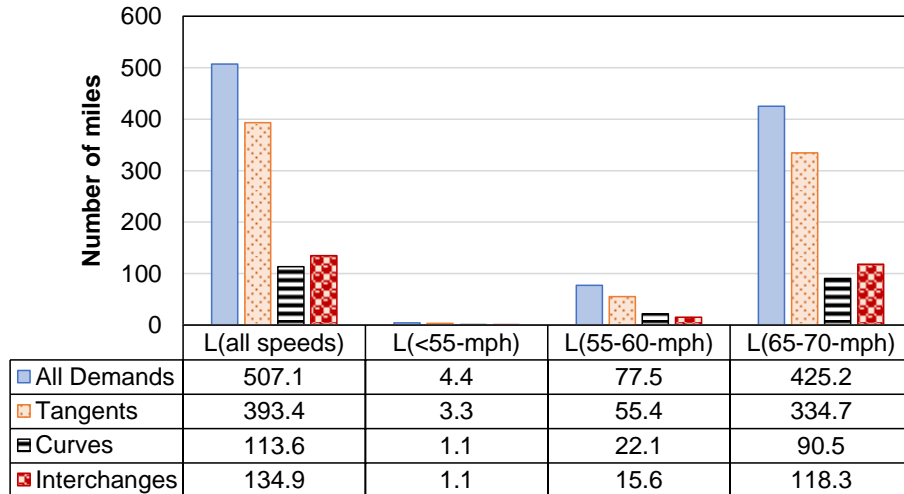


Figure 19. Total number of miles with friction and texture observations on each friction demand category.

4.2.2. Representative Friction and Texture Values

Friction and texture measurements on each site were aligned on the segments resulting from the friction demand categorization. Crash records are reported for both traffic directions; however, in the database these crashes are mile-posted using only the inventory direction. Hence, to keep consistency, for those sites where friction/texture were measured in both traffic directions the measurements were combined as if they were a single dataset using the milepost information. Afterwards, the friction and texture records that were organized in the inventory direction were assigned to each homogeneous segment and the representative friction and texture values on each segment was set as the 10th percentile and the 50th percentile of the continuous observations, respectively. Chapter 2 and Appendix E provide additional details.

To increase the sample size available for analysis, the performance models derived in Chapter 3 were used to back-cast friction and texture for the Group-2 sites. A back-casted value for a given site is a prediction made using the friction or texture performance models for a cumulative traffic value lower than the cumulative traffic at the first friction or texture measurement. For this group, the crash record dates from January 2010 to April 2023 were available, so depending on the first testing date some sites obtained one to up to three back-casted values. For these sites the first friction/texture observation was collected in 2020, the total traffic repetitions accumulated until the date friction/texture were recorded is denoted as T_{meas} in Figure 20, and this traffic value was used as the starting point for the back-calculation.

Based on the finding of the analysis conducted in Appendix H, the back-calculation is made in periods of 13-months, i.e., the traffic accumulated during the 13-month (ΔT) window before T_{meas} is subtracted from T_{meas} . For texture, the resulting traffic ($T_{meas} - \Delta T$) value is replaced in Equation (18) to predict the *MPD*. For friction, if the $T_{meas} - \Delta T$ value is higher than T_{max} , the second part of Equation (17) is used to make the prediction, otherwise the second order polynomial is used to make the prediction. This process is repeated sequentially as long as the 13-month period does not overlap with the overlay period, in other words as long as the difference $T_{meas} - \Delta T$ do not include part of the overlay period. The overlay period is defined as a 13-month window centered around the overlay date included in Appendix D. The total number of miles available for the threshold

definition, after combining the observed friction and texture with the back-casted values, is depicted in Figure 21.

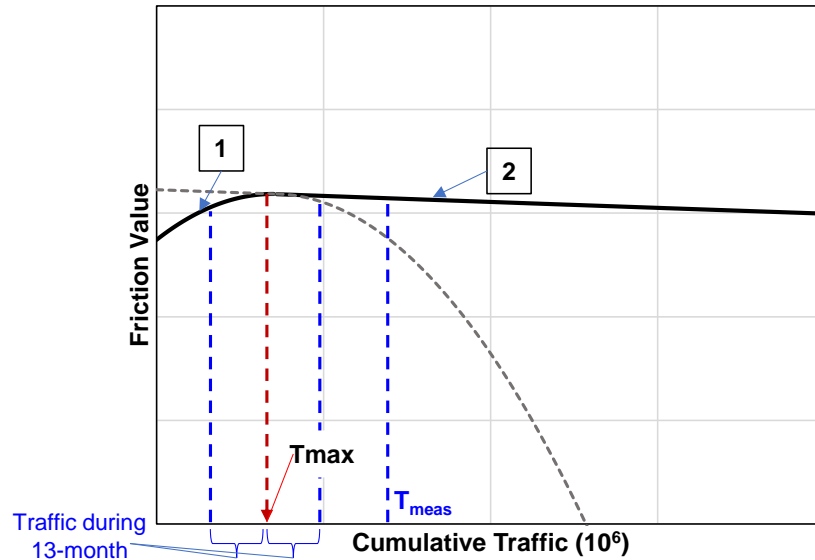


Figure 20. Back-cast prediction process.

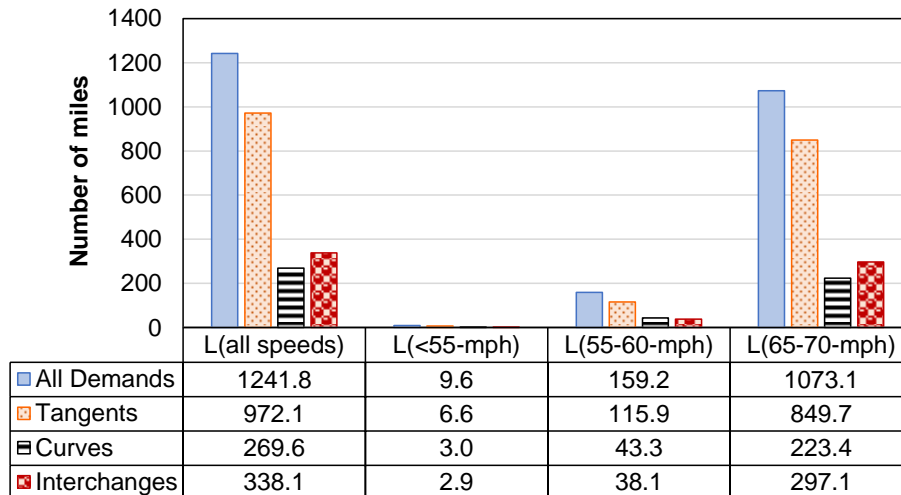


Figure 21. Total number of miles available for threshold determination after combining the observed friction and texture with the back-casted values.

4.2.3. Crash Rates Estimation Procedure

To calculate the crash rates used for threshold analysis, segments (both measured and back-casted) were first grouped by their friction and texture values. The bin width used for these grouping was set based on the method from Li et al. (27), i.e., the bin width was selected as that a minimum of 1-mile of friction/texture data was included in each bin. As a result, the probability density function of friction and texture data used bin widths of 0.05 units for the friction histogram and 0.20-mm for the *MPD* histogram. For each bin, a representative crash rate was calculated by combining the total crashes, cumulative traffic, and total length of segments in that bin. These values were obtained by analysis period, which was 13-months long and centered around either a measurement

or back-casted friction/texture value. The rationale and justification for choosing a 13-month analysis window is provided in Appendix H.

Once the segments were in their respective bin, each was reviewed to make sure that the analysis window did not coincide with the month the overlay was recorded as being placed (see Table D.1 and Table D.2), the six-months preceding the overlay month, or the six-months after the overlay month. This 13-month timeframe centered around the overlay month was referred to as the ‘overlay’ period. Data during this period is omitted from crash rate estimation because it is believed that work zone activities and other uncertainties in the construction process might affect crash numbers.

Once grouped and reviewed for the overlay period, the number of collisions and the number of vehicle-miles traveled were totaled for each bin. The expressions used to compute the crash rate are provided in Equation (19) to (21).

$$R_B = \sum_{i=1}^{n=M_B} \left(\frac{N_i}{VMT_i} \right) \times 10^8 \quad (19)$$

$$VMT_i = \sum_{j=1}^{13} MADT_{ij} \times 30 \times L_i \quad (20)$$

$$N_i = \sum_{j=1}^{13} \#Crashes_j \quad (21)$$

where;

- R_B = crash rate on bin B , in 100 million vehicle-miles traveled,
- VMT_i = vehicle-miles traveled on Site i in a 13-month period,
- N_i = number of lane departure wet crashes in a 13-month period on Site i ,
- $\#Crashes_j$ = number of lane departure wet crashes on Site i in month j ,
- $MADT_{ij}$ = monthly average daily traffic on Site i in month j , and
- L_i = length of the site i , in miles.

The unit of the crash rate computed, either for an individual site or for a given friction/texture bin, is 100-million crashes per million vehicle-miles traveled in a 13-month period, shortened as 100-Mvmt₁₃.

4.2.4. Estimating the Investigatory and Intervention Thresholds

Two analyses were conducted to estimate the investigatory and intervention threshold values. First, Method 3 of the Guide for Pavement Friction (GPF) was applied. By using this method, individual friction and texture thresholds could be estimated. Next, the combined effect of friction and texture was analyzed using a sequential Logit model. For both analyses, the demand categories and the observed and back-casted friction values were used, as indicated in Figure 21. Also, although in Figure 21 the available number of miles per friction demand category is segregated further by the speed limit, it is clear that the majority of the dataset was collected in facilities with a speed limit of 65 or 70 mph. For this reason, the effect of the speed limit on the investigatory thresholds will be evaluated only for Category 1, i.e., all demand combined. For both methods, the same nomenclature is used as summarized in Table 11.

Table 11. Nomenclature used for the proposed thresholds.

Abbreviation	Meaning
FN_{INV}	Investigatory friction threshold
FN_{INT}	Intervention friction threshold
MPD_{INV}	Investigatory MPD threshold
MPD_{INT}	Intervention MPD threshold

Analysis 1: GPF Method 3

Using the procedure described in the previous two sections, friction and texture histograms and their associated crash rates were obtained for each friction demand category. The thresholds were defined based on visual inspection to determine the inflection point where crash rates start increasing rapidly. The different elements involved in the analysis are depicted in Figure 22. In this schematic, the vertical left axis shows the histogram frequency, the horizontal axis shows the mid-point of the histogram bins, the vertical right axis depicts the lane departure wet (LD-Wet) crash rate associated with each histogram bin. As mentioned above, a LD-Wet crash rate is estimated using Equation (19) for each histogram bin. These estimated values are represented by the continuous orange line. A power model fitted to the crash rates computed on the histogram bins is calibrated as indicated in Equation (22). This model is represented with the tick dashed black line. Finally, the thin dashed black lines represent the two slopes computed as described above.

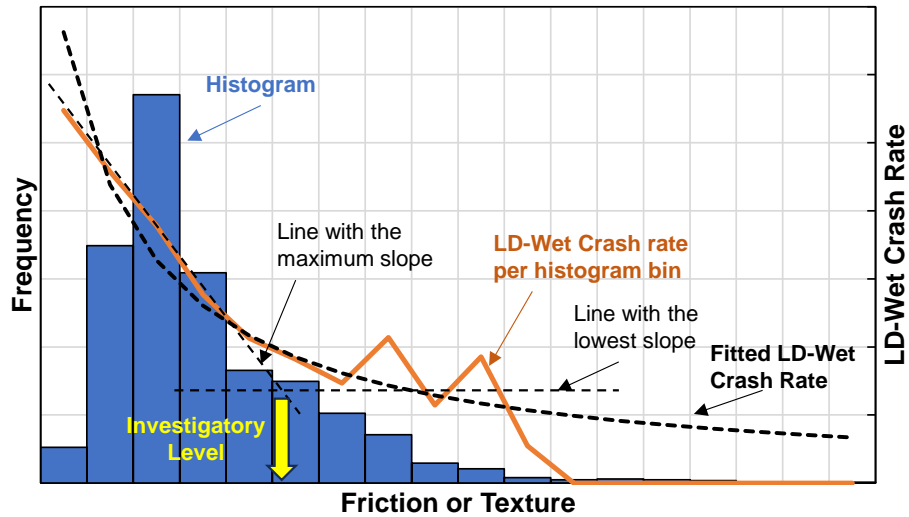


Figure 22. Graphical representation of the elements for GPF Method 3.

$$R_k = a \cdot X^b \quad (22)$$

where;

R_k = crash rate of friction/texture histogram bin k ,

X = mid-point friction or texture bin, and

a and b = parameters to be estimated.

As shown in the figure, for the purposes of establishing crash rate functions and calculating slopes, the crash rates were positioned at the mid-point of their respective bin. For example, the crash rate calculated from the sites in the texture bin covering MPD values between 0.4 and 0.6 mm was positioned at MPD equal to 0.5 mm. Also as shown, the maximum slope line was computed using

each pair of consecutive bins to identify the maximum slope. This maximum slope was used to draw a line, through the average of the two crash rates that produced the maximum slope and that delineates the highest crash rate variation. A similar process was implemented using the lowest slope calculated between two consecutive bins, which was used to identify the average crash rate level associated with the lowest variation with respect to either friction or texture, a horizontal line was drawn around this average crash rate. The intersection point of both lines defines the investigatory level. For some friction demand categories there were anomalies in the crash rate profile described in Figure 22. See for example the friction histogram for tangents shown in Figure I.10. In cases like that, engineering judgment was applied to define the line with the maximum slope. Finally, as depicted in Figure 21 the segments with a speed limit lower than 55-mph constitute the smallest sample proportion in the database. Hence, these were combined with the 55-60 mph segments to determine the investigatory threshold. For the all of the friction demand categories, the intervention threshold is set as 75% of the investigatory level, following the practice of FAA (29) and NCHRP-108 GPF (7).

Analysis 2: Sequential Logit

The alternative method used to define skid resistance thresholds is based on the structure of a sequential Logit. The model consists of four nests, as shown in Figure 23, where each nest is a binary model. The options for each nest are the $P(L_k \leq R_k < U_k)$ and $P(R_k \geq U_k)$, where the first element indicates the probability the crash rate (R_k) is greater than or equal to a lower boundary (L_k) but lower than an upper boundary (U_k); the second term is the corresponding complement. The model calibrates all the nested binary models at once. In this sense, if k is the current nest, then the probabilities in nest $k+1$ depends on $P(R_k \geq U_k)$.

For example, in the first nest of Figure 23, the probability of observing a crash rate between 0 and 10 is $P(0 \leq R_k < 10)$, then the probability of observing a crash rate greater than or equal to 30 would be $[1 - P(0 \leq R_k < 10)] \times [1 - P(10 \leq R_k < 30)]$. The limits of each nest, i.e., the crash rates of 10, 30, and 60 100-Mvmt₁₃, were established based on the cumulative distribution of the lane departure wet crash rate. In the same order, these three values represent the 50th, 75th, and 90th percentile of the crash rate, respectively.

In a binomial Logit model, the dependent variable, Y , can take one of two values 0.0 or 1.0, i.e., injury or non-injury, fatal or non-fatal crashes. It is also possible, as is the case here, that Y is defined as a categorical variable, which would indicate whether or not the observed crash rates are between certain values. Assuming $\pi_i = Pr(Y_i = 1)$, the general shape of the binomial logit model is given in Equation (23).

$$Logit(\pi_i) = \log \left[\frac{\pi_i}{1 - \pi_i} \right] = X_i \beta \quad (23)$$

where;

X_i = a vector of explanatory variables, i.e., risk factors, and

β = a vector of regression coefficients.

Based on Equation (23), the odds on each nest are defined as indicated in Equation (24).

$$Logit(\pi_{k,i}) = \log \left[\frac{\pi_{k,i}}{1 - \pi_{k,i}} \right] = \beta_0 + \beta_1 \times Speed_i + \beta_2 \times [MPD_i \cdot Friction_i] \quad (24)$$

where;

- $\pi_{k,i}$ = probability of observing a crash rate for Segment i , $R_{k,i}$, between L_k and U_k ,
- $Speed_i$ = speed limit of Segment i ,
- MPD_i = mean profile depth segment i ,
- $Friction_i$ = friction value representative of Segment i , and
- k = is the number of nests in the model.

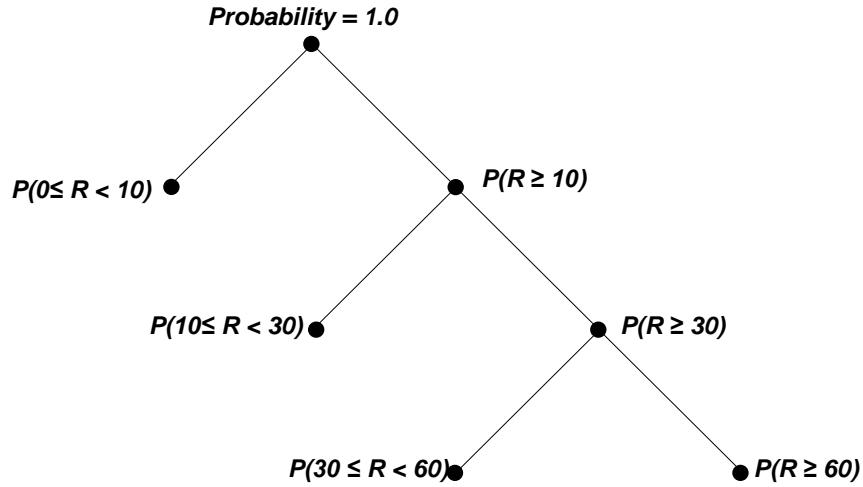


Figure 23. Sequential Logit model structure.

If the probability computed when both friction and texture are equal to their corresponding investigatory levels, FN_{INV} and MPD_{INV} , is taken as the base of comparison, the relative risk of observing a texture/friction value above or below the investigatory level can be estimated using Equation (25). In this sense, the relative risk (RR) concept can be used to evaluate the implications of having one, or both, skid resistance parameters below their corresponding investigatory values. If, an allowable risk ratio is defined, the RR could serve as a tool to refine the definition of the intervention levels.

$$RR(MPD_i, FN_i) = \frac{P(R < R_k | MPD_i, FN_i)}{P(R < R_k | MPD_{INV}, FN_{INV})} \quad (25)$$

where;

- RR = relative risk,
- MPD_i = any given MPD value,
- FN_i = any given friction number,
- MPD_{INV} = investigatory MPD level, and
- FN_{INV} = investigatory FN level.

4.3. Results

The observed and back-casted values are compared against the wet-lane departure crash rate in Figure 24. As shown, there is consistency between the two datasets and no bias is induced. The percentile distribution of the lane departure wet crash rates is included in Table 12. As shown, most of the sites have a lane departure wet crash rate below 30 100-Mvmt₁₃.

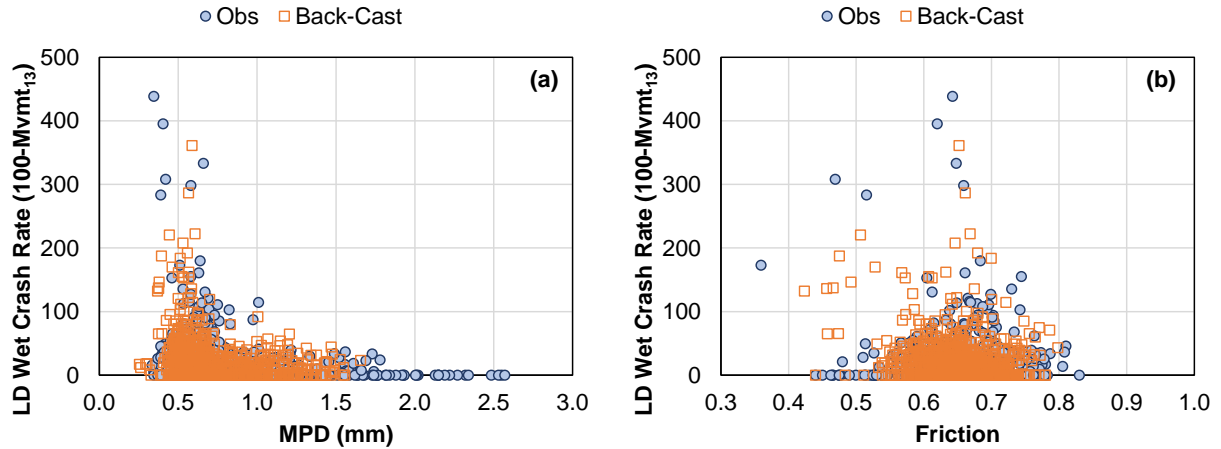


Figure 24. Observations available to determine thresholds for: (a) *MPD* and (b) friction.

Table 12. Lane departure wet crash rate, in 100-Mvmt₁₃, percentile distribution across the different observations.

Observations	Crash Rate (100-Mvmt ₁₃)				
	P ₂₅	P ₅₀	P ₇₅	P ₉₅	Max
All Sites	0	7.9	25.2	69.8	395.5
Raw Obs.	0	5.6	24.0	68.8	395.5
Back-Casted	0	9.4	27.0	72.0	361.1

4.3.1. GPF Method 3

Friction

Sites were grouped by friction demand category and for each category the friction histogram was obtained; then, for each histogram bin crash rate was computed using Equation (19). For example, Figure 25 and Figure 26 shows the friction histogram for all Category-1 segments and only Category-1 segments at 65-70 mph, respectively. Individual plots for each category are included in Appendix I.

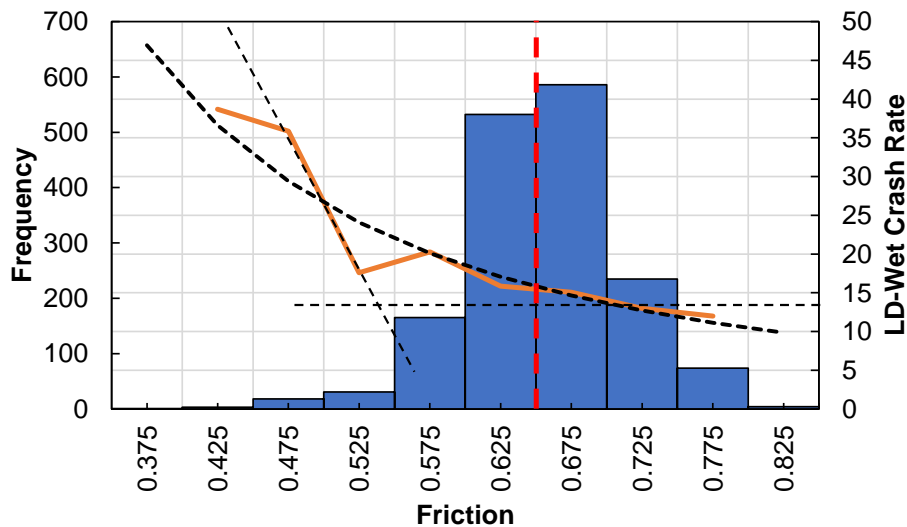


Figure 25. Wet lane departure crash rate variation as a function of Friction for Category-1.

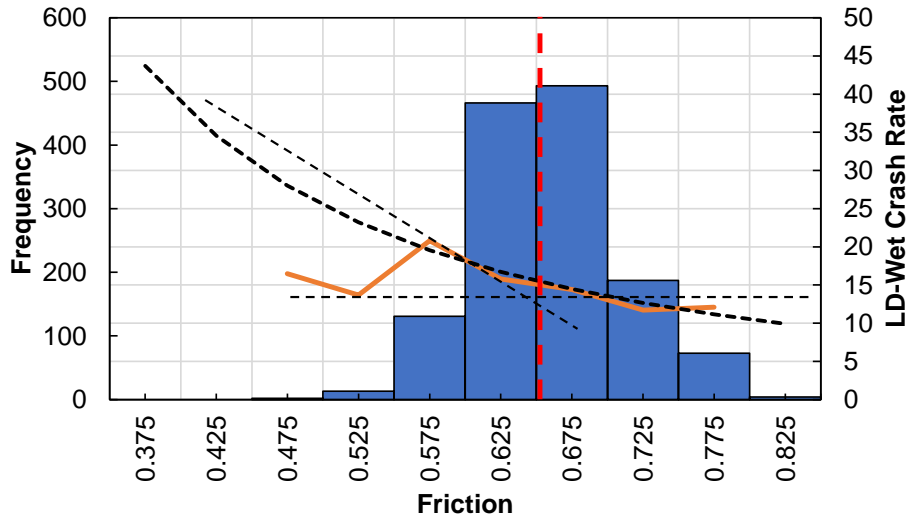


Figure 26. Wet lane departure crash rate variation as a function of Friction for Category-1 at 65-70 mph.

The thresholds were defined using the GPF-Pivot estimation method. Accordingly, the crash rates were inspected to identify the friction value at which crash rates start to increase rapidly. If one conducts a visual inspection of Figure 25 and Figure 26 and looks for the FN_{INV} at which the wet lane departure crash rate starts to increase rapidly, the thresholds for Category-1 and Category-1 at 65-70 mph are 0.53 and 0.62, respectively. By following a similar procedure for all the other friction demand categories, the investigatory friction thresholds are summarized in Table 13. It must be noted that individual thresholds were evaluated for different speed limits, but those were only obtained for Category-1.

Table 13. Investigatory and intervention Friction Thresholds estimated with the GPF-Pivot method.

Parameter	All Combined	Speed Limit		Tangents	Curves	Interchanges
		65-70	55-60			
FN_{INV}	0.53	0.62	0.51	0.57	0.60	0.65
FN_{INT}	0.39	0.45	0.38	0.43	0.45	0.49

Texture

After categorizing the sites based on the friction demand, the texture histogram for each demand category was obtained. As mentioned in the Methodology section, the effect of the speed limit was evaluated only for Category-1. Then, for each bin in the histogram the wet lane departure crash rate was computed using Equation (19). Examples of such plots are presented in Figure 27 and Figure 28, for Category-1 (all demand combined) and for Category-1 segments at 65-75 mph, respectively. In both figures, the red line represents the mean MPD of all segments. Individual plots for each category are included in Appendix I. The elements shown in Figure 27 and Figure 28 are described in Figure 22.

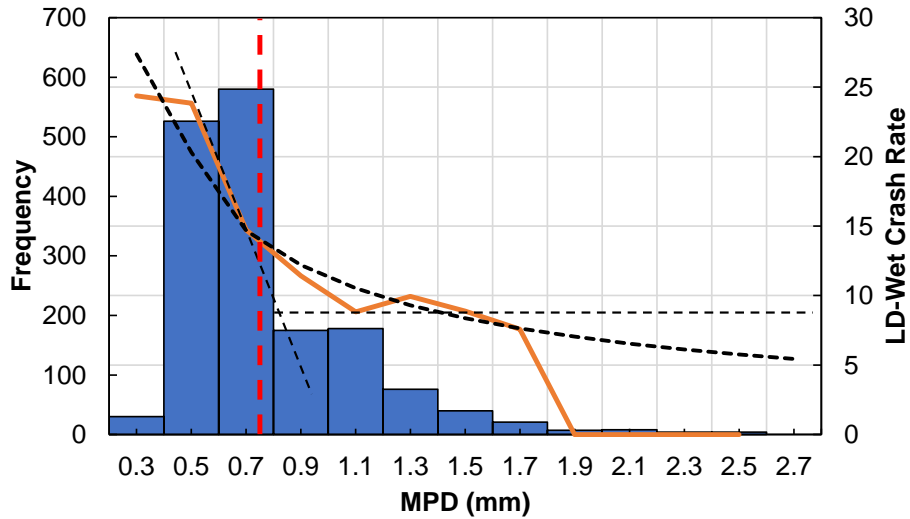


Figure 27. Wet lane departure crash rate variation as a function of MPD for Category-1.

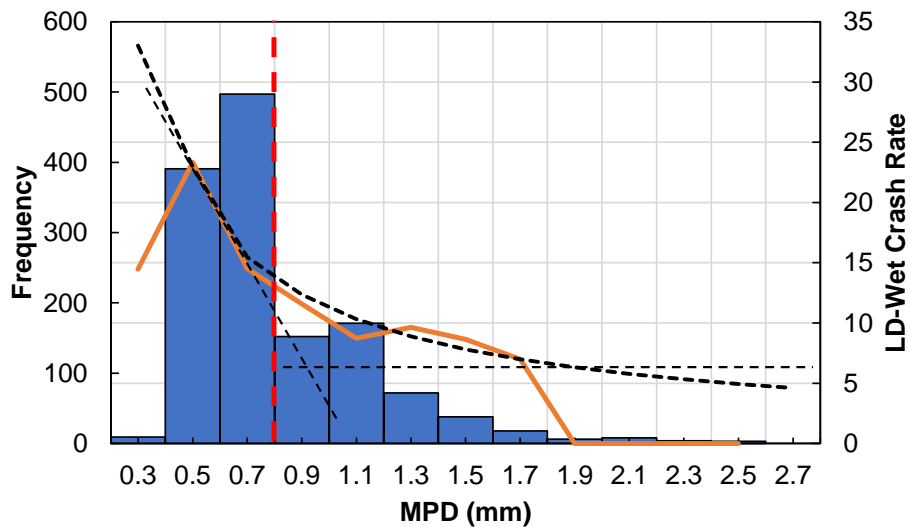


Figure 28. Wet lane departure crash rate variation as a function of MPD for Category-1 using only segments with a speed limit of 65-70 mph.

Two distinct regions are observed in Figure 27 and Figure 28. One region (MPD above approximately 1 mm) where crash rates are mostly constant and then a second region (MPD at or below 1 mm) where crash rates seem to be increasing linearly. Based on the analytical process described in Section 4.2.4, the data in Figure 27 and Figure 28 is found to yield a MPD_{INV} values of 0.8 mm and 0.9 mm, respectively. After following a similar procedure for the other friction demand categories, the MPD_{INV} summarized in Table 14 are found. It must be noted that individual thresholds were evaluated for different speed limits, but those were only obtained for Category-1.

Table 14. Investigatory and intervention *MPD* thresholds estimated with the GPF-Pivot method.

Parameter	All Combined	Speed Limit		Tangents	Curves	Interchanges
		65-70	55-60			
<i>MPD_{INV}</i>	0.80	0.90	0.67	0.76	0.88	0.90
<i>MPD_{INT}</i>	0.60	0.68	0.50	0.57	0.66	0.68

4.3.2. Sequential Logit Regression

To calibrate Equation, (24) both the ‘raw’ observations and the back-casted values were used as if they were a single database. To calibrate the model, the MATLAB ‘mnrfit’ function was used. The resulting coefficients are summarized in Table 15. These coefficients define the odd-ratio on each nest as indicated in Equation (26) to (28).

Table 15. Coefficients of the sequential Logit model.

Parameter	Crash Rate Nests		
	π_1	π_2	π_3
β_0	-0.69 ¹	-1.22 ¹	-1.09 ²
β_1	-0.16 ¹	0.14 ²	0.25 ²
β_2	2.68 ¹	2.05 ¹	2.43 ²

¹Significant at a 95% confidence level; ²significant at a 90% confidence level.

$$\pi_1 = \frac{P(0 \leq R < 10)}{P(R \geq 10)} = \text{Exp}(\beta_0 + \beta_1 \times \text{Speed}_i + \beta_2 \times [\text{MPD}_i \cdot \text{Friction}_i]) \quad (26)$$

$$\pi_2 = \frac{P(10 \leq R < 30)}{P(R \geq 30)} = \text{Exp}(\beta_0 + \beta_1 \times \text{Speed}_i + \beta_2 \times [\text{MPD}_i \cdot \text{Friction}_i]) \quad (27)$$

$$\pi_3 = \frac{P(30 \leq R < 60)}{P(R \geq 60)} = \text{Exp}(\beta_0 + \beta_1 \times \text{Speed}_i + \beta_2 \times [\text{MPD}_i \cdot \text{Friction}_i]) \quad (28)$$

For each nest, the total probability must add to 1.0, i.e., Equation (29) must be satisfied. Hence, individual probabilities can be solved on each nest. For example, the odd ratio for first nest is defined in Equation (30). Solving for $P(0 \leq R < 10)$ in Equation (29) results in the expression shown in Equation (31), then $P(R \geq 10)$ is equal to $[1 - P(0 \leq R < 10)]$.

$$P(L_k \leq R_k < U_k) + P(R_k \geq U_k) = 1 \quad (29)$$

$$\frac{P(0 \leq R < 10)}{P(R \geq 10)} = \text{Exp}(-0.69 - 0.16 \times \text{Speed}_i + 2.68 \times [\text{MPD}_i \cdot \text{Friction}_i]) \quad (30)$$

$$P(0 \leq R < 10) = \frac{1}{1 + 1/\text{Exp}(-0.69 - 0.16 \times \text{Speed}_i + 2.68 \times [\text{MPD}_i \cdot \text{Friction}_i])} \quad (31)$$

Consequently, one can compute the probabilities in the following nests by assuming the events are mutually exclusive and independent. By doing so, the $P(10 \leq R < 30)$ is defined as shown in Equation (32).

$$P(10 \leq R < 30) = P(R \geq 10) \times \left[\frac{1}{1 + 1/\text{Exp}(-1.22 + 0.14 \times \text{Speed}_i + 2.05 \times [\text{MPD}_i \cdot \text{Friction}_i])} \right] \quad (32)$$

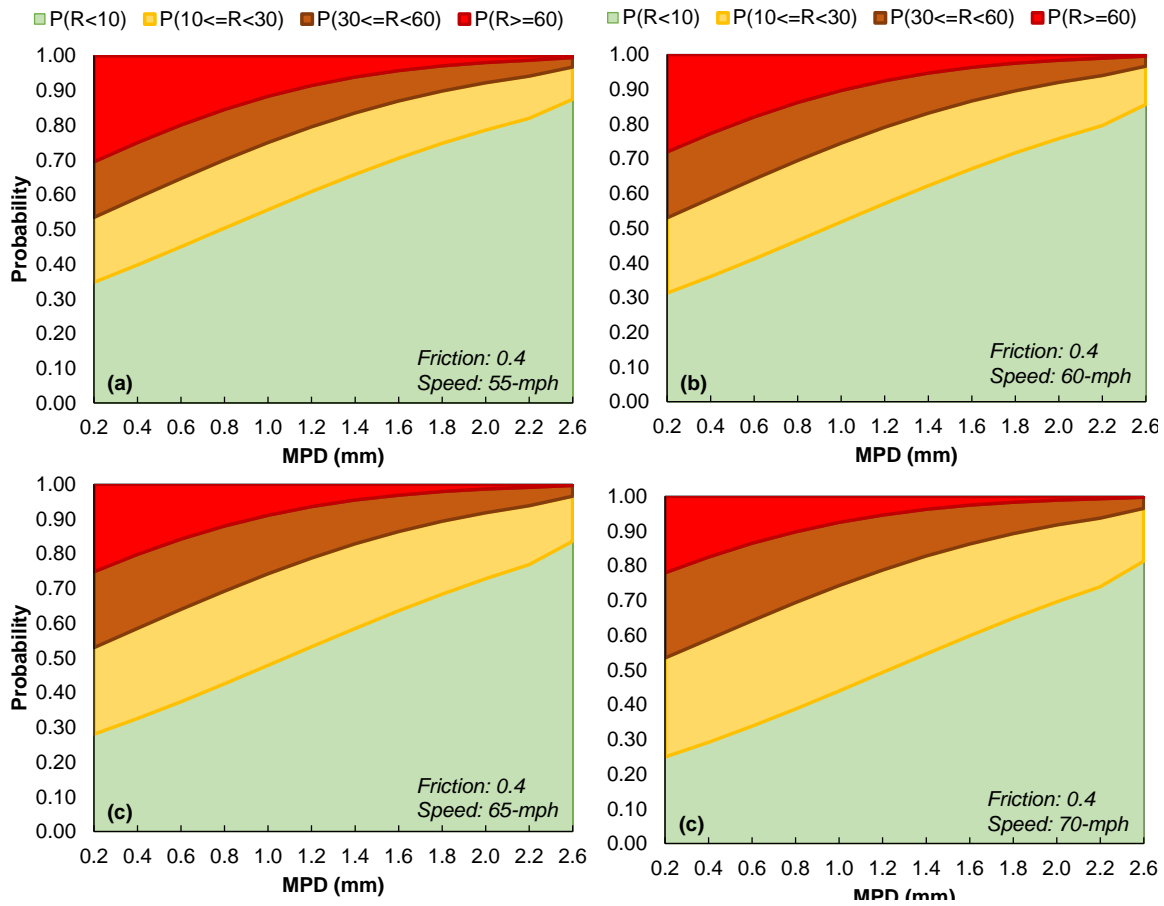


Figure 29. Probability $P(L_k \leq R_k < U_k)$ as a function of texture and a fixed friction of 0.4, for Category-1 at: (a) 55-mph, (b) 60-mph, (c) 65-mph, and (d) 70-mph.

After doing so, one can observe how the probability of being at a given crash rate level varies as a function of different values of the predictors. An example of such variation is depicted in Figure 29, where the model was used to evaluate the effect of MPD and speed limit, at a fixed friction of 0.4, on the four crash rates levels. As shown in the figure, the probability of observing the highest crash rate levels increases when MPD decreases and the speed limit increases.

For example, if the MPD is set equal to 1-mm in all four plots in Figure 29, then the $P(R < 10)$ is 56, 52, 48, and 44% for each speed limit evaluated. While the $P(R < 60)$ is 88, 90, 91, 93%, for 55, 60, 65, and 70-mph, respectively. This model can also be used to evaluate the effect of increasing friction at a certain level if all the other factors remain constant. Following the previous example, if the speed limit is 70-mph, the MPD is 1-mm, and if friction increases from 0.4 to 0.8 the probabilities of each crash rate level will change as indicated in Figure 30. As shown, that friction increases from 0.4 to 0.8 will reflect in a reduction of the chances of observing a crash rate greater than 30, i.e., $P(R < 30)$ went from 74% to 92%.

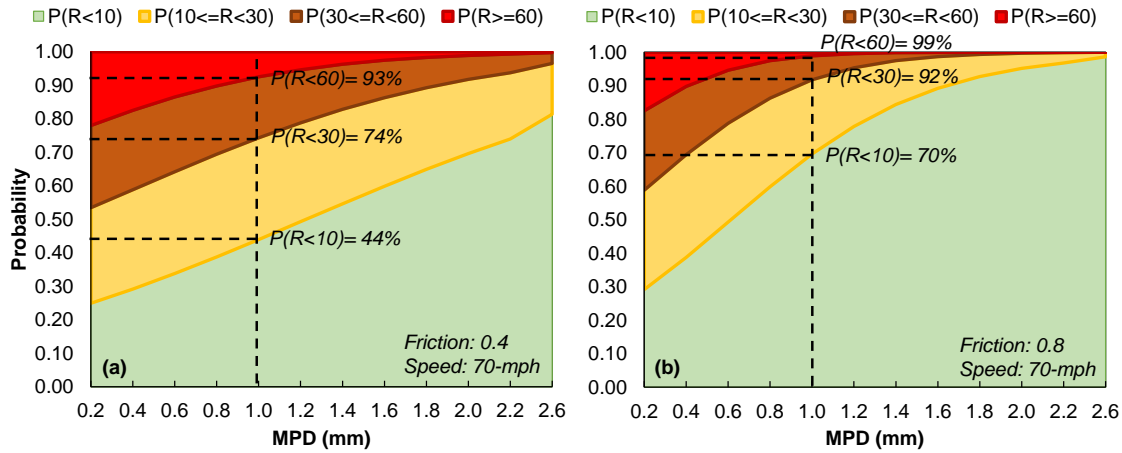


Figure 30. Probability $P(L_k \leq R_k < U_k)$ for: (a) friction = 0.4 and (b) friction = 0.8.

The results shown in Figure 29 and Figure 30 can be generalized by computing all the possible combinations of friction and texture at a given speed limit. This analysis results in a three-dimensional surface, which can be visualized in two dimensions by using a contour plot like the ones shown in Figure 31. In this figure, the darker the color, the higher the probability that the crash rate will be below 10 100-Mvmt₁₃ ($P(R < 10)$). For example, for a posted speed limit of 55-mph, if friction is 0.7 and MPD is 1-mm there is a 74% chance the crash rate will be less than 10 100-Mvmt₁₃. If friction reduces to 0.5, to maintain the same level of probability the MPD must be equal to 1.4-mm. For these two friction-texture combinations, if the speed limit increases from 55 to 70-mph, the $P(R < 10)$ reduces to 64% for the combination of $MPD = 1.0$ -mm and friction 0.7, and $MPD = 1.4$ -mm and friction = 0.5, respectively. By using this contour plot, it is possible to identify friction and texture combinations that lead to the same probability, or risk level.

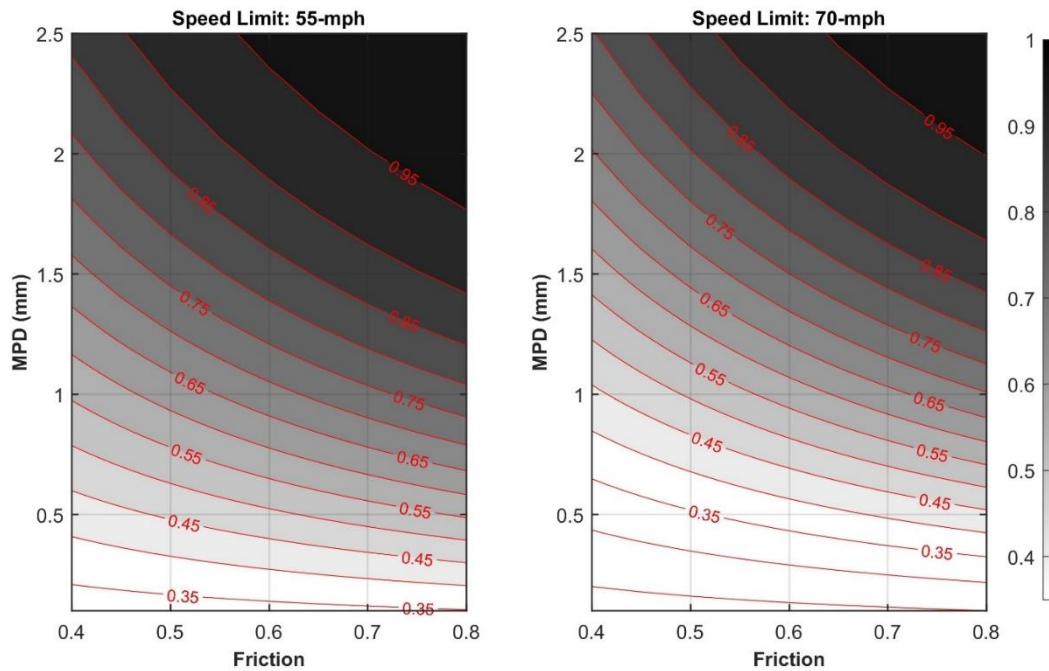


Figure 31. $P(R < 10)$ envelope for a speed limit of 55-mph (left panel) and 70-mph (right panel).

One way to communicate the individual friction/texture investigatory thresholds estimated with the GPF-Pivot method is by computing the probabilities associated when the *MPD* and friction reach their respective investigatory thresholds. As before, the intervention level is set as 25% below the investigatory level and an optimum value is set as 25% above the investigatory level. Intermediate values can be defined as needed. For example, if the thresholds estimated for Category-1 using the GPF method for friction and texture are used, yields an investigatory level for friction of 0.53 and for texture of *MPD* = 0.80 mm, see Table 13 and Table 14.

In that case, the 50% interval around the investigatory friction is 0.4 to 0.7 (25% below and above FN_{INV} , respectively), and for the *MPD* is 0.6 mm to 1 mm (25% below and above MPD_{INV} , respectively). Using Equation (26) when $FN = 0.53$, $MPD = 0.80$ mm, and speed limit is equal to 55-mph, the $P(R < 10)$ is calculated as 58%. In the case FN is now the intervention level of $FN = 0.4$ but *MPD* is still equal to 0.8 mm, $P(R < 10) = 50\%$. If instead, FN is still 0.4 but the *MPD* is now at the intervention level of 0.6-mm, $P(R < 10) = 45\%$.

Based on these probabilities, the relative risk is calculated with Equation (25) and $RR(MPD = 0.8, FN = 0.4) = 50/51 = 0.98$, and the relative risk $RR(MPD = 0.6, FN = 0.4) = 45/51 = 0.78$. The higher the *RR* the better. A summary of the different *RR* values computed based on $P(R < 10)$ is presented in Table 16. Similar tables can be made by using other probabilities, such as the $P(R < 30)$ or $P(R < 60)$.

Table 16. Relative risk based on $P(R < 10)$ for different speed limits.

Friction	<i>MPD</i> (mm)					Speed Limit
	0.6	0.7	0.8	0.9	1	
0.4	0.78	0.83	0.87	0.92	0.96	55-mph
0.5	0.85	0.91	0.96	1.02	1.08	
0.54	0.88	0.94	1.00	1.06	1.12	
0.6	0.92	0.99	1.05	1.12	1.18	
0.7	0.99	1.06	1.14	1.21	1.28	
0.4	0.76	0.81	0.86	0.91	0.96	60-mph
0.5	0.84	0.90	0.96	1.02	1.08	
0.54	0.87	0.93	1.00	1.07	1.13	
0.6	0.91	0.99	1.06	1.13	1.20	
0.7	0.99	1.07	1.15	1.23	1.31	
0.4	0.75	0.80	0.85	0.90	0.96	65-mph
0.5	0.83	0.89	0.96	1.02	1.09	
0.54	0.86	0.93	1.00	1.07	1.14	
0.6	0.90	0.98	1.06	1.14	1.22	
0.7	0.98	1.08	1.17	1.26	1.34	
0.4	0.73	0.79	0.84	0.90	0.95	70-mph
0.5	0.81	0.88	0.95	1.03	1.10	
0.54	0.85	0.92	1.00	1.08	1.16	
0.6	0.90	0.98	1.07	1.16	1.24	
0.7	0.98	1.08	1.19	1.29	1.38	
Color code:	$RR < 0.9$	$0.9 \leq RR \leq 1$	$RR > 1$			

4.4. Recommended Friction and Texture Thresholds

Table 13 and Table 14 summarize the values of friction and texture at which crash rates show a visible increase with continued reductions. There, the data is segregated by demand categories and, when all data is combined, by traffic speed. To develop final recommended friction and texture thresholds, additional assessments are needed. A summary of the aggregate crash rate computed for each friction demand category and their respective investigatory thresholds is presented in Figure 32. In this figure, the values from Table 13 and Table 14 are shown along with the different crash rate curves to emphasize the uncertainty and variability in the curves estimated for each demand category. It is noted that in Figure 32 (a), for the interchange category the data used to define the investigatory threshold did not include the values associated with a friction bin below 0.575, because the number of interchange segments with friction values below 0.575 was too small to obtain a reliable crash rate estimate. Figure 32 (b) shows for the case of texture that while the values developed by the GPF method are systematically different for each category, the overall crash rate curves are similar and thus choosing a single representative value does not have much impact on the final expected crash rates. On the other hand, Figure 32 (a) shows greater differentiation in crash rates by demand category for friction.

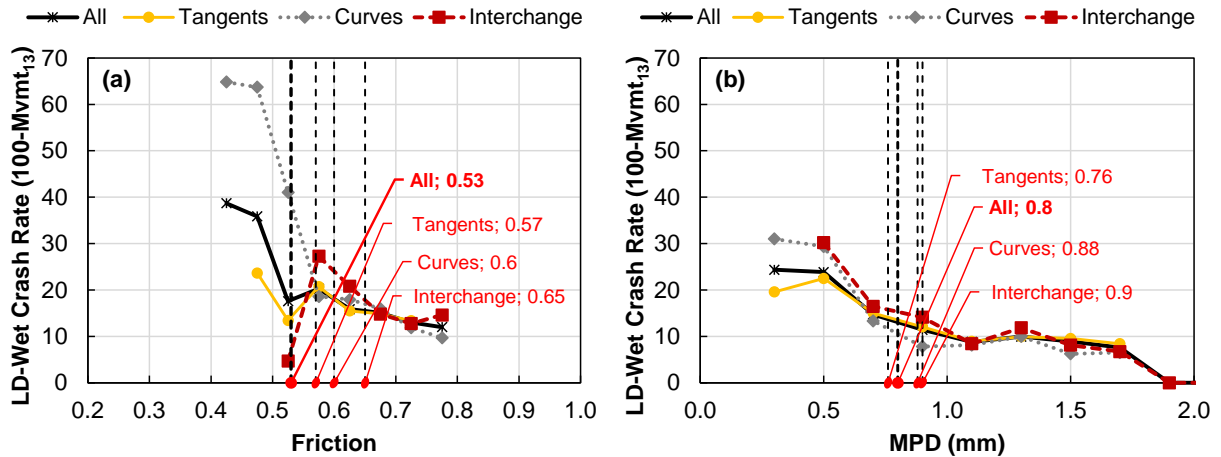


Figure 32. Investigatory Thresholds for the different demand categories for (a) Friction and (b) MPD.

It must be noted that the speed dependent thresholds evaluated for Category-1 are not included in Figure 32, because even though a value was obtained for the segments at 55-60 mph and 65-70 mph, the sample size of the former group is limited, and more observations are needed to proposed reliable speed dependent thresholds. Also, as shown in Figure 32 (a) the friction investigatory level of curves and tangents is close, 0.57 for tangents and 0.60 for curves. In contrast, the interchange has a distinct value of 0.65. Consequently, it seems feasible to recommend the value of 0.57 for curves and tangents, from now on referred as non-interchange segments, and the value of 0.65 for those segments inside an interchange influence area.

According to the NCHRP 108 GPF, pavement segments with measured friction/texture values at or below an assigned investigatory level are subject to a detailed site investigation to determine the need for remedial action, such as erecting warning signs, performing more frequent testing and analysis of skid resistance data and crash data, or applying a short-term restoration treatment. In other words, this threshold flags the need for a detailed evaluation. In contrast, pavement segments

with friction/texture values at or below the intervention level, require remedial actions that may consist of immediately applying a restoration treatment or programming a treatment into the maintenance or construction work plan and/or erecting temporary warning signs.

Hence, based on this need for site specific investigations, for friction there is much greater separation by demand categories, and it is recommended that demand category dependent thresholds be chosen. In the case of texture, based on the similarity of crash rate curves as a function of *MPD*, a single representative *MPD* value is recommended for the investigatory levels. The value for this investigatory level is selected from the combined Category 1 analysis. The proposed investigatory level and the associated intervention levels are summarized in Table 17. As noted above, even though the data available suggested that lane departure, wet crash rates were lower on facilities with a 55-60 mph speed limit than on those with a 65-70 mph speed limit, the recommended thresholds are the same for both. More data should be collected to have enough certainty to recommend a lower threshold limit for such facilities.

Table 17. Recommended investigatory thresholds.

Variable	Non-Interchanges	Interchanges
FN_{INV}	0.57	0.65
FN_{INT}	0.43	0.49
MPD_{INV} (mm)	0.80	0.80
MPD_{INT} (mm)	0.60	0.60

Having recommended the investigatory and intervention thresholds, an example is presented to illustrate the process needed to establish the demand categories for each segment and the corresponding thresholds. Figure 33 shows the geometry of Site 101 with the location of the tangents, curves, and interchanges identified. The total length of the site is 6.56 miles, 3.13 miles are characterized as curves (red lines in Figure 33) and 3.42 miles are tangents (blue lines in Figure 33). There are two interchanges along Site 101 and most of the segments that fall inside the interchanges' area of influence are curves (1.20 miles).

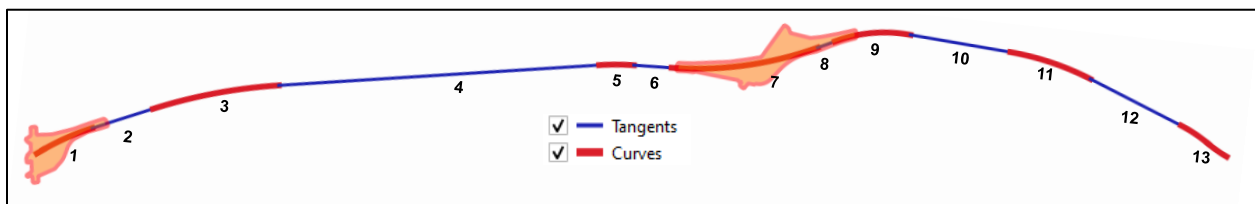


Figure 33. Friction demand categories definition for Site 101.

As presented in Table 17 the highest intervention threshold corresponds to interchanges. Any segment that is inside an interchange area of influence is categorized as Interchange in Table 18. For example, Segment 2 is a tangent with a total length of 0.34 miles; 0.07 miles of this segment is within the first interchange (leftmost one in Figure 33) and therefore is designated as an Interchange in Table 18 (from milepost 0.32 to 0.39), the remaining 0.27 miles are outside the interchange area and is designated as Tangent in Table 18. Once all the segments are categorized, the values of Table 17 are used to define the investigatory and intervention levels, respectively as shown in Table 18.

Table 18. Assigning the investigatory and intervention levels for the segments of Site 101.

Segment	Friction Demand	Milepost		Investigatory Levels		Intervention Levels	
				MPD (mm)	Friction	MPD (mm)	Friction
		From	To				
1	Interchange	0	0.32	0.80	0.65	0.60	0.49
2	Interchange	0.32	0.39	0.80	0.65	0.60	0.49
2	Tangent	0.39	0.66	0.80	0.57	0.60	0.43
3	Curve	0.66	1.35	0.80	0.57	0.60	0.43
4	Tangent	1.35	3.05	0.80	0.57	0.60	0.43
5	Curve	3.05	3.24	0.80	0.57	0.60	0.43
6	Tangent	3.24	3.44	0.80	0.57	0.60	0.43
7	Curve	3.44	3.47	0.80	0.57	0.60	0.43
7	Interchange	3.47	4.23	0.80	0.65	0.60	0.49
8	Interchange	4.23	4.32	0.80	0.65	0.60	0.49
9	Interchange	4.32	4.44	0.80	0.65	0.60	0.49
9	Curve	4.44	4.73	0.80	0.57	0.60	0.43
10	Tangent	4.73	5.27	0.80	0.57	0.60	0.43
11	Curve	5.27	5.72	0.80	0.57	0.60	0.43
12	Tangent	5.72	6.26	0.80	0.57	0.60	0.43
13	Curve	6.26	6.56	0.80	0.57	0.60	0.43

Following this example, if friction and texture are measured in Site 101, they should be first compared against the investigatory levels shown in Table 18. If the measured friction or texture of a given segment are below the investigatory level but above the intervention threshold, a detailed safety evaluation should be conducted. On the other hand, if the measured value is below the intervention level a maintenance treatment may be needed and a study must be carried out to determine the treatment type that best fits the site geometry and surface characteristics.

4.5. Cost-Benefit Analysis

As detailed in Appendix J, a cost-benefit analysis was carried out to assess the implications of the threshold values identified in this study. The analysis considered three different scenarios that were defined in close consultation with the project steering committee and intended to evaluate the effect of including safety requirements in the pavement maintenance planning and execution. The three scenarios evaluated were:

- Business-As-Usual Scenario (S1): maintenance is done as usual, i.e., without considering the available skid resistance and the expected number of lane departure wet collisions.
- Maintenance-With-Safety (S2): the available friction and texture is used to estimate the expected number of collisions in the network and using the combination of performance models and intervention thresholds evaluate whether a pavement needs to be rehabilitated or not.
- Safety-Risk-Balance (S3): the decision of whether a site needs to be rehabilitated is based on the sequential Logit model, which is used to estimate the probability of surpassing a given crash rate. A site is rehabilitated if the calculated probability is greater than a certain risk level.

Based on the recommendations of the project steering committee, two maintenance alternatives were evaluated: OGFC and UTBWC. The former was assumed to be used only in the western

administrative divisions, whereas the latter was used for the eastern divisions. The analysis evaluated two uncertainties associated with the maintenance strategies: the expected life and the expected structural damage. The combination of these two factors defined a set of maintenance strategies. In the case of the OGFC, three strategies were defined that represented a low-structural damage, a high-structural damage, and a modified/moderate case. The low-structural case assumes the top surface is milled and replaced every 5-years, and a full-depth replacement (OGFC + underneath dense layer) is replaced only every 10-years. The high-structural case considers that a full-depth replacement is needed every 5-years, and the modified-structural damage considers the full-depth is made every 8-years. In contrast, for the UTBWC two strategies were evaluated, low-structural damage and modified-structural damage. For the former the top surface is milled every 7-years, and a full-depth replacement is conducted after 14-years. The modified-structural condition evaluates the case where a full-depth replacement is made every 10-years.

The detailed cost-benefit analysis is presented in Appendix J. The friction and texture data collected by WDM was used to illustrate the proposed analysis method. One of the main inputs in the analysis was the set of intervention thresholds defined in this chapter, summarized in Table 17. A simplified life-cycle cost analysis was conducted, and the main conclusions obtained were:

- Of the strategies evaluated, the most efficient way to increase safety may be to use coarse-graded dense mixes that provide a mean initial texture value of 0.8-mm (measured with the Ames AccuTexture 100) and a minimum friction of 0.50 (measured with Moventor Skiddometer BV-11 at 60-mph). It is noted that potential long-term structural performance implications from such a mix were not included in the assessment. It was assumed that such a mix, if it were possible, would perform equivalent to the NCDOT's current surface mixtures.
- While the precise cost implications varied by scenario evaluated, all scenarios showed a benefit-cost ratio from using the OGFC and UTBWC greater than one. A minimum benefit-cost ratio of 4.5 was obtained and the maximum observed was 12. As outlined below, there are some limitations with respect to the assumptions made in the cost/benefit analysis and the ability to consider other cost implications that limit the research team's ability to confidently state whether such cost/benefit ratios could be achieved in practice.
- The current *MPD* and friction values of the portion of the network evaluated suggest North Carolina has texture values that fall below the proposed investigatory level. In contrast, friction values, in the majority of cases, exceed the proposed investigatory level. Hence, increasing the texture across the network should be the primary target of the NCDOT.

There are some main limitations in this analysis:

- The mobilization cost incurred to monitor those sites where either friction or texture is below their candidate investigatory threshold is not included.
- It is assumed that once a surface is treated, the initial *MPD* is equal to the average value of that surface type, instead this should be modeled as a random variable.
- The analysis here only evaluated primary economic effects, i.e., those directly related to the pavements. However, there are secondary and tertiary economic implications that may affect how well the calculated cost/benefit ratios would match real cost/benefits. Some of the other economic implications that were not included in the analysis are: i) the budgetary implications of widespread implementation of the friction/texture thresholds and rehabilitation strategies and the agency operational adjustments that would be needed for

such implementation; ii) the longer-term impact of shifting funding priorities on the maintenance, operations, and conditions of the entire transportation system in North Carolina to complete the activities resulting from the PFMP; iii) the time and cost required for contractors to get familiar and train their personnel to construct the different surface treatments to ensure that they perform well; iv) the availability and possible impacts on the supply and cost of component materials required for these treatments; and v) the impacts to sustainability and the costs/benefits from downstream effects (if any) of the use of these treatments (e.g., changes in the balance of waste materials at material suppliers, an imbalance in the amount of RAP generated versus what is used, impacts of increased construction times and lane closures over the life of the pavement that would be needed to construct and maintain these treatments, etc.).

The limitations noted above are considered substantial and should be addressed for before applying the findings here to make far reaching policy decisions. Had the analysis performed in this study not shown a cost/benefit ratio greater than one, then it would have been clear that the effort to better understand and quantify these secondary and tertiary effects was not worthwhile.

4.6. Summary

In this chapter, two evaluation approaches were applied to define a set of friction and texture investigatory thresholds. The first approach included two versions of the Guide for Pavement Friction Method 3, here named as Pivot method. The second approach relied on a statistical model known as the sequential Logit. This analysis showed:

- Interchanges have the highest friction/texture demand among all the categories evaluated. This situation can be explained if one considers that, depending on the number of entries and exits, the number of conflicts (convergence or divergence of traffic flows) expected in the area of influence of an interchange is considerably higher than that one could expect on a curve or tangent.
- As expected, the highest friction/texture demand occurs at a 65-70 mph speed limit. At 70-mph, the risk of hydroplaning is higher given the ratio between the hydroplaning speed and vehicle speed.
- It has been shown that the sequential Logit model is advantageous over the traditional Pivot method because it can account for the interaction effect between friction and texture. This feature allows one to define the required texture constrained to a certain available friction. The challenge with implementing the Logit model lie in the lack of a quantified assessment for the NCDOT relating crash rate probability and acceptable risk.
- Both the Pivot method and sequential Logit model were calibrated with the data at hand. The outcomes of both methods can be improved by including more observations, and in particular, expanding the dataset of OGFC and UTBWC sites. Other surface types, like chip seals, micro surfacing or portland concrete pavements can be incorporated to improve the model accuracy and generality.

5. CONCLUSIONS AND RECOMMENDATIONS

5.1. Conclusions

On the basis of the research conducted in this study, the following conclusions have been reached:

- For a dense-graded mixture, the statistical analysis on the initial friction variation as a function of mixture composition suggests that the highest friction percent changes are associated with a high proportion of fines, P_{200} , and with a high asphalt content, %AC.
- To get accurate predictions of friction and texture performance it is necessary to account for heterogeneity in the deterioration process. In this research, this heterogeneity was modeled using random effect models. These random effect terms are estimated during the calibration process and so for the calibration set these quantities are known for each site. To use the friction and texture performance model on sites that were not part of the calibration process, there are three possible options (ordered according to their accuracy level): i) set the random effects equal to the average values of the random effects observed in the calibration set; ii) estimate the random effects from mixture composition; and iii) estimate the random effects by using at least two friction/texture observations. These three situations were detailed in Appendix G.
- Texture performance models have higher accuracy than the friction models, which is attributed to an overall, more stable variation in MPD between measurements.
- Friction generally reduces over time due to the cumulative effect of traffic repetitions that cause aggregate polishing after an initial increase in some cases. However, as observed in some sites, friction can increase in presence of moderate to severe raveling processes, typical of old surfaces. Future versions of the proposed performance models should incorporate the raveling distress information stored in NCDOT PMS database.
- Independently of the method used to establish and evaluate friction/texture candidate thresholds, road segments were grouped by friction demand category. Interchanges have the highest friction/texture demand among all the categories evaluated. This situation can be explained if one considers that, depending on the number of entries and exits, the number of conflicts expected in the area of influence of an interchange is considerable higher than one could expect on a curve or tangent.
- The sequential Logit model has a substantial advantage over the traditional Method 3 of the NCHRP 108 for defining friction and texture thresholds because it can account for the interaction between friction and texture on safety. This feature allows one to define the required texture constrained to a certain available friction. Also, due to its simple form, the equations of the sequential Logit can be easily applied to an entire network to identify those locations that might require a detailed analysis.
- The candidate thresholds and the performance models were used to demonstrate the efficacy of the proposed framework. The analysis included primary construction and rehabilitation costs. The results indicate that it may be economically feasible to treat the network to maintain a minimum friction and texture levels. Benefit-cost ratios between 4.5 to 12 were obtained. However, other economic components, such as budgetary implications of treating the entire primary road network were not accounted for in the analysis.

5.2. Recommendations

Based on the aforementioned conclusions, the research team makes the following recommendations;

5.2.1. PFMP Recommendations

- For a given pavement, it is ideal to measure friction across the different seasons to calibrate a model that describes the seasonal variation for local conditions.
- For new pavements, it is recommended to collect four equally spaced measurements during the first year of construction. Then, measurements should be conducted in the summer.
- Avoid collecting friction or texture measurements in sites with more than 20 consecutive dry days. More chances exist that dust and contaminants could affect the observations.
- Interstates, US-routes, curves, ramps, and intersections should be prioritized to receive the highest measurement frequency.
- Friction should be measured at 40-mph and 60-mph. The 40-mph is relevant in ramps and intersections. The thresholds proposed here were set based on friction at 60-mph.
- For quality control, it is recommended that the NCDOT define a roadway section for device calibration/verification.
- The recommended friction and texture thresholds shown in Table 17, presented in Chapter 4 and repeated here for convenience, could be used to monitor the safety performance of facilities with speed limits above 55 mph on North Carolina’s primary road network, but continual monitoring and refinement should be carried out as more data becomes available.

Table 19. Recommended investigatory thresholds.

Variable	Non-Interchanges	Interchanges
⁽¹⁾ FN_{INV}	0.57	0.65
⁽¹⁾ FN_{INT}	0.43	0.49
⁽²⁾ MPD_{INV} (mm)	0.80	0.80
⁽²⁾ MPD_{INT} (mm)	0.60	0.60

(1) FN_{INV} and FN_{INT} specific for Moventor Skiddometer BV-11 at 60-mph
(2) MPD_{INV} and MPD_{INT} specific for AMES AccuTexture 100

5.2.2. Future Research Recommendations

- Characterize friction and texture for other surface treatments, such as microsurfacing, chip seals, diamond grinding, grooving, etc.
- Conduct research to evaluate the use of coarser gradations or alternative surface types in North Carolina pavements.
- Conduct research to develop a method to account for friction and texture demands during the mixture design and/or mixture placement process.
- Friction and texture performance models can be improved by incorporating a variable that quantifies the raveling process experienced by the pavement. Currently, for the primary roadway network, the NCDOT PMS database stores the area of the pavement with four possible raveling severity levels, none, light, moderate, and severe. It is expected that the higher the extent of the raveling process, the higher the expected change in macrotexture and friction. Clustering techniques can also be used to improve the accuracy of the friction models.

- The sequential Logit model discussed in Chapter 4 should be calibrated for different friction demand categories and should incorporate data collected on a wider variety of surface types. Additionally, the NCDOT should conduct a study to define its allowable risk for each crash rate level.

This page is intentionally blank

6. IMPLEMENTATION AND TECHNOLOGY TRANSFER PLAN

The Traffic Safety Unit and Materials and Test Unit of the NCDOT will be the primary users of this product. The products of this research will be used by the NCDOT to predict friction and texture performance on roadways and to understand when measurements represent a potential hazard exists. It can also be used to help identify asphalt mixtures with potential friction and macrotexture issues and develop better guidelines, specifications, and operational controls (if necessary) for recently overlaid pavements. Though many factors exist on individual facilities, these steps could lead to reduced overall lane-departure, wet collision rates on these pavements.

For follow-up activities, the research team believes that the NCDOT could consider the following activities:

- allocating resources to evaluate a larger proportion of pavements with 55-60 mph speed limits in order to modify the recommended threshold limits for such facilities;
- allocating resources to investigate the efficacy of alternative surface treatment strategies in order to maximize the benefit-cost ratio on a facility-by-facility basis;
- allocate resources to validate the recommended investigatory and intervention threshold limits and to refine these limits to better account for friction demand, including refinement of the recommended limits for facilities with 55-60 mph speed limits; and
- allocate resources to refine and develop a quality assurance protocol for newly constructed pavements to ensure appropriate friction and texture is achieved at construction and flag pavements that require mitigation early.

This page is intentionally blank

7. REFERENCES

1. de León Izeppi, Edgar, Gerardo W. Flintsch, and Ross McCarthy. *Evaluation of Methods for Pavement Surface Friction, Testing on Non-Tangent Roadways and Segments*. No. FHWA/NC 2017-02. North Carolina. Dept. of Transportation, 2017.
2. Underwood, S. B., C. Castorena, B. Goenaga, and P. Rogers. *Evolution of Pavement Friction and Macrotexture After Asphalt Overlay*. No. FHWA/NC 2020-11. North Carolina. Dept. of Transportation, 2021.
3. Pérez-Acebo, H., Gonzalo-Orden, H., Findley, D. J., & Rojí, E. (2020). A skid resistance prediction model for an entire road network. *Construction and building materials*, 262, 120041.
4. Pomoni, M., C. Plati, A. Loizos, and G. Yannis. Investigation of Pavement Skid Resistance and Macrotexture on a Long-Term Basis. *International Journal of Pavement Engineering*, 2020, pp. 1–10.
5. Pranav, C., M. T. Do, and Y. C. Tsai. Analysis of High-Friction Surface Texture with Respect to Friction and Wear. *Coatings*, Vol. 11, No. 758, 2021.
6. Gonzalez, O. *Evaluation of Pavement Surface Friction Seasonal Variation*. Master Thesis. Virginia Polytechnic Institute and State University, Virginia, 2009.
7. Hall, J. W., Smith, K. L., Titus-Glover, L., Wambold, J. C., Yager, T. J., & Rado, Z. (2009). Guide for pavement friction. *Final Report for NCHRP Project, 108*.
8. Ahammed, M. A., and S. L. Tighe. Concrete Pavement Surface Textures and Multivariables Frictional Performance Analysis: A North American Case Study. *Canadian Journal of Civil Engineering*, Vol. 35, No. 7, 2008, pp. 727–738.
9. Ahammed, M., and S. L. Tighe. Early-Life, Long-Term, and Seasonal Variations in Skid Resistance in Flexible and Rigid Pavements. *Transportation Research Record: Journal of the Transportation Research Board*, No. 2094, 2009, pp. 112–120.
10. Woodward, W. D. H., Woodside, A. R., & Jellie, J. H. (2002). Development of Early Life Skid Resistance for High Stone Content Asphalt Mixes. In *Proceedings of the 3rd International Conference on Bituminous Mixtures and Pavements, Held Thessaloniki, Greece, November 2002*. (Vol. 2).
11. Jayawickrama, P. W., and B. Thomas. Correction of Field Skid Measurements for Seasonal Variations in Texas. *Transportation Research Record: Journal of the Transportation Research Board*, No. 1639, 1998, pp. 147–154.
12. Cenek, P. D., D. J. Alabaster, and R. B. Davie. *Seasonal and Weather Normalisation of Skid Resistance Measurements*. Transfund New Zealand Research Report No. 139. 1999.
13. Wu, Z., and C. Abadie. Laboratory and Field Evaluation of Asphalt Pavement Surface Friction Resistance. *Frontiers of Structural and Civil Engineering*, Vol. 12, No. 3, 2018, pp. 372–381.
14. Miao, Y., J. Li, X. Zheng, and L. Wang. Field Investigation of Skid Resistance Degradation of Asphalt Pavement during Early Service Skid Resistance Degradation of Asphalt Pavement. *International Journal of Pavement Research and Technology*, Vol. 9, No. 4, 2016, pp. 313–320.
15. West, R., D. Timm, B. Powell, N. Tran, F. Yin, B. Bowers, C. Rodezno, F. Leiva, A. Vargas, F. Gu, R. Moraes, and M. Nakhaei. *Phase VII (2018-2021) NCAT Test Track Findings*. Alabama, 2021.

16. Fwa, T. F. Skid Resistance Determination for Pavement Management and Wet-Weather Road Safety. *International Journal of Transportation Science and Technology*, Vol. 6, No. 3, 2017, pp. 217–227.
17. Flintsch, G. W., K. K. Mcghee, E. D. L. Izeppi, and S. Najafi. *The Little Book of Tire Pavement Friction*. 2012.
18. de Leon Izeppi, E., G. Flintsch, S. Katicha, K. McGhee, R. McCarthy, and K. Smith. *PFM Program Utilizing CFME and State-of-the-Practice Safety Analysis Demonstration*. Washington, 2019.
19. National Highway Traffic Safety Administration (NHTSA). *MMUCC Guideline: Model Minimum Uniform Crash Criteria*. 2017.
20. Goenaga, B., N. Matini, D. Karanam, and B. S. Underwood. Disruption and Recovery: Initial Assessment of COVID-19 Traffic Impacts in North Carolina and Virginia. *Journal of Transportation Engineering, Part A: Systems*, Vol. 147, No. 4, 2021, p. 06021001.
21. Bíl, M., R. Andrášik, J. Sedoník, and V. Cícha. ROCA – An ArcGIS Toolbox for Road Alignment Identification and Horizontal Curve Radii Computation. *PLoS ONE*, Vol. 13, No. 12, 2018.
22. Kogbara, R. B., E. A. Masad, E. Kassem, A. Scarpas, and K. Anupam. A State-of-the-Art Review of Parameters Influencing Measurement and Modeling of Skid Resistance of Asphalt Pavements. *Construction and Building Materials*, Vol. 114, 2016, pp. 602–617.
23. Alhasan, A., I. Nlenanya, O. Smadi, and C. A. MacKenzie. Impact of Pavement Surface Condition on Roadway Departure Crash Risk in Iowa. *Infrastructures*, Vol. 3, No. 2, 2018, p. 14.
24. Zhang, Z., and L. Gao. A Nested Modelling Approach to Infrastructure Performance Characterisation. *International Journal of Pavement Engineering*, Vol. 19, No. 2, 2018, pp. 174–180.
25. Chen, D., and N. Mastin. Sigmoidal Models for Predicting Pavement Performance Conditions. *Journal of Performance of Constructed Facilities*, Vol. 30, No. 4, 2016, p. 04015078.
26. Huo, X., J. Leng, Q. Hou, and H. Yang. A Correlated Random Parameters Model with Heterogeneity in Means to Account for Unobserved Heterogeneity in Crash Frequency Analysis. *Transportation Research Record: Journal of the Transportation Research Board*, Vol. 2674, No. 7, 2020, pp. 312–322.
27. Li, J. Q., Wang, K., Liu, W., & Yu, W. (2020). *Utilizing pavement friction and texture data for the reduction of traffic crashes and delays* (No. FHWA-OK-21-01). Oklahoma. Department of Transportation.
28. Goenaga, B., B. S. Underwood, C. Castorena, and P. Rogers. Early Friction and Texture Evolution After an Asphalt Overlay. *Transportation Research Record: Journal of the Transportation Research Board*, 2023.
29. US Department of Transportation, F. A. A. (FAA). *Advisory Circular Subject: Measurement and Maintenance of Skid-Resistant Airport Pavement Surfaces*. 2016.
30. Leandri, P., and M. Losa. Peak Friction Prediction Model Based on Surface Texture Characteristics. *Transportation Research Record: Journal of the Transportation Research Board*, Vol. 2525, No. 3, 2015, pp. 91–99.
31. Henry, J. J. *NCHRP Synthesis 291: Evaluation of Pavement Friction Characteristics*. 2000.
32. Wu, Z., and B. King. *Development of Surface Friction Guidelines for LADOTD - Report No. FHWA/LA.11/485*. 2012.

33. Association mondiale de la Route World Road Association (PIARC). *Experiment to Compare and Harmonize Texture and Skid Resistance Measurements*. 1995.
34. Radó Zoltán. *A Study of Road Surface Texture and Its Relationship to Friction*. Ann Harbor, 1994.
35. Wilson, D. J. *An Analysis of the Seasonal and Short-Term Variation of Road Pavement Skid Resistance*. 2006.
36. Kokkalis, A. G. Prediction of Skid Resistance from Texture Measurements. *Proceedings of the Institution of Civil Engineers: Transport*, Vol. 129, No. 2, 1998, pp. 85–93.
37. Brittain, S. *PUBLISHED PROJECT REPORT PPR739 Calculation of Local Equilibrium Correction Factors for the 2014 Skid Resistance Surveys S Brittain*. 2015.
38. Jayawickrama, P. W., and B. Thomas. Correction of Field Skid Measurements for Seasonal Variations in Texas. *Transportation Research Record: Journal of the Transportation Research Board*, No. 1639, 1998, pp. 147–154.
39. Szatkowski, W. S., and J. R. Hosking. *The Effect of Traffic and Aggregate on the Skidding Resistance of Bituminous Surfacing*, Transport and Road Research Laboratory. 1972.
40. Rezaei, A., and E. Masad. Experimental-Based Model for Predicting the Skid Resistance of Asphalt Pavements. *International Journal of Pavement Engineering*, Vol. 14, No. 1, 2013, pp. 24–35.
41. Rezaei, A., and E. Masad. Experimental-Based Model for Predicting the Skid Resistance of Asphalt Pavements. *International Journal of Pavement Engineering*, Vol. 14, No. 1, 2013, pp. 24–35.
42. Grady, J. E., and W. P. Chamberlin. Groove-Depth Requirements for Tine-Texture Pavements. *Transportation Research Record: Journal of the Transportation Research Board*, Vol. 836, 1981, pp. 49–72.
43. Drakopoulos, A., T. H. Wenzel, S. F. Shober, and R. B. Schmiedlin. Crash Experience on Tined and Continuously Portland Cement Concrete Pavements. *Transportation Research Record: Journal of the Transportation Research Board*, Vol. 1639, No. 1, 1998, pp. 140–146.
44. Rao, S., H. T. Yu, L. Khazanovich, M. I. Darter, and J. W. Mack. Longevity of Diamond-Ground Concrete Pavements. *Transportation Research Record: Journal of the Transportation Research Board*, Vol. 1684, No. 1, 1999, pp. 128–136.
45. Saghafi, M., I. N. Abdallah, and S. Nazarian. Practical Specimen Preparation and Testing Protocol for Evaluation of Friction Performance of Asphalt Pavement Aggregates with Three-Wheel Polishing Device. *Journal of Materials in Civil Engineering*, Vol. 34, No. 1, 2022.
46. ASTM E1911-09. *Standard Test Method for Measuring Paved Surface Frictional Properties Using the Dynamic Friction Tester*. 2009.
47. ASTM E303-93 (Reapproved). *Standard Test Method for Measuring Surface Frictional Properties Using the British Pendulum Tester*. 2018.
48. BS EN 12697 - 49. *Bituminous Mixtures. Test Methods for Hot Mix Asphalt - Determination of Friction after Polishing*. 2014.
49. AASHTO. *Standard Practice for Sample Preparation and Polishing of Unbound Aggregates for Dynamic Friction Testing - AASHTO PP 103*. 2020.
50. ASTM D3319-11. *Standard Practice for the Accelerated Polishing of Aggregates Using the British Wheel*. 2017.

51. Khasawneh, M. A., and M. A. Alsheyab. Effect of Nominal Maximum Aggregate Size and Aggregate Gradation on the Surface Frictional Properties of Hot Mix Asphalt Mixtures. *Construction and Building Materials*, Vol. 244, 2020.
52. Masad, E., A. Rezaei, A. Chowdhury, and P. Harris. *Predicting Asphalt Mixture Skid Resistance Based on Aggregate Characteristics*. 2009.
53. Masad, E., A. Rezaei, A. Chowdhury, and T. Freeman. *Field Evaluation of Asphalt Mixture Skid Resistance and Its Relationship to Aggregate Characteristics*. 2010.
54. Zhao, Y., T. Xu, X. Huang, and Z. Li. Gradation Design of the Aggregate Skeleton in Asphalt Mixture. *Journal of Testing and Evaluation*, Vol. 40, No. 7, 2012.
55. Lin, C., and W. Tongjing. Effect of Fine Aggregate Angularity on Skid-Resistance of Asphalt Pavement Using Accelerated Pavement Testing. *Construction and Building Materials*, Vol. 168, 2018, pp. 41–46.
56. Khasawneh, M. A., and R. Y. Liang. Air Void Effect on Frictional Properties of Existing Asphalt Pavement Surfaces. *International Journal of Pavements*, Vol. 10, 2011, pp. 62–71.
57. Liu, Y., T. F. Fwa, and Y. S. Choo. Effect of Surface Macrotexture on Skid Resistance Measurements by the British Pendulum Test. *Journal of Testing and Evaluation*, Vol. 32, No. 4, 2004.
58. Goodman, S. N., Y. Hassan, and A. O. A. el Halim. Preliminary Estimation of Asphalt Pavement Frictional Properties from Superpave Gyrotory Specimens and Mix Parameters. *Transportation Research Record: Journal of the Transportation Research Board*, Vol. 1949, No. 1, 2006, pp. 173–180.
59. Woodward, D., P. Millar, C. Lantieri, C. Sangiorgi, and V. Vignali. The Wear of Stone Mastic Asphalt Due to Slow Speed High Stress Simulated Laboratory Trafficking. *Construction and Building Materials*, Vol. 110, 2016, pp. 270–277.
60. Praticò, F. G., and R. Vaiana. A Study on Volumetric versus Surface Properties of Wearing Courses. *Construction and Building Materials*, Vol. 38, 2013, pp. 766–775.
61. Magnoni, M., and F. Giustozzi. Evaluation of the Effect of Aggregates Mineralogy and Geometry on Asphalt Mixture Friction. *Journal of Civil & Environmental Engineering*, Vol. 6, No. 3, 2016.
62. Alsheyab, M. A., and M. A. Khasawneh. Quantifying the Effect of Modified Mixture Volumetrics and Compaction Effort on Skid Resistance of Asphalt Pavements. *International Journal of Pavement Engineering*, 2020.
63. Sullivan, B. W. Development of a Fundamental Skid Resistance Asphalt Mix Design Procedure. 2005.
64. FHWA. Pavement Friction Management: Technical Advisory. <https://www.fhwa.dot.gov/pavement/t504038.cfm>. Accessed Jul. 19, 2021.
65. Heitzman, M., and J. Moore. *Evaluation of Laboratory Friction Performance of Aggregates for High Friction Surface Treatments*. 2017.
66. AASHTO. *Highway Safety Manual*. 2010.
67. Noyce, D. A., H. U. Bahia, J. Yambo, J. Chapman, and A. Bill. *Incorporating Road Safety into Pavement Management: Maximizing Surface Friction for Road Safety Improvements*. 2007.
68. Wallbank, C., H. Viner, L. Smith, and R. Smith. *The Relationship between Collisions and Skid Resistance on the Strategic Road Network PPR 806*. 2016.
69. Pulugurtha, S. S., D. Ph, P. R. Kusam, and K. Patel. Relationship between Pavement Macrotexture and Crash Incidences on North Carolina Roads. *FHWA/NC 2007-1*, 2008.

70. Srinivasan, R., and D. Carter. *Development of Safety Performance Functions for North Carolina*. 2011.
71. Srinivasan, R., D. Carter, and K. Bauer. *Safety Performance Function Decision Guide: SPF Calibration versus SPF Development*. 2013.
72. Srinivasan, R., D. Carter, and K. Bauer. *Safety Performance Function Development Guide: Developing Jurisdiction-Specific SPF*. 2013.
73. Galgamuwa, U., J. Du, and S. Dissanayake. Bayesian Spatial Modeling to Incorporate Unmeasured Information at Road Segment Levels with the INLA Approach: A Methodological Advancement of Estimating Crash Modification Factors. *Journal of Traffic and Transportation Engineering (English Edition)*, Vol. 8, No. 1, 2021, pp. 95–106.
74. Katicha, S. W., J. Houry, and G. Flintsch. Spatial Multiresolution Analysis Approach to Identify Crash Hotspots and Estimate Crash Risk. *Journal of Transportation Engineering, Part A: Systems*, Vol. 147, No. 5, 2021.
75. Katicha, S. W., and G. W. Flintsch. Multiscale Vehicular Expected Crashes Estimation with the Unnormalized Haar Wavelet Transform and Poisson's Unbiased Risk Estimate. *Journal of Transportation Engineering, Part A: Systems*, Vol. 144, No. 8, 2018.
76. Hauer, E. *Observational Before-After Studies in Road Safety. Estimating the Effect of Highway and Traffic Engineering Measures on Road Safety*. 1997.
77. Thakali, L. *Nonparametric Methods for Road Safety Analysis*. Thesis for the degree of Doctor of Philosophy. University of Waterloo, Waterloo, Ontario, Canada, 2016.
78. Ye, Z., and D. Lord. Estimating the Variance in Before-after Studies. *Journal of Safety Research*, Vol. 40, No. 4, 2009, pp. 257–263.
79. Zoubir, A., and D. Iskander. *Bootstrap Techniques for Signal Processing*. Cambridge: Cambridge University Press., 2004.
80. Fisher, N. I., and P. Hall. Bootstrap Confidence Regions for Directional Data. *Journal of the American Statistical Association*, Vol. 84, No. 408, 1989, pp. 996–1002.
81. Efron, B. *Bootstrap Methods: Another Look at the Jackknife*. 1992.
82. Zhang, Y., Z. Ye, and D. Lord. Estimating Dispersion Parameter of Negative Binomial Distribution for Analysis of Crash Data: Bootstrapped Maximum Likelihood Method. *Transportation Research Record*, No. 2019, 2007, pp. 15–21.
83. Ong, G. P., and T. F. Fwa. Wet-Pavement Hydroplaning Risk and Skid Resistance: Modeling. *Journal of Transportation Engineering*, Vol. 133, 2007, pp. 590–598.
84. Izeppi, E. de L., G. Flintsch, S. Katicha, K. McGhee, and R. McCarthy. *Locked-Wheel and Sideway-Force Continuous Friction Measurement Equipment Comparison and Evaluation Report FHWA-RC-19-001*. Washington, 2019.
85. Flintsch, G. W., E. de León Izeppi, V. Bongioanni, S. W. Katicha, K. Meager, E. Fernando, R. Perera, and K. K. McGhee. *NCHRP Research Report 964 Protocols for Network-Level Macrotexture Measurement*. Transportation Research Board, Washington, D.C., 2021.
86. Highways Agency, T. S. W. G. and D. for R. D. N. I. *HD28 Skidding Resistance (7.3.1) Design Manual for Roads and Bridges*. 2015.
87. Transport Agency, N. *T10:2002 New Zealand Specification for State Highway Skid Resistance Management*. 2012.
88. Wallman, C.-G., and H. Åström. *Friction Measurement Methods and the Correlation between Road Friction and Traffic Safety. A Literature Review*. 2001.
89. AASHTO. *A Policy on Geometric Design of Highways and Streets*. 2018.

90. Federal Highway Administration (FHWA). *Manual of Uniform Traffic Control Devices for Street and Highways*. 2009.
91. Milstead, R., X. Qin, B. Katz, J. Bonneson, M. Pratt, J. Miles, and P. Carlon. *Procedures for Setting Advisory Speeds on Curves - FHWA-SA-11-22*. 2011.
92. Tsai Yichang (James), P. (Lucas) Yu, T. Liu, Z. Yang, and A. Steel. *Enhanced Network-Level Curve Safety Assessment and Monitoring Using Mobile Devices*. Georgia, 2021.
93. Merritt, D. K., C. Lyon, and B. Persaud. *Evaluation of Pavement Safety Performance*. 2015.
94. Wang, H., and Z. Wang. Evaluation of Pavement Surface Friction Subject to Various Pavement Preservation Treatments. *Construction and Building Materials*, Vol. 48, 2013, pp. 194–202.
95. Li, L., K. C. P. Wang, and Q. J. Li. Geometric Texture Indicators for Safety on AC Pavements with 1 Mm 3D Laser Texture Data. *International Journal of Pavement Research and Technology*, Vol. 9, No. 1, 2016, pp. 49–62.
96. Hosseini, A., A. Faheem, H. Titi, and S. Schwandt. Evaluation of the Long-Term Performance of Flexible Pavements with Respect to Production and Construction Quality Control Indicators. *Construction and Building Materials*, Vol. 230, 2020, p. 116998.
97. Wang, H., Z. Wang, R. J. Blight, and E. C. Sheehy. Derivation of Pay Adjustment for In-Place Air Void of Asphalt Pavement from Life-Cycle Cost Analysis. *Road Materials and Pavement Design*, Vol. 16, No. 3, 2015, pp. 505–517.
98. Hider, S., G. Musunuru, and K. Chatti. Effect of Sample Size and Methods on Percent within Limits for Quality Control and Assurance. 2017.
99. Stroup-Gardiner, M., and E. R. Brown. *NCHRP Report 441*. 2000.
100. Global Modeling and Assimilation Office (GMAO). MERRA-2 StatD_2d_slv_Nx: 2d,Daily,Aggregated Statistics Single-Level Assimilation, Single-Level Diagnostics V5.12.4. https://disc.gsfc.nasa.gov/datasets/M2SDNXSLV_5.12.4/summary. Accessed Jun. 4, 2022.
101. Hauer, E., and B. N. P. Problem of Identifying Hazardous Locations Using Accident Data. *Transportation Research Record: Journal of the Transportation Research Board*, 1994, pp. 531–540.
102. Hauer, E. Identification of Sites with Promise. *Transportation Research Record: Journal of the Transportation Research Board*, No. 1542, 1996, pp. 54–60.
103. Lord, D., and L. F. Miranda-Moreno. Effects of Low Sample Mean Values and Small Sample Size on the Estimation of the Fixed Dispersion Parameter of Poisson-Gamma Models for Modeling Motor Vehicle Crashes: A Bayesian Perspective. *Safety Science*, Vol. 46, No. 5, 2008, pp. 751–770.
104. Agrawal, R., and D. Lord. *Effects of Sample Size on Goodness-of-Fit Statistic and Confidence Intervals of Crash Prediction Models Subjected to Low Sample Mean Values*. 1950.
105. Karanam, D., B. Goenaga, and B. S. Underwood. *Quantifying Uncertainty with Pavement Performance Models: Comparing Bayesian and Non-Parametric Methods*. 2023.
106. Campbell, M. J., and M. J. Gardner. *Calculating Confidence Intervals for Some Non-Parametric Analyses*. 1988.
107. Alper, J. S., and R. I. Gelb. *Standard Errors and Confidence Intervals in Nonlinear Regression: Comparison of Monte Carlo and Parametric Statistics*. 1990.
108. Ye, Z., and D. Lord. Estimating the Variance in Before-after Studies. *Journal of Safety Research*, Vol. 40, No. 4, 2009, pp. 257–263.

109. NCDOT. *Pavement Design Procedure AASHTO 1993 Method*. 2017.
110. Galvis Arce, O. D., and Z. Zhang. Framework to Estimate the Benefit–Cost Ratio of Establishing Minimum Pavement Friction Levels for Roadway Networks. *International Journal of Pavement Engineering*, Vol. 23, No. 7, 2022, pp. 2135–2147.

This page is intentionally blank

APPENDIX A. DETAILED LITERATURE REVIEW

Introduction

This appendix presents a summary of the literature on the issues relevant to friction and texture, their measurement, their relationship with crash risk, and approaches to managing friction. The appendix is organized as follows:

- Section 2 presents a summary of the friction mechanism, the main models used to represent the friction variation with speed, and the friction variation during a braking maneuver. Also, the current state-of-the art for friction and texture performance models are discussed.
- Section 3 includes the main techniques used to characterize the skid resistance of both aggregates and asphalt concrete mixes. Here aspects such as the laboratory specimen preparations, as well as the equipment used to measure friction and simulate the traffic polishing are discussed.
- Section 4 discusses the effect of the mixture composition in the available friction and texture. Key aspects such as the use of Superpave Gyratory Compactor samples for estimating as-constructed friction and texture, the effect of binder modifiers in friction, and the most used friction treatment, are included in this section.
- Next, Section 5 presents a detailed description of the techniques available to quantify the crash risk in a road segment, topics such as the most common variables and the model structure are discussed. Also, this section briefly describes the mechanism behind a ‘before-after’ study, and the potential of using non-parametric methods to overcome the problem of a limited sample size.
- Section 6 presents the main elements of a Pavement Friction Management Program (PFMP), the methodology that can be used to set Investigatory Levels (ILs) for a highway network, and the aspects to consider for defining friction demand categories.
- Finally, the last section covers the main conclusions and knowledge gaps.

Pavement Friction

Wet pavement friction is a measure of the force generated when a tire slides on a wet pavement surface. Typically, wet pavement friction is also referred to as ‘skid resistance’ and can be found in the literature by either of these names. Skid resistance reduces when the relative speed between the sliding surfaces increases, a.k.a. between vehicle tire and pavement surface.

During the braking process, the rotational speed of the tire starts decreasing at a higher rate than the vehicle speed; therefore, the slip speed, which is zero when the vehicle is at a free rolling mode, will increase until it reaches the maximum value of the vehicle speed. Equation (33) shows the relationship between the vehicle speed (V) in mi/h and the slip speed (S), where ω is the angular velocity of the tire in rad/s, r is the tire radius in ft and V_P is the average peripheral speed of the tire in mi/h (see Figure A.1). If the vehicle is at rolling-free mode V_P is nearly equal to V , and the slip speed will be zero (7, 17).

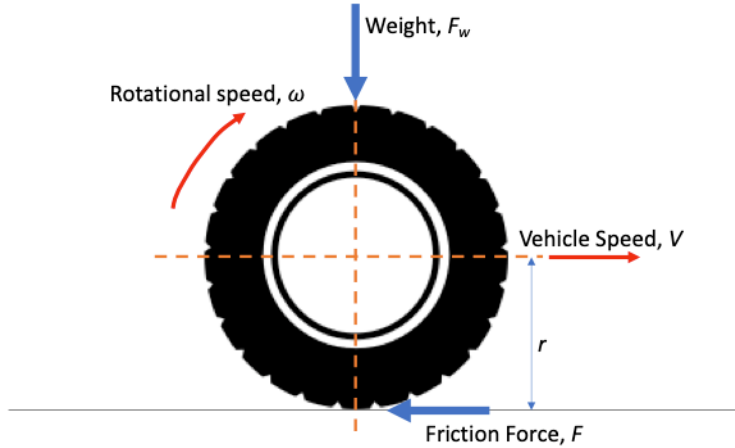


Figure A.1. Friction concept schematic.

$$S = V - V_p = V - (0.68 \times \omega \times r) \quad (33)$$

The slip ratio is defined by Equation (34).

$$SR = \frac{S}{V} \times 100 \quad (34)$$

As soon as the braking maneuver starts, V_p begins decreasing and S increases until the slip ratio (SR) reaches the critical value, $S_{critical}$, which typically occurs at a $SR = 10-25\%$ (3, 4). At that point a peak in the value of the coefficient of friction (μ_{peak}) occurs, see Figure A.2. This friction is the maximum value that can be produced between the tire and the pavement while the wheel has not been fully locked. After the $S_{critical}$ the coefficient of friction start reducing until it reaches a constant value (μ_{slip}) that is maintained when the wheel is fully locked (22).

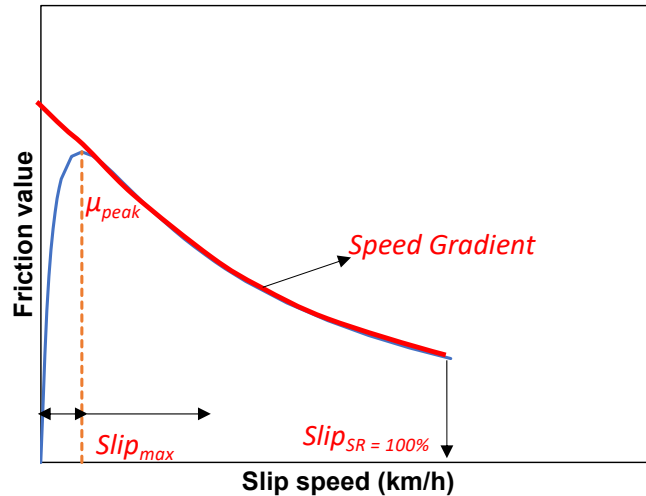


Figure A.2. Friction variation during a braking maneuver.

Existing friction models can be divided into three types: theoretical, empirical, and semi-empirical models (30). Theoretical models focus attention on evaluation of the effects on friction of rubber properties and surface characteristics of pavements; they generally refer to ideal surfaces, and the extension of results to real surfaces is not easy or possible in many cases. Empirical models derive

directly from regression operations according to experimental results (linear or exponential model structures) and most try to relate the friction coefficients to kinematic parameters. In this case, the pavements used for characterization are existing surfaces, and the obtained model is significant only for that specific combination of surface, tire, and external conditions. To address this problem, semi-empirical models have been introduced; they appear to be more practical since computation is considerably reduced compared with theoretical models.

In the literature, friction models have focused on describing the variation of friction values after the peak (μ_{peak}) (7, 13, 22, 32), highlighted in red in Figure A.2. Furthermore, these models focus on predicting the behavior of the speed gradient which is defined as the inverse of the derivative of the friction-speed curve (30). The most popular functional form used to describe the red curve in Figure A.2 is the exponential function (31). The most common semi-empirical models available in literature are the Penn State model and the PIARC model that have served as the basis for standardizing friction values measured with different devices, and the RADO model. These models are described in detail in the next section.

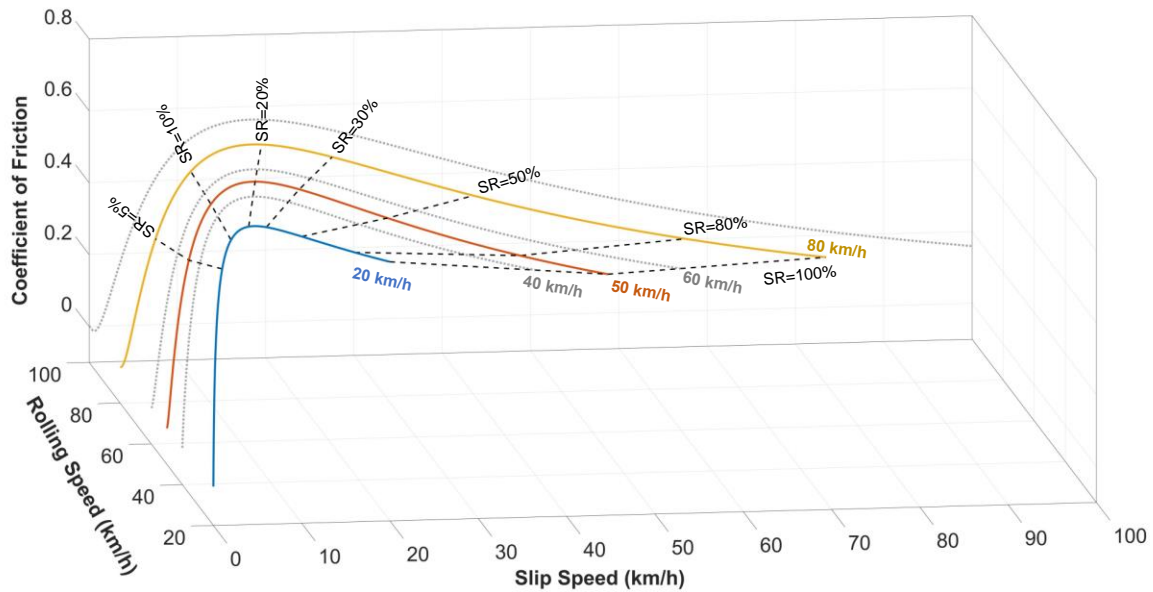


Figure A.3. Three-dimensional representation of the friction surface.

Finally, as indicated in Equation (33) the slip speed S depends on the vehicle speed, hence a braking maneuver as the one depicted in Figure A.2 is a snapshot of the friction variation observed during a braking process made at a given slip speed S . In consequence, the complete friction variation as a function of vehicle speed and slip speed is a three-dimensional surface like the one presented in Figure A.3. In this figure, the black dashed lines represent the friction variation with vehicle speed at a constant slip ratio SR . Most of the Continuous Friction Measurement Equipment (CFME) use a SR that varies between 10-20% and the traditional Lock-Wheel Skid Tester (LWST) uses a SR equal to 100%. If one looks at the three-dimensional surface depicted in Figure A.3 in a two-dimensional plane, then one can appreciate something like the curves presented in Figure A.4.

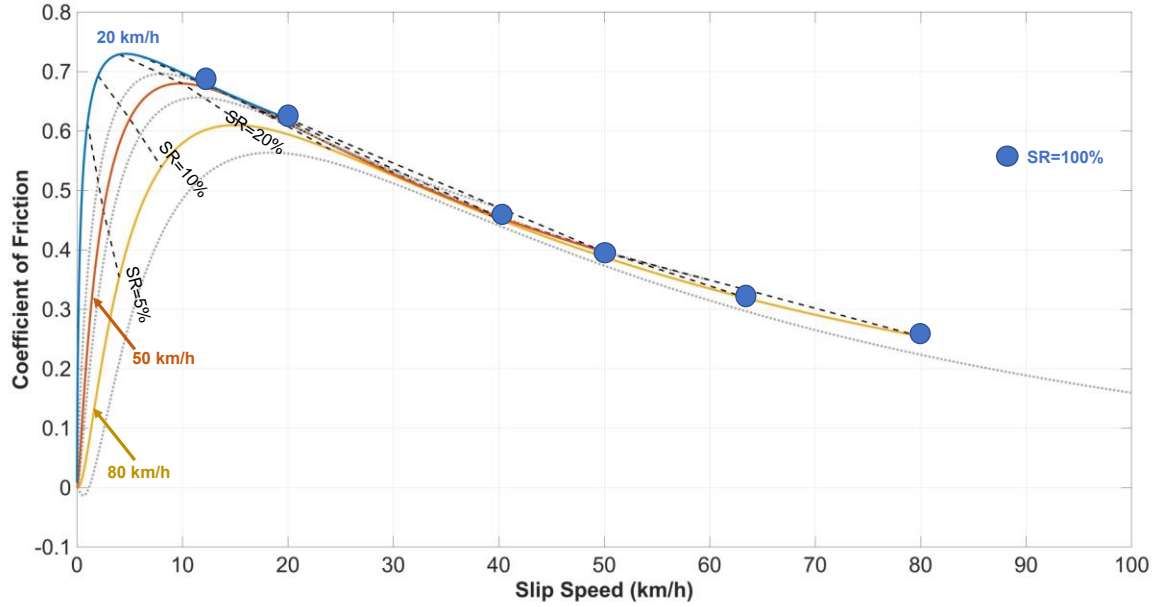


Figure A.4. Two-dimensional representation of the friction surface.

Modeling Friction Variation with Slip Speed

Penn State Model

The Penn State model describes the relationship of friction (μ) and slip speed (S) in an exponential form as shown in Equation (35).

$$\mu = \mu_0 e^{\left(-\frac{PNG}{100} \times S\right)} \quad (35)$$

where;

μ_0 = is the intercept of friction at zero speed, and

PNG = is the percent normalized gradient as defined in Equation (36).

$$PNG = -\frac{100}{\mu} \frac{d\mu}{dS} \quad (36)$$

It has been demonstrated that PNG is constant with speed and therefore Equation (35) is obtained by rearranging Equation (36) and integrating from $S = 0$ to S . Furthermore, it was discovered that PNG is highly correlated with macrotexture and that μ_0 can be predicted from microtexture (friction properties dictated by the aggregate properties, such as mineralogy, shape, and abrasion resistance).

Figure A.5 shows Penn State model predictions for two cases that have the same $F60$ (friction at 60 km/h), one pavement with good microtexture but poor macrotexture, and other with poor microtexture and good macrotexture. As indicated in the figure, though these two pavements have the same friction at 60 km/h they behave differently at different slip speeds. This example demonstrates the need for specifying more than a single value (such as $F60$ using the Penn State model) to describe the skid resistance of a pavement.

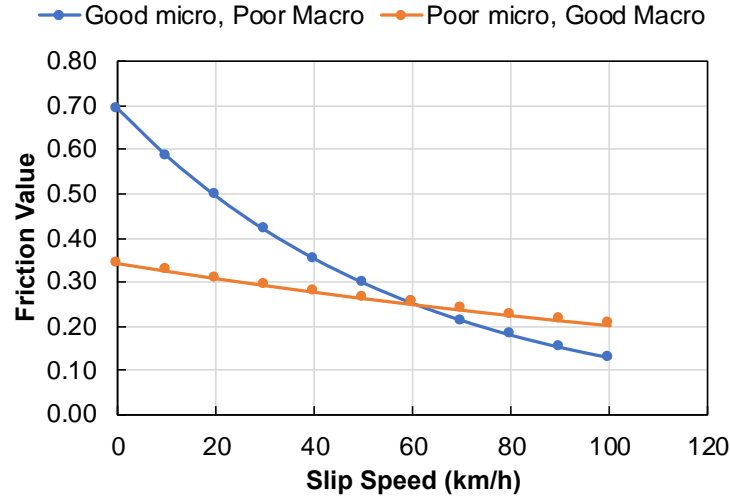


Figure A.5. Illustrative example of the friction variation as a function of the slip speed for two pavements with different macrotexture characteristics.

PIARC Model

The PIARC model is based on the Penn State Model, but in Equation (35) the inverse of PNG is defined as the speed constant S_p and the intercept is shifted to 60 km/h, as shown in Equation (37).

$$F(S) = F60 \times e^{\left(\frac{60-S}{S_p}\right)} \quad (37)$$

where;

$F(S)$ = is the friction at slip speed S , and

$F60$ = is the friction at 60 km/h (38 mph).

As indicated above, the PNG and consequently the S_p is highly correlated to surface macrotexture, whereas μ_0 depends on the surface microtexture. Hence, the PIARC model assumes the friction at 60 km/h (40-mph) is a good representation of the surface microtexture. However, more recently, researchers have advocated to use a better representation of μ_0 by considering the maximum friction (μ_{peak}) in the model derivation (13, 30). One example of this representation is the RADO model discussed below.

The International PIARC Experiment to Compare and harmonize texture and skid resistance measurements was conducted in Belgium and Spain in the fall of 1992. Forty-seven different friction and texture testers from sixteen countries participated. These systems measured 67 different parameters (33 texture parameters and 34 friction parameters). The various friction systems included side force, fixed slip, and locked wheel mechanisms. Each friction tester was operated at three speeds: 30, 60, and 90 km/h (18, 36, and 54 mph), and each tester made two repeated runs at each speed. Texture was measured by both stationary and mobile equipment (33). All texture measurements were made on dry surfaces before any water was applied to the roadway. As a control, a microtexture measurement was made before and after the skid testers made their tests. This data was used to show that there were no statistically significant changes occurring during the testing.

The Penn State Model was chosen as the basis for the analysis of the data from the PIARC experiment and the development of the International Friction Index (*IFI*). The harmonization

process allows skid resistance to be measured by any of the measurement methodologies and the result reported on a common scale. The *IFI* consists of two parameters, one is the wet pavement friction (S_p) that is related with the *MPD*, and the other is the calibrated wet friction at 60 km/h (40 mph) denoted as *F60*. The advantage of the *IFI* is that the value of *F60* for a pavement will be the same regardless of the slip speed, which permits the test vehicle to operate at any safe speed, for example, at higher speeds on high-speed highways and lower speeds in urban situations. When the *IFI* is reported one must include both the S_p and *F60*.

The calculus of the *IFI* consist of the following steps (ASTM E1960-07):

1. Measure and compute the *MPD*.
2. Measure the friction at a given speed slip speed S , this will be the $FR(S)$.
3. Calculate the speed constant, S_p in km/h, using the following equation:

$$S_p = 14.2 + 89.7 \times MPD . \quad (38)$$

4. Using the S_p coefficient obtained in the last step, adjust the friction measurement made at the slip speed S , i.e. $FR(S)$, to obtain the friction at 60 km/h, i.e. $F(60)$, using Equation (39).

$$F(60) = FR(S) \times e^{\frac{(S-60)}{S_p}} \quad (39)$$

5. The final step in the harmonization is the calibration of the equipment used for measurement, by regression of the adjusted measurement $FR(60)$, with the calibrated friction number $F(60)$:

$$F(60) = A + B \times FR(60) . \quad (40)$$

RADO Model

As a tire changes from the free rolling condition to the locked wheel condition under braking, the friction increases from zero to a peak value and then decreases to the locked wheel friction, as indicated in Figure A.2. According to Rado (34), the friction before the peak is mainly related to tire properties, whereas the friction after the peak depends on the pavement surface characteristics. Different from the preceding models, the RADO model describes the entire friction-slip speed curve and serves as the basis for the ABS braking system. Equation (41) presents this model.

$$\mu(S) = \mu_{\max} \times e^{\left(- \left[\frac{\ln(S/S_{\max})}{C} \right]^2 \right)} \quad (41)$$

where;

$\mu(S)$ = friction at slip speed S ,

μ_{\max} = maximum friction value,

S_{\max} = slip speed at the maximum friction, and

C = shape factor that determines the skewed shape of the friction curve.

The PIARC and Penn State model are a particular case of the RADO model, the S_p constant is the inverse of the derivative of the friction curve $\mu(S)$ at slip speed S equal to 60 km/h and at slip ratio $SR = 100\%$, when it is transformed to a logarithmic form.

In the PIARC friction model, which is primarily intended for long-term monitoring of the pavement, the steady state value of friction, $F(S)$, is calculated. This value occurs at 100% slip

(fully locked wheel), and it decreases with increasing slip speed. Although the *IFI* describes the friction experienced by a driver in emergency braking, when the transient part happens so quickly that only the steady state needs to be used, cars with ABS follow a different pattern. In these cases, a different model that captures the influence of the tire design and material in addition to texture, slip speed, and measuring speed is needed and the RADO model serves as this alternative (30).

An example of the RADO model derivation is presented in Figure A.6. Part (a) of this figure depicts the friction variation with vehicle speed; these friction values were collected in road section with homogeneous surface, i.e., a pavement that was recently overlaid sufficiently long to collect measurements at different speeds. The yellow points are the arithmetic average computed in increments of 10 km/h (6.3-mph). An exponential model was fit to the yellow points obtaining the model shown in Figure A.6 (a).

It is important to notice that Figure A.6 shows the friction variation with vehicle speed, but the BV-11 uses a $SR = 17\%$. So, in order to apply the model described by Figure A.2 it is necessary to use Equation (34) to compute the slip speed. To derive the RADO model for this pavement, the procedure described by Leandri and Losa (30) was applied. According to these authors, for each slip speed it is necessary to estimate the three parameters of Equation (41); three observations are needed for this purpose and these can be obtained as follows:

- The observed friction should be equal to the prediction made with the RADO model; this is the friction at V_i should be equal to $\mu(0.17 \times V_i)$.
- The RADO model, $\mu(S)$, and the *IFI* curve, $F(S)$, have the same tangent, and
- The RADO model, $\mu(S)$, and the *IFI* curve, $F(S)$, have the same value at the same slip speed and at the same slip ratio ($SR = 100\%$).

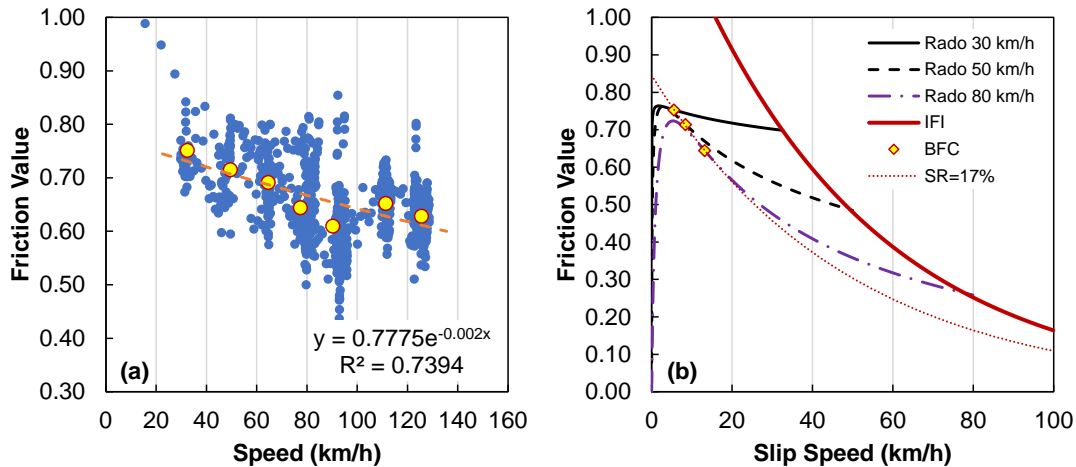


Figure A.6. (a) Friction values collected with the BV-11 Moventor Skiddometer, and (b) Rado Model development.

These conditions are stated in Equation (42). Finally, because in the derivation is necessary to use the *IFI* model, the model fitted with yellow points in Figure A.6 (a) is used to calculate the friction corresponding to a slip speed equal to 60 km/h.

$$\min \left(\sum_{i=1}^3 \left\{ \left(BFC(V_i) - \mu(0.17 \times V_i) \right)^2 + \left(F(V_i) - \mu(V_i) \right)^2 + \left(\frac{\partial F(V_i)}{\partial S} - \frac{\partial \mu(V_i)}{\partial S} \right)^2 \right\} \right) \quad (42)$$

where;

BFC = friction coefficient measured with the BV-11 at a given speed (V_i),

$\mu(S)$ = friction predicted with the RADO model, and

$F(S)$ = friction predicted with the IFI model.

The resulting RADO model for each vehicle speed (30 km/h, 50 km/h, and 80 km/h) are illustrated in Figure A.6 (b). As depicted in this figure, this methodology can be used to calibrate the RADO model by fitting the three curves simultaneously, this procedure can be used to fully describe the available friction for a given pavement.

Modeling Friction and Texture Variation with Traffic/Time

Figure A.7 shows the general model that is internationally accepted to represent skid resistance performance over time (3). For a new pavement, an initial skid resistance increase appears if the aggregates are covered by a bituminous film. After the bituminous film is worn away, the aggregate microtexture is exposed to traffic and, hence, skid resistance increases. Then, once exposed, aggregates suffer from a normal polishing process and their friction level is reduced, until an equilibrium phase is achieved, where the skid resistance tends to follow an asymptotic.

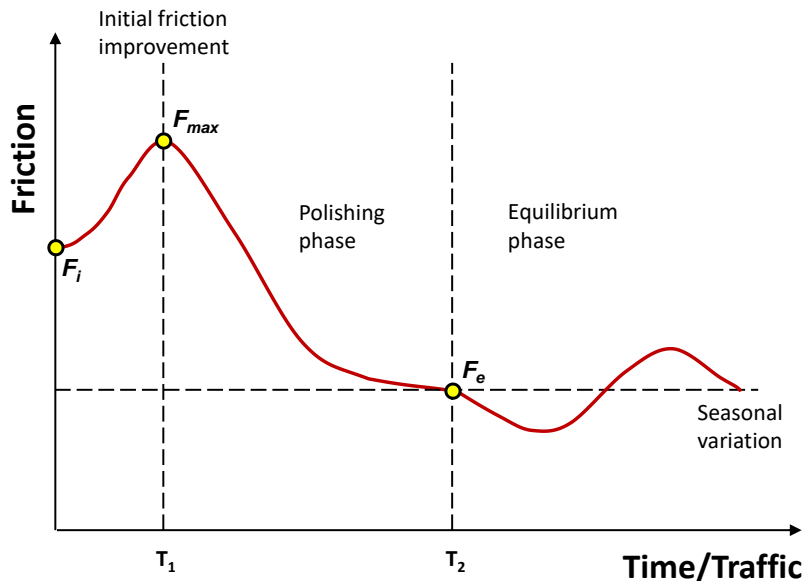


Figure A.7. Skid resistance variation with time or traffic.

No consensus exists about the duration of each phase. For the elimination of the bitumen cover of the aggregates ($age < T_1$), it depends on the binder type and heavy traffic characteristics. For example, in Spain it has been observed T_1 might last 2 or 3 months for dense graded AC mixes, but it may extend during the whole life cycle of the pavement surface for Stone Mastic Asphalt (SMA) mixes (10). Similarly, the results of the FHWA/NC 2020-11 project (2) suggested friction can increase as much as 50% of the initial value after construction, and on average it takes 4.0 million traffic repetitions for this increment to occur. In contrast Woodward et al. (10), have found T_1 might last 4 years for polymer modified mixes. Regarding the polishing phase duration (the time between T_1 and T_2) the published literature has reported a range from approximately five years (35) to one year (36).

On the other hand, once the equilibrium phase is reached (after T_2), if everything remains constant (traffic levels and weather patterns) the only friction variation is due to a seasonal effect. On dry roads, generally in the summer, the polishing effect action of traffic is dominant, but, when the road pavements are wet for long periods, normally in winter, surfaces recover some of their former texture and harshness (7). Since road agencies must assure a minimum friction on the roads in their network, knowing the minimum level of skid resistance available is a vital interest in their pavement management system and, hence, it is preferable to evaluate the network in the summer.

The British highway agency (BHA) applies a seasonal correction factor ($C_{seasonal}$) for those measurements that are collected during the winter when considering the seasonal variation. The BHA characterize the friction at a network level during the summer when the friction is at its lowest values, to capture year to year variation it is necessary to measure friction every year and correct the measurements to remove any atypical fluctuation. This correction is done comparing each measurement with the average of the past three measurements (37), as shown in Figure A.8. For modeling the seasonal variations of skid resistance, sinusoidal models have been the dominant model type proposed in the literature (12, 38).

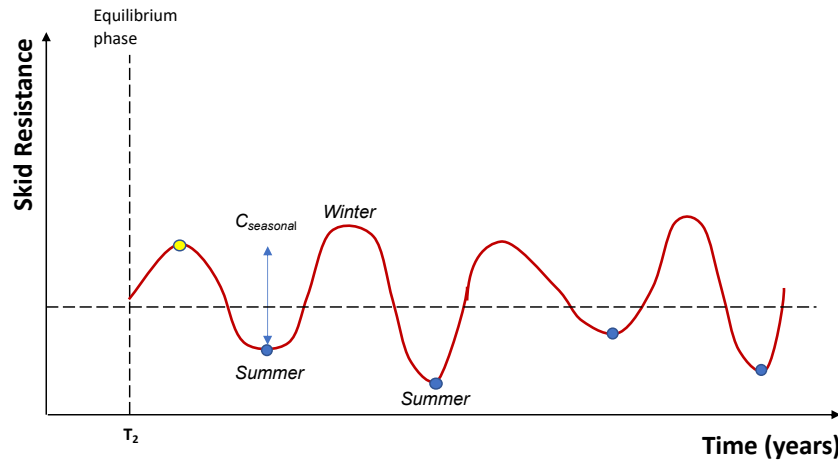


Figure A.8. Data collection plan used by the British Highway Agency (BHA).

The amount of polishing has been found to be proportional to the traffic intensity (usually expressed in vehicle per day per lane or heavy vehicles per day per lane), not to the cumulative traffic (number of vehicles that passed during the period of analysis). In fact, some authors had reported that if traffic intensity is reduced, friction degradation due to polish may recover to some extent (35). This effect is also shown in Figure A.9.

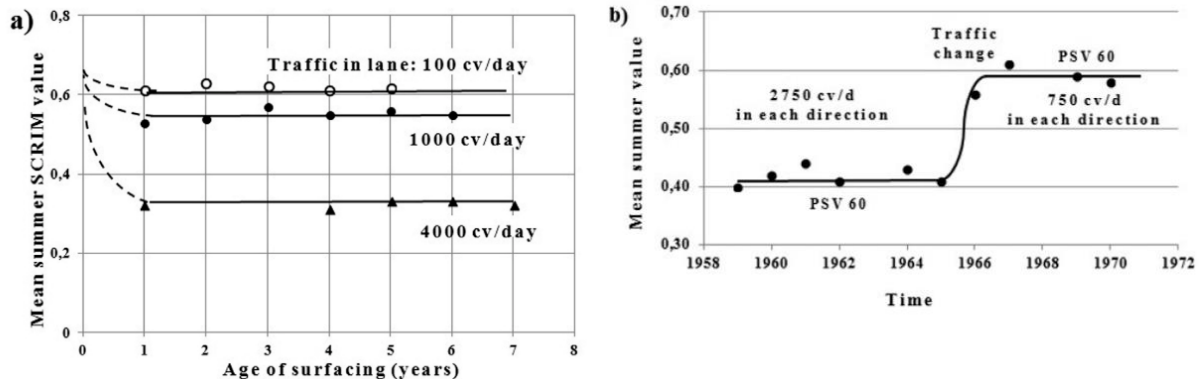


Figure A.9. Mean Summer SCRIM coefficient (MSSC) variation: (a) with constant heavy traffic volume, (b) with changing heavy traffic volume (35).

The general macrotexture performance model, depicted in Figure A.10, includes four components: initial macrotexture (M_i), equilibrium macrotexture (M_e), time to equilibrium (T_1), and the harmonic characteristics of the seasonal effect. The general model suggests that macrotexture is maximum immediately after construction and decreases as the binder film wears off from the aggregate. Some have suggested that the densification of the surface asphalt mixture also contributes to a reduction in the macrotexture (13). It is generally accepted and proven that texture values do not vary substantially due to the traffic polishing effect and the only source of variation is caused by the seasonal effect. It is important to note that other factors may contribute to an increase in macrotexture during a pavement’s service life. For example, age-induced raveling/loss of surface fines may increase the surface texture (4). In the following sections a summary of the most relevant work proposed to describe each of these phases is presented.

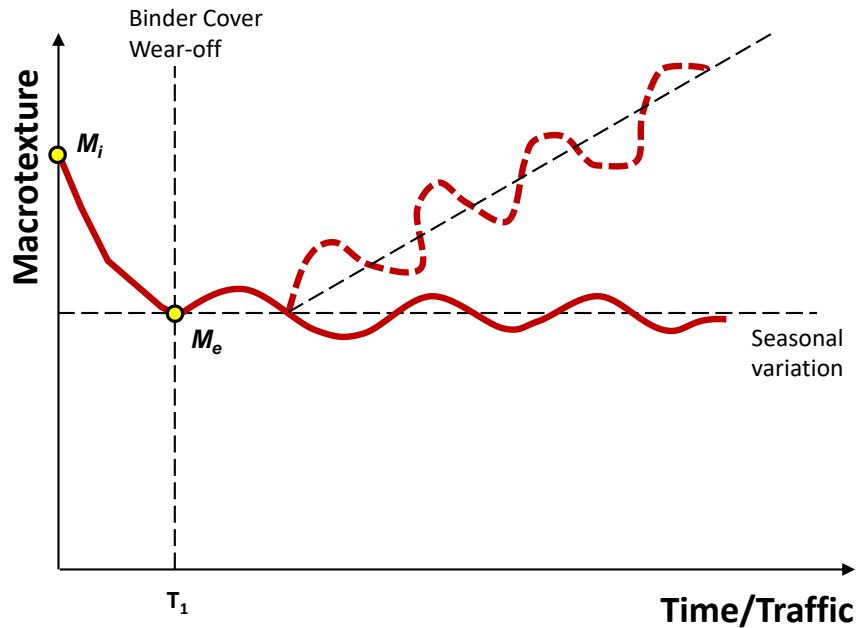


Figure A.10. Macrotexture variation with time or traffic.

Early Friction and Texture Development (Before T_1)

With respect the early friction and texture development different models have been developed to relate the mixture volumetric properties to the friction and texture measured in the lab, also a few of these have also evaluated the relationship between the lab measurements and the field observations.

Polishing Phase (Between T_1 and T_2)

One of the first friction prediction models was proposed by Szatkowski and Hosking (39) who used a dataset collected in the period of 1960 to 1970 across 139 roadway segments. The Skid Friction Coefficient (SFC) values were an average value of mean summer values with known aggregate PSV which resulted in the development of Equation (43) and Equation (44) with a coefficient of determination R^2 equal to 0.92 and 0.84, respectively. This model does not account for seasonal variation explicitly, so it is necessary to standardize the measurements first.

$$MSSC = 0.024 + 0.663 \times 10^{-4} \times Q_{CV} + 1 \times 10^{-2} \times PSV \quad (43)$$

$$MSSC = 0.024 + 0.15 \times 10^{-4} \times Q_{TV} + 1 \times 10^{-2} \times PSV \quad (44)$$

where;

$MSSC$ = Mean summer scrim coefficient measured by a SCRIM device at 50 km/h,

PSV = Polish stone value of the aggregates (with a range of 0 to 100),

Q_{CV} = number of commercial vehicles per lane per day (a commercial vehicle is defined as one with a mass greater than 1500 kg), and

Q_{TV} = number of total vehicles per lane per day.

This equation set the basis for the development of a friction management program in the United Kingdom, because it allowed one to predict the friction values as a function of the traffic intensity and the aggregate properties of the mix. This equation also showed that the effect of traffic on the SFC is not cumulative from year to year. Nevertheless, a more complete research study was conducted and demonstrated that Equation (43) and (44) predicted higher values on roads with lower levels of heavy traffic and underestimated the available friction with higher levels of heavy traffic volumes.

Based on Equation (43), New Zealand proposed Equation (45) with a coefficient of determination R^2 equal to 0.28. After a slight correction to Equation (45) (for example, accounting for the fact that in the United Kingdom derivation only straight segments were included in the analysis, while in New Zealand all type of segments were evaluated, including curves and ramps) and comparing the predictions with the ones made with Equation (43), the New Zealand department of transportation proposed Equation (46).

$$SFC_{50} = 0.018 + 0.311 \times 10^{-4} \times CVD + 0.637 \times 10^{-2} \times PSV \quad (45)$$

where;

SFC_{50} = mean summer scrim coefficient measured at 50 km/h using a SCRIM device.

CVD = number of commercial vehicles per lane per day (a commercial vehicle is one with a mass greater than 3500 kg), and

PSV = Polish stone value of the aggregates (with a range of 0 to 100).

$$PSV = 100 \times ESC_{50} + 0.00663 \times CVD + 2.6 \quad (46)$$

where;

ESC_{50} = Equilibrium skid resistance coefficient, i.e., the SCRIM coefficient measured at 50 km/h and corrected for seasonal and yearly variations.

Another approach was made by Jayawickrama and Thomas (38), who developed a model for describing the seasonal variation of the friction numbers. The authors used LWST for collecting friction biweekly at three different climate regions in Texas. For each region, the measurements were collected at two different sites meaning a total of six locations were analyzed. Then the authors related the observed friction variation with the observed climate record and obtained Equation (47). A reduced variant of the model shown in Equation (47) can be made to analyze only the long-term variation of the skid resistance. For this model, the only explanatory variable is the Julian calendar days (JD).

$$SN_{64} = 32.28 - 0.14 \cdot TEMP_5 + 0.031 \cdot RF_5 - 0.66 \cdot \sin\left[\left(\frac{2\pi}{365}\right)JD\right] + 13.53 \cdot I_1 - 3.12 \cdot I_2 - 2.78 \cdot I_3 + 9.52 \cdot I_4 + 7.43 \cdot I_5 \rightarrow R^2 = 0.917 \quad (47)$$

where;

SN_{64} = Skid number at 64 km/h (~40 mph),

$TEMP_5$ = Average of daily temperatures for the 5 days before the measurements,

RF_5 = Cumulative rainfall over the 5-day period before the measurements,

JD = Julian calendar day, and

I_1, \dots, I_5 = Indicator variable that identify the pavement section.

Similar work was conducted in New Zealand by Cenek et al. (12), who used a long-term friction value measured using a British Pendulum Tester and a Grid Tester in a manual mode. The authors proposed the functional form shown in Equation (48) to account for yearly seasonal variations. The idea of this function was that friction measurements could be made at any time in the year and then corrected to a certain predefined period of interest. For example, correcting the winter measurements to equivalent summer values. The authors mentioned in their report that the BPT model is more accurate because more data was available for calibration.

For the British Pendulum Tester

$$BPN = BPN_{terminal} - 5 \cdot \cos\left(\frac{2\pi}{365.25} \cdot JD\right) \quad (48)$$

For the GripTester

$$GN = GN_{terminal} + 0.002 \cdot \cos\left(\frac{2\pi}{365.25} \cdot JD\right)$$

where;

$BPN_{terminal}$ = BPN measured,

BPN = BPN corrected for seasonal variation,

$GN_{terminal}$ = Grip number measured in tow mode,

GN = Grip number measured in tow mode corrected for seasonal variation, and

JD = Julian calendar day.

Texas A&M University researchers developed a friction prediction model based on both laboratory and field measurements. Rezaei and Masad (40) described the complete process of the model, which included two phases: in the first phase a model that relates the friction variation with the number of polishing cycles applied in the lab was developed, and in the second phase a model that relates the traffic intensity, i.e., the number of vehicle pass observed in the field was combined with the model developed in phase one. The model developed in phase one was calibrated using a Dynamic Friction Tester (DFT) at 20 km/h and a Circular Track Meter (CTM). The model that relates the *IFI* with the mixture properties is shown in Equation (49) (41).

$$IFI(N) = a_{mix} + b_{mix} \times \exp(-c_{mix} \times N) \quad (49)$$

where;

IFI = is the international friction index,

$a_{mix}, b_{min}, c_{mix}$ = coefficients of the model and represent the terminal, initial and rate of change, respectively, and

N = number of polishing cycles, expressed in thousands.

In the second phase, the authors developed a skid resistance prediction model, which included the aggregate texture and gradation of the aggregates and traffic volume from field measurements. The traffic modification factor (*TMF*) was defined as follows:

$$TMF = \frac{AADT(\text{for outer lane}) \times \text{years in service} \times 365}{1000} \quad (50)$$

The relationship between the *TMF* and the number of polishing cycles *N*, was derived using a non-linear least square regression analysis of the expression shown in Equation (51). Consequently, combining Equation (49) and (51) the *IFI* can be expressed by Equation (52). This Equation shows that the decrease of skid resistance depends on the aggregate characteristics but in both cases, it tends to an asymptotic value after polishing cycles.

$$N = TMF \times 10^{(1/(A+B \times b_{mix} + 1/c_{mix}))} \quad (51)$$

where;

A, *B*, *C* = regression coefficients equal to -0.421, -58.95, and $5.8.34 \times 10^{-6}$, respectively.

$$IFI(TM F) = a_{mix} + b_{mix} \times \exp\left(-c_{mix} \times TMF \times 10^{(1/(A+B \times b_{mix} + 1/c_{mix}))}\right) \quad (52)$$

The Wisconsin Department of Transportation (WDOT) uses the model developed by Russell to predict *FN* as a function of asphalt material properties, age of pavement, traffic conditions, and climate. The model is shown in Equation (53).

$$FN = 41.4 - 0.00075 \cdot D^2 - 1.45 \cdot \text{Log}(LAVP) + 0.245 \cdot LAWEAR \quad (53)$$

where;

FN = friction number calculated for a LWST at 40-mph,

D = %dolomite in the mix,

LAVP = lane accumulated vehicle passes, and

LAWEAR = aggregate wear in Los Angeles machine.

Finally, Perez-Acebo et al. (3) developed a model similar to the one shown in Equation (43) for the region of Viscaya in Spain. During the analysis the authors evaluated different variables such as AADT, pavement structure, material properties, aggregate polish resistance, and rainfall intensity. The authors concluded that friction may be predicted using traffic intensity and aggregate *PSV* values and confirmed that friction is not related to pavement age or cumulative traffic.

In the case of texture Miao et al. (14) evaluated the degradation of mean texture depth (*MTD*) with traffic and developed the model structure indicated in Equation (1). To develop these models, field tests were collected seven times in two years. Two highway sections were included in the field test, covering four surface types. Macrotexture was characterized using the Sand Patch Test (SPT).

$$MTD = a \cdot \text{Log}(\text{Traffic}) + b \quad (54)$$

where;

a and *b* = regression coefficients that take the value shown in Table A.1.

MTD = mean texture depth measured with a SPT, in mm.

Table A.1. Fitting coefficients of the logarithmic model for MTD (14).

Surface Type	Dense Mixes	Rubber Asphalt Concrete	SMA	UTWC
<i>a</i>	-0.1406	-0.1245	-0.0648	-0.0978
<i>b</i>	0.6128	0.8733	0.8542	0.9906
<i>R</i> ²	0.815	0.901	0.594	0.831

Wu and Abadie (13) conducted a similar study to characterize friction and texture in the laboratory and then validated their results with field observations. They also observed a texture variation like the one shown in Equation (1), i.e., texture values decays with traffic repetition, though they did not estimate the model coefficients. In addition, the raveling process described in Figure A.10 has been observed by at the National Center for Asphalt Technology (NCAT) facility. Several field observations have been conducted as part of the Phase VII (2018-2021) of the NCAT Test Track findings (15). In these experiments a power growth in texture values has been observed until which texture values seem to remain constant. Interestingly though, in some cases traffic seems to be the causative factor, in others the best descriptor of this process in the pavement age.

Portland Concrete Pavements

Using two-year data from 11 pavement section in the state of New York, Grady and Chamberlin (42) estimated the decay in grooved textures and developed models relating skid number with mean groove depths as well as with traffic passes, the proposed models are shown in Equation (55) to Equation (57).

$$\text{Log}(SN_{40}) = 1.64 - 0.13\text{Log}(CVP) \rightarrow R^2 = 0.79 \quad (55)$$

$$MTD = 0.037 - 0.0044mvp \rightarrow R^2 = 0.17 \quad (56)$$

$$MGD = 0.128 - 0.013mvp \rightarrow R^2 = 0.16 \quad (57)$$

where;

*SN*₄₀ = skid number measured at 40-mph with a LWST,

CVP = cumulative vehicle passes, in millions,

MTD = mean texture depth, in in.,

mvp = million vehicle passes, and

MGD = mean groove depth, in in.

In 1998, Drakopoulos et al. (43) presented the model used by the Wisconsin Department of Transportation (WDOT) for estimating the deterioration of transversely tined concrete pavement surface friction over time. The model is shown in Equation (58), but was limited to single-tine texture only. Additionally, the positive sign associated with HV is counterintuitive because friction is expected to reduce with an increase in heavy vehicle percentage in the design lane. An *R*² of the model was not provided in the paper.

$$\text{Log}(FN) = 3.99 - 0.0419\text{Log}(LAVP) - 0.00129DOL + 0.00474HV \quad (58)$$

where;

FN = predicted friction number at 60 km/h (40-mph)

LAVP = summation of all vehicles expected to pass over the surface during the design life, in millions,

DOL = limestone, dolomite, or ankerite content of coarse aggregate materials, in % weight, and

HV = percentage of heavy vehicles in the design lane.

On the other hand, Rao et al. (44) suggested a regression model to estimate the longevity of diamond ground concrete pavements as a function of age and climate as indicated in Equation (59). It should be noticed that the model shown in Equation (59) does not include a traffic variable. The service life observed in the pavements used in the study was around 10 years, after which re-grinding or another measured was required.

$$MTD = 0.887 - 0.152(1 + 0.233Freeze) \text{Log}(Age) \rightarrow R^2 = 0.83 \quad (59)$$

where;

MTD = mean texture depth, in mm,

$Freeze$ = dummy variable defined as 1: wet/dry non freeze and 0: wet/dry freeze), and

Age = age of the pavement since the grinding was applied.

Ahammed and Tighe (8) studied the long-term friction variation in portland concrete pavements (PCP). One challenge of this surface type is to provide a durable surface with adequate skid resistance for economy and safety. The authors examined the long-term frictional performance of eight different surface textures on 197 sections within the long-term pavement performance database (LTPP). The analysis showed that tined and (or) grooved textures maintain consistently higher skid resistance over time and the surface friction of concrete pavements is less sensitive to ambient temperature. Another interesting finding was that friction values seem to be more sensitive to the cumulative traffic volume than to the cumulative axle-load.

The surface texture methods analyzed by Ahammed and Tighe were longitudinal tine, broom drag, burlap drag, grooved float, astroturf drag plus longitudinal tine, and burlap drag plus transverse tine. The independent variables evaluated to describe friction were vehicle speed in km/h (S); compressive strength of concrete in MPa (CS); cumulative traffic passes of all vehicles in thousands (V) equal to age x AADT; cumulative traffic passes of passenger cars in thousands (VPC); cumulative traffic passes of trucks in thousands (VT); and percent of trucks (TP). The texture characteristics were incorporated in the model by a set of categorical variables: texture code (TC), 1 for grooved and 0 for dragged; texture rank (TR), 1 for drag plus transverse tine, 2 for drag plus longitudinal tine, 3 for longitudinal tine, 4 for grooved float or diamond ground-groove, 5 for burlap or broom drag, and 6 for astroturf drag; texture factor (TF), 1.16 for drag plus transverse tine, 1.10 for drag plus longitudinal tine, 1.02 for longitudinal tine, 0.98 for grooved float or diamond ground-groove, 0.92 for burlap or broom drag, and 0.85 for astroturf drag.

The models developed by Ahammed and Tighe are summarized in Equation (60) to (64).

$$FN = 63.467 - 0.322S + 4.278TC - 0.041VPC - 0.131VT + 0.065CS \rightarrow R^2 = 0.461 \quad (60)$$

$$FN = 74.140 - 0.321S - 2.316TR - 0.041VPC - 0.119VT + 0.075CS \rightarrow R^2 = 0.484 \quad (61)$$

$$FN = 76.293 - 0.325S - 2.291TR - 0.054V - 0.040TP + 0.050CS \rightarrow R^2 = 0.498 \quad (62)$$

$$FN = 23.877 - 0.319S + 42.250TF - 0.026VPC - 0.139VT + 0.072CS \rightarrow R^2 = 0.478 \quad (63)$$

$$FN = 26.535 - 0.319S + 41.355TF - 0.052VPC - 0.037VT + 0.053CS \rightarrow R^2 = 0.487 \quad (64)$$

Finally, more recently, Gu et al. evaluated a model to predict the SN measured with a LWST and the SR measured with a SCRIM tester. For this purpose, the authors collected a series of sequential measurements at NCAT, friction was quantified by a LWST and a SCRIM machine, whereas

texture was characterized by the CTM. The experimental design considered three measurement speeds (30, 40, and 50-mph), and three air temperatures (morning, noon, and afternoon measurements). The resulting models are shown in Equation (65) and (66).

$$SN = C_1 + 65.51 - 0.3056 \cdot V + 4.068 \cdot MPD - 0.1549 \cdot T_{air} \quad (65)$$

$$SR = C_2 + 80.739 - 0.2527 \cdot V + 1.122 \cdot MPD - 0.4448 \cdot T_{air} \quad (66)$$

where;

C_1 and C_2 = are regression coefficients dependent on surface type (i.e, dense graded, OGFC, SMA, HFST, and chip seal) and aggregate type (i.e., limestone and granite),

SN = skid number measured with a LWST,

SR = scrim reading measured with a SCRIM machine,

V = measurement speed, mph,

MPD = mean profile depth measured with a CTM, in., and

T_{air} = air temperature in Celsius degrees.

Knowledge Gaps

The most popular friction related index currently used is the *IFI*, this index assumes that the microtexture friction component can be described by the friction value measured at 60 km/h (40-mph), whereas the speed gradient fully depends on the macrotexture. However, this model has some flaws:

- Currently, researchers most commonly advocate describing microtexture using static observations, such as the ones collected with a DFT at 20 km/h (12-mph). Typically, these measurements are combined with other aggregates friction characteristics, such as the polish resistance measured with a TWPD or Los Angeles test.
- Though in the original PIARC test different friction measurement techniques were used, most of the applications with the *IFI* model, especially in the U.S., have used a LWST to characterize friction. There is a need to expand these observations using CFME.
- The speed gradient in the *IFI* model was described solely with the *MPD*. But nowadays, it has been shown there are other texture parameters that better correlate with friction.
- The friction variation models with time/traffic have not directly incorporated the seasonal variation. This effect, as shown by some researchers, may cause significant variations in the friction values. Also, most of these models have been derived using a LWST or a BPT.
- In the U.S., a few works have been made to relate the traffic polishing resistance simulated in the lab with the actual polishing observed in the field. However, these works have used a LWST to characterize friction in the field.

Laboratory Evaluation of Skid Resistance

Currently, there are a few options available to measure friction in the lab, as indicated in Table A.2. From these alternatives, the Dynamic Friction Tester (DFT) is currently the most popular because it solves some of the weakness of the British Pendulum Tester (BPT) but keeps the portability and capability of measuring friction both in the lab and in the field. The Wehner/Schulze (W/S) device is used mostly in Europe; however, is the most expensive option and can only be used in the laboratory.

Table A.2. Devices used for friction measurement in the laboratory (7, 45).




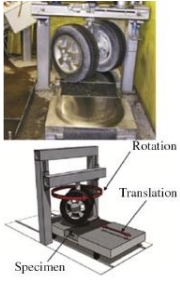
Dynamic Friction Tester (DFT) (46)	British Pendulum Tester (BPT) (47)	Wehner/Schulze Friction Test Device (W/S) (48)
Three 20-mm by 16-mm rubber sliders located at 120° on a rotary disc friction head accelerate to a tangential speed of 80 km/h while water is sprayed on the surface at a rate of 3.6 liters per min. The motor is then stopped, and the head assembly is lowered so that the contact pressure between the rubber pads and specimen with outer and inner diameters of 356 and 203 mm is 150 kPa. The system records the friction speed curve during the test.	A 25-mm by 32-mm rubber slider attached to a 1,500-g weight is released from a locked position to contact the surface of an 89-mm by 45-mm specimen. The elevation to which the slider arm swings is the friction value.	Three 30-mm by 15-mm rubber sliders positioned at 120° on the rotary disc friction head accelerate to a tangential speed of 100 km/h while water is sprayed on the surface to create a film thickness of about 0.5 mm. The motor is then stopped, and the head assembly is lowered so that the contact pressure between the rubber pads and surface of the circular specimen with a diameter of 225 mm is 200 kPa. The system records the friction-speed curve during the test.

Except for the W/S device that has the capability of simulating traffic polishing, these devices are coupled with separate equipment to simulate traffic polishing. The most common coupled system nowadays is the DFT-TWPD, where TWPD stands for Three Wheel Polishing Device. See Table A.3 for references of each device.

Aggregate Skid Resistance Contribution

The recently published AASHTO provisional standard titled “PP103, Provisional Standard Practice for Sample Preparation and Polishing of Unbound Aggregates for Dynamic Friction Testing” recommends the use of a TWPD for polishing and a DFT for measuring the friction of aggregates (49). AASHTO PP 103 recommends using a polishing device that has three patterned pneumatic tires and can exert 0.65 ± 0.02 kN (146 ± 5 lbs) to the test surfaces. Besides the TWPD and the DFT, a circular casting mold made of stainless steel (or another suitable material) capable of molding a specimen is needed. The dimensions of this mold are such that it has an outside diameter of 355.6 mm (14 in.), an inside diameter of 209.6 mm (8.25 in.), and height of 25 mm (1 in.) as indicated in Figure A.11 (a). The circular mold is capped with a sturdy metal plate of 10 kg (22 lbs) and placed in a square sample holder for friction testing with the DFT, see Figure A.11 (b) and (c), respectively.

Table A.3. Device used to simulate traffic polishing in the laboratory (7, 45).

Three Wheel Polishing Device (TWPD) (49)	British Wheel Test (Polished Stone Value - PSV) (50)	Wehner/Schulze Device (W/S) (48)	Aachen Polishing Machine (APM)
<p>Three 203-mm-diameter and 51-mm-wide rubber tires attached to a rotating weighted carriage travel over the specimen surface at 60 rpm while a total load of 68 kg is applied to the specimen surface.</p>	<p>A 203-mm-diameter and 51-mm-wide rubber-tired wheel rotates at a speed of 320 rpm while applying a 400-N load on a ring of specimens. During the polishing process, a mixture of silicon carbide grit and water is fed to the surface.</p>	<p>Three conical roller rubbers rotate at 500 rpm over the specimen surface while applying a contact pressure of 400 kPa. During the polishing process, a mixture of 5% quartz powder and 95% water is pumped onto the surface.</p>	<p>A pair of passenger car wheels (165/75 R14) with a tire pressure of 2 bar moves across the specimen surface in a combined rotational and translational motion while a 1,500-N load and polishing agents and water are applied to the surface.</p>
			

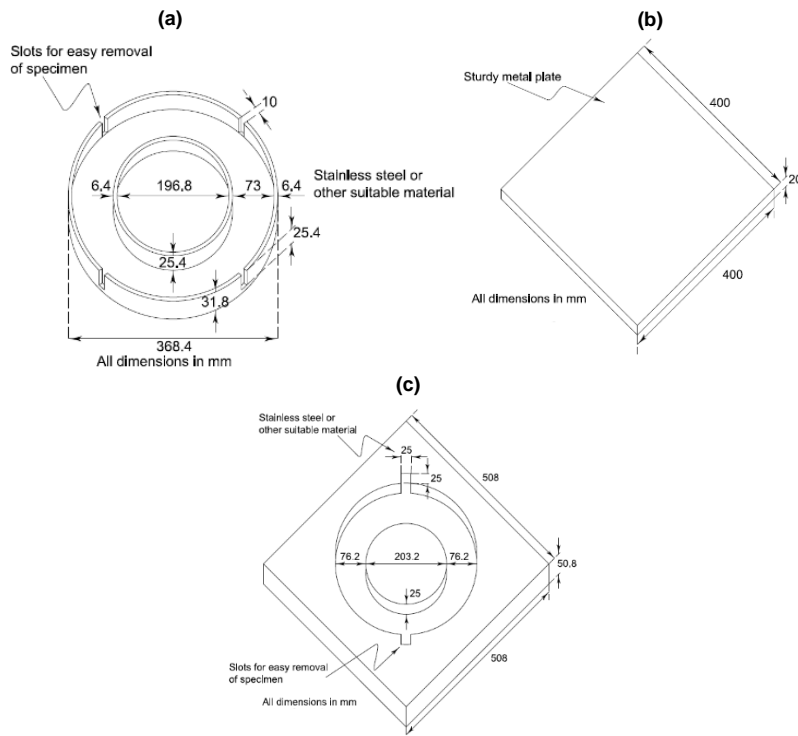


Figure A.11. (a) Circular casting mold, (b) capping mold, and (c) square sample holder (49).

The standard includes two methods, Method A for unbound coarse aggregate (passing 12.5 mm sieve and retained in 9.5 mm sieve) and Method B for fine aggregates (passing 4.75 mm sieve and retained on the 1.18 mm sieve) used for pavement surface treatments. Both methods consist of the following steps:

- Step 1: grease the circular mold.
- Step 2: manually place one layer of the aggregates and pack them very tightly placing the flat face downwards.
- Step 3: fill the voids between the aggregates using fine sand or glass beads.
- Step 4: pour a mixture of polyester resin, extender pigment, and silica in top of the aggregates.
- Step 5: place the capping mold on top of the mold the squeeze out the extra bounding agent and form a smooth surface. The specimen must be demolded after a minimum of 12 hours. The specimens look like the one shown in Figure A.12.



Figure A.12. Finished specimen (49).

The procedure described above might take more than 15 hours to obtain a single test result. Also, this method is costly and each specimen costs around \$30 (45). Recently, Saghafi et al. (45) analyzed the protocol of the AASHTO PP 103-20 and proposed a modification to reduce both the cost and time of the specimen preparation. The study consisted of two phases, the first compared the results from a new proposed aggregate specimen preparation method with the AASHTO PP 103 method using four different aggregate sources. The second phase focused on quantifying the variability of results obtained with the DFT-TWPD equipment, here the authors analyzed the role of the tires in the TWPD, the variability between TWPD devices, method to arrange aggregates, the role of the DFT rubber pads slider life, and the effect of the tire's tread in the TWPD. The main differences between the Saghafi et al. proposed specimen preparation method and the AASHTO method are the formula and type of the bounding agents and the aggregate tightness.

The formula and type of the bounding agent is detailed in Figure A.13. The authors compared the friction value at the beginning as well as the friction-polishing cycle curve and found there is no statistical difference between the sample preparation procedures. The other modification was the tightness of the aggregates, as shown in Figure A.14. The tight structure proposed in the AASHTO PP 103 is achieved by manually placing each aggregate to ensure the maximum packaging. In contrast, Saghafi et al. proposed placing a batch of aggregate and then carefully arranging them, which resulted in some gaps among adjacent particles. The differences in the friction performance results from specimens prepared with different voids are statistically insignificant at a 95%

confidence level. The operator performance in preparing the mosaic of aggregates may not affect the friction results significantly, if the aggregate matrices are reasonably tight (according to the authors less than 16% gaps between aggregates).

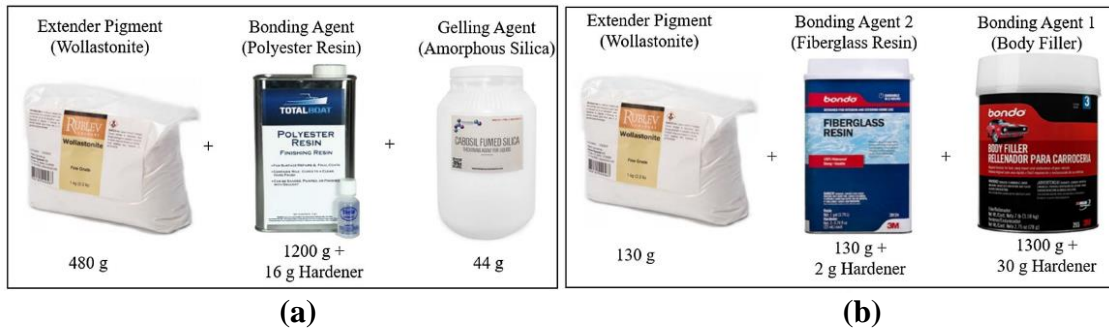


Figure A.13. Bonding agent ingredients for aggregate specimen preparation: (a) AASHTO PP 103-20 bonding agent formula, and (b) new bonding agent formula of Saghafi et al. (45).

With these modifications, Saghafi’s et al. method allows preparing a specimen in just 5 hours, in comparison to the more than 15 hours required by the AASHTO PP 103 procedure. Also, it reduces the specimen cost to around \$10/specimen (in contrast to the \$30/specimen of the AASHTO PP 103) because it uses less blending agent.

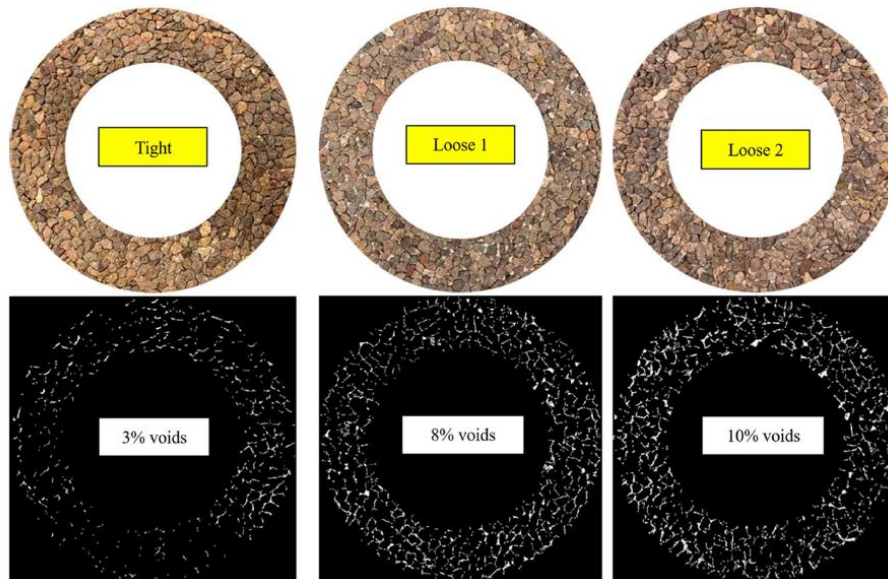


Figure A.14. Comparing the aggregate arrangement in the specimen preparation.

Other interesting findings presented by Saghafi et al. are:

- The same results can be obtained with a solid tire instead of pneumatic tire (the tire type recommended by the AASHTO standard). This is important because this tire type is more cost effective and could be safer for the TWPD operation. The reproducibility of the three identical fabricated TPWDs was not an issue at a 95% confidence level.
- No statistically significant differences were observed between the DF_{20} values of the new and used rubber pads (used more than 200 times for DFT measurements). The final rubber pad’s life of 200 ± 50 times is reasonable.

- The flat-free tires with and without tread showed similar polishing performance. The tread depth does not seem to significantly affect the polishing performance of the tires.

Asphalt Concrete Surface Skid Resistance Quantification

The TWPD is used to simulate the polishing of a pavement surface by traffic to evaluate the friction characteristics of asphalt mixes. This procedure has been standardized in the AASHTO provisional standard PP 104-20 “Sample Preparation and Polishing of Asphalt Mixture Specimens for Dynamic Friction Testing”. This standard is to be used with compacted asphalt mixture slab specimens; other specimen preparation procedures would be needed for assembling a group of gyratory cylinders to be polished using a TWPD.

Equipment

The equipment used to prepare the sample and the devices used to measure friction are specified as follows:

- **Sample compaction device:** A machine capable of uniformly compacting an asphalt mixture within a rigid mold to a specified height to achieve a specified density. This compaction may be accomplished using linear kneading compaction, plate compaction, or manual impact compaction.
- **Specimen mold:** A rigid specimen mold with dimensions that permit the compaction of a 508 × 508 mm (20 × 20 in.) asphalt mixture slab specimen. In some cases, a dynamic friction tester (DFT) will accommodate a smaller sample, in which case, the resulting compacted asphalt mixture slab specimen shall be no less than 400 mm (16 in.) wide.
- **Non-Stick Paper:** Paper or other material that does not readily adhere to an asphalt mixture.
- **Metal Partition:** For full-scale slab specimens, a metal partition capable of dividing the asphalt mixture into four quadrants.
- **Transfer Funnel:** A metal device with a tapered end capable of transferring an asphalt mixture from pans into the four quadrants created by the splitter.
- **Thermometers:** Armored, glass, or dial type thermometers with metal stems for determining the temperature of aggregates, binder, and asphalt mixtures up to 204°C (400°F) and readable to 2°C (5°F).
- **Balance:** A balance meeting the requirements of AASHTO M 231, Class G 5, for determining the mass of aggregates, binder, and asphalt mixtures.
- **Oven:** An oven thermostatically controlled to ± 3°C (5°F), for heating aggregates, binder, asphalt mixtures, and equipment as required. The oven shall be capable of maintaining the temperature required for asphalt mixture conditioning in accordance with R 30.
- **Three-Wheel Polishing Device (TWPD):** A polishing device that has three patterned pneumatic tires and can exert 0.65 ± 0.02 kN (146 ± 5 lbs) through the tires to the test surfaces. The device’s height shall be adjustable to accommodate sample heights of 25 mm (1.0 in.) to 50 mm (2.0 in.).
- **Tire:** The tire size shall be 2.80/2.50-4 and shall maintain a pressure of 240 ± 34 kPa (35 ± 5 psi) and a tread depth of no less than 2 mm (0.1 in.). The tire tread shall have a ribbed pattern. The tire tread shall be free of any visible contamination. When replacement is necessary, all tires shall be replaced at the same time with tires having the same tread pattern as the tires being replaced.

- **Dynamic Friction Tester (DFT):** A device used to measure pavement surface friction values as is described in ASTM E1911.

Material and Equipment Preparation

Unless the compactor equipment has internal heating, place assembled mold and other appropriate compaction tools that will be in contact with the sample in an oven set to the desired compaction temperature a minimum of 30 min prior to compaction. Determine mass of total asphalt mixture needed to achieve desired height and air voids. A common target air voids is 7 ± 1 percent for dense graded and gap- graded asphalt mixtures. A higher target air voids, such as 15 ± 2 percent, should be used for open-graded asphalt mixtures. Equation (67) shows how to calculate the total mixture mass.

$$m_T = (lwt)(G_{mm} \cdot \rho_w) \left[\frac{100 - V_a}{100} \right] \quad (67)$$

where;

- m_T = total mass of asphalt mixture to construct a slab in g,
- l = length of slab, to the nearest 0.1 mm,
- w = width of slab, to the nearest 0.1 mm,
- t = desired thickness of slab, to the nearest 0.1 mm,
- G_{mm} = theoretical maximum specific gravity of the asphalt mixture,
- ρ_w = density of water, 0.001 g/mm³, and
- V_a = desired percent air voids of slab.

Material Preparation

- **Step 1:** Prepare four batches of asphalt mixture. Determine the total mass of each batch by dividing m_T by 4.
- **Step 2:** Mix each batch separately and set aside.
- **Step 3:** Place all four pans in an oven for $2 \text{ h} \pm 5 \text{ min}$ at the compaction temperature.

Specimen Preparation Procedure

- **Step 1:** Pour one of the asphalt mixture batches from one pan into the transfer funnel, then into one quadrant (see Figure A.15). Pour the next asphalt mixture batch into the transfer funnel and then into the quadrant diagonally across from the first quadrant. Repeat for the other two batches. Carefully remove the metal partition.



Figure A.15. Technician pouring a batch into the partitioned compaction mold.

- **Step 2:** Spade the combined asphalt mixture batches with a large trowel until the asphalt mixture is a relatively uniform depth. Level the asphalt mixture with the trowel, taking care

not to segregate the particles. Each asphalt mixture batch should be kept in the vicinity of the quadrant in which it was poured.

- **Step 3:** Compact the asphalt mixture until desired height is achieved. Depending on the compaction method, the bottom of the slab could be the ideal side for most testing.
- **Step 4:** Ensure there is no more than a 1 mm departure in any of the areas to be tested by the DFT that is not related to mixture surface texture. The slab should be stored on a rigid plate such as an approximately 25 mm (1 in.) thick piece of plywood to protect against deformation. Do not stack slabs or place the slab on a non-flat surface.

Sample Polishing Procedure

- **Step 1:** Measure the initial friction value by the dynamic friction tester (DFT) according to ASTM E1911. Use a template to guide the location of the DFT, as shown in Figure A.16, so the friction measurement path aligns with the TWPD polishing path.



Figure A.16. DFT placed into a guide template.

- **Step 2:** Remove the slab from the DFT and slide the specimen under the wheel assembly of the TWPD. Position the specimen so that the slab is against the back and side spacers, as shown in Figure A.17. One revolution of the polishing carriage corresponds to one pass made by all three wheels. 100,000 revolutions have been found to be sufficient to polish most compacted asphalt mixes to the terminal friction value. Intermittent friction values may be obtained, if desired, to capture the rate of polishing of the asphalt mixture before it reaches its terminal friction value.



Figure A.17. Properly positioned specimen in the TWPD.

- **Step 3:** Measure the friction value by the DFT according to ASTM E1911 in the same friction measurement path used to obtain the initial friction value.

Knowledge Gaps

In this section the laboratory protocols to evaluate the skid resistance performance have been presented. As shown, there is a separate protocol to evaluate the aggregate polishing resistance and another to evaluate asphalt concrete. Both protocols are still in development and are currently a provisional standard. A few gaps still exist for the implementation of these protocols:

- The TWPD, which is the most used polishing device in the US, uses slab geometry. However, there are some challenges with this geometry, one of this is the fabrication of the specimens which may take a few days. In terms of QC this poses a problem because agencies need to fabricate an extra specimen for friction testing.
- The second knowledge gap is the incompatibility of the testing machine with the SGC sample geometry. The SGC specimens are collected in most of the QC/QA programs, also the field cores collected to control asphalt densities have a similar geometry. However, none of these can be tested using a DFT or a TWPD.
- The results of this test have not been incorporated into a friction performance model in the field. In the previous section it was shown that some models use aggregate resistance as a predictor of friction performance in the field; however, the aggregate polishing resistance has not been incorporated in a formal model yet.
- A cheaper alternative to the couple DFT/TWPD is the BPT/PSV, though these devices have some flaws like repeatability, or susceptibility to higher variations, they work with a SGC geometry (in the case of the BPT) and can test aggregate polishing resistance at a fraction of the cost of a TWPD.

Effect of Mixture Volumetrics on Skid Resistance

HMA volumetrics and compaction are strongly influenced by aggregate type and gradation, binder type, mixing and compaction temperatures, level of compaction and compaction type (31). In the Superpave mix design protocol three trial blends that cover a range of gradations are sufficient. The phase diagram used to represent the mix volumetric distribution is depicted in Figure A.18. As shown, the aggregates represent the largest volumetric component, and the total asphalt content consists of an absorbed portion and an effective fraction that covers the aggregates and fills the voids.

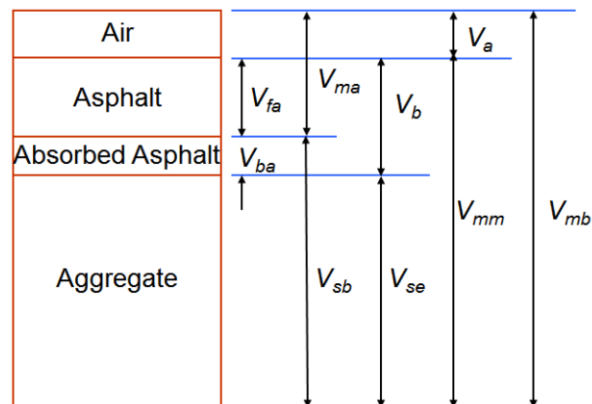


Figure A.18. Asphalt mixture volumetrics.

where;

- V_{mb} = bulk volume of compacted mixture,
- V_{mm} = voidless volume of mixture,
- V_{se} = volume of aggregates (based on G_{se}),
- V_{ma} = voids in mineral aggregates,
- V_{ba} = volume of absorbed binder,
- V_a = volume of air,
- V_b = volume of binder,
- V_{sb} = volume of aggregates (based on G_{sb}), and
- V_{fa} = voids filled with asphalt.

The aggregate component of asphaltic mixtures plays a significant role in pavement friction since aggregate constitutes approximately 95% by weight and 90% by volume of asphalt mixtures (51). Friction adhesion is mostly a micro-surface component that is provided by the aggregate mineralogy and shape. The hysteresis depends on the surface macrotexture and depends on the gradation, binder content and compaction of the mixture. Many researchers have concluded that coarser mixes with aggregates with a high portion of fracture and irregularities produce better friction performance (7, 22).

Different studies have been conducted to explain the relationship between aggregate gradation and skid resistance (10, 31–33, 39, 52, 53). One of these studies is the one by Zhao et al. (54) who conducted a laboratory test using five gradations with different design curves and different NMASs to get the attenuation law of skid resistance. The results showed that the mass content of the coarse aggregate above 4.75 mm and the maximum aggregate size had significant influence on skid resistance of pavement. At the same time, the maximum size of aggregate should be determined by taking into consideration the layer thickness and temperature and so on.

In another study, Lin and Tongjing (55) evaluated the effect of fine aggregate angularity (FAA) on the skid-resistance of asphalt pavements. To achieve this objective, four fine aggregates with various FAA values were used in stone matrix asphalt (SMA) and conventional asphalt concrete (AC), separately. The Model Mobile Load Simulator (MMLS3) was used to simulate the effect of traffic load on the skid-resistance of compacted mixes. A BPT was used to quantify friction and the sand patch test was used to measure *MTD*.

These simulations allowed Lin and Tongjing to investigate the changes of skid-resistance on both the micro and macrotexture by the traffic polishing. The results lead the authors to conclude that with the increase of loading repetitions, both the micro and macrotexture skid-resistance of HMA decreased. They also found that, generally the initial skid-resistance can be used to predict the final skid-resistance. Finally, at some time, after a certain number of repetitions skid-resistance reached a constant level. It seems that fine aggregate angularity had a significant impact on *MTD* while little effect on *BPN*, which means the fine aggregate angularity may not significantly affect skid-resistance on the microtexture level.

Several studies investigated the effect Air Voids Volume (V_a) on the surface fractional properties of HMA pavements. It has been shown that friction changes as the air void decreases over the life span of pavements (56–58). However, this change may correlate without causation and studies such as (22, 56), have concluded that percent of V_a is not a key factor to characterize pavement surface frictional properties. Also, in the other hand some researchers (59–61) have observed the

V_a controls the macrotexture values, measured by MTD , and found that MTD is directly proportional to V_a .

Alsheyab and Khasawneh (62) have suggested it would be more meaningful to evaluate surface friction based on other volumetric measures following a more comprehensive approach by relying on V_a and V_{be} rather than V_a alone. That is, V_a is generally expressed as a ratio of V_a over the V_{mb} , where V_{mb} is typically affected by compaction effort. Consequently, V_{mb} decreases if the level of compaction increases while keeping the aggregate volume in the mix unchanged.

According to Sullivan (63), while the design of asphalt mixtures for friction requirements will most likely not involve mixtures near the critical air void level, any movement of the mix gradation away from the maximum density line tends to increase texture. This change may also increase the field air void content in the mixture, which can in turn reduce mix stability, increases aging, increases permeability, and reduces fatigue life. These effects are schematically represented in Figure A.19, where the arrows indicate the increasing tendency of the material property. Therefore, when designing an asphalt mixture for friction, any significant departure from the maximum density line will need to be compensated for by changing binder contents and/or changing binder grades.

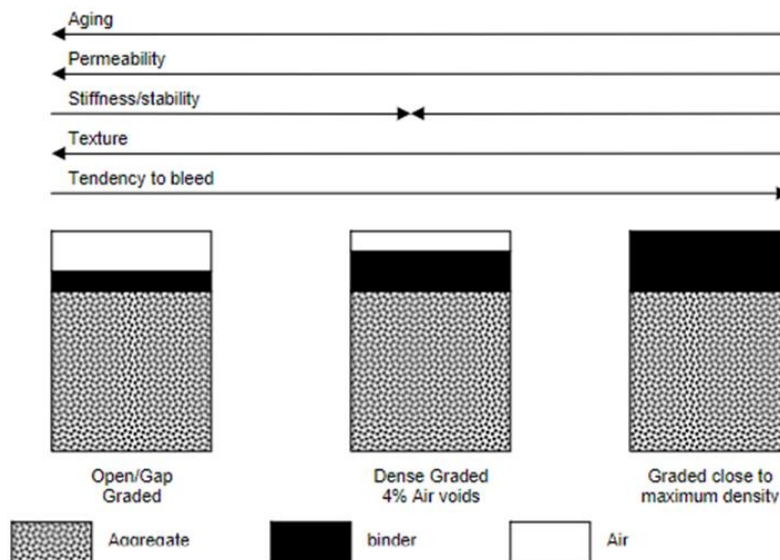


Figure A.19. Asphalt mixture phase diagram (63).

Observations with a Superpave Gyrotory Compactor (SGC)

Khasawneh and Alsheyab (51) evaluated the surface characteristics of SGC HMA specimens made of local resources. The surface frictional properties were characterized using the BPT and the SPT. Asphalt mixtures were prepared using a PG70-10 binder, mixed with crushed limestone aggregate with three Nominal Maximum Aggregate Size (NMAS) 19 mm, 12.5 mm, and 9.5 mm, and involving two types of gradations for each NMAS, fine and coarse gradations. The study found that fine-graded mixtures provide higher microtexture (quantified with the BPN) and lower macrotexture values compared to coarse-graded mixtures. There was a significant difference between the surface frictional properties from the top surface and the bottom surface of the SGC specimen. The top surface exhibited a greater MTD than the bottom surface, and the opposite was true for BPN readings. Moreover, the surface frictional properties of mixtures' top surfaces were

significantly affected by the NMAS and aggregate gradation type. An increase in the NMAS causes and increase in macrotexture but a reduction in microtexture. On the other hand, the bottom surface was affected only by the gradation type due to migration of fine materials toward the bottom surface during compaction.

Khasawneh and Alsheyab proposed the models presented in Equation (68) and (69) to relate the top and bottom MTD and Equation (70) and (71) to relate the top and bottom BPN .

$$MTD_B = 0.3167 \cdot e^{0.2695 \cdot MTD_T} \rightarrow R^2 = 0.449 \quad (68)$$

$$\frac{MTD_B}{MTD_T} = 0.4278 \cdot MTD_T^{-0.762} \rightarrow R^2 = 0.891 \quad (69)$$

$$BPN_B = 45.751 \cdot BPN_T^{0.1419} \rightarrow R^2 = 0.215 \quad (70)$$

$$\frac{BPN_B}{BPN_T} = 0.00010 \cdot BPN_T^2 - 0.0342 \cdot BPN_T + 2.893 \rightarrow R^2 = 0.907 \quad (71)$$

where;

MTD_B = mean texture depth measured with a SPT in the bottom surface of a SGC specimen, (mm),
 MTD_T = mean texture depth measured with a SPT in the top surface of a SGC specimen, (mm),
 BPN_B = friction number measured with a BPT in the bottom surface of a SGC specimen, and
 BPN_T = friction number measured with a BPT in the top surface of a SGC specimen.

In a similar work, Goodman et al. (58) evaluated the surface frictional properties obtained with a SGC specimen. However, in addition Goodman et al. collected a series of field cores that were part of the quality control process and compared the friction and texture measured in the SGC specimens with the values obtained with the field cores. Friction was characterized with a BPT, whereas texture was characterized with the SPT. Also, because at the moment of the study the City of Ottawa was in a transition from Marshall to Superpave methodology the authors included both kinds of mixes.

For both the lab and field specimens the volumetric properties such as the $AC\%$, bulk relative density, V_a , VMA , VFA , DBR , and gradation were measured. The laboratory cores were cut in half, so the bottom and top surface were tested separately. It was immediately clear that the added confinement imposed on the bottom surface of the gyratory specimens by the mold led to a reduction in macrotexture depth compared with the top surface. The authors proposed Equation (72) to predict MTD of the field cores from the MTD measured with the SGC specimens. In the case of friction, it was not possible to obtain a relationship between the BPN measured in the SGC specimens and the field cores.

$$MTD_{field} = 1.14(MTD_T)^2 - 0.81(MTD_T) + 0.40 \rightarrow R^2 = 0.99 \quad (72)$$

where;

MTD_{field} = mean texture depth measured with the SPT in the surface of a field core, (mm), and
 MTD_T = mean texture depth measured with the SPT in the top surface of a SGC specimen, (mm).

Finally, Goodman et al. also developed a set of expressions to relate the field MTD and BPN with the mixture volumetrics as indicated in Equation (73) and (74), respectively.

$$MTD_{field} = -0.24 + 0.981 \cdot \left(\frac{FM \cdot VMA}{P_{4.75} \cdot BRD} \right) \rightarrow R^2 = 0.95 \quad (73)$$

$$BPN_{field} = 42.32 + 2.95 \cdot \left(\frac{P_{4.75} \cdot BRD}{FM \cdot AC} \right) \rightarrow R^2 = 0.69 \quad (74)$$

where;

MTD_{field} = mean texture depth measured with the SPT in the surface of a field core, (mm),

BPN_{field} = friction number, measured with the BPT in the surface of a field core,

FM = aggregate finesses modulus,

VMA = voids in the mineral aggregates,

$P_{4.75}$ = percent of aggregates retained on 4.75 mm sieve,

BRD = bulk relative density of the compacted field, and

AC = percent by mass of binder contained in the mix.

Effect of Modifiers

Changing asphalt binder properties can be easily achieved through the usage of asphalt mixture modifiers. Modifiers are known for their ability to enhance the properties of asphalt mixtures and ultimately the performance of pavements against stresses caused by repeated traffic loading. It is also expected that the modified asphalt binder might affect the resulting friction. Alsheyab and Khasawneh (62) conducted a study to evaluate the surface frictional characteristics of Superpave specimens based on their volumetric properties, modifier type and compaction level. This study is based on asphalt mixtures prepared using a PG64–10 fresh asphalt binder and crushed limestone aggregate. Three different asphalt modifiers were used, crumb tire rubber (CTR), microcrystalline synthetic wax (MSW), and nano silica (NS). The SPT for macrotexture evaluation and the British Pendulum Tester (BPT) for microtexture evaluation was utilized.

The specimens were adjusted to 4% air voids and compacted, using the SGC, at two compaction efforts with Design Number of Gyration (N_{des}) equal to 119 and 82 to simulate high and low levels of traffic, respectively. A decrease in V_a and V_{be} values were observed at higher levels of compaction. To analyze the combined effect of these two variables, the variable P_v was defined using Equation (75).

$$P_v = \frac{V_a}{V_{be}} \times 100\% \quad (75)$$

It was concluded that asphalt modifiers could influence V_a and V_{be} , which would result in different surface frictional characteristics, additional investigation was recommended. CTR-Modified mixtures provided the highest values of MTD and BPN , respectively. Hence, CTR as an asphalt modifier, could ensure adequate levels of macrotexture and microtexture needed for adequate frictional characteristics of asphalt pavements. This inference could be attributed to the direct relationship between V_a and macrotexture and between V_{be} and microtexture.

High-Surface Friction Treatment

The High Friction Surface (HFS) has been used as one of the low-cost safety countermeasures to address high friction demand concerns on curved roadways. It was developed in the 1960s in the U.K. by the Greater London Council and the Transport and Road Research Laboratory to restore friction on high-crash road sections (7). The used aggregate for this treatment type is calcinated bauxite (64, 65). A properly constructed HFS on pavements in good condition typically maintains a high friction value throughout its expected life. Based on some studies, the typical HFS life ranges from 7 to 12 years, and the benefits surpass the cost when the HFS is more than 7 years.

However, this treatment can fail earlier, and the main reported causes are in the form of delamination, aggregate loss (the most common), or cohesion failure (5). In the field, the friction performance of a HFS is like the one shown in Figure A.21. As depicted, the HFS maintains almost a constant friction value during most of its life; however, at some point when the aggregate loss accelerates the friction value starts decaying abruptly.

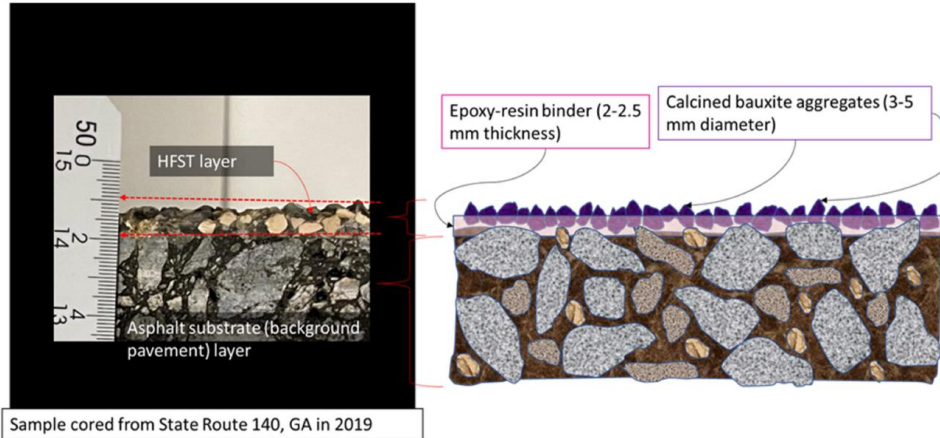


Figure A.20. Cross section of HFS and illustration showing the typical dimensions of epoxy and calcinated bauxite (5).

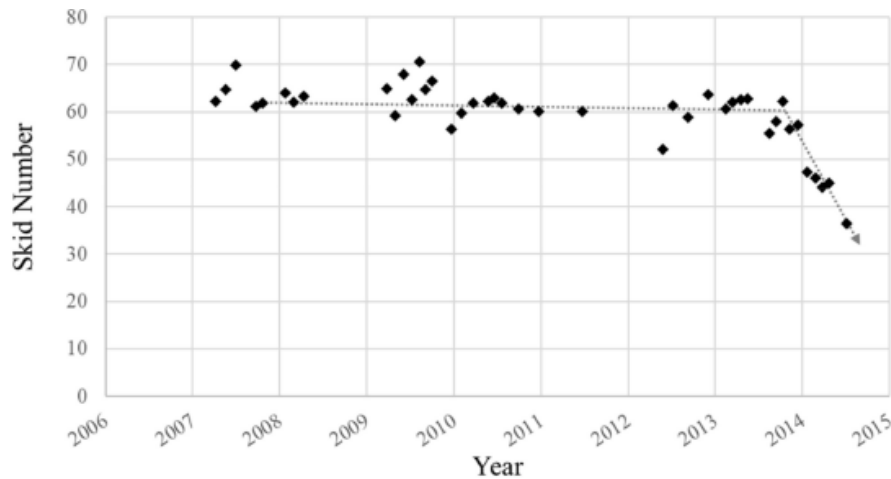


Figure A.21. Evolution of friction of a HFS surface (5).

Pranav et al. (5) conducted a detailed analysis to characterize the different stages of aggregate loss using texture parameters. Tests were conducted on selected HFS locations with different aggregate loss severity levels at the NCAT Test Track. Friction tests were performed using a DFT. The surface texture was measured by means of a high-resolution 3D pavement scanning system. Three texture parameter types were considered: 1) parameters related to aggregate characteristics, Equations (76) to (78), 2) parameters related to the distribution of the aggregates, Equation (79), and projected area of the surface intersect with a plane located at a depth below 1 mm of the highest peak, see Figure A.20, and 3) parameters related to the aggregate loss physical process, i.e., Abbott curve shown in Figure A.22.

$$S_q = \sqrt{\frac{1}{MN} \sum_{j=1}^N \sum_{i=1}^M z^2(x_i, y_i)} \quad (76)$$

$$S_{dq} = \sqrt{\frac{1}{(M-1)(N-1)} \sum_{j=1}^N \sum_{i=1}^M \left[\left(\frac{z(x_i, y_j) - z(x_{i-1}, y_j)}{\Delta x} \right)^2 + \left(\frac{z(x_i, y_j) - z(x_i, y_{j-1})}{\Delta y} \right)^2 \right]} \quad (77)$$

$$S_{sc} = -\frac{1}{2} \Delta \frac{1}{n} \sum_{k=1}^n \left(\frac{z(x_{p+1}, y_q) + z(x_{p-1}, y_q) - 2z(x_p, y_q)}{\Delta x^2} + \frac{z(x_p, y_{q+1}) + z(x_p, y_{q-1}) - 2z(x_p, y_q)}{\Delta y^2} \right) \quad (78)$$

$$S_{ds} = \frac{\text{Number of peaks}}{(M-1)(N-1)\Delta x \Delta y} \quad (79)$$

where;

- S_q = root mean square height,
- S_{dq} = mean quadratic slope, to characterize the steepness of asperities,
- S_{sc} = curvature of the asperities (at a peak located at x_p and y_q),
- S_{ds} = density, to characterize the number of asperities in the surface,
- M = number of points measured in the 'X' direction,
- N = number of points measured in the 'Y' direction,
- $z(x,y)$ = measured elevation at point (x,y) , and
- Δ = profile asperity width.

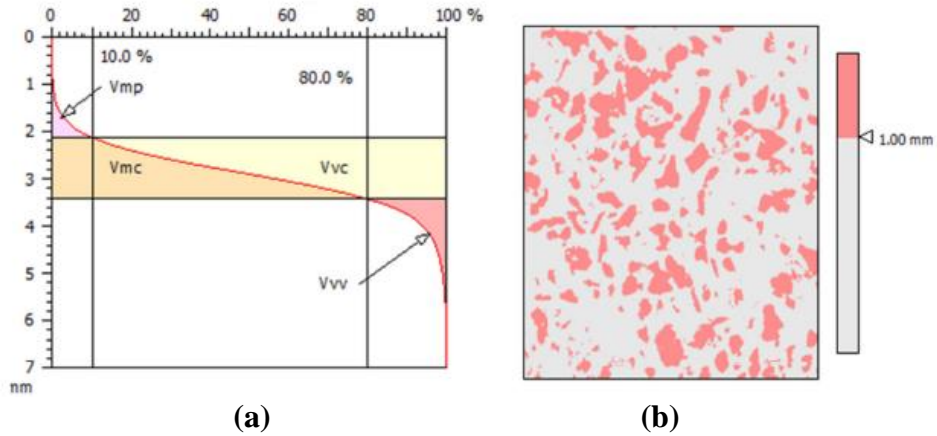


Figure A.22. (a) Abbott curve and the volume parameters and (b) projected area (5).

where;

- V_{mp} = peak material volume,
- V_{mc} = core material volume,
- V_{vc} = valley void volume, and
- V_{vv} = core void volume.

The software MountainsMap was used to: 1) replace unmeasured points by interpolating with the nearing neighbors, 2) remove extreme values (0.025% at each end), and 3) level the surface using a regression plane. As values of the texture parameters should reflect the part of the surface that is

in contact with the rubber slider (pad of the DFT), it was decided to apply a morphological filter to obtain an envelope of the surface. This envelope represents the possible ‘contact’ of the rubber with the HFS aggregates.

Once all of the parameters described in the above equations were calculated, Pranav et al. made a correlation with friction values, and they found that seven of the nine parameters are highly correlated with friction and can capture the ‘abrupt’ deterioration process shown in Figure A.21. From these parameters, those with the highest correlation were found to be S_{ds} , S_{dq} , and S_{sc} .

Knowledge Gaps

With respect to the effect of the mixture volumetrics in the early friction and texture characteristics, most researchers recognize that the aggregate gradation is the main factor affecting macrotexture values. Likewise, they recognize that the coarse fraction of the gradation is the one that contributes the most to friction values. There is a promising application of SGC samples to control friction and texture values in the field; however, as mentioned in the previous section, there is still not a standard procedure to evaluate friction performance on SGC specimens. Some aspects still require more research:

- The models developed with a SGC specimen used a SPT to characterize texture. However, other devices such as the Ames portable laser can produce a more reliable and precise quantification of the surface characteristics, both in the lab and the field.
- Changing asphalt binder properties can be easily achieved through the usage of asphalt mixture modifiers. However, these changes might affect the resulting surface friction. Although initial findings suggests that asphalt modifiers could influence the air voids and the volume of effective binder in the mix, which would result in different surface frictional characteristics, additional investigation is recommended to evaluate the effect of each type of modifier.
- Though some work has been done to understand the effect of asphalt modifiers, a substantial contribution to evaluate the effect of high RAP/RAS content in the surface friction has not been presented to date. Moreover, there is no study evaluating this effect in long-term friction and texture performance.
- As indicated, the main failure mechanism in the HFST is the aggregate loss. Despite some techniques are available to quantify the change in texture parameters due to this aggregate loss, most of them are based on high-resolution lasers, and bases on aerial parameters. However, new laser devices can collect 3D surface profiles at high speeds, this in the future will allow aerial parameters at a network level. More research is needed to evaluate the correlation of these parameters with friction.

Modeling Crashes

Typically, safety of a roadway is expressed using crash frequency or crash rates. The crash rate can be calculated through Equation (80).

$$R_i = \frac{10^8 \cdot C_i}{365 \cdot Y \cdot AADT_i \cdot L_i} \quad (80)$$

where;

- R_i = crash count per million-mile vehicle traveled for segment i ,
- C_i = observed crash count for segment i ,

Y = number of years in the period of analysis,
 $AADT_i$ = average annual daily traffic for segment i , and
 L_i = roadway segment length (in miles).

In the highway safety community, crash rates are no longer the primary index used to describe crashes, because R_i implicitly assumes that crashes and traffic are proportional, while research has shown that crashes increase with $AADT$ in a nonlinear fashion. Because a crash event is a random variable that depends on several factors, the Highway Safety Manual (HSM) (66) uses an empirical-Bayes (EB) approach to account for the regression to the mean effect (this is the name used in statistics to recognize the fact that after an extreme event – in this case an unusual high number of crashes – the next observation will be closer to the mean value of the site). The mean value of a site is calculated using a Safety Performance Function (SPF).

Crash counts are assumed to follow a negative binomial distribution (NB), this distribution can represent the situation when the variance of the random variable X (number of crashes) $V(X)$ is higher than the mean $E(X)$.

$$E(X) = \lambda_i = \exp\left(\beta_0 + \sum_{j=1}^k \beta_j Z_{ij}\right) \quad (81)$$

where;

λ_i = expected average number of crashes for section i ,
 β_0, β_i = parameters to be estimated, and
 Z_{ij} = value of predictor variable j for section i .

The HSM (66) uses the NB model to generate SPFs in highway safety management practice as a network-level screening process to identify sites that have elevated crash risk and to assess the potential benefits of surface treatments. The SPF crash predictions are considered as average expected values for a site as a function of geometry variables and traffic volumes. The EB method combines SPF values with the observed number of crashes as follows:

$$EB_i = W_i \cdot \lambda_i + (1 - W_i) \times X_i \quad (82)$$

$$W_i = \frac{1}{1 + \lambda_i \times \alpha} \quad (83)$$

where;

EB_i = EB estimate number of crashes for the road segment i ,
 W_i = weight term for road segment I , see Equation (83),
 α = over-dispersion parameter of the SPF,
 λ_i = prediction of the expected number of crashes using the SPF, and
 X_i = observed number of crashes.

To assess benefits of surface treatments in a PFMP, statistically reliable estimates of average expected crash counts are required. This information is provided by the SPF if one includes friction as a safety factor.

Noyce et al. (67) studied the relationship between friction number and crashes (both total and wet only). In both cases it was not possible to observe a significant trend between crashes and FN . Afterwards, crash data were further analyzed to select only skid-related crashes. Crash types evaluated included those that involved heavy braking, skidding, or loss of vehicle control. Several

of the previously selected skid crashes were eliminated via this process since no contributing factors could be found between the crash and the associated pavement characteristics. Although the frequency of crashes is quite low, there is some evidence to suggest that the crashes happened in the latter years of the analysis period where friction numbers tended to reduce. Although no statistically significant correlation was found.

In 2016, Wallbank et al. (68) conducted a study to update the relationships between collisions and skid resistance used in the U.K. Strategic Road Network. For this purpose, roads were grouped by category and the preferred length of analysis was defined as 500-m for motorways and 200-m for all other roads. In their analysis the authors used the data available in the period of 2010 to 2013 and included only segment of roads with at least three friction measurements during this period. The researchers defined the collision risk as the number of collisions divided by the total amount of traffic (in vehicle kilometers), and the skid resistance averaged in 0.05 increments. It was observed that for most of the road categories the proportion of collisions which were wet collisions increased slightly at lower levels of skid resistance. A similar trend was evident when examining the proportion of wet collisions that were skidding collisions.

Next, Wallbank et al. used a multivariate generalized linear regression to calibrate the SPF shown in Equation (84). The independent variables that were tested are skid resistance, rut depth, texture depth, curvature (1/radius), gradient, and road crossfall. After calibration, not all the models (one for each road category) included skid resistance as an independent variable, and the proportion of variance explained by each model was always less than 20%.

$$N_{crashes} = L \cdot T^\alpha \cdot \exp[\beta_0 + \beta_1 x_1 + \dots + \beta_n x_n] \quad (84)$$

where;

- $N_{crashes}$ = number of collisions,
- L = segment length,
- T = cumulative traffic flow, and
- α, β_i = coefficients to be estimated.

In the case of North Carolina, Srinivasan and Carter (69–72) have made a complete summary of the calibration process of the SPFs used by the NCDOT to screen the network and identify sites with high number of crashes. The procedure described by the HSM (66) to: 1) update the SPF proposed by the HSM and 2) to develop their own SPF was followed. The specific process performed by Srinivasan and Carter is summarized thusly:

1. Identify facility types for which the applicable Part C of the HSM predictive model can be calibrated.
2. Select sites for calibration of the predictive model for each facility type.
3. Obtain data for each facility type applicable to a specific calibration period.
4. Apply the applicable Part C predictive model to predict total crash frequency for each site during the calibration period.
5. Compute calibration factors to use in Part C predictive model.

For the second task they developed different SPF for segment lengths for predicting nine types of crashes:

- Total Crashes
- Injury and fatal crashes (K, A, B, C)
- Injury and fatal crashes (K, A, B)

- PDO crashes
- Lane departure crashes – These included crashes with the First Harmful Event = (1) Ran off road – right, or (2) Ran off road – left, or (3) Ran off road – straight, or (19) Fixed object, or (27) Head on, or (29) Sideswipe, opposite direction.
- Single vehicle crashes (includes animal crashes)
- Multi vehicle crashes
- Wet crashes – These included crashes with Road Surface Condition = (2) Wet or (3) Water (standing, moving)
- Night crashes – These included crashes with Ambient Light = (4) Dark – lighted roadway, or (5) Dark – roadway not lighted, or (6) Dark – unknown lighting

The first SPF, the one recommended by the HSM, has only *AADT* and Length as descriptor, for use in the network screening:

$$N_{crashes} = L \cdot e^{\alpha} AADT^{\beta} \quad (85)$$

where;

- $N_{crashes}$ = expected number of crashes per year,
- L = length of the section, in miles,
- $AADT$ = annual average daily traffic, and
- α and β = model coefficients, estimated as part of the negative binomial regression model.

The second SPF includes more variables and are intended for crash prediction:

$$N_{crashes} = L \cdot \exp(\alpha + \beta_1 \cdot f_1(AADT) + \beta_2 \cdot f_2(Z_2) + \beta_3 \cdot f_3(Z_3) + \dots) \quad (86)$$

where;

- $N_{crashes}$ = expected number of crashes per year,
- L = length of the section, in miles,
- $\alpha, \beta_1, \beta_2, \dots$ = model coefficients, estimated as part of the negative binomial regression model,
- f_1, f_2, f_3, \dots = represent functions for including each one of the independent variables,
- $AADT$ = annual average daily traffic, and
- Z_2, Z_3, \dots = specific site characteristics: AADT, terrain, shoulder type and shoulder width.

None of the functional forms currently available by the NCDOT includes any variable related to pavement condition. Additionally, though some of the models resulted with an R^2 greater than 0.7, most of them have an R^2 lower than 0.3.

Works like the one conducted by Wallbank (68) and Srinivasan and Carter (69–72) are numerous and can be found elsewhere in the literature. Though most of these works predict general crash trends, they show high variability and low prediction capabilities. For this reason, some authors have tried to account for factors that explain heterogeneity in the crash occurrence in the network. Galgamuwa et al. (73) incorporated spatial correlation to account for crash clustering depending on the road geometry (ramps, bridges, etc.). Huo et al. (26) incorporated correlated random parameters in the SPF to model heterogeneity in the expected number of crashes, to in this way account for unobserved heterogeneity in crash frequencies.

In one attempt to incorporate spatial correlation, Katicha et al. (74) developed a methodology to estimate the expected number of crashes based on the spatial distribution of crash events. The proposed spatial multiresolution analysis (SMA) method works like bandwidth kernel density

estimation (KDE). The SMA method is based on the Haar wavelet transform, which is like the KDE method with the additional benefit of allowing the bandwidth to be different at different road segments depending on how homogenous the segments are. Furthermore, the optimal bandwidth (the number of adjacent segments that have the same number of crashes) at each road segment is determined solely based on the data by minimizing an unbiased estimate of the mean square error for Poisson data called Poisson’s unbiased risk estimate (PURE). A detailed reference to the PURE derivation can be found in (75).

Katicha et al. have reported their proposed SMA method can outperform the EB method because it incorporates the spatial variation of the expected number of crashes, but at the same time is a simple method that can be easily applied using a macro in Microsoft Excel. To apply the method, it is necessary to summarize the number of crashes in a uniform interval, e.g., every 0.1-mile, or every 1-mile. An example of this kind of crash ‘profile’ is illustrated in Figure A.23, where the dashed purple line represents the number of crashes observed in a period of five years (2015-2019). As indicated, there are two locations where a higher number of crashes occur. By using the SMA method, red line in Figure A.23, it is possible to predict the expected number of crashes based on this spatial pattern, but just using the crash profile.

To do a similar prediction using the EB method it will be necessary to account for variables that describe the geometry (for example, there are ramps in milepost 11.7 and 13) of the road, the pavement condition, weather condition, etc. In some cases, such variables may not be available and the SMA method is a good alternative to estimate the variation in the expected number of crashes along a road.

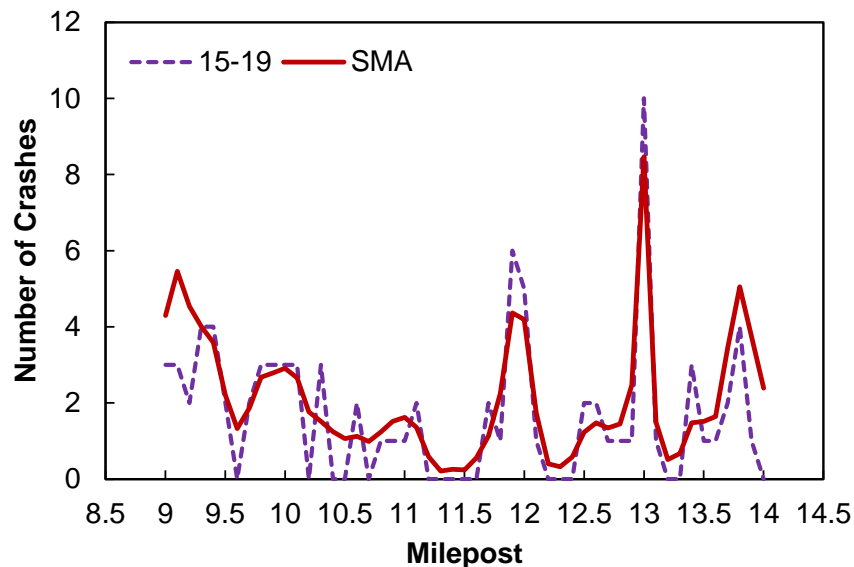


Figure A.23. Application of the SMA method to predict the variation in the expected number of crashes.

Before-and-After Analysis

The before-after study is a commonly used method for measuring the safety effects of a single treatment or a combination of treatments in highway safety (76). Short of a controlled and fully randomized study design, this type of study is deemed superior to cross-sectional studies since many attributes linked to the converted sites where the treatment (or change) was implemented

remain unchanged. As the name suggests, it implies that a change occurred between the “before” and “after” conditions.

Before-after studies can be grouped into three types: the simple (naïve) before-after study; the before-after study with control groups; and the before-after study using the EB technique (also using a control group) (66). According to Hauer (76), the traditional before-after study (no matter which type is used) can be accomplished using two tasks. The first task consists of predicting the expected number, π , of target crashes for a specific entity (i.e., intersection, segment) or series of entities in the “after” period had the safety treatment not been implemented. The second task consists of estimating the number of target crashes, λ , for the specific entity in the “after” period with the treatment in place.

The term “after” means the time period after the implementation of a treatment; correspondingly, the term “before” refers to the time before the implementation of the treatment. In most practical cases, either π or λ can be applied to a composite series of entities where a similar treatment was implemented at each entity.

The effect of the treatment on safety is judged by comparing π and λ after defining the following difference and ratio terms;

$\delta = \pi - \lambda$; defined as the reduction in the ‘after’ period of the expected number of target crashes,
or
 $\theta = \lambda/\pi$, defined as the ratio of what safety was with the treatment to what it would have been without the treatment.

When $\theta < 1$, the treatment is effective, when $\theta > 1$ it is harmful to safety. Also, $100 \times (1 - \theta)$ is the percent reduction in the expected accident frequency. As indicated above, π and λ are expected values. Expected values are never known, but can be estimated from observed data, this is $\hat{\pi}$ and $\hat{\lambda}$. The difference between the many variants of before-after studies resides in the methods used to obtain $\hat{\pi}$ and $\hat{\lambda}$.

Before-After Study for a Single Entity

The sequence of steps used to conduct a before-after study for a single entity (road segment or intersection) are the followings:

1. **Estimate λ and predict π .** In the case of λ it can be estimated from the counts of ‘after’ crashes. The prediction of π will depend on the statistical method chosen (naïve, methods of moments, or EB).
2. **Estimate $Var(\hat{\lambda})$ and $Var(\hat{\pi})$.** The variance estimates will depend on the method chosen to obtain the estimate and predict λ and π , respectively. Typically, it is assumed that the count of accidents is Poisson distributed and the counts in the ‘before’ and ‘after’ period are mutually independent. Therefore, $Var(\hat{\lambda}) = \hat{\lambda}$ and $Var(\hat{\pi}) = \hat{\pi}$.
3. **Estimate $\hat{\delta}$ and $\hat{\theta}$ using Equation (87) and (88), respectively.**

$$\hat{\delta} = \hat{\pi} - \hat{\lambda} \quad (87)$$

$$\hat{\theta} = \frac{\hat{\lambda}}{\hat{\pi}} \cdot \left[\frac{1}{1 + \frac{VAR(\hat{\pi})}{(\hat{\pi})^2}} \right] \quad (88)$$

4. Estimate the variance of $\hat{\delta}$ and $\hat{\theta}$ using Equation (89) and (90), respectively.

$$VAR(\hat{\delta}) = VAR(\hat{\pi}) + VAR(\hat{\lambda}) \quad (89)$$

$$VAR(\hat{\theta}) = (\hat{\theta})^2 \left[\frac{\left(\frac{VAR(\hat{\lambda})}{(\hat{\lambda})^2} \right) + \left(\frac{VAR(\hat{\pi})}{(\hat{\pi})^2} \right)}{\left(1 + \frac{VAR(\hat{\pi})}{(\hat{\pi})^2} \right)^2} \right] \quad (90)$$

Before-After Study for a Group of Entities

Usually, the safety effect is estimated after a treatment has been applied to a set of entities. If these are numbered as $j = 1, 2, \dots, n$, then for each entity j , an estimate of $\hat{\pi}(j)$ and $\hat{\lambda}(j)$ $\lambda(j)$ is obtained. See Step 1 of the previous section. Similarly, the variance in the expected number of crashes for each entity is estimated according to Step 2 of previous section, this is $VAR(\hat{\pi}(j))$ and $VAR(\hat{\lambda}(j))$. To draw overall conclusions, the following sums are conducted:

$$\pi = \sum_{j=1}^n \pi_j \quad (91)$$

$$\lambda = \sum_{j=1}^n \lambda_j \quad (92)$$

And the variance for each quantity is obtained as follows:

$$VAR(\hat{\pi}) = \sum_{j=1}^n VAR(\hat{\pi}_j) \quad (93)$$

$$VAR(\hat{\lambda}) = \sum_{j=1}^n VAR(\hat{\lambda}_j) \quad (94)$$

It is important to notice that one main assumption in the steps to conducting a before-after study according to the descriptions in the previous paragraphs is that crash counts follow a Poisson process, in which the variance is equal to the mean. However, many authors have observed this is not the case because crash events are highly over dispersed, therefore the best representation should be NB not Poisson (66, 73, 75). The argument to use the NB distribution over the Poisson is that the mean, or expected value, is unknown, therefore the variance should be estimated conditioned in the observed crash counts, this is $f(X_j | \pi_j)$.

Parametric Method

In a parametric approach, the conditional probability of crash frequency is assumed to follow a specific distribution defined by a set of parameters. Two techniques, namely Maximum Likelihood and Bayesian Estimation are commonly used to estimate the parameters of the conditional probability functions (66). Among the most used probability functions are Poisson, NB, Poisson-Log Normal, and Zero-Inflated models (77).

Because of the closed form of the Poisson-Gamma distribution, i.e., the closed form and the conjugate distribution, it is used to derive the SPF distribution proposed in the HSM (66). The NB distribution can be viewed as a Poisson distribution where the Poisson parameter, the mean μ , is itself a random variable, distributed according to a Gamma distribution. Therefore, if the means of the Poisson distribution of a group of entities is assumed to be gamma distributed, $\eta = \{ \eta_1, \eta_2, \dots, \eta_n \} \sim \text{Gamma}(\phi, \mu/\phi)$, it can be shown that the marginal distribution (the mean conditioned in the data) becomes the conjugate Poisson-Gamma distribution. In this case, ϕ is defined as the inverse dispersion parameter of the Poisson-Gamma distribution. The mean and variance of η are defined as μ and μ^2/ϕ , respectively. Now, in the case of a group of entities where the observed number of crashes of each individual entity is conditioned by the mean η , the variance for a series of observed values is calculated using the conditional variance identity theorem. So, if $Y = \sum_{j=1}^n \eta(j)$ the variance of Y is $\text{VAR}(Y) = n\mu + n\mu^2/\phi$. Where μ can be approximated by the mean value of entities:

$$\hat{\mu} = \frac{1}{n} \sum_{j=1}^n \eta(j). \quad (95)$$

Some limitation exists with the parametric methods, for example, it is necessary to pre-define the characteristics of the conditional probability function, which in some cases may lead to erroneous results. Also, to estimate the coefficients of the model it is necessary to establish prior information for each coefficient and the correlation or absence of correlation between the variables in the model.

Non-Parametric Method

The nonparametric approach is different from the parametric approach because it does not require specification of model functional form, especially in an equation structure, for the relation between dependent and independent variables. Therefore, the estimation is purely data-driven and is expected to be less biased as this approach avoids the misspecification issues of parametric models (77). Some nonparametric methods are artificial neural network (ANN), classification and regression tree (CART), multivariate adaptive regression splines (MARS), and most recently Bootstrap re-sampling. From these, the bootstrap sampling is of interest because is easy to implement and the number of observations needed for the analysis is substantially less than the other methods (77, 78).

Generally, bootstrapping provides a resampling simulation approach to estimate standard errors and other measures of statistical precision by repeatedly and randomly sampling subsets of data from the original dataset. The bootstrap method was first introduced in 1979 to estimate the variance of a sample mean and was then applied in more complicated problems, such as the parametric model and in estimating regression parameters (77). The bootstrap method is distribution-free and makes no assumption about the distribution of the observed data. Furthermore, the bootstrap method is usually not limited by the number of observations needed to

get a good estimate of the mean and variance of the data, although it is suggested to use a sample size larger than five observations (79–82).

The idea behind bootstrap sampling is the following (18, 19): if Y is a random variable that comes from a probability distribution F (F can be the normal distribution, Poisson, Negative Binomial, etc.), and if one has at hand a realization y (the observed data) of the random variable Y , it is possible to calculate a statistic with this realization, like for example calculating the mean or the standard deviation, generally speaking a statistic $T(y)$. Then, if one considers that all the elements of y are independent and identically distributed from distribution F , it is possible to estimate the distribution of values for the statistic $T(y)$ by considering that a set of ‘realizations’ of Y can be constructed by randomly sampling y , with replacement several times.

Ye and Lord (78) compared the parametric method described in the previous section with the bootstrap sampling and concluded that bootstrap re-sampling can be used to estimate the variance of crash events and provides a similar result of that of Poisson-Gamma parametric method. A random sampling with replacement is one where each value of the population sample can be selected more than once. For example, in Table A.4 it is shown the number of crashes observed in a road for 30 months, a random sample of ten elements generated with replacement can be: {4, 12, 4, 7, 6, 11, 9, 11, 10, 6}. As indicated in this example, the first number sampled was 4, next for the second value the 4 was still a possible outcome but 12 was chosen, then in the third sampled value 4 was chosen again, a similar process was followed for the remaining values. Collecting samples in this way guarantees independence of the elements within a sample and guarantees independence between samples.

Table A.4. Generated crash data to illustrate the Bootstrap method.

Month	1	2	3	4	5	6	7	8	9	10	11	12	13	14	15
Crashes	3	4	3	7	7	9	7	3	7	6	12	8	11	7	4
Month	16	17	18	19	20	21	22	23	24	25	26	27	28	29	30
Crashes	6	4	7	10	6	6	2	6	7	4	7	6	9	10	10

The expected number of crashes per month for the site of Table A.4 is $198/30 = 6.60$. By applying the bootstrap method to the data of Table A.4, it is possible to estimate the standard deviation and confidence interval of the mean. To do this the following properties are defined:

- Define number of bootstrap samples (S): 10,000,
- Define number of elements for each sample S_k : ten elements are sampled with reposition from Table A.4,
- For each sample the average number of crashes is calculated as indicated in Table A.5. Hence, in total there are 10,000 observations of the expected number of crashes; the standard deviation of these observations is 0.799 and the 95% confidence interval of the expected value is (5.0, 8.2).

As shown with this example, the bootstrap sample allows one to estimate the uncertainty (confidence intervals and standard deviation) of a statistic of interest. The bootstrap has several good features in dealing with small sample problems. First, unlike the classic procedures, the bootstrap does not rely on theoretical distributions and thus does not require strong assumptions of the sample and the distribution (79, 80). This attribute is convenient since it is usually difficult to obtain accurate parameters for a certain distribution given the small samples. Moreover, by bootstrapping, the original sample is duplicated many times. Hence, the bootstrap can treat a small

sample as the virtual population and generate more observations from it (81). Finally, the bootstrap is a rather simple technique and does not require a sophisticated mathematical background for its use (78).

Table A.5. Bootstrap samples generated with the observations of Table A.4.

Sample #	Month										Crash/month
	1	2	3	4	5	6	7	8	9	10	
1	4	12	4	7	6	11	9	11	10	6	8.00
2	7	4	3	4	4	2	10	7	11	4	5.60
3	11	12	6	10	12	6	7	7	2	4	7.70
⋮	⋮	⋮	⋮	⋮	⋮	⋮	⋮	⋮	⋮	⋮	⋮
10000	6	10	2	11	9	6	2	11	3	7	6.70

Knowledge Gaps

Although the HSM method provides a powerful tool to evaluate crash risks, in particular, North Carolina has a set of SPFs for several road classes, none of these directly incorporates pavement surface condition as one of the predictors. Additionally, as many researchers have shown, there is a strong spatial correlation in crash events and the current HSM method does not account for this correlation. For this reason, more research is still needed in the following areas:

- Incorporating friction and/or texture in a SPF for North Carolina.
- Incorporating spatial correlation in the prediction of crash frequencies. Alternatives such as the spatial multiresolution analysis can improve the correlation between crash risks and friction or texture.
- In the U.S. just a few attempts have been made to define an investigatory level threshold. Most of these works have focused solely on friction not in texture. There is a need to evaluate the combined effect of these components.
- The use of non-parametric methods, such as the bootstrap sample, to level the limited sample size in the before-after studies.

Pavement Friction Management Program

Given the inherent high complexity of a crash event, it is extremely difficult to identify all the contributing factors that may impact its occurrence. However, many authors agree that some of these factors are pavement surface condition, traffic speed, traffic volume, road geometry and human factors (7, 16, 17, 83). Moreover, the AASHTO Highway Safety Manual (HSM) indicates that the factors that generally contribute to crash events can be categorized as: human factors, vehicle factors, and roadway condition and characteristics factors (66).

Highway Safety is a key element in a Pavement Management System (PMS) because monitoring the road features and surface conditions that are related with crash frequencies may allow the agencies to identify a potential hazard and apply countermeasures that reduce both frequency and severity of crashes (67). Hence, it is inferred that a Pavement Friction Management Program (PFMP) must communicate with the PMS to obtain the required inputs for characterizing the materials of the road surface but also to obtain other variables such as road geometry and traffic volume, just to mention a few. The relationship between a PFMP and a PMS is illustrated in Figure A.24. This framework has been developed based on the recommendations presented in the “Guide for Pavement Friction” NCHRP 108 GPF (7), and the FHWA-RC-20-009 report “Pavement Friction Management Program Utilizing Continuous Friction Measurement Equipment and State-of-the-Practice Safety Analysis Demonstration Project” (18).

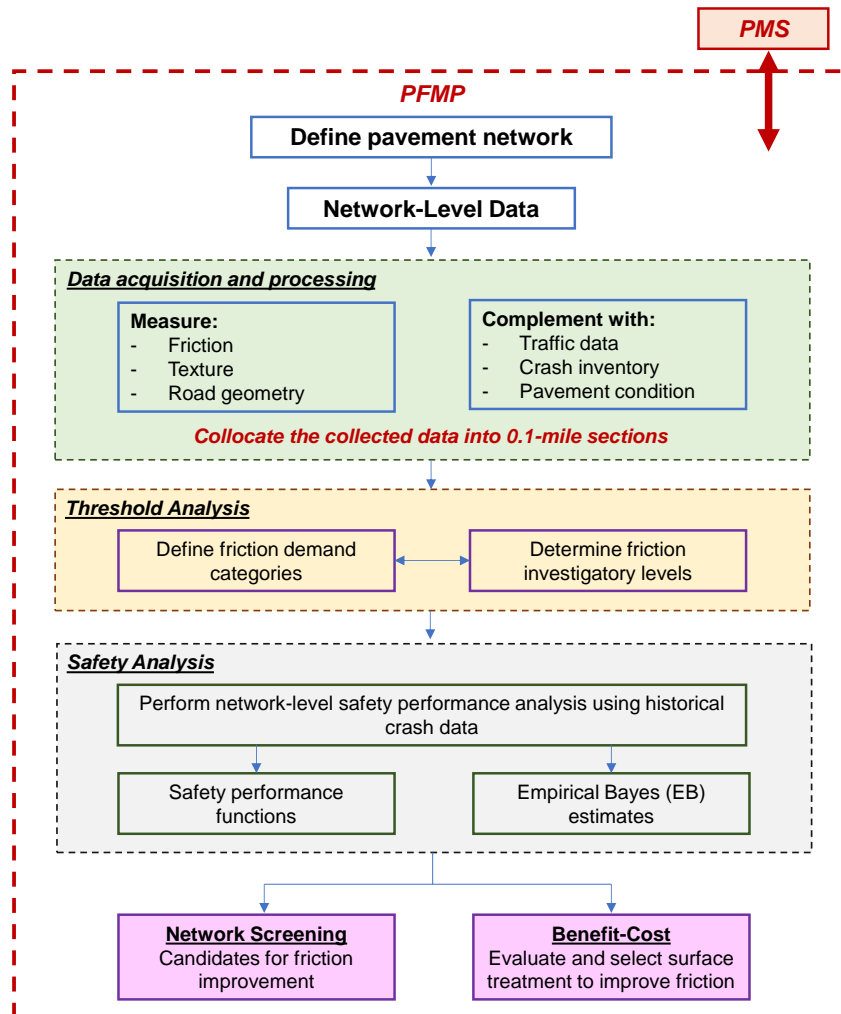


Figure A.24. Elements of a pavement friction management program.

As indicated in Figure A.24, while in a PMS the roads in a network are divided into sections, defined based on the structural composition (number of layers, thicknesses, etc.), the construction history (age of construction and maintenance activities), and traffic (volume and composition). In a PFMP the network is divided according to the friction demand. The section length of a road segment included in a PFMP is generally driven by the shortest practical length where the confidence in the quality of the data is high and the length is practical from an analysis perspective (7). In the study developed by de Leon Izeppi et al. (18), the experience with four DOTs resulted in sections that were 0.1-mi in length. Crash and pavement surface data need to be over a 3-year period. The surface characteristics data should be verified from the state PMS. Similarly, the U.K. has used a segment length that varied from 500 m to 200 m (0.3-mi to 0.15-mi) (68). In consequence, aggregating the information every 0.1-mi seems like a good starting point. To establish the framework depicted in Figure A.24 it is necessary to collect both texture and friction at a network level. In another work, de Leon Izeppi et al. (84) provided evidence of the benefit of using a CFME to monitor pavement friction.

In the case of Macrotexture, different indices and devices have been used in the literature to describe the texture characteristics. Still the most widely used among state highway agencies are *MPD*, *MTD*, and *RMS* (7). However, other indices such as Skewness (*Rsk*) and Kurtosis (*Rku*)

seem promising, and some agencies have started to include them in their PFMP (85). Also, with increasing computational power, more research has been published related to aerial parameters. Based on the initial analysis presented so far, it appears that aerial parameters correlate better with friction (5).

Finally, during the NCHRP 10-98 (85) several equipment manufacturers that each used different technology to measure texture were analyzed. The experiment considered testing speed and exposure time for the laser sensors. The experiment also used a reference measurement beam manufactured to collect static reference texture data using a high-resolution laser and collected data on a series of manufactured surfaces. The main conclusions from that experiment were:

- Single-spot and line-laser *MPD* results should not be used inter-changeably when longitudinal pavement texturing is present. Single-spot lasers are not capable of adequately capturing longitudinal pavement texture when compared to line lasers.
- Most off-the-shelf macrotexture equipment measurement results are repeat-able and generally agree well with one another if similar sensing technologies are used.
- The use of commercially available walking macrotexture measuring equipment with a line laser appears to be the most practical method to collect reference profiles to verify and/or certify high-speed macrotexture measuring devices.
- Engineered surfaces with properly prepared surfaces can and probably should be used to test the accuracy of line-laser-equipped reference walking devices.
- The use of a line laser oriented at a 45° angle to the travel direction appears to be the most practical solution for measuring pavements with a longitudinal or transversal engineered macrotexture (like a grooved PCC pavement).

Establishing Investigatory Thresholds

Investigatory friction threshold levels (IL) are threshold values of friction that identify locations where friction may be at a level that may increase the risk of a crash. These levels trigger the need for an investigation to determine if remedial action is warranted. Hall et al. (7) has proposed three methods to establish these thresholds. This methodology was developed based on a friction monitoring program that uses the LWST and thus de Leon Izeppi et al. (18) has proposed a methodology for determining ILs using CFME. In the next subsections, first the three methods from Hall et al. (7) are described using a set of examples developed by de Leon Izeppi et al. (18), and then the methodology proposed by de Leon Izeppi et al. will be analyzed.

NCHRP 108 (GPF) Method (7)

The Guide for Pavement Friction (GPF) has proposed three methods to determine the investigatory thresholds. To apply these methods, it is necessary to divide the network into 0.1-mile segments and group these segments by friction demand category. However, it is important to keep in mind that the GPF bases on the use of LWST data and new research has proved that using a LWST to characterize friction at a network level is not ideal, because it is quite difficult to match specific friction location with crashes.

- **Method 1: Establishing thresholds using pavement friction data only.** The main problem with this method is that relies completely in the capacity to observe a change in the friction rate of deterioration, which may be complicated because friction is a long-term process with a gradual deterioration rate. An example of this method is presented in Figure

A.25. As depicted, this plot shows a deterioration of friction over time; however, the rate of friction loss does not have a demonstrable significant increase at a certain point in time.

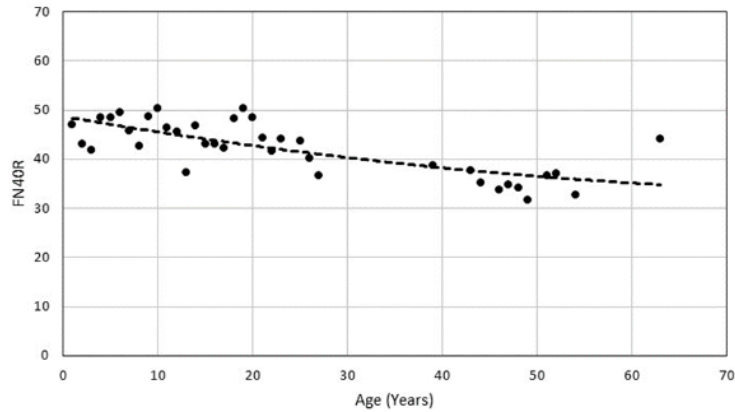


Figure A.25. LWST friction versus pavement age for divided, non-event friction demand segments (Method 1) (18).

- Method 2: Establishing thresholds using both historical friction data and crash data.** For this method it is necessary to plot friction data against pavement age, in addition it is necessary to plot crash data on the same graph. An example of this method is illustrated in Figure A.26. A problem associated with this method is confronted when there are zero dry crash counts, which makes the wet/dry crash ratio undividable. Also, like Method 1 it is hard to identify a change in friction rates that may be linked to crash data variation.

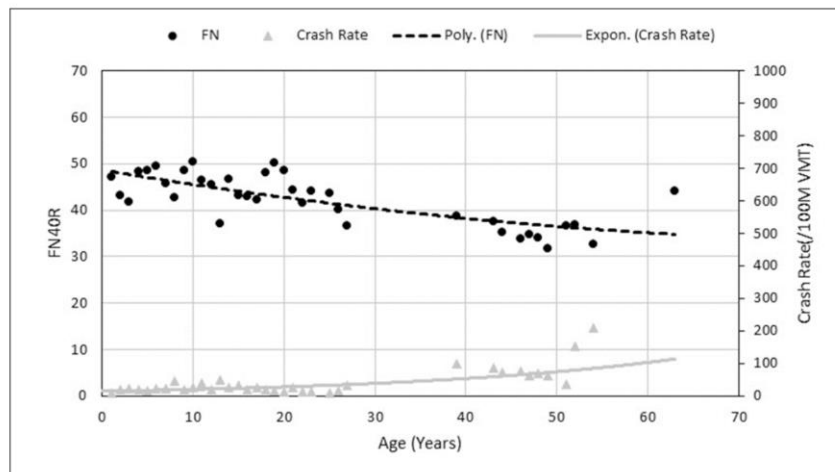


Figure A.26. Graph LWST friction versus pavement age for divided, non-event friction demand segments (method 2) (18).

- Method 3: Establishing thresholds using pavement friction distribution and crash rate – friction trend.** Plot the histogram of all friction values and plot the wet-to-dry crash ratio for each friction bin for each friction demand category. Again, when there are zero dry crash counts the wet/dry ratio is undividable. The investigatory threshold is established as the friction mean minus x-standard deviations, where x-standard deviations correspond to the level where crash rates begin to increase considerably. The problem with this method is that crashes are averaged by friction bin, which may not be representative of the risk at

all individual locations with the same friction number. Also, as indicated in Figure A.27 there is not an evident increase in crash ratio at a certain friction value.

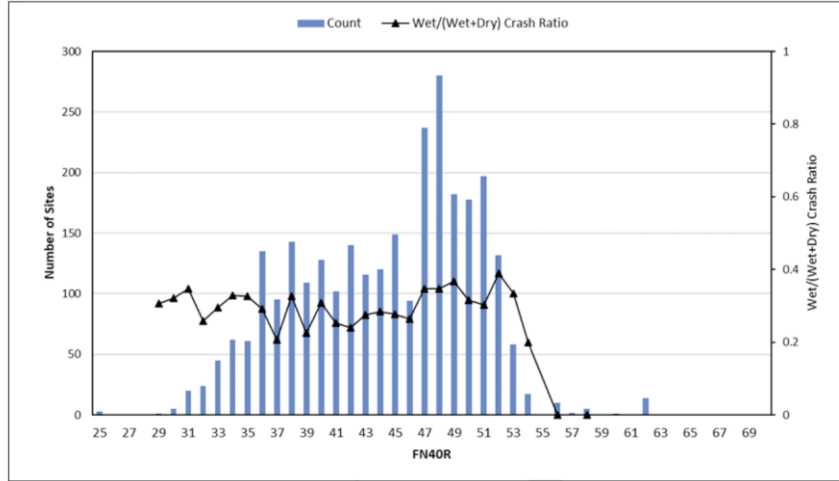


Figure A.27. LWST friction distribution and wet/(wet+dry) crash ratio for divided non-event friction demand segments (Method 3) (18).

Establishing Friction Investigatory Thresholds using CFME data

de Leon Izeppi et al. (18) has proposed a constrained least square (CLS) method to directly compute the investigatory threshold. CLS uses linear regression modeling to fit two lines of crash risk data that intersect at a single point. The optimum point of intersection, x_i , is the value of friction that minimizes the mean square error (MSE). This is an objective approach in which the IL is obtained by mathematical methods not just visual observations. An example of this approach is depicted in Figure A.28.

$$\begin{bmatrix} \hat{\beta} \\ z \end{bmatrix} = \begin{bmatrix} 2A^T A & C^T \\ C & 0 \end{bmatrix}^{-1} \begin{bmatrix} 2A^T y \\ 0 \end{bmatrix} \tag{96}$$

$$y(x) = \begin{cases} a_1 x + b_1; & x \leq x_i \\ a_2 x + b_2; & x > x_i \end{cases} \tag{97}$$

$$C = [x_i \quad 1 - x_i \quad -1] \tag{98}$$

where;

- β = estimated vector of parameters (a_i and b_j) contained skid resistance,
- A = matrix of predictors, column of ones for the intercept,
- y = response vector, i.e., crash counts or crash rates, and
- z = lagrange multiplier, and the value is not of interest in the analysis.

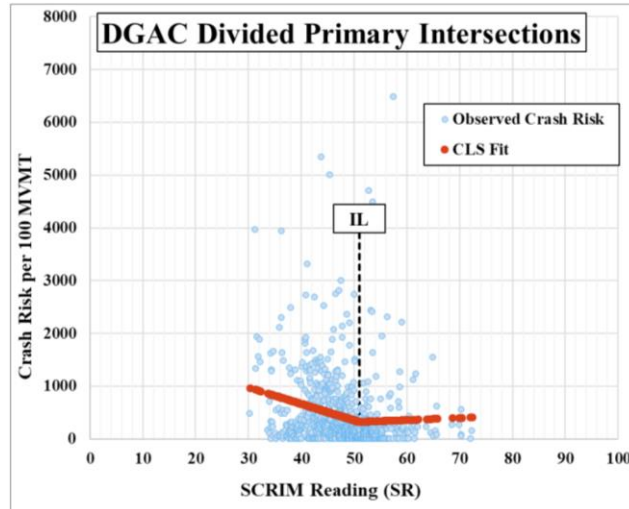


Figure A.28. Investigatory levels determined with CLS regression (18).

Using this approach and the database of four states, de Leon Izeppi et al. computed a set of preliminary investigatory thresholds, these are summarized in Table A.6. Important to keep in mind for this analysis friction was characterized by a SCRIM machine and friction values have been standardized to 50-mph. In addition, the authors stated the data samples were not as robust as necessary to establish statistically sound values for the ILs of friction.

Table A.6. Illustrative state ILs of friction for different friction demand categories (18).

Friction Demand Categories	State A	State B	State C	State D
Interstates Non-Events	N/A	30-35	40-45	30-35
Divided Primary Non-Events	N/A	35-40	40-45	30-35
Undivided Non-Events	N/A	40-45	N/A	50-55
All Non-Events	35-40	N/A	N/A	N/A
Horizontal Curves	N/A	50-55	N/A	50-55
Intersections, Ramps, etc.	45-50	50-55	N/A	55-60

Friction and Texture Thresholds

In the U.S. the most used device to characterize friction is the LWST (84). Regardless of the methodology used, the numerical skid resistance value associated with a specific pavement is usually presented as a two-digit constant, determined by multiplying the measured friction coefficient by 100 (though sometimes the number is left as a decimal). This number is described as the friction number (*FN*) or skid number (*SN*), note that *FN* rather than *SN* is the preferred abbreviation. *FN* is usually followed by the speed value at which the friction measurement was taken and the type of tire (i.e., *FN50S* represents the friction measurement taken at 50 mph with a smooth tire).

The previous notation is mainly used to summarize the results of the LWST. However, because the use CFME is becoming more and more common nowadays, it is also customary to finding the acronym of *SR* (scrim reading) or *GN* (grid number), depending on the device that has been used. The threshold established by the WDOT is based on the model given by Equation (53). This model states a desirable minimum predicted *FN* of 35 but does not differentiate between factors such as microtexture and macrotexture. Based on Equation (53) the WDOT has set the recommended *FN* values shown in Table A.7.

Table A.7. Typical skid resistance value ranges measured with a LWST (67).

FN40S	Recommendations
<30	Take action to correct pavement
≥30	Acceptable for low volume roads
31-34	Monitor pavement frequently
≥35	Acceptable for heavily traveled roads

Different numerical values of skid resistance are used outside of the U.S. In U.K. the road surface friction on the English Strategic Road Network (SRN) is managed through the requirement for skid resistance and texture depth (68). The requirements have been in place since the 1980s and were last reviewed prior to the 2004 update to the skid resistance Standard (HD28). The HD28 standard is based on routine measurements, the data from which trigger investigations of individual sites where the skid resistance is low. The thresholds to trigger site investigations (Investigatory Levels, ILs) are indicated in Table A.8. These thresholds were set for friction measured with a Scrim Machine, and corrected for seasonality and standardized to a speed of 50 km/h.

Table A.8. Site categories and investigatory levels from HD28 (86).

Site Category and Definition	IL for Skid Resistance					
	0.30	0.35	0.40	0.45	0.50	0.55
A Motorway						
B Non-event carriageway with one-way traffic						
C Non-event carriageway with two-way traffic						
Q Approaches to and across minor and major junctions, approaches to traffic signals and roundabouts						
K Approaches to pedestrian crossings and other high-risk situations						
R Roundabout						
G1 Gradient 5-10% longer than 50 m						
G2 Gradient >10% longer than 50 m						
S1 Bend radius <500 m – carriageway with one-way traffic						
S2 Bend radius <500 m – carriageway with two-way traffic						

In Table A.8, dark shading indicates the range of ILs that will normally be used on the SRN for each type of site. Lighter shading indicates lower ILs that can be used for low-risk situations, such as locations with low traffic or where the risks normally present are mitigated. The overall concept is that higher ILs are assigned at locations where the risk of collisions involving skidding is greater, thereby attempting to achieve an equalization of risk. An IL is defined for every element of the network, by determining which site category is most appropriate to each location and then selecting an appropriate IL from within the range for that site category, Table A.8. The objective of setting an IL is to assign a level of skid resistance appropriate for the risk on the site, at or below which further investigation is required to evaluate the site-specific risks in more detail.

Sites with the same category may have different levels of risk of skidding crashes. So, there is flexibility to set different ILs for different sites within the same category. This allows sites where the risk of skidding crashes is potentially higher to have a higher IL and possibly be treated to maintain a higher level of skid resistance. The process to set an IL for an element of the network is depicted in Figure A.29. According to the HD28 standard, once the IL is established it must be revisited every three years. All sites where the measured friction is at or below the IL shall be investigated. The objective is to determine whether a surface treatment is justified to reduce the risk of vehicles skidding, whether some other form of action is required, or whether no action is

currently required. If no action is taken, sites will automatically be reviewed again following the next skid resistance measurement if they remain at or below the IL. Figure A.30 depicted the initial investigation scheme proposed in the HD28 standard. It is recommended to make this analysis in sections of 100-m length.

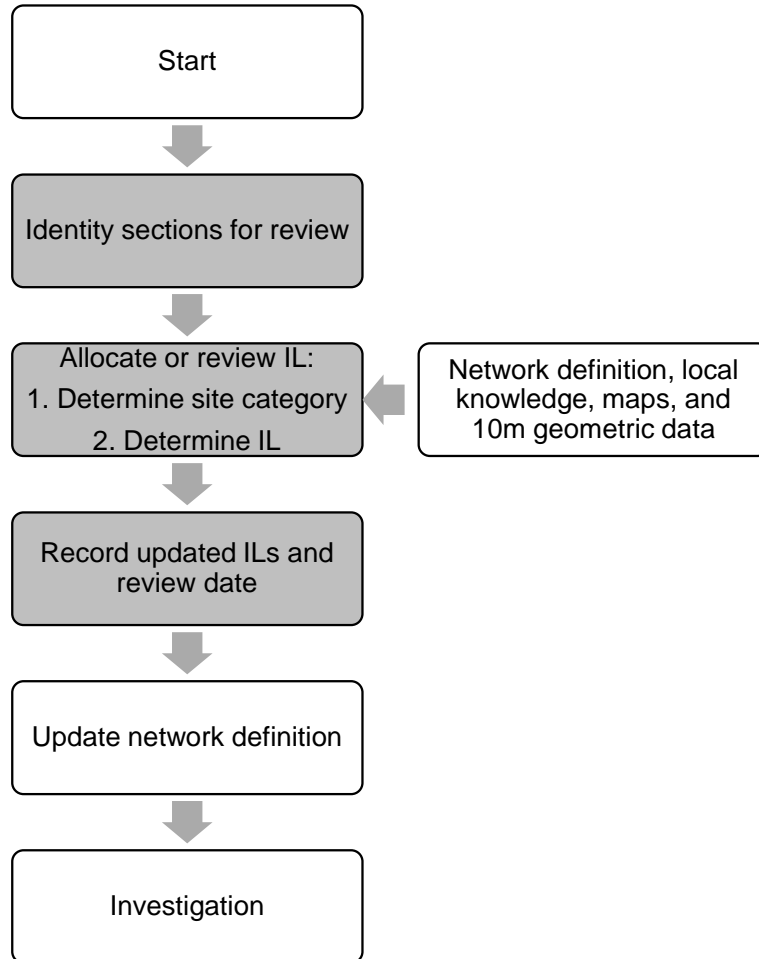


Figure A.29. Setting the investigatory level (86).

In New Zealand, the T10 pavement specification established that the SCRIM must be used for measuring friction. The measurements must be conducted throughout the whole primary network during the summer months. Table A.9 summarizes the skid resistance ILs used in New Zealand. Finally, using a series of historical values collected in the state of Washington using the SCRIM machine, Flintsch et al. (1) proposed the limits shown in Table A.10 for skid resistance investigatory levels.

As noted, all the references presented above have tried to establish an investigatory threshold that can be used to flag locations for further evaluation. References indicating an intervention level are scarce, and because of the high complexity associated with a crash event, is better to identify sites that may represent a hazard in terms of friction and start monitoring them. In addition, the literature review found that none of the state agencies in the U.S. are using a surface texture characteristic for evaluating safety performance. Despite this situation, a lot of work has been done trying to

relate both friction and macrotexture with crash rates or total number of crashes, and it has been found that the macrotexture is a better predictor than friction.

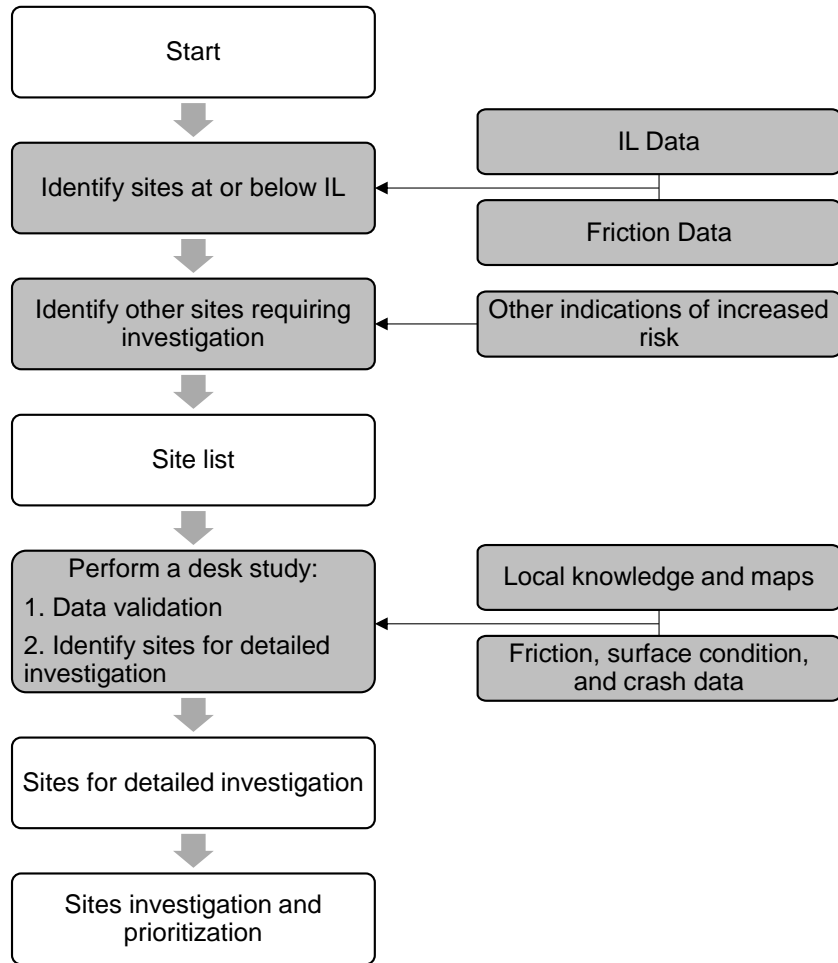


Figure A.30. Initial investigation scheme (86).

Table A.9. T10:2002 Skid Resistance Investigatory Levels in New Zealand (87).

Site Category	Description	Notes	Investigatory Level (ESC)			Skid Assessment Length (m)
5	Divided carriageway	Even free	0.35			100
4	Normal roads	Undivided carriageways only (event free)	0.45			100
3d	Roundabouts, circle only	Circular section only				60
3b and 3c	Down gradients 5%-10%	Includes motorway on/off ramps	0.45			50
3a	Approaches to junctions					60
2	Urban curves R<250 m	All risks	0.50			50
	Rural curves R<250 m	Low risks Med risks High risks	0.45	0.50	0.55	
	Rural curves, 250<R<400 m	Low risks Med risks High risks	0.40	0.50	0.55	
	Down Gradients > 10%	Includes on ramps with ramp metering	0.50			
1	Highest priority	Railway level crossing, approaches to roundabouts, traffic lights, pedestrian crossings, and similar hazards.	0.55			60

Table A.10. SCRIM Friction Thresholds Using GPF Method 3 (1).

Type of Roadway	SR Investigatory Level
Divided	30-35
Undivided	50-55
Curves	50-55
Intersections	55-60

Similar to friction, defining a threshold for macrotexture that represents a safe condition is a difficult task. However, some studies have brought some ideas about this; for example, the work of Pulugartha (69) established that the *MPD* must be greater than 1.524 mm but less than 3.048 mm, in order to reduce the number of crashes. Likewise, the work of Flinstch et al. (1) recommended that the *MPD* must be greater than 0.8 mm for roads with a speed limit of 50 mph, and 1.0 mm for roads with a speed limit of 70 mph. Similar attempts have been made in the United Kingdom and New Zealand as shown in Table A.11 and Table A.12. These tables show the minimum *MPD* a new pavement surface should have to provide a safe operating condition.

Skid resistance performance has also been studied in detail by the Federal Aviation Administration (FAA). The FAA conducted a set of measurements with different devices and different pavement surface characteristics and published the Advisory Circular (AC) No. 150/5320-12D (29) based

on the results. This AC contains guidelines and procedures for pavement evaluation with friction measuring equipment, and maintenance of high skid-resistant pavements. Table A.13 is shown below as a reference for the measurement frequency recommended by the FAA. In addition, the FAA recommended that friction should be measured at either 40 mph (65 km/h) or 60 mph (95 km/h). The lower speed provides an indication of the overall microtexture/contaminant/drainage condition of the pavement surface. The higher speed provides an indication of the condition of the surface's macrotexture. According to the FAA, a complete survey should include tests at both speeds. Since friction values depends on both tire properties and the pavement surface the FAA has recommended a set of minimum and threshold for trigger maintenance for some popular devices as indicated in Table A.14.

Table A.11. Requirements for Initial Texture Depth for Trunk Roads Including Motorways, U.K. (1).

Road Type	Surfacing Type	Average/1,000 m	Average/10 measures
High Speed roads >50 mph	Thin surface overlay Agg. Size<14 mm	MTD > 1.3 mm (MPD 1.4 mm)	MTD > 1.0 mm (MPD 1.0 mm)
	Surface treatments	MTD > 1.5 mm (MPD 1.6 mm)	MTD > 1.2 mm (MPD 1.25 mm)
Lower Speed roads <40 mph	Thin surface overlay Agg. Size<14 mm	MTD > 1.0 mm (MPD 1.4 mm)	MTD > 0.9 mm (MPD 0.9 mm)
	Surface treatments	MTD > 1.2 mm (MPD 1.25 mm)	MTD > 1.0 mm (MPD 1.0 mm)
Roundabout, high speed>50 mph	All surfaces	MTD > 1.2 mm (MPD 1.25 mm)	MTD > 1.0 mm (MPD 1.0 mm)
Roundabout, low speed <40 mph	All surfaces	MTD > 1.0 mm (MPD 1.0 mm)	MTD > 0.9 mm (MPD 0.9 mm)

Table A.12. Minimum Macrotexture Requirements for New Zealand (87).

Permanent Speed Limit PSI (km/h)	Minimum macrotexture – Mean Profile Depth (mm)					
	Chip Seal		Asphalt Concrete ESC > 0.40		Asphalt Concrete ESC < 0.40	
	ILM ¹	TLM ¹	ILM ¹	TLM ¹	ILM ¹	TLM ¹
PSL < 50	1.00	0.70	0.40	0.30	0.50	0.50
50 < PSL < 70	1.00	0.70	0.40	0.30	0.70	0.50
PS > 70	1.00	0.70	0.40	0.30	0.90	0.70

¹ ILM = Investigatory level for macrotexture; TLM = Threshold level for macrotexture

Table A.13. FAA recommended friction survey frequency (29).

Number of daily minimum turbojet aircraft landings per runway end	Minimum friction survey frequency
Less than 15	1 year
16 – 30	6 months
31 – 90	3 months
91 – 150	1 month
151 – 210	2 weeks
Greater than 210	1 week

Table A.14. FAA recommended friction level classification for runway pavement surfaces (29).

Device	40 mph (65 km/h)		60 mph (95 km/h)	
	Minimum	Main. Plan.	Minimum	Main. Plan.
Airport surface friction tester	0.50	0.60	0.34	0.47
Safegate friction tester	0.50	0.60	0.34	0.47
Dynatest runway friction tester	0.50	0.60	0.41	0.54
Griptester Friction Meter	0.43	0.53	0.24	0.36
Halliday Technologies RT3	0.45	0.55	0.42	0.52
BV-11 Skiddometer	0.50	0.60	0.34	0.47
Mu Meter	0.42	0.52	0.26	0.38
NAC Dynamic Friction Tester	42	52	28	38
Norsemeter RUNAR (fixed 16% slip)	0.45	0.52	0.32	0.42
Tatra Friction Tester	0.48	0.57	0.42	0.52

Within normal ranges, low skid resistance does not cause crashes although, depending on the circumstances, it may be a significant contributory factor (86). The level of skid resistance, even on a polished surface, will generally be adequate to achieve normal acceleration, deceleration and cornering maneuvers on sound surfaces that are wet but free from other contamination. However, higher skid resistance is required to allow maneuvers that demand higher friction to be completed safely, e.g., to stop quickly or corner sharply. Higher skid resistance can therefore reduce crashes in cases where drivers need to complete a more demanding maneuver to avoid a crash (86). Crash analyses have therefore proposed that a relationship exists between measured friction and crash risk. However, these relationships are not precise and differences in skid resistance may account for only a relatively small part of the difference in crash risk between individual sites because of all the other factors involved (68).

The reduction of friction with speed depends on surface type and texture depth. As such, sites with low skid resistance and low texture depth should be prioritized. The typical reduction of friction experienced by traffic with speed and the influence of texture depth is illustrated in Table A.15. The effect of texture depth becomes apparent at speeds as low as 50 km/h but becomes increasingly significant at higher speeds (86).

In this line, the National Transportation Safety Board and FHWA concluded that about 70 percent of wet pavement crashes could be prevented or minimized by improved pavement surface friction (64). Wallman and Astrom (88) developed a relationship between pavement friction and roadway crash rate, revealing that higher friction can significantly reduce the crash rate Table A.16.

Friction Demand Categories

Identifying the level of friction needed by the driving public is the important first step in a PFMP. However, because of the great number of factors that may affect the friction developed in the tire-pavement interface, there is not a universal criterion for defining the existing friction demand levels, nevertheless there is a consensus that a rational estimate can be developed by evaluating the array of factors comprising by four broad categories (7, 17, 22):

- highway alignment,
- highway features/environment,
- highway traffic characteristics, and

- driver/vehicle characteristics.

However, because the driver/vehicle characteristics such as driver skills and age, vehicle tire characteristics, and vehicle steering capabilities, are difficult to assess in terms of friction demand, they are rarely included in a PFMP.

Table A.15. Typical reduction in skid resistance experienced by traffic compared with SCRIM machines measurements (86).

Speed	Mean Texture Depth (mm)		
	Below 0.5	0.5-0.8	Above 0.8
50 km/h	40%	30%	25%
120 km/h	70%	60%	50%

Table A.16. Friction coefficients and crash rate (88).

Frictional Coefficient	Crash Rate (injuries per million vehicle km)
<0.15	0.80
0.15-0.24	0.55
0.25-0.34	0.25
0.35-0.44	0.20

Highway Alignment

Friction demand is highly influenced by the highway geometry (its horizontal and vertical alignment). The amount of friction required increases with increasing complexity of the highway horizontal alignment, the grade of the vertical alignment, and the stopping sight distance requirements. The relationship between side-force friction for horizontal curves (the most critical horizontal alignment), vehicle speed, radius of curvature, and highway cross-section (super-elevation) is defined using the following AASHTO Green Book equation (89):

$$F_s = \frac{V^2}{15 \times R} - e \quad (99)$$

where;

F_s = side-force friction demand, in lb,

e = super-elevation rate, ft/ft,

V = speed, mi/hr, and

R = radius, ft.

As the speed increases, the force required to maintain a circular path eventually exceeds the force that can be developed at the pavement-tire interface and super-elevation. At this point, the vehicle begins to slide in a straight line, tangential to the highway alignment. In addition to the vehicle speed, the curve radius and the super-elevation, F_s is a function of climate, tire condition, and driver comfort while performing maneuvers (e.g., braking, making sudden lane changes, and making lateral movements within a lane).

For the vertical alignment, the AASHTO green book defines the Stopping Sight Distance (SSD) as the distance required for a driver (with a 1 m eye height) to clearly see an object of 0.15 m (0.5 ft) or more in height on the highway with enough distance to perceive, react and brake the car to a stop on a poor wet pavement. The SSD distance is calculated using the Equation (100), as shown,

this distance is the arithmetic sum of two distances, the distance traveled while the driver perceives the obstacle in the road, and the distance required to bring the car to a stop once the driver starts braking (89).

$$SSD = (1.47 \times v \times t) + \frac{V^2}{30(\mu \pm G)} \quad (100)$$

where;

SSD = stopping sight distance, ft,

t = driver reaction time, in s,

G = longitudinal grade, percent, and

V = speed, mi/hr.

As shown in Equation (99) and (100) besides the vehicle velocity and acceleration of gravity, the other inputs are the radius of curvature and the road superelevation grade. However, these two parameters are hard to obtain at a network level. In the other hand, in terms of curve safety, two things are critical for transportation agencies to determine: the curve advisory speed limit and the types, spacing, and locations of the curve signs that need to be placed. To determine the curve advisory speed and the placement of the curve warning signs, transportation agencies should follow the Manual on Uniform Traffic Control Devices (MUTCD) guidelines (90), which contain information regarding the determination of curve advisory speeds and curve sign locations. The curve advisory speed is unarguably the most important factor in terms of horizontal curve safety because the driving speed is the only thing that a driver can control when navigating a vehicle along a curve. It is emphasized that the curve advisory speed is not the safe speed for every type of vehicle under every condition; it is a speed obtained by a defined testing procedure that provides comfort and safety for most driving conditions. Historically, the advisory speed has been set as the 85th percentile of the free-flow vehicle operating speed (91).

The FHWA (91) have proposed six methods to establish the advisory speed for curves, these are:

- Direct Method
- Texas A&M Transportation Institute (TTI) Curve Speed Model – Compass Method
- TTI Curve Speed Model – GPS Method
- TTI Curve Speed Model – Design Method
- Ball-Bank Indicator (BBI) Method
- Accelerometer Method

The direct method asks a tester to drive over a curve at various speeds and determine the appropriate curve advisory speed subjectively. The compass method is used in combination with other methods (e.g., BBI), the purpose of the compass is to obtain the curve radius; therefore, we do not consider it as an individual method to obtain the curve advisory speed. Similarly, the GPS method is used merely to obtain the curve radius and should not be listed individually. The ball-bank indicator (BBI) method and the accelerometer method are the two methods that are widely adopted and commercialized. They both utilize digital sensors mounted on a vehicle to indirectly calculate the curve safety-related characteristics (91).

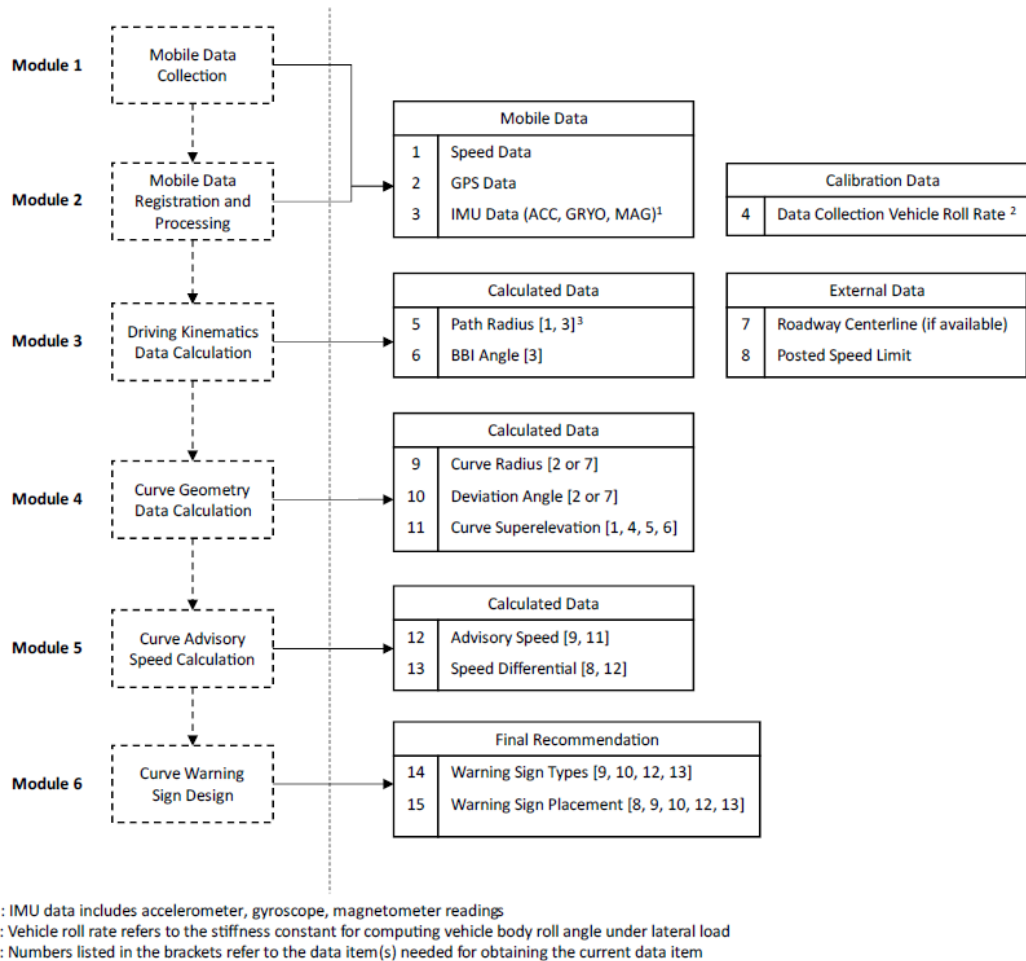


Figure A.31. Data collection and computational framework and data items for network-level curve safety assessment using mobile devices (92).

The Georgia Department of Transportation (GDOT) has conducted the research project 19-17 titled “Enhanced Network-Level Curve Safety Assessment and Monitoring Using Mobile Devices” (92), the main objective of this research effort was to define a protocol that bases on smartphones devices to characterize road geometry (radius of curvature and superelevation) and to assist in the speed advisory determination for the GDOT curves.

The authors of the GDOT Research Project 19-17 (92) proposed the framework depicted in Figure A.31. As shown, the framework consisted of six modules starting from the mobile data collection protocols and finalizing with the curve warning sign design. Of particular interest are Module 1 to 4, because using a smartphone mounted in vehicle it is possible to back calculate the geometry details of a curve by driving through the curve at normal operating conditions. Most of the back calculations are based on the BBI angle estimation. Based on the results shown in the GDOT RP19-17 the results seem promissory and can help the NCDOT to characterize their curves. This information is of particular interest to properly characterize the friction demand categories.

The BBI index (referred also as BBI angle) is calculated using vehicle kinematics equations and refers to the movement of the vehicle measured in degrees of deflection, and is indicative of the combined effect of superelevation, lateral (centripetal) acceleration, and vehicle body roll (92).

Highway features/environment

Highway features/environment is an important but hard-to-measure characteristic of traffic flow that can significantly influence pavement friction. These characteristics depend on the presence and type of median barriers, the presence or absence of specially designed lanes (e.g., left, or right turn lanes), number of conflict situations (e.g., intersections, ramps, exits/access), and more important depends on the setting (urban or rural) (7). In general, as the highway environment becomes more difficult and complex, significantly higher levels of friction are required to help drivers perform the necessary maneuvers (e.g., is expected higher friction demand in urban areas).

Highway traffic characteristics

Traffic characteristics that influence friction demand are traffic volume, composition, and speed. As traffic volume increases the number of conflicts also increases. The risk associated with any maneuver is elevated especially in high-speed areas. Also, for the same traffic levels, traffic composition may significantly affect the friction demand, mainly because in comparison to passenger cars, the trucks have worse steering capabilities, require longer distances to stop, and their tires produce less friction (7). Finally, vehicle speed is the most important variable influencing friction demand. As can be seen in Figure A.32, the friction developed at the tire-pavement interface reduces as the vehicle speed increases (this phenomenon is aggravated in wet conditions). The speed at which the friction demand is exactly equal to the available friction is known as the Skid Limit, or Speed of Impending Skid. Finally, increasing speed (above 40 mph [60 km/h]) increases the likelihood of hydroplaning, which is a major cause of wet-weather crashes. Besides, the higher the speed, the higher the severity in a collision.

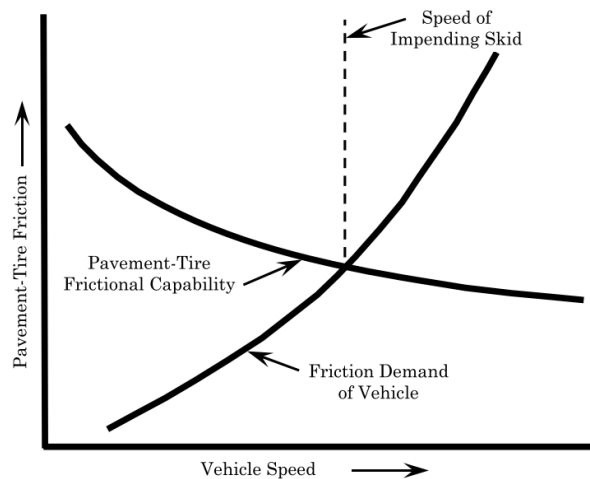


Figure A.32. Conceptual relationship between friction demand, speed, and friction availability (7).

Knowledge Gaps

This section has summarized the elements that constitute a PFMP, explained the available methods used to establish a friction investigatory threshold, and discussed the aspects needed to set the friction demand categories. After reviewing the relevant literature related to these topics there are some important knowledge gaps.

- In the case of North Carolina, information related to highway alignment is not easily available at a network level, in particular the super elevation and curve radius. Surrogates of

this information, such as the BBI index can be used, but it is necessary to evaluate the relationship of this index with crash risk and friction. The BBI is a cheap alternative that can be used to supplement North Carolina's PFMP.

- Though the thresholds proposed by FAA serve as a reference, it is important to notice these values were envisioned for airports. To set investigatory levels for a highway network it is necessary to include crash risks, which can be estimated by means of a SPF.
- Although there are some references in the U.S. for friction and texture thresholds, most of these references are based on a LWST.
- Despite texture being easier to measure at a network level, most agencies do not have a measurement protocol for texture. Moreover, the attempts to use texture information as a predictor in a SPF are quite limited.
- In the PFMP structures available in the literature, the component that relates friction and texture in the field has not been explored. In fact, in the U.K. or New Zealand there are no references for the quality control process of friction and texture in the field. It is imperative that such protocol becomes available among practitioners.

Conclusions

Based on the literature reviewed in previous sections, the following statements can be made.

- The most accurate representation of the friction variation with speed and slip ratio is provided by the RADO model. To calibrate this model for a given pavement requires friction observations for at least three different speeds. By using this model, it is possible to account for more realistic friction mechanisms such as those of an ABS braking system and are suitable for Continuous Friction Measurement Equipment (CFME) where the slip ratio (SR) is around 15-20%.
- The most used equipment for collecting static friction and texture measurements are the Dynamic Friction Tester (DFT) and the Circular Track Meter (CTM). These two devices are coupled with the Three-Wheel Polishing Device (TWPD) to evaluate aggregate and pavement surfaces traffic polishing resistance.
- Static texture measurements, such as the ones obtained with portable laser devices, provide a more complete description of the surface texture than the one provided by the CTM.
- Correlating aerial texture parameters to friction seems promising.
- The recommended statistical function to model crash events is the negative binomial. A complete Safety Performance Function (SPF) should include traffic, geometry, and pavement condition indicators.
- Crashes are spatially correlated. This correlation needs to be accounted for to improve the relationship with friction. To identify a relationship between friction, or texture, and crashes it is necessary to aggregate crashes in no more than 1-mile increments. Finer resolutions, such as 0.1-mile or 0.5-mile, are desired.
- Non-parametric methods, such as bootstrap sampling can be useful to overcome the small-sample problem after an overlay.
- A sound SPF function for each friction demand category is needed to establish friction and texture investigatory thresholds.

To establish the friction demand categories, it is necessary to obtain specific road geometry details, such as cross-slope, super elevation, and curvature radius, for each element in the network. In the case of North Carolina, this information is not available for all the road segments.

APPENDIX B. MIXTURE VOLUMETRICS OF TESTED SITES

Table B.1. Group-1 sites selected for friction and texture measurements.

Site	Route Type ¹	Mix Type	#Obs.	AC%	VFA	VMA	P ₂₀₀	Cc	P _{4.75}	P _{2.36}	AADT ²
1	I	S9.5C	3	6.4	75.7	17.3	6.3	0.5	75	60	19,242
2	I	S9.5C	3	6.3	77.2	18.2	7.5	0.6	78	65	13,719
3	US	S9.5B	4	5.7	76.0	17.2	5.7	1.1	70	53	4,382
4.1	I	UTBWC	4	5.5	0.0	0.0	4.1	5.1	42	24	57,930
4.2	I	S9.5D	5	6.0	76.5	17.3	5.8	0.8	68	48	41,683
5	I	UTBWC	7	5.5	0.0	0.0	3.5	2.0	44	27	41,799
6	I	S9.5D	9	5.6	76.5	16.7	5.8	0.8	68	52	76,546
7	I	S9.5D	7	5.7	76.0	16.7	6.5	0.8	74	63	50,469
8	NC	S9.5C	8	5.7	77.8	16.9	5.8	1.2	71	52	4,415
9	NC	S9.5C	6	6.4	77.8	18.4	6.7	1.0	79	65	5,984
11	NC	S9.5C	4	6.0	76.9	17.3	7.2	0.7	82	63	41,446
12	US	S9.5B	3	5.4	75.3	16.2	6.2	0.7	75	56	18,711
13	US	S9.5C	1	6.5	77.5	17.9	7.2	0.8	82	67	62,603
14	US	S9.5B	6	6.2	76.9	17.3	7.3	0.6	83	64	12,580
15	NC	S9.5C	6	6.2	78.5	17.9	6.9	0.6	77	62	620
16	NC	S9.5C	6	6.8	78.8	18.9	7.0	0.7	78	65	1,205
17	US	S9.5C	7	5.7	74.1	17.4	5.9	0.5	75	56	13,747
18	US	S9.5D	8	5.7	75.5	16.5	6.1	0.6	72	57	25,341
19	US	S9.5C	7	6.0	76.9	17.3	7.2	0.8	82	67	47,510
23	I	S9.5C	4	6.0	76.6	17.1	7.0	0.9	76	60	16,500
24	NC	S9.5C	2	5.8	76.6	17.5	5.9	1.3	73	59	7,660
27	US	S9.5B	5	5.5	73.1	16.0	6.4	1.1	74	61	22,801
28	NC	S9.5D	3	6.6	77.7	18.7	7.8	0.8	79	65	13,723
29	NC	S9.5C	5	6.3	79.6	19.5	7.0	0.8	75	61	12,991
30	NC	S9.5C	2	5.3	75.3	16.2	6.4	1.0	75	53	21,696
33	US	S9.5C	9	5.6	75.5	16.6	6.7	0.6	70	57	16,306
34	US	S9.5C	2	5.7	77.0	16.8	6.8	0.4	73	57	18,247
35	US	S9.5C	2	5.8	74.4	17.2	6.4	0.6	76	58	18,247
36	NC	S9.5C	2	6.3	76.0	17.5	6.2	0.4	71	56	29,362
37	US	S9.5C	2	6.9	77.0	18.4	6.6	0.5	75	65	11,602
39	US	S9.5C	1	5.4	74.5	15.9	5.2	0.7	73	58	6,142
40	US	OGFC	2	6.3	36.3	30.0	2.9	1.2	38	11	21,500
41	I	S9.5C	2	5.4	16.1	75.8	6.0	0.8	72	57	5,300
42	US	S9.5C	2	6.0	17.2	76.2	6.1	0.8	71	57	4,300
43	NC	OGFC	2	6.2	30.0	39.7	2.9	1.2	43	12	21,000
44	I	UTBWC	2	5.5	22.0	50.1	4.9	4.1	42	20	51,500
45	US	S9.5C	3								16,500

¹I: Interstates, US: US-Routes, and NC: State-Routes ²AADT year 2019

Table B.2. Group-2 sites selected for friction and texture measurements.

Site	Route Type ¹	Mix Type	#Obs.	AC%	VFA	VMA	P ₂₀₀	Cc	P _{4.75}	P _{2.36}	AADT ²
101	US	UTBWC	2	5.5	34	29.6	2.3	1.4	24	9	8,900
102	I	UTBWC	2	5	0	0	5.4	6	40	25	65,500
103.1	US	UTBWC	2	5.5	0	0	4.1	5.1	42	24	62,500
103.2	US	S9.5C	2	-	-	-	-	-	-	-	60,500
104.1	I	UTBWC	2	-	-	-	-	-	-	-	51,000
104.2	I	UTBWC	2	-	-	-	-	-	-	-	51,000
105.1	US	UTBWC	2	5	0	0	4.7	0.3	40	27	19,500
105.2	US	UTBWC	2	-	-	-	-	-	-	-	19,500
106.1	US	S9.5C	2	-	-	-	-	-	-	-	36,000
106.2	US	S9.5C	2	-	-	-	-	-	-	-	37,000
106.3	US	S9.5C	2	-	-	-	-	-	-	-	41,000
106.4	US	S9.5B	2	-	-	-	-	-	-	-	44,000
107	I	UTBWC	2	5	0	0	4.1	2.5	41	28	58,000
108.1	US	S9.5C	2	-	-	-	-	-	-	-	17,500
108.2	US	S9.5C	2	-	-	-	-	-	-	-	17,000
108.3	US	S9.5C	2	-	-	-	-	-	-	-	15,500
109	I	S9.5C	2	5.6	74.5	15.8	6.4	1	72	58	11,500
110.1	US	S9.5B	2	-	-	-	-	-	-	-	34,500
110.2	US	S9.5B	2	-	-	-	-	-	-	-	33,500
111.1	I	JCP	2	-	-	-	-	-	-	-	84,000
111.2	I	UTBWC	2	-	-	-	-	-	-	-	54,500
111.3	I	UTBWC	2	-	-	-	-	-	-	-	58,000
111.4	I	OGFC	2	-	-	-	-	-	-	-	58,000
111.5	I	UTBWC	2	-	-	-	-	-	-	-	64,000
112	I	S9.5C	2	6	77	17.7	6.2	0.8	69	52	55,000
113	I	OGFC	2	6.3	30	36.3	2.9	1.2	38	11	21,500
114.1	I	OGFC	2	-	-	-	-	-	-	-	44,500
114.3	I	S9.5C	2	-	-	-	-	-	-	-	58,000
115	US	OGFC	2	6.2	0	29.9	3	2.2	34	14	11,000
116	US	OGFC	2	6.5	40.3	30.8	3	2.8	25	15	15,500
117.1	I	S9.5C	2	-	-	-	-	-	-	-	58,000
117.2	I	OGFC	2	-	-	-	-	-	-	-	36,500
117.3	I	UTBWC	2	-	-	-	-	-	-	-	62,000
118	I	UTBWC	2	-	-	-	-	-	-	-	33,500
119.1	US	UTBWC	2	-	-	-	-	-	-	-	82,000
119.2	US	S9.5C	2	-	-	-	-	-	-	-	79,000
119.3	US	S9.5C	2	-	-	-	-	-	-	-	75,500
119.4	US	S9.5C	2	-	-	-	-	-	-	-	44,000
120.1	US	S9.5C	2	-	-	-	-	-	-	-	69,000
120.2	US	S9.5C	2	-	-	-	-	-	-	-	28,000
121	I	S9.5D	2	6.2	76.5	16.6	4.2	1.4	72	51	85,000
122	US	S9.5C	2	6.2	76.6	17.1	7.6	1.2	79	61	46,000
123.1	I	S9.5D	2	-	-	-	-	-	-	-	40,500
123.2	I	S9.5C	2	-	-	-	-	-	-	-	35,000
124	I	S9.5C	2	-	-	-	-	-	-	-	1,000
125	I	Diamond Grind	2	-	-	-	-	-	-	-	138,000
126	I	UTBWC	2	-	-	-	-	-	-	-	48,500

Site	Route Type ¹	Mix Type	#Obs.	AC%	VFA	VMA	P ₂₀₀	Cc	P _{4.75}	P _{2.36}	AADT ²
127	US	S9.5C	2	5.8	77	16.5	5.1	0.9	76	55	30,000
128	I	S9.5D	2	6	76.6	17.3	7.1	0.9	78	64	44,500
129.1	I	OGFC	2	-	-	-	-	-	-	-	27,000
129.2	I	OGFC	2	-	-	-	-	-	-	-	55,500
129.3	I	OGFC	2	-	-	-	-	-	-	-	55,500
130.1	US	OGFC	2	-	-	-	-	-	-	-	19,500
130.2	US	S9.5C	2	-	-	-	-	-	-	-	17,500
131	I	UTBWC	2	5	0	0	4.1	2.5	41	28	61,500
132.1	US	S9.5C	2	-	-	-	-	-	-	-	28,000
132.2	US	S9.5C	2	-	-	-	-	-	-	-	28,000
132.3	US	S9.5C	2	-	-	-	-	-	-	-	28,000
133	US	Crack Seal	2	-	-	-	-	-	-	-	26,000
134	I	OGFC	2	5.9	30.5	34.1	2.9	1.3	24	8	22,000
134.1	I	OGFC	2	-	-	-	-	-	-	-	65,000
134.2	I	OGFC	2	-	-	-	-	-	-	-	47,500
135	US	S9.5C	2	5.6	75.5	16.3	6.4	0.4	70	56	32,000
137.1	US	S9.5C	2	-	-	-	-	-	-	-	32,500
137.2	US	S9.5C	2	-	-	-	-	-	-	-	36,000
138	I	S9.5C	2	6	76	16.8	5.5	0.7	74	52	27,500
139.1	I	S9.5D	2	-	-	-	-	-	-	-	38,000
139.2	I	S9.5D	2	-	-	-	-	-	-	-	34,000
140	US	S9.5B	2	6.5	77.6	18.6	6.5	0.9	84	58	16,000
141.1	I	UTBWC	2	-	-	-	-	-	-	-	74,000
141.2	I	S9.5C	2	-	-	-	-	-	-	-	122,000
142	I	S9.5C	2	5.6	74.6	16	6.3	0.5	70	55	18,000
143.1	I	OGFC	2	-	-	-	-	-	-	-	47,000
143.2	I	S9.5D	2	-	-	-	-	-	-	-	46,000
144	US	UTBWC	2	5.2	33	29.2	3.2	1.6	28	13	30,000
145	US	S9.5C	2	6.9	76.4	17.9	6.8	0.8	81	67	32,000
146	I	S9.5D	2	5.2	76.5	16.8	6	1	71	53	65,000
147	US	S9.5C	2	6.2	76	16.2	5	0.8	73	60	22,000
148.1	US	S9.5C	2	-	-	-	-	-	-	-	20,000
148.2	US	S9.5C	2	-	-	-	-	-	-	-	27,000
149	US	OGFC	2	6	42.8	28.1	2.5	1.5	33	12	18,500
150.1	I	S9.5C	2	-	-	-	-	-	-	-	22,500
150.2	I	S9.5C	2	-	-	-	-	-	-	-	44,000
150.3	I	S9.5C	2	-	-	-	-	-	-	-	44,500
150.4	I	S9.5C	2	-	-	-	-	-	-	-	26,500
151	I	S9.5C	2	6	76.5	17.9	4.9	1.1	71	49	19,000
152	I	UTBWC	2	5	0	0	4.1	3.3	42	18	68,500
153.1	US	S9.5C	2	-	-	-	-	-	-	-	21,000
153.2	US	S9.5C	2	-	-	-	-	-	-	-	21,000
154	I	S9.5C	2	6.2	77.8	18	6	0.6	78	65	16,000
155	US	S9.5C	2	6.3	77	18.1	7.2	0.8	80	65	15,500
156	I	JCP	2	-	-	-	-	-	-	-	83,500
157.1	US	UTBWC	2	-	-	-	-	-	-	-	18,500
157.2	US	UTBWC	2	-	-	-	-	-	-	-	18,500
158	US	S9.5C	2	6.2	77.8	18	7.5	0.6	78	65	23,500

Site	Route Type ¹	Mix Type	#Obs.	AC%	VFA	VMA	P ₂₀₀	Cc	P _{4.75}	P _{2.36}	AADT ²
159	I	S9.5C	2	5.9	77.5	17.1	6.6	0.9	73	57	28,500
160	US	S9.5C	2	6.2	77.5	18.2	6.6	0.6	66	51	35,000
161	US	Crack Seal	2	-	-	-	-	-	-	-	14,500
162	US	S9.5B	2	5.8	79	16.3	5.6	0.9	73	55	14,000
163	I	S9.5C	2	5.8	75.6	16.4	6.1	0.8	70	55	104,000
164	NC	JCP	2	-	-	-	-	-	-	-	46,500
165.1	US	S9.5C	2	-	-	-	-	-	-	-	38,500
165.2	US	S9.5C	2	-	-	-	-	-	-	-	39,500
165.4	US	OGFC	2	-	-	-	-	-	-	-	77,000
165.5	US	S9.5C	2	-	-	-	-	-	-	-	48,500
166.1	US	S9.5C	2	-	-	-	-	-	-	-	15,000
166.2	US	S9.5C	2	-	-	-	-	-	-	-	32,500
167	I	S9.5D	2	5.3	75	15.8	5.4	0.7	72	56	41,000
168	I	OGFC	2	6	0	0	2.7	2.8	39	15	35,500
169	NC	S9.5B	2	5.4	75	16	6.2	1.1	72	59	7,800
170.1	US	OGFC	2	-	-	-	-	-	-	-	30,500
170.2	US	OGFC	2	-	-	-	-	-	-	-	21,000
171.1	US	S9.5C	2	-	-	-	-	-	-	-	20,000
171.2	US	S9.5C	2	-	-	-	-	-	-	-	4,000

¹I: Interstates, US: US-Routes, and NC: State-Routes ²AADT year 2019

APPENDIX C. DEVICE COMPARISON

This appendix presents the results of a comparison between the two devices used in this project for collecting friction and texture measurements at a network level. These measurements were conducted by KPR engineering and WDM USA. For friction, KPR used the Moventor Skiddometer, BV-11, and WDM used the Sideways-Force Coefficient Routine Investigation Machine (SCRIM). In the case of texture, KPR used the AMES High-Speed Texture Profiler (HSTP), and WDM used a mounted laser in the SCRIM machine.

Friction Comparison

The friction coefficient can be measured in the longitudinal or in the lateral direction. In the first case, the main plane of the testing tire is parallel to the direction of travel, whereas in the second case the tire has a yaw angle with the respect the direction of movement.

In this sense, the BV-11 is a longitudinal friction testing machine that has the following specifications:

- Mode of Braking: Continuous slip ratio of 17%.
- Tires: Two references and one measuring tire, smooth.
- Water film thickness: A uniform water depth of 1 mm in front of testing tire.
- Measuring speed: Measuring speed range of 20 to 160 km/h (12.5 to 100 mph).
- Frequency of results reported: Friction averaged every 3 m (10 ft).
- Measurement location: right wheel path (RWP) of outermost lane.

On the other hand, the SCRIM is a side-force friction testing machine, meaning the resulting friction value is a lateral friction coefficient, and has the following specifications:

- Mode of Braking: Variable slip ratio.
- Yaw angle: 20 degrees (resulting in an approximate 34% slip ratio).
- Tires: Smooth tire (narrow).
- Water film thickness: A uniform water depth of 0.5 mm in front of testing tire.
- Measuring Speed: variable speed, but as close as possible to 50-mph.
- Frequency of results reported: Scrim Reading (*SR*) averaged every 8 m (26.4 ft).
- Measurement location: left wheel path (LWP) of outermost lane.

The reported *SR* is processed using two corrections factors that intends to remove the effect of a testing speed different than 50 mph and a pavement temperature different than 25. The first correction is made with Equation (101) and the second correction is made using Equation (102).

$$SR(\text{at } 64.37 \text{ km/h}) = SR(S) \cdot \frac{-0.015 \cdot S^2 + 4.765 \cdot S + 799.25}{1043.82} \quad (101)$$

$$SC = \frac{SR(\text{at } 64.37 \text{ km/h})}{0.548 + \frac{44.69}{92.3 + 0.48 \cdot (T_{air} + T_{surface})}} \quad (102)$$

where;

SR(*S*) = SCRIM reading at testing speed *S*,

SC = Standardized SCRIM coefficient,

S = Testing speed in km/h,

T_{air} = air temperature in Celsius degrees, and
 $T_{surface}$ = pavement surface temperature in Celsius degrees.

To help differentiate between the values reported by the two devices, a named convention was employed; the friction resulting from KPR's records is referred as FN , whereas the value obtained from WDM's measurements is referred as SC . In summary, both devices measure a different friction response, the BV-11 characterizes friction longitudinally whereas the SCRIM does it laterally. Also, other fundamental aspects such as the slip ratio, measurement speed, and testing wheel path are different. Because of all these differences, it might be difficult to find a good correlation between the two devices.

Texture Comparison

Both devices collected the texture profile of the tested wheel path and then processed the raw profile using the ISO-13473-1 standard. The texture parameter used in this analysis was the Mean Profile Depth (MPD). To help differentiate between the values reported by the two devices, a nomenclature based on subscript was employed; the MPD resulting from KPR's records do not have subscript, whereas the value obtained from WDM's measurements was labeled as MPD_{SCRIM} . The characteristics of the two devices are indicated below.

KPR used the AMES HSTP with the following specifications:

- Measuring Speed: 25 to 65 mph (40 to 104 km/h)
- Laser frequency: 100 kHz.
- Frequency of results reported: every 3 m (9.84 ft).
- Measurement location: right wheel path (RWP) of outermost lane.

In the case of WDM, the laser mounted in the SCRIM machine has the following specifications:

- Measuring Speed: variable speed, but as close as possible to 50-mp.
- Laser frequency: 64 kHz.
- Frequency of results reported: every 8 m (26.4 ft).
- Measurement location: left wheel path (LWP) of outermost lane.

Segments Selected for Comparison

In 2022 WDM established a contract with the NCDOT for testing 5,161 miles of state-maintained roadways (primarily full control, 55+ mph) for a single-lane survey, both directions as part of a multi-year effort to characterize friction and texture at a network level. Between September and October of 2022, WDM collected approximately 4,715 miles of data, which was approximately 91% of the year 1 collection scope. On the hand, KPR engineering collected the data used in this project to characterize performance and define a set of investigatory thresholds as part of two research projects, FHWA/NC 2020-11 and FHWA/NC 2022-05. For this comparison, the observations from the latter project were used, i.e., Group-2 sites listed in Table 2. These measurements were obtained from April 2020 to July 2023.

Because the measurements were made at different dates, the observations collected by KPR with the closest date to that of the WDM were selected for the analysis. In this sense, KPR's records from June/July 2022 were compared to WMD's data from September – October 2022. These resulted in a total of 95 sites for comparison. The distribution of the friction and texture values collected by the two companies is presented in Figure C.1 and Figure C.2 respectively. In these figures, Part (a) contains the values measured by KPR, while Part (b) shows the observations made

by WDM. It must be noted that for KPR the values plotted included all the observations collected (October 2019 to July 2023) and two data series are shown, the observations depicted in blue, and the back-cast values shown in orange. A full description of both data series is included in Chapter 4.

In the case of friction, see Figure C.1, the *FN* is 0.026 units lower than the *SC*, but in general terms the two distributions are similar and if one makes a t-test evaluation is noted the two distributions are not different. It can be seen from Figure C.2 that the mean *MPD* from KPR's observations is 0.24 mm lower than the mean *MPD_{SCRIM}*, whereas the median *MPD* is 0.25 mm lower than the median of *MPD_{SCRIM}*.

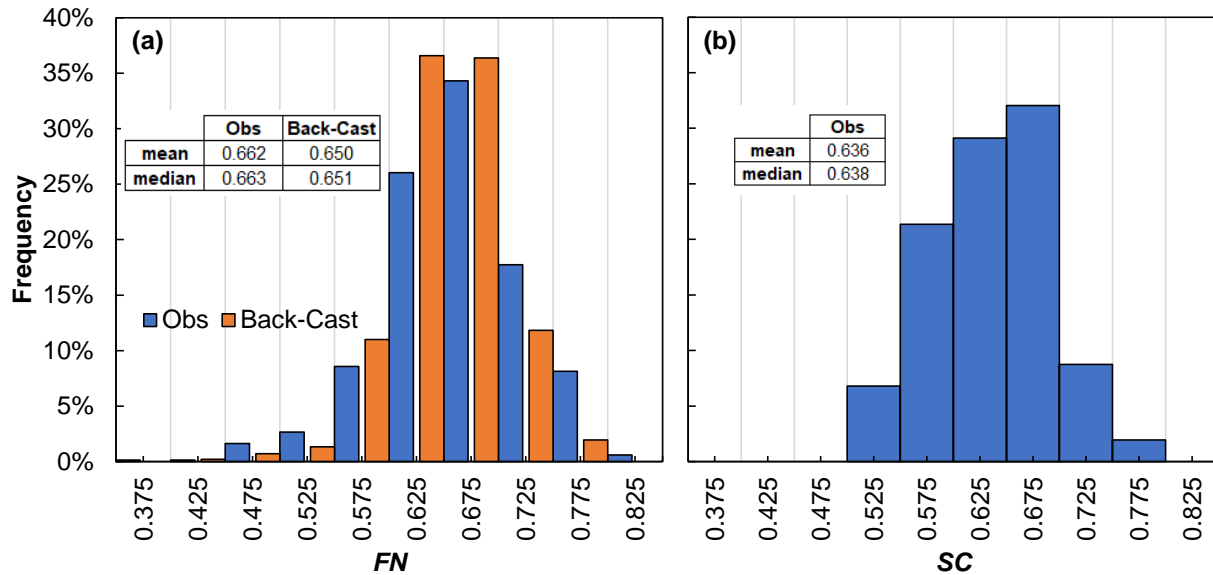


Figure C.1. Distribution of friction values measured with (a) BV-11 and (b) SCRIM.

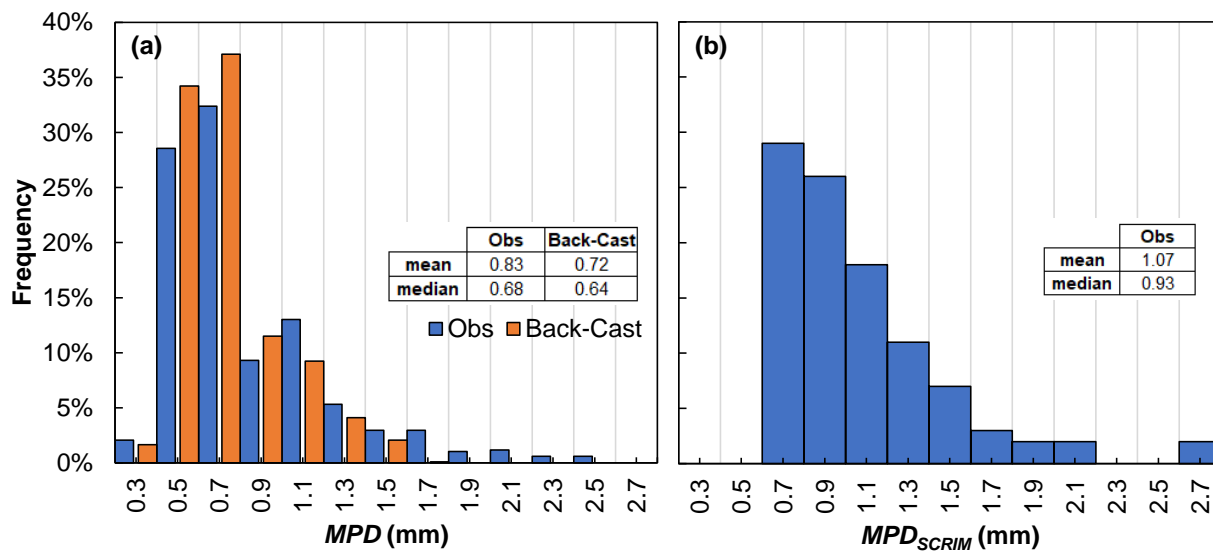


Figure C.2. Distribution of *MPD* values measured with (a) AMES HSTP and (b) SCRIM.

Methodology

Overview

Based on the data description presented above, the two datasets were compared as indicated below:

- For each site, the average friction and *MPD* was computed across the entire site. To facilitate the comparison process, only the inventory direction was used for each site. Also, the measurements made by KPR were made based on the extension of a given rehabilitation project, whereas WDM measurements were made based on route inventory. This means that the extent of WDM's dataset is longer than KPR's. Hence, to unify the spatial window used to compute this average, the milepost limits of the KPR records were used for both datasets.
- After calculating the average values, a scatter plot was created, and the box plot of the mean differences were used to evaluate possible outliers as discussed in the next section.
- Next, once the possible outliers are removed, a simple linear regression is made between the two records, using KPR values as the explanatory variable and WDM records as the response. These linear regression models were calibrated using all the observations combined, and calibrated for individual surface types, i.e., dense-graded mixtures, OGFC, and UTBWC.
- This process was made in sequence, first for texture and later for friction. In this sense, if an outlier is identified for texture, this site is also labeled as an outlier for friction and the data pair was removed from the analysis. Then, the same outlier and linear regression evaluation was conducted for friction.

Outlier Analysis

Outlier analysis was conducted in two steps. First, outliers were identified from the texture data and then outliers were identified from the friction data. In both cases these basic process was the same; first, a boxplot was used to highlight those pair values that resulted in a mean difference greater than or equal to 1.5 times the interquartile range (IQR), whereas the IQR is defined as the arithmetic difference between the 75th percentile and the 25th percentile of the distribution of the mean differences, second for each of the highlighted sites a manual verification process was conducted to verify that the surface type was the same in both measurement dates, to verify that no rehabilitation has been conducted in the time between measurements.

After computing the mean *MPD* of both datasets for each site, the scatter plot shown in Figure C.3 (a) was made. Afterwards, for each site the difference between the mean *MPD* and the difference between the *MPD_{SCRIM}* was calculated and then the distribution of this difference across all sites is presented in Figure C.3 (b). Based on this distribution, the 75th percentile and the 25th percentile are 0.25 and 0.13 mm, respectively. Hence the IQR is equal to 0.12 mm and a site will be flagged as a potential outlier if the value of $MPD_{SCRIM} - MPD$ is greater than or equal to $0.25 + 3 \times 0.12$ mm = 0.62 mm or lower than or equal to $0.13 - 3 \times 0.12$ mm = -0.24 mm.

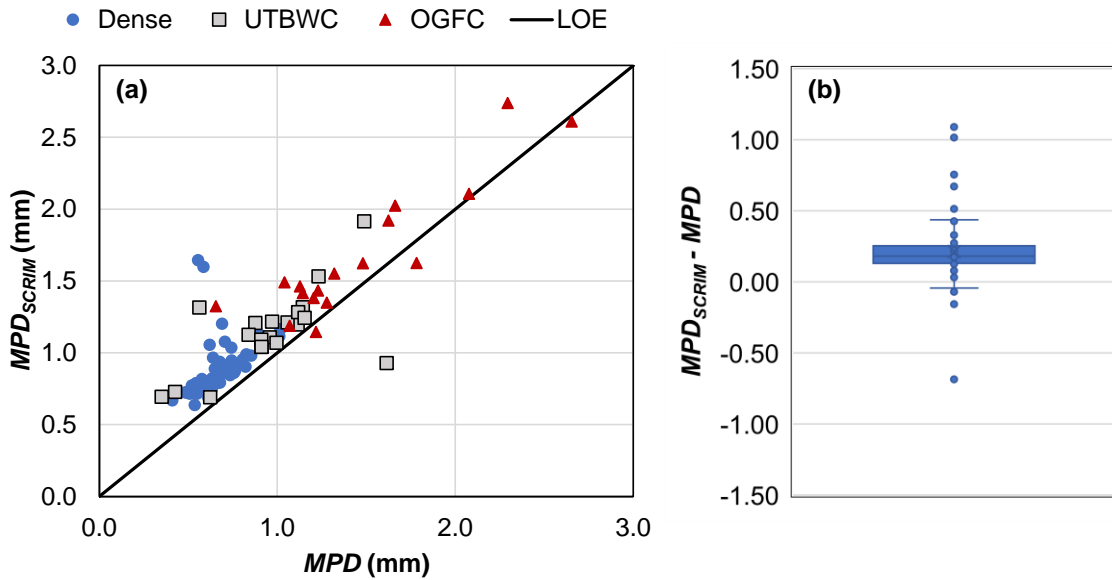


Figure C.3. (a) Scatter plot of the MPD comparisons and (b) Box plot of the MPD mean differences.

An example of a site that was labeled as an outlier is included in Figure C.4. The data shown in this figure is for Site 139.1, which has a dense-graded surface. WDM collected more than 25 miles on this route and in consequence it captured the surface texture of pavements with different surface types and pavement age, as evidenced by the variation in MPD_{SCRIM} values along these 25 miles. In contrast, KPR measurements were made on the limits of the rehabilitation project made in 2013, from milepost 0.0 to milepost 4.9. Figure C.4 (b) shows a zoomed in view of this portion of the measurements and the mean of both datasets in this milepost range are $MPD_{SCRIM} = 1.65$ mm and $MPD = 0.56$ mm, respectively. The difference between the two means is 1.01 mm, which is greater than the limit value of 0.62 mm calculated above.

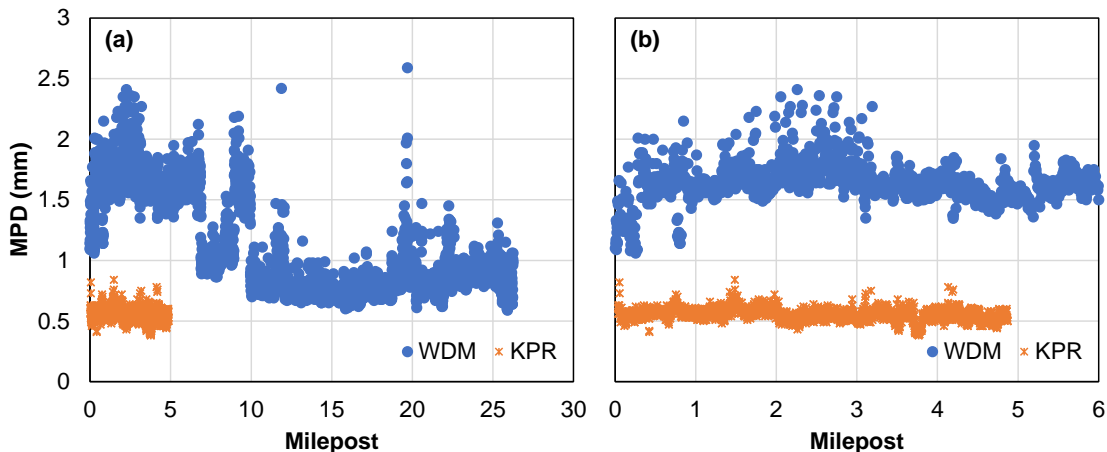


Figure C.4. (a) MPD values on Site 139.1 and (b) Portion of the dataset selected to compute the mean.

Similarly, an example of a site that was kept for the analysis is depicted in Figure C.5. This is Site 111.4 that has an OGFC surface type. As indicated in Part (a) of Figure C.5 WDM collected their

measurements in a spatial window of 22 miles, including pavements with different ages and surface types, while KPR made its measurements between milepost 11.6 and 14.0. As a result, the mean MPD values were computed using the 11.6 to 14.0 milepost range for both datasets and $MPD_{SCRIM} = 1.38$ mm and $MPD = 1.20$ mm. The difference between the two means is 0.18 mm which is lower than the limit value of 0.62 mm.

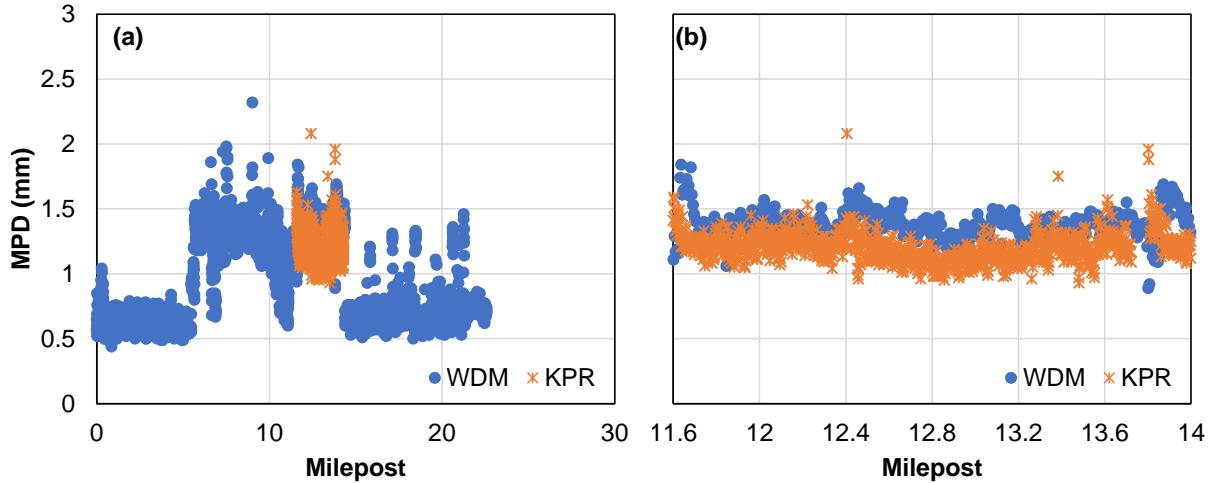


Figure C.5. (a) MPD values on Site 111.4 and (b) Portion of the dataset selected to compute the average MPD .

As indicated in the methodology section, the sites where the difference in the MPD values of the two datasets was flagged as a potential outlier were also removed from the analysis for friction. For instance, Site 139.1 shown in Figure C.4 and flagged as an outlier during the texture analysis was removed from the dataset for friction. This was made because the outliers in the previous analysis were mostly caused by a site that was rehabilitated between measurements, or because the overlap of the two datasets was not sufficient, i.e., there number of miles that have measurements collected with both datasets is less than 0.5 miles.

Likewise, the mean friction using the two datasets was computed for each site, i.e., FN and SC . It must be noted that the SC is presented in decimal format, not in percentage. Afterwards, the difference of the two means was calculated and the distribution of the differences was obtained. Figure C.6 (a) and (b) show the scatterplots of the friction values after removing the outliers from the texture analysis and the box plots of the difference between the means, respectively. Based on the distribution shown in Figure C.6 (b), the 75th percentile and the 25th percentile of the difference in mean friction is 0.02 and -0.06. Hence the IQR is equal to 0.08 and a site will be flagged as a potential outlier if the value of $SC - FN$ is greater than or equal to $0.02 + 3 \times 0.08$ mm = 0.26 or lower than or equal to $-0.06 - 3 \times 0.08$ mm = -0.31.

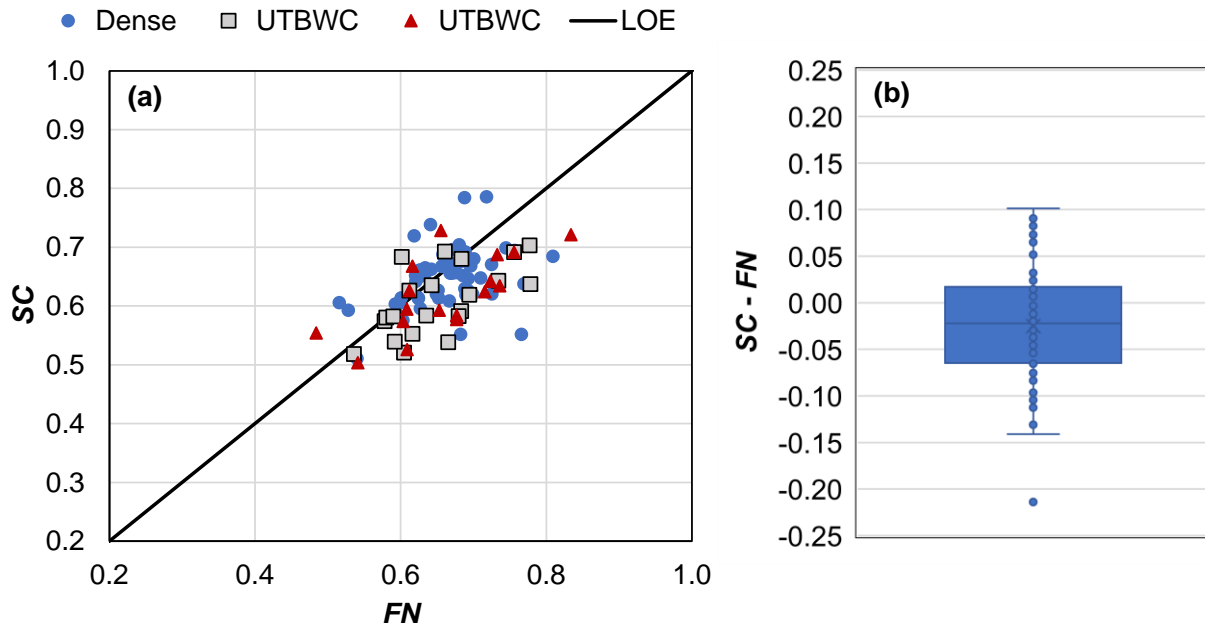


Figure C.6. (a) Scatter plot of the friction comparisons and (b) Box plot of the friction means differences.

For example, Site 111.4 that has an OGFC surface type, analyzed in the previous section, has been used again to illustrate the outlier identification process. The friction values collected with the BV-11 and the SCRIM are plotted in Figure C.7 (a). As shown, WDM collected their measurements in a spatial window of 22 miles, including pavements with different ages and surface types, while KPR made its measurements between milepost 11.6 and 12.3. As a result, the mean friction values were computed using the 11.6 to 12.3 milepost range for both datasets and $SC = 0.57$ and $FN = 0.60$. The difference between the two means is -0.03 which is higher than the lower limit value of -0.31 .

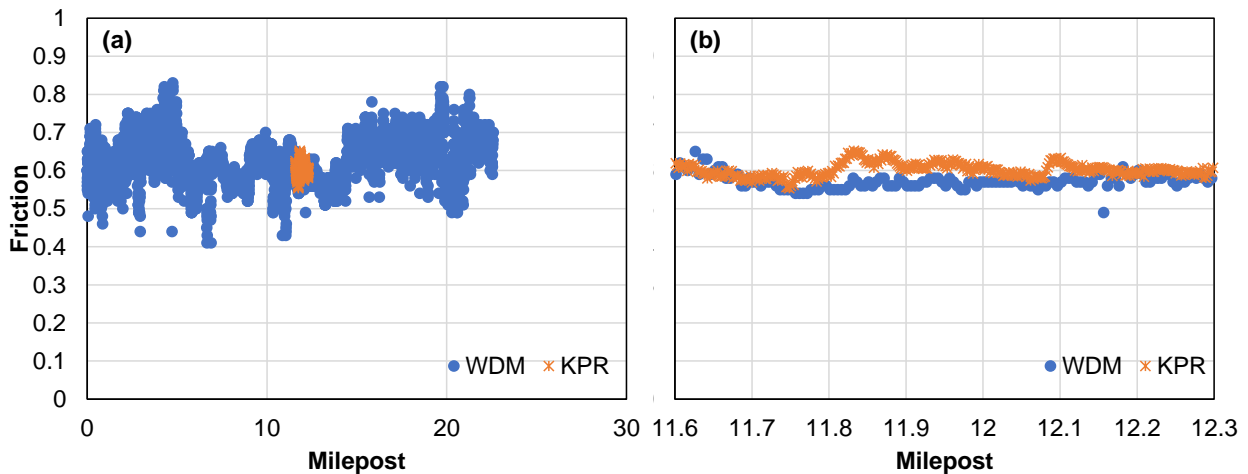


Figure C.7. (a) Friction values on Site 111.4 and (b) Portion of the dataset selected to compute the mean.

In summary, 84 out of the 95 data pairs remained available for comparison after removing the outliers detected during the texture analysis. Then, after conducting the statistical evaluation for these 84 data pairs, 79 remained for evaluation.

Results

Friction

The scatter plot of the friction pairs of values is presented in Figure C.8. For the comparison, four models were developed: i) using all sites independently of the surface type, ii) one for dense-graded mixtures, iii) one for OGFC, and iv) another for UTBWC. These models are presented in Figure C.9. As shown in Part (b) to (d) of Figure C.9, except for the UTBWC model the slope of the regression equations is close to 0.50. Hence, for the model that uses all sites independently of the surface type, see Part (a), the slope was constrained to be equal to 0.5. This model is also shown in Equation (103) and indicates that on average the SC is 0.31 units higher than half of the FN .

It must be noted that the comparison presented here has been made for FN collected at 60-mph, whereas the SC were collected and standardized to a measurement speed of 50-mph. This difference in the representative speed, joined with the fact the two measurements were collected in different wheel paths and each device represent a different friction response (longitudinal vs lateral friction response), could have contributed to the low statistical significance of the models.

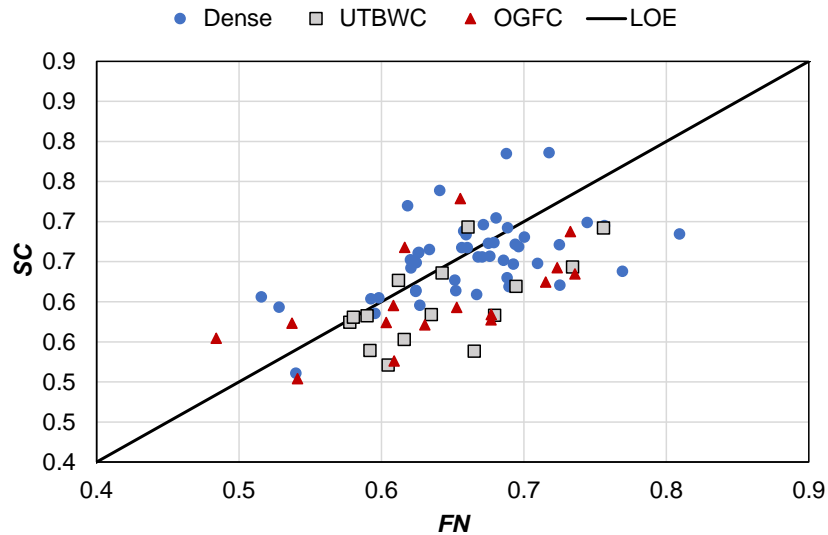


Figure C.8. Scatter plot for friction comparisons after removing outliers.

$$SC = 0.31 + 0.5 \times FN \quad (103)$$

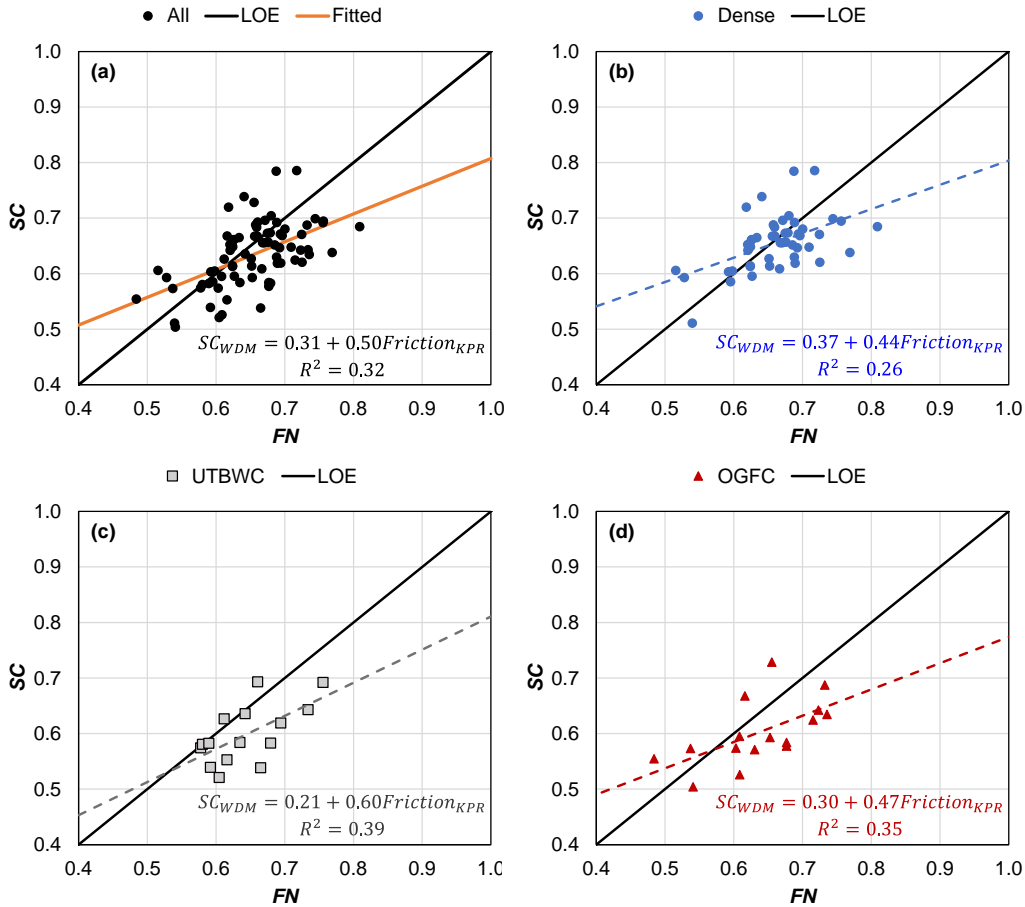


Figure C.9. Friction regression model proposed for: (a) all sites combined, (b) dense-graded, (c) UTBWC, and (d) OGFC.

Texture

The scatter plot of Figure C.3 (a) was recreated using only these 84 sites and is presented in Figure C.10. Like with the friction analysis, four models were developed: i) using all sites independently of the surface type, ii) one for dense-graded mixtures, iii) one for UTBWC, and iv) another for OGFC. These models are presented in Figure C.11. As shown in Part (b) to (d) of Figure C.11, except for the dense-graded model the slope of the regression equations is close to one. Hence, for the model that uses all sites independently of the surface type, see Part (a), the slope was constrained to be equal to one. This model is also shown in Equation (104) and indicates that on average the MPD_{SCRIM} is 0.2 mm higher than the MPD measured with the AMES HSTP.

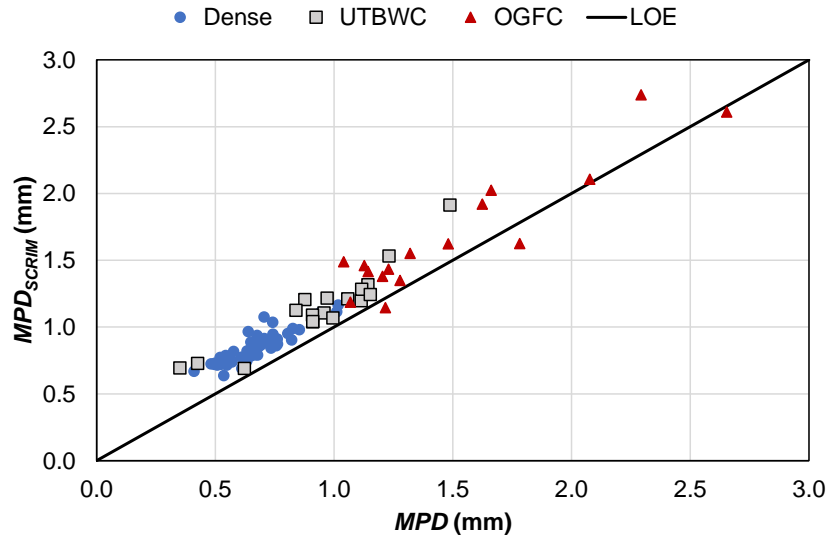


Figure C.10. Scatter plot for MPD comparisons after removing outliers.

$$MPD_{SCRIM} = 0.2 + MPD \quad (104)$$

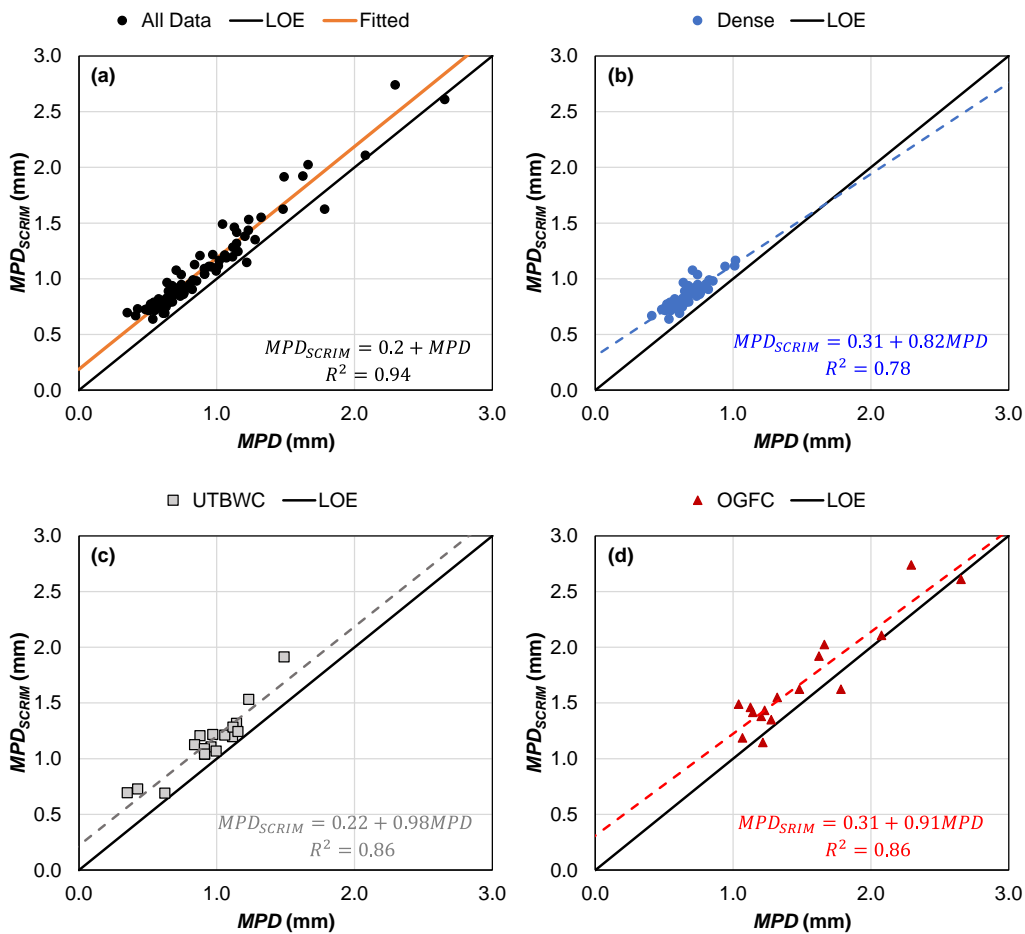


Figure C.11. MPD regression model proposed for: (a) all sites combined, (b) dense-graded, (c) UTBWC, and (d) OGFC.

Conclusions and Recommendations

Based on the results shown in this appendix, it is concluded that there is a strong relationship between the *MPD* measured by KPR with the AMES HSTP and the *MPD* measured by WDM using the SCRIM machine (MPD_{SCRIM}). The proposed model indicated that on average MPD_{SCRIM} is 0.2 mm higher than the *MPD* from the KPR instruments. In contrast, it is concluded that there is not a sound statistical relationship between the longitudinal friction value measured by KPR using the BV-11 (*FN*) and the SCRIM coefficient (*SC*) measured by WDM using the SCRIM machine. It is noted that different results between instruments measuring the same quantity (*MPD* in this case) or closely related quantities (friction via *FN* or *SC* in this case) is not unusual. As discussed in the literature review, efforts to better homogenize measurements across instruments continue to be carried out and future standardization efforts may further help to obviate the need for the kinds of correlation studies performed here.

In consequence, Equation (104) can be used to relate the proposed set of investigatory and intervention *MPD* thresholds proposed using the AMES HSTP. But it is not recommended to use the correlations presented here to relate the *SC* measurements with the proposed friction investigatory and intervention thresholds presented in Chapter 4.

APPENDIX D. FRICTION AND TEXTURE TESTING DATES

Table D.1. Friction Measurements.

Sites	Overlay	Date1	Date2	Date3	Date4	Date5	Date6	Date7	Date8	Date9
1	Oct-19	Oct-19	Apr-20	Jun-20						
2	Oct-19	Oct-19								
3	Oct-19	Oct-19	Apr-20	Oct-20	Feb-21					
4.1	Oct-19	Oct-19	May-20	Jul-20	Oct-20					
4.2	Apr-20	Apr-20	Jul-20	Oct-20	Jun-22	Mar-23				
5	Oct-19	Oct-19	May-20	Jul-20	Oct-20	Nov-21	Mar-23			
6	Oct-19	Oct-19	May-20	Jul-20	Oct-20	Feb-21	Jun-21	Dec-21	Mar-23	
7	Aug-19	Nov-19	Apr-20	Aug-20	Nov-20	Feb-21	Jul-21	Feb-22	Aug-22	
8	Apr-20	Apr-20	Aug-20	Oct-20	Jan-21	Mar-21	Jun-21			
9	Oct-19	Nov-19	Aug-20	Nov-20	Feb-21	Jul-21				
11	Mar-20	Aug-20	Nov-20	Feb-21	Jul-21					
12	Oct-19	Oct-19								
13	Nov-20	Nov-20								
14	Oct-19	Oct-19	Apr-20	Jul-20	Oct-20	Jan-21	Jul-21			
15	Oct-19	Nov-19	Apr-20	Aug-20	Nov-20	Mar-21	Jul-21			
16	Oct-19	Nov-19	Apr-20	Aug-20	Nov-20	Mar-21	Jul-21			
17	Oct-19	Nov-19	Apr-20	Jul-20	Oct-20	Jan-21	Mar-21	Jun-21		
18	Oct-19	Nov-19	Apr-20	Aug-20	Nov-20	Mar-21	Dec-21	Mar-23		
19	Apr-20	Apr-20	Aug-20	Nov-20	Feb-21	Jul-21	Feb-22	Aug-22	May-23	
23	Nov-19	Apr-20	Aug-20	Nov-20	Mar-21					
24	Jun-20	Jun-20	Jan-21							
27	Jun-20	Jul-20								
28	Mar-20	Jun-20	Aug-20	Nov-20						
29	Aug-20	Aug-20								
33	Jun-20	Jun-20	Aug-20	Oct-20	Jan-21	Mar-21	Jun-21	Dec-21	Jun-22	Mar-23
35	Jun-21	Nov-21	May-22							
36	Aug-21	Oct-21	May-22	Aug-22						
37	Sep-21	Sep-21	Nov-21							
39	Oct-21	Nov-21	Sep-22							
40	Sep-22	Oct-22								
41	Jun-22	Jul-22								
42	Jun-22	Jul-22								
43	May-22	Jun-22								
44	Sep-22	Sep-22								
101	Jun-17	May-20	May-22							
102	Jun-16	May-20								
103.1	Jun-16	Jul-20								
103.2	Jun-12	May-20								
104.1	Jun-10	May-20	Apr-22							
104.2	Jun-14	May-20	Apr-22							
105.1	Jun-08	May-20	May-22							
105.2	Jun-08	May-20	May-22							
106.1	Jun-16	Apr-20	Apr-22							
106.2	Jun-15	Apr-20	Apr-22							
106.3	Jun-12	Apr-20	Apr-22							
106.4	Jun-14	Jul-20	Apr-22							
107	Jun-12	Apr-20	Apr-22							
108.1	Jun-12	Jun-20	Jun-22							
108.2	Jun-12	Jun-20	Jun-22							
108.3	Jun-13	Jun-20	Jun-22							
109	Jun-14	Jun-20	Jun-22							
110.1	Jun-17	Jun-20	Jun-22							

Sites	Overlay	Date1	Date2	Date3	Date4	Date5	Date6	Date7	Date8	Date9
110.2	Jun-14	Jun-20	Jun-22							
111.1	Jun-13	May-20	May-22							
111.2	Jun-13	May-20	May-22							
111.3	Jun-14	May-20	May-22	Aug-22	Nov-22	Jan-23	Mar-23			
111.4	Jun-16	May-20	May-22							
111.5	Jun-13	May-20	May-22							
112	Jun-16	May-20	Jun-22							
113	Jun-11	Jul-20	Jul-22							
114.1	Jun-15	Jun-20	Jun-22							
114.3	Jun-12	Jul-20	Jun-22							
115	Jun-13	May-20	May-22							
116	Jun-13	May-20	May-22							
117.1	Jun-14	Jun-20	Jun-22							
117.2	Jun-17	Jun-20	Jun-22							
117.3	Jun-17	Jun-20	Jun-22							
118	Jun-17	Jul-20	Jun-22							
119.1	Jun-17	Jun-20	Jun-22							
119.2	Jun-14	May-20	May-22							
119.3	Jun-15	May-20	May-22							
119.4	Jun-12	May-20	May-22							
120.1	Jun-17	Jun-20	Jun-22							
120.2	Jun-17	May-20	May-22							
121	Jun-17	Apr-20	Apr-22							
122	Jun-14	Apr-20	Apr-22							
123.1	Jun-12	Jul-20	Jun-22							
123.2	Jun-12	Jul-20	Jun-22							
124	-	Mar-20	Apr-22							
125	Jun-18	May-20	May-22							
126	Jun-17	May-20	May-22							
127	Jun-13	May-20	May-22							
128	Jun-16	Jul-20	Jul-22							
129.1	Jun-13	Apr-20	Jun-22							
129.2	Jun-08	May-20	Jun-22							
129.3	Jun-15	Jul-20	Jun-22							
130.1	Jun-12	Apr-20	Apr-22							
130.2	Jun-12	Apr-20	Apr-22							
131	Jun-15	May-20	Apr-22							
132.1	Jun-13	Apr-20	Apr-22							
132.2	Jun-13	Apr-20	Apr-22							
132.3	Jun-13	Apr-20	Apr-22							
133	Jun-16	Apr-20	Apr-22							
134	Jun-16	Jul-20	Jul-22							
134.1	Jun-16	May-20	May-22	Aug-22	Oct-22	Feb-23	Mar-23	Jun-23		
134.2	Jun-17	May-20	May-22							
135	Jun-17	May-20	Jul-22							
137.1	Jun-17	Apr-20	Apr-22							
137.2	Jun-15	Apr-20	Apr-22							
138	Jun-15	May-20	Jun-22							
139.1	Jun-18	May-20	Jun-22							
139.2	Jun-18	May-20	Jun-22							
140	Jun-17	May-20	Jun-22							
141.1	-	May-20	Jun-22							
141.2	-	May-20	Jun-22							
142	Jun-12	May-20	May-22	Nov-22	Jan-23	Mar-23	Jun-23			
143.1	Jun-13	Jul-20	Jul-22							

Sites	Overlay	Date1	Date2	Date3	Date4	Date5	Date6	Date7	Date8	Date9
143.2	Jun-16	Jul-20	Jul-22							
144	Jun-12	Jul-20	Jul-22							
145	Jun-13	Jul-20	May-22							
146	Jun-14	May-20	Jun-22	Oct-22	Feb-23	Mar-23	Jun-23			
147	Jun-05	May-20	May-22							
148.1	Jun-05	May-20	May-22							
148.2	Jun-05	May-20	May-22							
149	Jun-12	Apr-20	Apr-22							
150.1	Jun-12	May-20	May-22							
150.2	Jun-13	Apr-20	Apr-22							
150.3	Jun-16	Apr-20	Apr-22							
150.4	Jun-16	May-20	May-22							
151	Jun-13	May-20	May-22							
152	Jun-15	May-20	May-22							
153.1	Jun-16	Jun-20	Jun-22							
153.2	Jun-14	Jun-20	Jun-22							
154	Jun-17	Jul-20	Jun-22							
155	Jun-11	Jul-20	Jun-22							
156	Jun-13	May-20	May-22							
157.1	Jun-12	Apr-20	Apr-22							
157.2	Jun-12	Apr-20	Apr-22							
158	Jun-16	Jun-20	Jun-22							
159	Jun-14	May-20	Jun-22							
160	Jun-14	May-20	Jun-22							
161	Jun-16	Apr-20	Apr-22							
162	Jun-16	May-20	May-22							
163	Jun-12	Jul-20	Jul-22							
164	Jun-13	Jul-20	Jul-22							
165.1	Jun-12	Jun-20	Jul-22							
165.2	Jun-12	Jul-20	Jul-22							
165.4	Jun-14	Jul-20	Jul-22	Nov-22	Mar-23	Jun-23				
165.5	Jun-16	Jul-20	Jul-22							
166.1	Jun-14	May-20	Jun-22							
166.2	Jun-16	May-20	Jun-22							
167	Jun-17	Jul-20	Jul-22							
168	Jun-19	Jul-20	Jul-22							
169	Jun-15	May-20	May-22							
170.1	Jun-12	Jul-20	Jul-22							
170.2	Jun-12	Jul-20	Jul-22							
171.1	Jun-13	May-20	Jun-22							
171.2	Jun-15	May-20	Jun-22							

Table D.2. Texture Measurement Dates.

Site	Overlay	Date1	Date2	Date3	Date4	Date5	Date6	Date7	Date8	Date9
1	Oct-19	Oct-19	Feb-20	Jun-20						
2	Oct-19	Oct-19								
3	Oct-19	Oct-19	Feb-20	Oct-20	Feb-21					
4.1	Oct-19	Oct-19	Feb-20	Jul-20	Oct-20					
4.2	Apr-20	May-20	Jul-20	Oct-20	Jun-22	Mar-23				
5	Oct-19	Oct-19	Feb-20	Jul-20	Oct-20	Nov-21	Mar-23			
6	Oct-19	Oct-19	Feb-20	Jul-20	Oct-20	Feb-21	Jun-21	Dec-21	Mar-23	
7	Aug-19	Nov-19	Feb-20	Aug-20	Nov-20	Feb-21	Jul-21	Feb-22	Aug-22	
8	Apr-20	Apr-20	Aug-20	Oct-20	Jan-21	Mar-21	Jun-21			
9	Oct-19	Nov-19	Feb-20	Aug-20	Nov-20	Feb-21	Jul-21			
11	Mar-20	Aug-20	Nov-20	Feb-21	Jul-21					
12	Oct-19	Oct-19								
13	Nov-20	Nov-20								
14	Oct-19	Oct-19	Feb-20	Jul-20	Oct-20	Jan-21	Jul-21			
15	Oct-19	Nov-19	Feb-20	Aug-20	Nov-20	Mar-21	Jul-21			
16	Oct-19	Oct-19	Feb-20	Aug-20	Nov-20	Mar-21	Jul-21			
17	Oct-19	Nov-19	Feb-20	Jul-20	Oct-20	Jan-21	Mar-21	Jun-21		
18	Oct-19	Nov-19	Feb-20	Aug-20	Nov-20	Mar-21	Dec-21	Mar-23		
19	Apr-20	Apr-20	Aug-20	Nov-20	Feb-21	Jul-21	Feb-22	Aug-22	May-23	
23	Nov-19	Dec-19	Aug-20	Nov-20	Mar-21					
24	Jun-20	Jun-20	Jan-21							
27	Jun-20	Jul-20								
28	Mar-20	Jun-20	Aug-20	Nov-20						
29	Aug-20	Aug-20								
33	Jun-20	Jun-20	Aug-20	Oct-20	Jan-21	Mar-21	Jun-21	Dec-21	Jun-22	Mar-23
35	Jun-21	Sep-21	Nov-21	May-22						
36	Aug-21	Sep-21	May-22	Aug-22						
37	Sep-21	Sep-21	Nov-21							
39	Oct-21	Nov-21	Sep-22							
40	Sep-22	Oct-22								
41	Jun-22	Jul-22								
42	Jun-22	Jul-22								
43	May-22	Jun-22								
44	Sep-22	Sep-22								
101	Jun-17	May-20	May-22							
102	Jun-16	May-20	Jun-22							
103.1	Jun-16	Jul-20	Jun-22							
103.2	Jun-12	Apr-20	Jun-22							
104.1	Jun-10	May-20	Apr-22							
104.2	Jun-14	Apr-20	Apr-22							
105.1	Jun-08	May-20	May-22							
105.2	Jun-08	May-20	May-22							
106.1	Jun-16	Apr-20	Apr-22							
106.2	Jun-15	Apr-20	Apr-22							
106.3	Jun-12	Apr-20	Jun-22							
106.4	Jun-14	Jul-20	Apr-22							
107	Jun-12	Apr-20	Apr-22							
108.1	Jun-12	Mar-20	Jun-22							
108.2	Jun-12	Mar-20	Jun-22							
108.3	Jun-13	Mar-20	Jun-22							
109	Jun-14	Mar-20	Jun-22							
110.1	Jun-17	Mar-20	Jun-22							
110.2	Jun-14	Mar-20	Jun-22							
111.1	Jun-13	May-20	May-22							

Site	Overlay	Date1	Date2	Date3	Date4	Date5	Date6	Date7	Date8	Date9
111.2	Jun-13	Mar-20	May-22							
111.3	Jun-14	Mar-20	May-22	Aug-22	Nov-22	Jan-23	Mar-23	Jun-23		
111.4	Jun-16	May-20	May-22							
111.5	Jun-13	Mar-20	May-22							
112	Jun-16	May-20	Jun-22							
113	Jun-11	Mar-20	Jul-22							
114.1	Jun-15	Jun-20	Jun-22							
114.3	Jun-12	Mar-20	Jun-22							
115	Jun-13	Mar-20	May-22							
116	Jun-13	May-20	May-22							
117.1	Jun-14	Mar-20	Jun-22							
117.2	Jun-17	Mar-20	Jun-22							
117.3	Jun-17	Mar-20	Jun-22							
118	Jun-17	Jun-20	Jun-22							
119.1	Jun-17	Jun-20	Jun-22							
119.2	Jun-14	May-20	May-22							
119.3	Jun-15	May-20	May-22							
119.4	Jun-12	May-20	May-22							
120.1	Jun-17	Mar-20	Jun-22							
120.2	Jun-17	May-20	May-22							
121	Jun-17	Apr-20	Apr-22							
122	Jun-14	Apr-20	Apr-22							
123.1	Jun-12	Mar-20	Jun-22							
123.2	Jun-12	Mar-20	Jun-22							
124	#N/A	Mar-20	Apr-22							
125	Jun-18	May-20	May-22							
126	Jun-17	May-20	May-22							
127	Jun-13	May-20	May-22							
128	Jun-16	Mar-20	Jul-22							
129.1	Jun-13	Apr-20	Jun-22							
129.2	Jun-08	Apr-20	Jun-22							
129.3	Jun-15	Jul-20	Jun-22							
130.1	Jun-12	Apr-20	Apr-22							
130.2	Jun-12	Apr-20	Apr-22							
131	Jun-15	Apr-20	Apr-22							
132.1	Jun-13	Apr-20	Apr-22							
132.2	Jun-13	Apr-20	Apr-22							
132.3	Jun-13	Apr-20	Apr-22							
133	Jun-16	Apr-20	Apr-22							
134	Jun-16	Mar-20	Jul-22							
134.1	Jun-16	May-20	May-22	Aug-22	Oct-22	Feb-23	Mar-23			
134.2	Jun-17	May-20	May-22							
135	Jun-17	May-20	Jul-22							
137.1	Jun-17	Apr-20	Jun-22							
137.2	Jun-15	Apr-20	Apr-22							
138	Jun-15	Apr-20	Jun-22							
139.1	Jun-18	Apr-20	Apr-22							
139.2	Jun-18	Apr-20	Apr-22							
140	Jun-17	Apr-20	Apr-22							
141.1	-	May-20	Jun-22							
141.2	-	May-20	Jun-22							
142	Jun-12	Feb-20	May-22		Nov-22	Jan-23	Mar-23			
143.1	Jun-13	Mar-20	Jul-22							
143.2	Jun-16	Mar-20	Jul-22							
144	Jun-12	Mar-20	Jul-22							

Site	Overlay	Date1	Date2	Date3	Date4	Date5	Date6	Date7	Date8	Date9
145	Jun-13	Jul-20	May-22							
146	Jun-14	May-20	Jun-22	Oct-22	Feb-23	Mar-23				
147	Jun-05	May-20	May-22							
148.1	Jun-05	May-20	May-22							
148.2	Jun-05	May-20	May-22							
149	Jun-12	Apr-20	Apr-22							
150.1	Jun-12	Feb-20	May-22							
150.2	Jun-13	Feb-20	Apr-22							
150.3	Jun-16	Feb-20	Apr-22							
150.4	Jun-16	Feb-20	May-22							
151	Jun-13	Mar-20	May-22							
152	Jun-15	Mar-20	May-22							
153.1	Jun-16	Feb-20	Jun-22							
153.2	Jun-14	Feb-20	Jun-22							
154	Jun-17	Jul-20	Jun-22							
155	Jun-11	Mar-20	Jun-22							
156	Jun-13	May-20	May-22							
157.1	Jun-12	Apr-20	Apr-22							
157.2	Jun-12	Apr-20	Apr-22							
158	Jun-16	Feb-20	Jun-22							
159	Jun-14	Mar-20	Jun-22							
160	Jun-14	Mar-20	Jun-22							
161	Jun-16	Apr-20	Apr-22							
162	Jun-16	May-20	May-22							
163	Jun-12	Mar-20	Jul-22							
164	Jun-13	Mar-20	Jul-22							
165.1	Jun-12	Mar-20	Jul-22							
165.2	Jun-12	Mar-20	Jul-22							
165.4	Jun-14	Mar-20	Jul-22							
165.5	Jun-16	Jul-20	Jul-22	Nov-22	Mar-23					
166.1	Jun-14	Mar-20	Jun-22							
166.2	Jun-16	Mar-20	Jun-22							
167	Jun-17	Mar-20	Jul-22							
168	Jun-19	Mar-20	Jul-22							
169	Jun-15	May-20	May-22							
170.1	Jun-12	Mar-20	Jul-22							
170.2	Jun-12	Mar-20	Jul-22							
171.1	Jun-13	Mar-20	Jun-22							
171.2	Jun-15	Mar-20	Jun-22							

APPENDIX E. ADDITIONAL CONSIDERATIONS FOR REPRESENTATIVE FRICTION VALUES

As mentioned in Chapter 2, each site was segmented into 0.1-mile sections, for each section the representative value was set as the 2.5th friction percentile and the 50th texture percentile. However, when sites are categorized by friction demand categories some sections may be too short to have reliable estimates of these percentiles because if the segment length is less than 0.4-miles only three to four 0.1-mile sections can be established. As a solution, it was decided to identify the percentile value computed over an entire site that produces a representative value that is similar to the one computed on the average of 0.1-mile segments.

Hence, three statistics were computed for each 0.1-mile segment: 2.5th, 10th, and 25th percentile. The statistics computed on the entire sites are: 2.5th, 10th, 25th, and 50th percentile. An example of such statistics for each analysis aggregation unit is depicted in Figure E.1. This procedure was conducted on the remaining sites and statistics computed over an entire site are compared against the average statistic computed over 0.1-mile segments. Three plots like the one presented in Figure E.2 were created.

The results indicated the following:

- The average 0.1-mile 2.5th friction percentile is equivalent to the 10th friction percentile calculated over the entire site.
- The average 0.1-mile 10th friction percentile is equivalent to the 25th friction percentile calculated over the entire site.
- The average 0.1-mile 25th friction percentile is equivalent to the 25th friction percentile calculated over the entire site.
- The average 0.1-mile 50th texture percentile is equivalent to the 50th texture percentile calculated over the entire site.

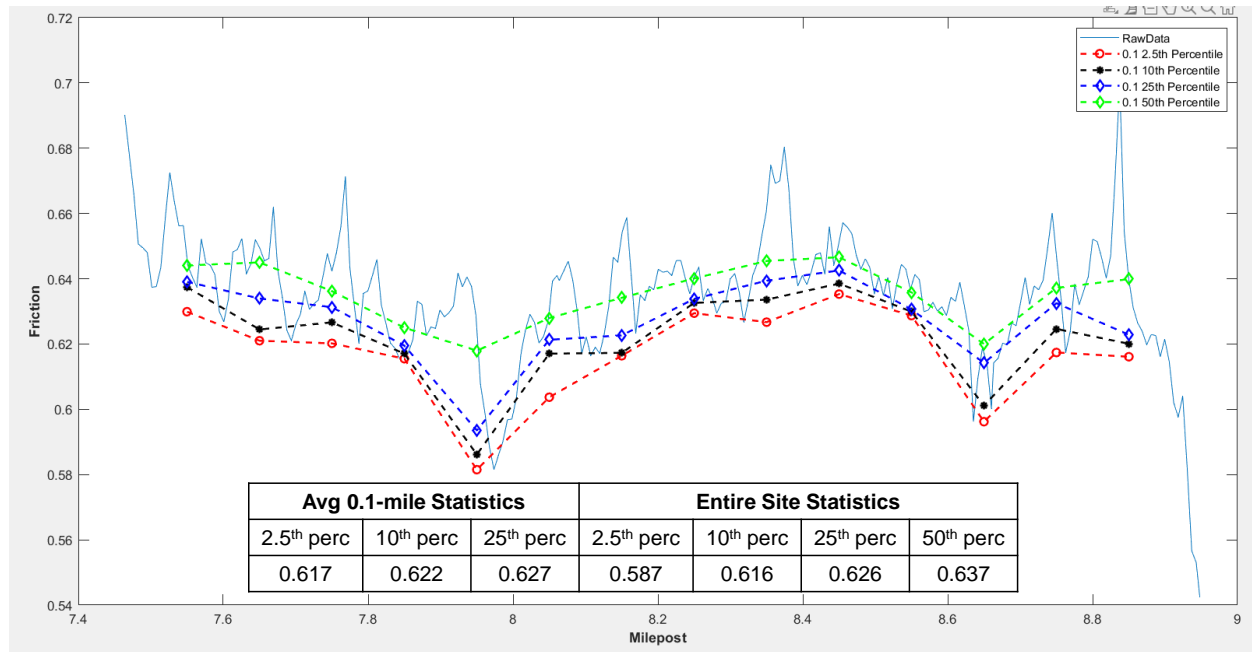


Figure E.1. Representative friction value for Site 111.3 NB.

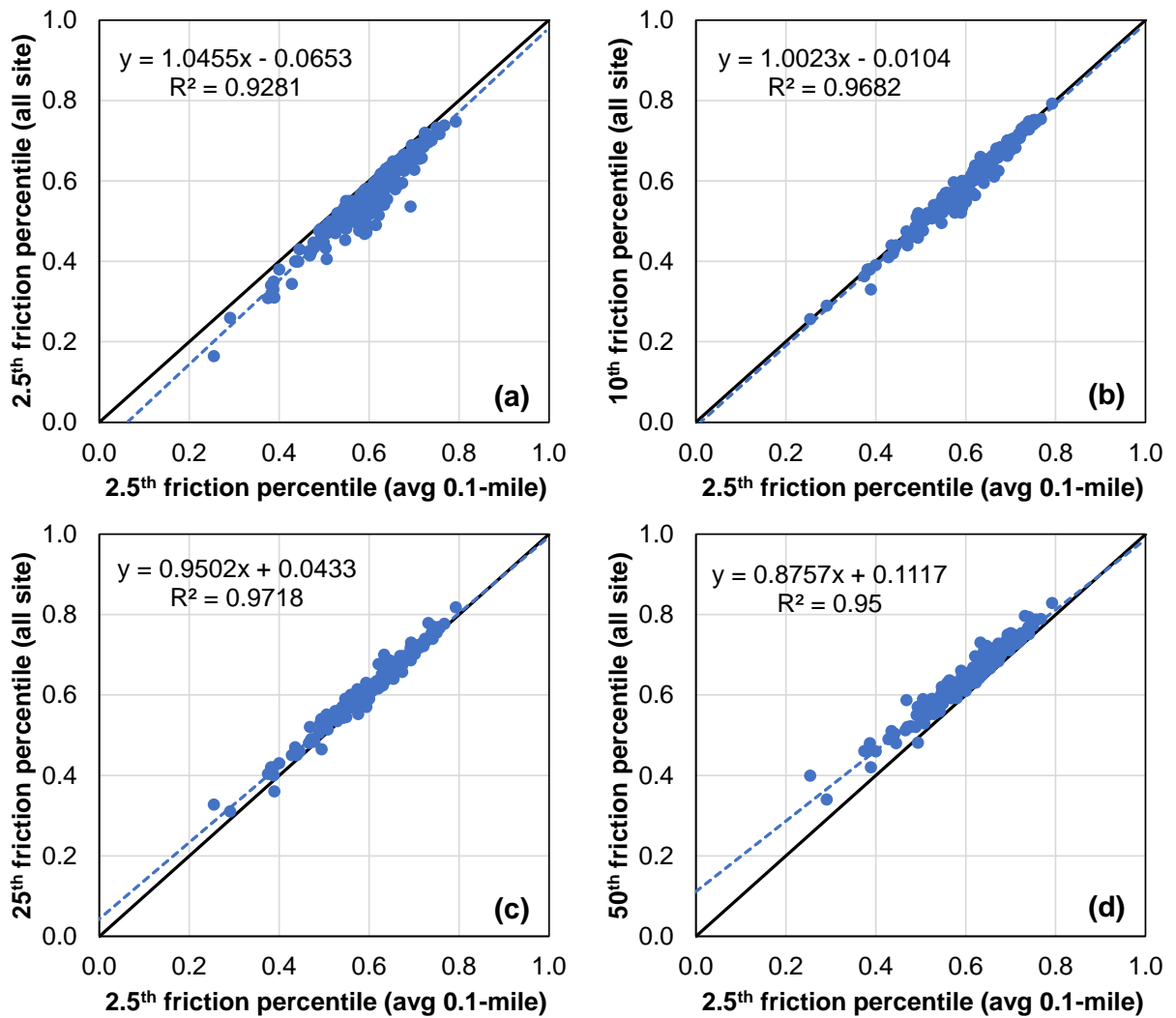


Figure E.2. Comparison of the average 0.1-mile 2.5th friction percentile against site statistics: (a) 2.5th friction percentile of the entire site, (b) 10th friction percentile of the entire site, (c) 25th percentile of the entire site, and (d) 50th percentile of the entire site.

APPENDIX F. FRICTION AND TEXTURE PREDICTION AFTER AN ASPHALT OVERLAY

Overview

Over the years, three elements have been considered basic and fundamental in any PFMP: i) a system for evaluating in-service pavements for friction, ii) a system for correlating available friction with wet-weather crashes, and iii) guidance on the design, construction, and maintenance of pavement surfaces with adequate surface friction throughout the pavement design life. In other words, it is necessary to measure friction and texture properties within the network to quantify the friction demand and understand the effect of pavement design and construction practices on the available friction values (93).

Moreover, there is evidence that there is often an increase in the wet crash rates after placement of new asphalt wearing courses (1). An initial decrease in friction and texture after placement of the new surface has been reported as one contributing factor to observed increases in wet crash rates (93, 94). Different researchers have used varying methodologies to incorporate friction demand into the mixture design process (7). However, most of the available studies have used laboratory specimens to measure friction and texture variation, which may not be representative of the field conditions.

Some attempts have been made to correlate laboratory friction and texture measurements with corresponding field measurements (13, 52, 53); however, most of these studies have used Locked-Wheel Skid Testers (LWST) to measure friction in the field. The LWST is the current standard procedure for network level friction measurement in the United States (7). It is a discrete (i.e., not continuous) sample-base test in which a measurement is taken over a 60-m (180-ft.) distance by locking a wheel on a tow-behind trailer. This method is reliable and does provide useful point information. However, reported values reflect averages across long distances through changing road conditions, and do not effectively differentiate the changes in friction along the route corridor (1). The LWST equipment has additional limitations. For example, it is difficult to conduct LWST tests in critical, high friction demand locations, such as horizontal curves or intersections, which tend to experience greater tire scrubbing and polishing that lead to loss of pavement friction.

An alternative to the LWST is the Continuous Pavement Friction Measurement Equipment (CFME), which is an established and proven approach that has been used for several decades in other countries. It is distinct from LWST because it allows a continuous reading of pavement friction in a section of road. The CFME is capable of measuring pavement friction through different types of geometries such as tangents, curves, and intersections, at a broad range of speeds (as high as 96 km/h (60 mph)). Measurements with a CFME can be reported at a spatial frequency as fine as 30-cm (1-ft), and for this reason many agencies around the world are shifting from the LWST to a CFME to better capture relationships between friction, texture, and crash frequencies (1).

Because the use of CFME to measure friction is a relative novel technique, especially in the United States, it has a disadvantage with respect to the relatively limited number of historical measurements. This lack of data makes it very challenging to define reliable friction deterioration models and there is not an accepted friction investigatory threshold nor an accepted friction intervention threshold for CFME measurements. Another disadvantage of the CFME is that the amount of information collected in each road is larger due to the finer resolution of the

measurements, which increases the computational effort and the resources required to store the data.

In terms of texture, practitioners and researchers are shifting from traditional static methods such as the Sand Patch Test (SPT) or the Circular Test Meter (CTM) towards high-speed profilers, because these profilers allow the collection of continuous texture measurements at a network level at the road operating speeds (95).

Therefore, based on the recent trend towards the implementation of a CFME as the standard for friction characterization at a network level and an overall lack of historical measurements on asphalt mixtures in the US, there is a need to develop a set of relationships between the current laboratory methods for characterizing friction and texture and the measurements collected with a CFME and high-speed laser profiler in the field. Furthermore, relationships between asphalt mixture composition and the friction and texture of new overlays could be used to identify locations with potential safety concerns based on mixture composition and can be used to control the construction quality of newly constructed asphalt surfaces.

Objectives

The objectives of this chapter were twofold:

- Identify the mixture compositional factors that affect the most the initial friction and texture properties.
- Develop a set of models that relate friction and texture values measured in the laboratory with the ones measured in the field using CFME and high-speed laser profilers.

Proposed Expressions to Relate Laboratory Observations, and Mixture Composition with Field Values

Sullivan (63) conducted a study that evaluated the implications of incorporating the friction demand required to provide a minimum stopping distance as an additional criterion during mixture design. The aggregate gradation was used to develop a relationship to predict in-service surface macrotexture, expressed as *MPD* reported by the CTM. Then, the microtexture component of the surface friction was expressed in terms of the polished aggregate friction value (PAFV), which is measured using the Polished Stone Value (PSV) test. These models were used to predict a vehicle stopping distance as a function of the mixture composition.

A more detailed evaluation was presented by Masad et al. (52, 53). In the first of these studies, the researchers focused on the lab procedures to characterize surface friction and texture and reported that the friction outcome of an asphalt mixture can be controlled and predicted based on the individual aggregate properties in conjunction with the mix characteristics. The polishing effect on aggregates was analyzed using the Micro-Deval test in conjunction with the aggregate imaging system test (AIMS) test. The AIMS, introduced by Masad et al. (52), is a method developed to measure the aggregate texture directly by a microscope and a digital image processing technique.

In the second part of the study, Masad et al. (53) conducted field observations to evaluate the friction (measured using a LWST and a Dynamic Friction Tester, DFT) and texture values (measured with a CTM). The main results of the study indicated that the initial friction microtexture is a function of the aggregate type and can be related to the DFT_{20} (friction value measured with a DFT at 20 km/h (12 mph)).

Later, Wu and Abadie (13) developed a surface friction prediction model that can be used during mixture design for wearing courses. In their study, twelve wearing course mixtures typically used in Louisiana were analyzed, including dense-graded and open-graded mixes with different aggregate sources. Each one of these mixtures were evaluated in the lab using the Three Wheel Polishing Device (TWPD). Then, friction and macrotexture were measured in the field on 22 different projects. The in-situ measurements were collected using a DFT, a CTM, and a LWST. Based on their findings, Wu and Abadie proposed a series of equations to predict the microtexture friction contribution, the expected surface macrotexture, and to estimate the expected LWST friction value at 60 km/h (40 mph).

While these studies have clearly identified a methodology to characterize predictive functions, they have largely relied on LWST or DFT to characterize friction in the field and most of them have used a static method such as the CTM to measure macrotexture. Today, CFME devices and high-speed lasers are used to survey friction and texture at a network level, respectively, and it is necessary to develop a relationship between the current lab protocols (either the British Pendulum Tester, BPT, or DFT for friction, and any static method to measure texture) and the values reported by high-speed devices in the field.

Also, previous models to predict friction and texture based on composition have relied on indices that are not part of routine measurements today, like the PSV or aggregate properties by AIMS. Thus, another need is to evaluate if friction and texture can be predicted from more conventional mixture compositional factors. Having such an expression will provide a valuable tool to verify the quality of newly constructed surfaces in terms of the as-constructed friction and texture characteristics.

Pavement Quality Control Program

Highway agencies around the world have developed different programs to ensure and enhance highway performance through inspection of asphalt paving productions and placement operations. In the U.S., most state highway agencies have been engaged in Quality Programs (QP) to follow asphalt mixes production, testing for consistency and quality from the stockpiles all the way to the finished road surfaces (96).

The elements of a QP are depicted in Figure F.1. As shown, the process starts with pavement design where parameters such as layer thicknesses, materials properties and mix design are defined. Then, certain acceptance quality characteristics (AQC) such as in-place density, binder content, aggregate gradation, etc. are measured during the production and construction of the pavement structure. The main goal of the QP is to compare the as-designed and the as-built pavement life to determine the required pay adjustment. Finally, performance surveys need to be conducted periodically to quantify deterioration rates and to identify condition thresholds that will be used as input in future pavement designs.

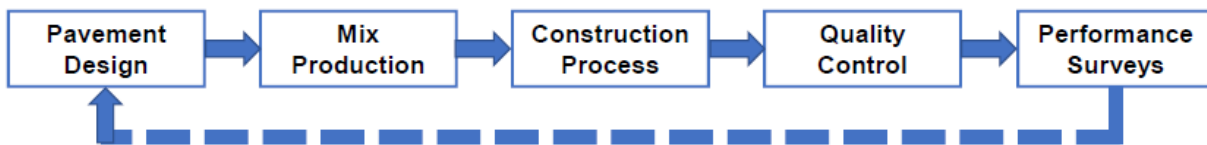


Figure F.1. Pavement construction quality program.

Mix production quality is controlled by lots. Typically, the AQC is collected by taking and testing a few samples. The statistics of an AQC of the lot determined based on the samples is used to make an inference on the overall construction quality (97). The most used quality measure to quantify the quality is percent within limits (PWL) (NCHRP Report 704). For performance related construction specification, the PWL value of a lot is related to its expected future performance (98). The advantage of the PWL is that captures both the mean and standard deviation in one parameter, facilitating the analysis of an AQC values distribution.

In this sense, to get a reliable expression to predict friction and texture in the field it is necessary to account for the three variable sources depicted in Figure F.2. First, the as-designed mixture volumetrics are needed, e.g., the selected binder content, gradation parameters, VMA, etc. These as-designed properties will vary during the production process, therefore samples from asphalt plants are needed to estimate this amount of variation. Finally, typically field cores are collected to verify compaction levels, although sometimes loose mixes are collected as well to estimate the variation the material experienced during the transport.

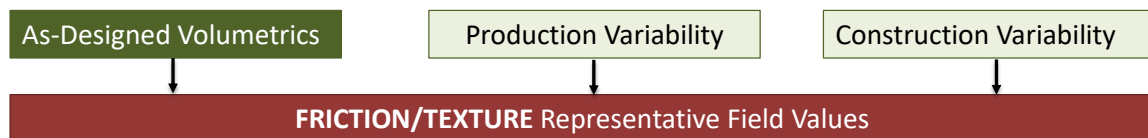


Figure F.2. Evaluating the effect of the pavement construction process.

Given the number of actors involved in this process, getting all these pieces of information is not an easy process. Hence, one way to capture the variability from the three different stages of the process is by using as-designed mixture volumetrics to represent the design process, get estimates of daily production variability on the asphalt plant the supplied the material (e.g., quantify the typical difference in the percent passing Sieve No. 200 the day the pavement studied was constructed), and incorporate measurements of the in-place condition, typically in-place density (estimated from field cores or measured directly with density gauges).

Data and Methods

The primary source of information used to meet the objectives established in this appendix are the field friction and texture measurements collected right after construction, see Chapter 2 and Appendix C, and the laboratory measurements obtained from the set of field cores extracted in sixteen of the 36 sites analyzed in Group 1 of sites, see Table 1.

The gradation of each mix is summarized using the coefficient of curvature, C_c , and coefficient of uniformity, C_u , defined in Equations (105) and (106), respectively. Both parameters are widely used to describe gradation shape and aggregate size distribution (99). For the gradation to be well graded, the value C_c must range between one and three, and for a single sized gradation both C_c and C_u are equal to one. In addition, a C_u greater than six indicates a densely graded material with a considerable range of particle size, while a C_u less than four indicates a uniformly graded material.

$$C_c = \frac{D_{30}^2}{D_{10} \times D_{60}} \quad (105)$$

$$C_u = \frac{D_{60}}{D_{10}} \quad (106)$$

where;

D_{60} = particle size at 60% finer,

D_{30} = particle size at 30% finer, and

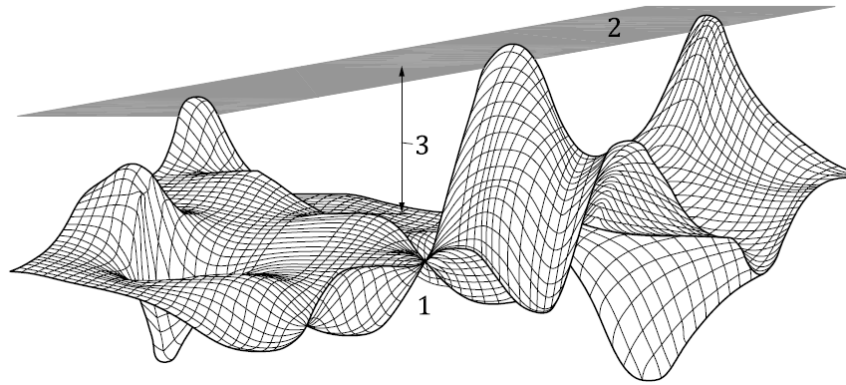
D_{10} = particle size at 10% finer.

The data described above was used in two different analyses.

- The relationship between the laboratory and field friction/texture values was characterized by using data from the sixteen sites where cores were taken after construction. In total, there were 42 cores, for a total of 42 field/lab pairs of observations. These expressions that relates as-designed composition and observations made on field cores (to get a representation of the variability of the construction process) can be used as a tool to control the quality of newly constructed surfaces, by using field cores to verify that the placed material meet friction/texture requirements.
- A model was calibrated to relate the average friction/texture values in the field, with the as-designed mix volumetric parameters, by using measurements from all 36 sites. For this purpose, the first after construction measurement was used; some sites have observations in both traffic directions, others just in one direction, in total there are 60 friction and texture values that can be contrasted against the mixture composition of each site. This model can be used to get an estimate of the expected friction/texture given the as-designed mixture composition.

For the laboratory measurements, friction was characterized using a BPT, the BPN was set as the average of four consecutive readings and the measurement process was carried out in accordance with the ASTM E303 specification. The texture surface was characterized using a volumetric technique based on the ASTM standard, and using a three-dimensional surface scanned with the AMES 9500 rapid laser texture scanner (rLTS) as indicated in Figure 6. These surfaces were processed in accordance with the ISO-13473; therefore, the AMES 9500 rLTS provides an estimate of the average *MPD*. As shown in Figure F.3, a surface is the graphical representation of the group of points collected with the lasers, and the texture depth is defined as the average difference between the plane that passes through the three highest peaks and each point of the surface.

It is important to notice that the surface used to calculate the *EMTD* as represented in Figure F.3 has been pre-processed in such a way that any slope has been suppressed and the mean value has been set to zero. With this in mind, the average peak is understood as the average of those positive elevations, i.e., the average of the points that are above the surface mean plane; similarly, the average valley depth is understood as the average of the negative elevations, i.e., the points located beneath the surface mean plane.



1: surface; 2: plane through three highest peaks of the surface, 3: mean texture depth.
Figure F.3. Illustration of the terms “surface” and estimated mean texture depth (EMTD)
(Taken from ISO-13473).

The CFME device and the laser scanner provide measurements over a long section of road, while the core results provide a point estimation of the field friction and texture. Thus, to compare the lab results against the field observations it was necessary to take an average of the continuous friction and texture measurements around the location of each core. It was decided to use a window of ± 76 m (250 ft) around the core location. An example of this procedure is illustrated in Figure F.4, where the continuous texture and friction profiles are plotted for Site 23, the yellow dots indicate the location where the cores were extracted, and the label next to the points are the mean values of the texture and friction, respectively, in the vicinity of the core location.

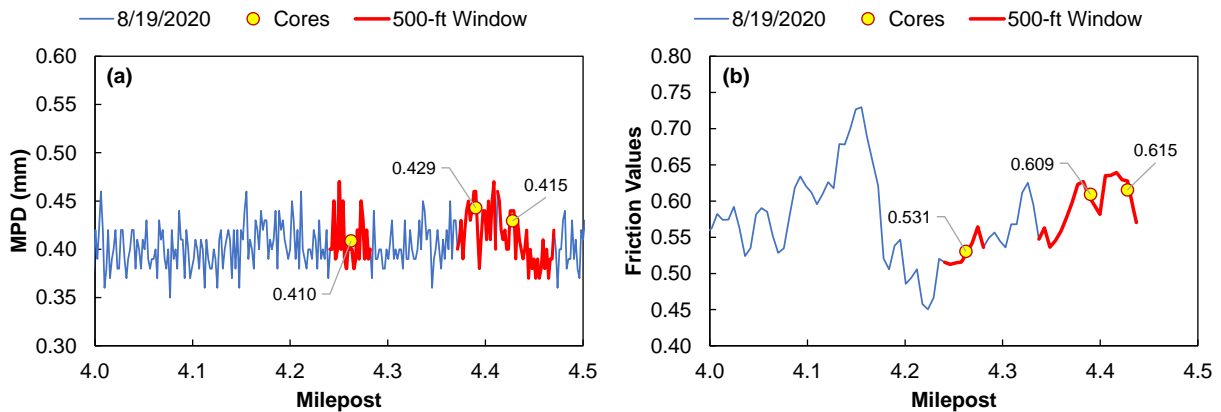


Figure F.4. Field measurements and core locations for Site 23: (a) MPD and (b) Friction value.

Results

The results of the field and lab measurements are summarized in Table F.1. It is important to mention that Site 34 only has pre-construction cores, the observations of these cores are compared against the observations of the cores from Site 35. This comparison is possible because before the overlay Sites 34 and 35 have the same surface JMF and both sites have almost the same age.

Table F.1. Summary of the observations from the field cores.

Site No.	Core	Friction	SPT	Parameters from Scanned Surface				Field Obs.	
		BPN	MTD (mm)	MPD (mm)	EMTD (mm)	Peak (mm)	Valley (mm)	MPD (mm)	Friction
8	C1	54	0.5	0.34	0.47	0.14	0.19	0.39	0.76
	C2	56	0.4	0.27	0.42	0.15	0.23	0.42	0.74
	C3	57	0.4	0.32	0.45	0.16	0.24	0.38	0.65
13	C1	74	0.3	0.15	0.32	0.11	0.13	0.31	0.46
	C2	53	0.4	0.26	0.41	0.10	0.14	0.30	0.47
	C3	55	0.3	0.13	0.30	0.12	0.12	0.30	0.43
14	C1	69	0.4	0.21	0.37	0.10	0.13	0.41	0.53
	C2	62	0.3	0.17	0.33	0.09	0.12	0.40	0.53
	C3	64	0.4	0.17	0.34	0.09	0.12	0.39	0.53
17	C1	56	0.5	0.31	0.44	0.15	0.22	0.38	0.62
	C2	52	0.5	0.36	0.49	0.15	0.21	0.40	0.60
	C3	57	0.4	0.21	0.37	0.11	0.17	0.38	0.56
23	C1	59	0.4	0.24	0.39	0.12	0.17	0.41	0.53
	C2	60	0.4	0.24	0.39	0.12	0.16	0.43	0.61
	C3	56	0.4	0.19	0.35	0.13	0.15	0.41	0.62
24	C1	54	0.3	0.23	0.38	0.15	0.19	0.33	0.68
	C2	56	0.4	0.22	0.38	0.12	0.17	0.33	0.67
	C3	61	0.4	0.22	0.38	0.11	0.15	0.34	0.65
	C4	60	0.4	0.26	0.41	0.12	0.19	0.36	0.68
27	C1	63	0.4	0.23	0.39	0.12	0.21	0.37	0.73
	C2	60	0.4	0.18	0.34	0.11	0.16	0.35	0.63
	C3	66	0.4	0.18	0.34	0.10	0.19	0.36	0.59
28	C1	52	0.3	0.16	0.32	0.10	0.15	0.31	0.50
	C2	50	0.3	0.15	0.32	0.09	0.13	0.33	0.50
	C3	51	0.4	0.16	0.32	0.09	0.14	0.30	0.53
30	C1	60	0.4	0.21	0.37	0.12	0.17	0.38	0.62
	C2	51	0.4	0.25	0.40	0.18	0.23	0.37	0.63
	C3	48	0.4	0.30	0.44	0.16	0.22	0.36	0.64
33	C1	55	0.4	0.26	0.41	0.14	0.17	0.35	0.51
	C2	50	0.4	0.20	0.36	0.11	0.17	0.37	0.55
	C3	60	0.3	0.19	0.35	0.11	0.18	0.35	0.56
35	C1	59	n.c.	0.10	0.30	0.14	0.14	0.30	0.55
	C2	59	n.c.	0.11	0.17	0.06	0.08	0.31	0.42
	C3	55	n.c.	0.09	0.15	0.06	0.08	0.29	0.42
	C4	55	n.c.	0.10	0.19	0.06	0.08	0.33	0.42
	C5	60	n.c.	0.13	0.29	0.13	0.12	0.31	0.52
37	C1	66	n.c.	0.15	0.31	0.08	0.13	0.28	0.50
	C2	55	n.c.	0.12	0.22	0.06	0.09	0.27	0.47
	C3	63	n.c.	0.13	0.37	0.06	0.09	0.28	0.47
39	C1	55	n.c.	0.26	0.36	0.14	0.26	0.34	0.70
	C2	62	n.c.	0.31	0.38	0.17	0.33	0.39	0.68
	C3	57	n.c.	0.24	0.31	0.14	0.24	0.36	0.67

n.c.: not collected.

Effect of Mixture Volumetrics on the Initial Representative Friction and Texture Values

As described above, the representative friction is defined as the average of the 2.5th friction percentile reported in 0.1-mile increments along a site. In the case of the *MPD*, the representative value was set as the average of the 50th *MPD* percentile. As indicated in Table F.1, there are 10 sites with pre-construction observations, which allows for comparison of the effects of the overlay on pavement friction and texture for these sections in Figure F.5 and Figure F.6, respectively.

These graphs indicate the effect of asphalt overlays on friction values is uniform because for five out of the ten sites, friction reduced (by an average of 17%), whereas in the other five sites, friction increased (by an average of 19%). In contrast, the effect of an overlay on the *MPD* is more evident because in 9 out of the 10 sites with pre-construction observations, the *MPD* reduced after the overlay (on average by 55%). Also, as shown in Figure F.6, the *MPD* is more sensitive to the surface type, because the UTBWC sites clearly stand out from the dense mixes, but the same does not occur in Figure F.5 in the case of friction.

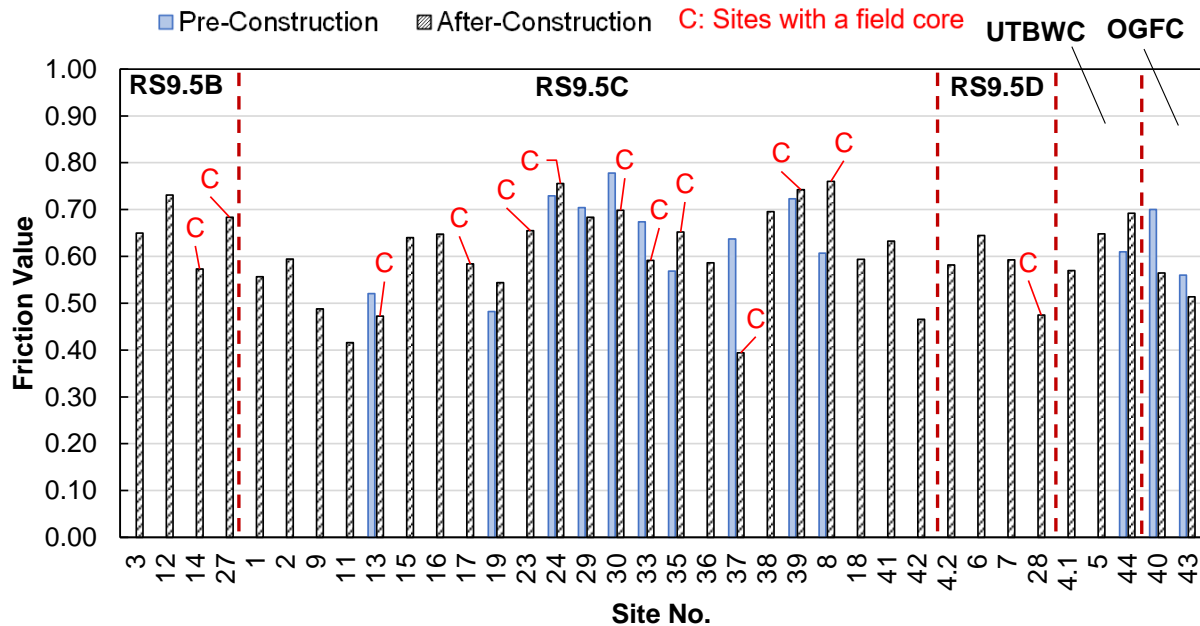


Figure F.5. Comparison of the representative friction before and after the overlay

Hence, a model that relates the as-designed mixture composition with the representative field friction and texture is proposed. The predictors evaluated as possible explanatory variables were the mixture volumetrics indicated in Table B.1. The response variable in the prediction models was set either as the representative friction ($Friction_{representative}$) or the representative *MPD* ($MPD_{representative}$). An iterative approach was followed where each variable of Table B.1 was used as the only explanatory parameter, then the most significant parameters were included in a multilinear regression model. The R^2 of the model and the significance of each parameter were computed and used to select the best model. Table F.2 and Table F.3 summarize the different models evaluated to predict the initial representative *MPD* and friction, respectively. The selected models are shown in Equation (107) and Equation (108).

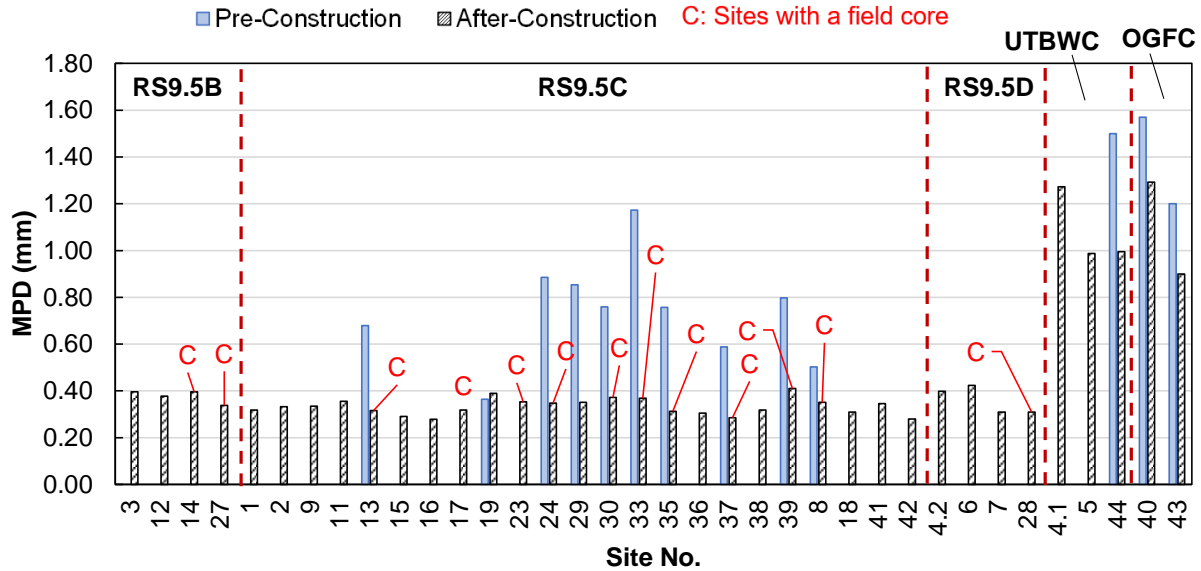


Figure F.6. Comparison of the representative *MPD* before and after the overlay.

Table F.2. Coefficients of the initial representative *MPD* models.

Model	Intercept	AC%	VMA	VFA	D_{60}	C_c	P_{200}	VFA* P_{200}	Adj. R^2
1	1.01*	-0.11*	-	-	-	-	-	-	0.12
2	1.51*	-	-0.07*	-	-	-	-	-	0.23
3	1.48*	-	-	-0.01*	-	-	-	-	0.91
4	0.09*	-	-	-	0.10*	-	-	-	0.66
5	0.15*	-	-	-	-	0.28*	-	-	0.53
6	1.04*	-	-	-	-	-	-0.11*	-	0.50
7	0.93*	-	-	-	-	-	-	-0.12*	0.68
8	1.29*	-	-	-0.01*	0.02*	-	-	-	0.91
9	1.22*	-0.05	-	-0.01*	-	0.09*	-	-	0.92
10	1.15*	-	-	-0.01*	0.03*	-	0.02***	-	0.92
11	1.15*	-	-	-	-0.01*	-	-	0.03*	0.70

*Significant at 95% confidence level, **significant at 90% confidence level, ***not significant.

$$MPD_{mean} = 1.22 - 0.009 \times VFA + 0.087 \times C_c - 0.046 \times (AC\% \cdot Dense); R^2 = 0.920 \quad (107)$$

where;

- MPD_{field} = average *MPD* measured in the field using a HSIP, in mm,
- C_c = coefficient of curvature, computed with Equation (105),
- Dense* = 1 for a dense mix, 0 otherwise,
- VFA* = percent of voids filled with asphalt, and
- AC%* = binder content in %.

Table F.3. Coefficients of the average friction models.

Mod	Inter.	AC%	VFA	D ₆₀	Cc	P ₂₀₀	MPD	R _{sk}	AC%*P ₂₀₀	Adj. R ²
1	1.26*	-0.11*	-	-	-	-	-	-	-	0.21
2	1.21*	-	-	-	-	-	-	-	-	0.10
3	0.71*	-	-0.002***	-	-	-	-	-	-	0.00
4	0.49*	-	-	0.03*	-	-	-	-	-	0.10
5	0.49*	-	-	-	0.12*	-	-	-	-	0.14
6	0.96*	-	-	-	-	-0.06*	-	-	-	0.24
7	0.54*	-	-	-	-	-	0.12***	-	-	0.00
8	0.55*	-	-	-	-	-	-	-0.09*	-	0.27
9	0.89*	-	-	-	-	-	-	-	-0.79*	0.29
10	1.03*	-0.08*	-	-	-	-	-	-0.07*	-	0.36
11	0.83*	-	-	-	-	-0.04*	-	-0.07*	-	0.37
12	0.79*	-	-	-	-	-	-	-0.07*	-0.58*	0.40

*Significant at 95% confidence level, **significant at 90% confidence level, ***not significant.

$$Friction_{mean} = 0.786 - 0.065 \times R_{sk} - 0.580 \times (AC\% \times P_{200}); R^2 = 0.40 \quad (108)$$

where;

$Friction_{field}$ = average friction measured in the field using a CFME,

R_{sk} = texture profile skewness,

AC% = binder content in %, and

P_{200} = percent passing sieve No. 200.

These models indicate the friction is affected by the surface skewness, which measures the amount of negative macrotexture, and by the interaction of the P_{200} and AC%. Higher skewness means the proportion of voids is higher than the proportion of peaks in the texture profile, resulting in lower representative friction values. The higher influence from the interaction of $P_{200} \times AC\%$ reflects a higher proportion of fines in the mix that might be covering the coarse aggregate, which might limit the coarse aggregate friction contribution.

Also, it is important to notice that the R^2 of the friction model is 0.40, meaning that this model explains just 40% of the data variability. More research is needed to improve the model accuracy; for instance, adding more observations by incorporating open-graded mixes, like increasing the number of UTBWC and/or adding Open-Graded Friction Courses (OGFC), could light a better relationship between volumetrics, R_{sk} , and MPD; another possibility is to incorporate the aggregate properties in the analysis, like abrasion, polishing resistance, shape, angularity, etc. These aggregate specific variables provide a representation of the microtexture friction component, which given the current model form might not be well represented.

On the other hand, the model given in Equation (107) for the representative MPD has an R^2 of 0.92; however, it was observed that this model is highly influenced by the four UTBWC sites that have the highest texture values. If these observations are removed, the R^2 of the model drops to 0.35. Thus, this model can differentiate between high friction mix designs and dense mixtures but is not as strong at differentiating between dense-graded mixes. In this sense, it is necessary to add more observations of open graded mixes to improve the model.

Nevertheless, these models bring a first estimate of the expected representative friction and texture value based on as-designed mixture volumetric properties. The values predicted are the expected

average values across several miles. The next section evaluates the use of laboratory measurements on field cores combined with mixture volumetrics to predict field friction and texture. Using laboratory measurements on field cores might be more accurate because these provide point estimates of the surface properties that bring more location-specific predictors.

Field Lab-Relationships

Basic Observations of Field-Lab Relationships

Initial comparisons of the field observations and the values collected in the field are presented in Figure F.7 and Figure F.8. The *BPN* is frequently used to represent friction contribution from the surface microtexture. Figure F.7 shows that there is no relationship between the *BPN*, and the field friction collected with the CFME. This result is expected because the CFME is conducted at high speeds whereas the *BPN* is the result of a static measurement. On the other hand, the *MPD* of the pre-construction cores is higher than their after-construction counterparts, in fact the average *MPD* among all the pre-construction cores was above 0.55 mm, whereas the average *MPD* among all after-construction cores was below 0.45 mm.

As indicated in both figures, since the pre-construction cores have the lowest friction and the highest *MPD* values, these observations have a strong influence in the linear trend because as illustrated in part (c) and (d) of Figure F.7 and Figure F.8, the trend changes considerably after removing these observations.

The pre-construction cores may have lower friction and higher texture due to the traffic polishing effect that can cause a densification of the material, peel-off of the binder cover from the aggregates, and loss of fines or raveling. Because the main objective is to analyze the early friction and texture development (one to two months after the overlay), only the cores collected after the overlay are used to develop the predictive models. These models are proposed to relate the as-designed mixture volumetrics, texture and friction specific parameters measured on the surface of a set of QA field cores, with the field friction and texture.

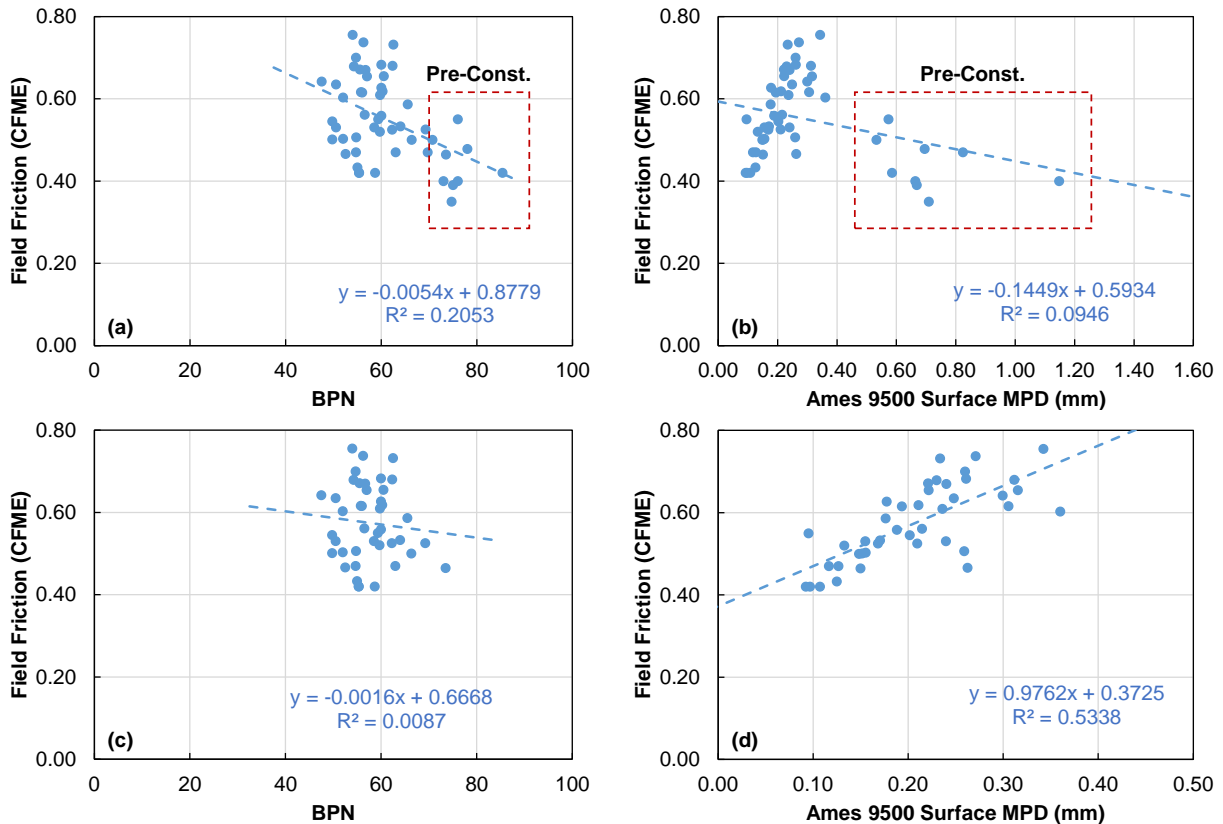


Figure F.7. Comparison of laboratory measurements with field friction: (a) *BPN*, (b) *MPD*, (c) *BPN* without pre-construction observations, and (d) *MPD* without pre-construction observations.

If one compares the average field friction, *MPD*, and *BPN* recorded with the pre-construction cores against the average of the values observed in after-construction cores a 31% increase in field friction is obtained as well as a 45% and 24% reduction in field *MPD* and *BPN*, respectively. Furthermore, if one computes the percent change using only the observations of Site 34 (pre-construction field cores) against the observations of Site 35 (after-construction field cores) an increase of 9% in field friction and a reduction of 52% and 23% in field *MPD* and *BPN*, respectively are observed. In the case of Site 37 and 39 the reduction in *MPD* was 53% and 45%, respectively.

Collectively, these results indicate that asphalt overlays have a more pronounced effect on texture than friction. As shown above, the *MPD* reduces on average 45%, but this reduction can be as high as 53%. Although there is not a clear relationship between the *BPN* and the field friction, on average the microtexture friction component reduces after an overlay. These two variables might not relate because, the *BPN* might be more sensitive to macrotexture components due to a higher relative hysterical engagement, i.e., lower speed and less ability to move relative to the surface plane. More observations are needed to get a better understanding of the microtexture friction component in the resulting skid resistance of a surface.

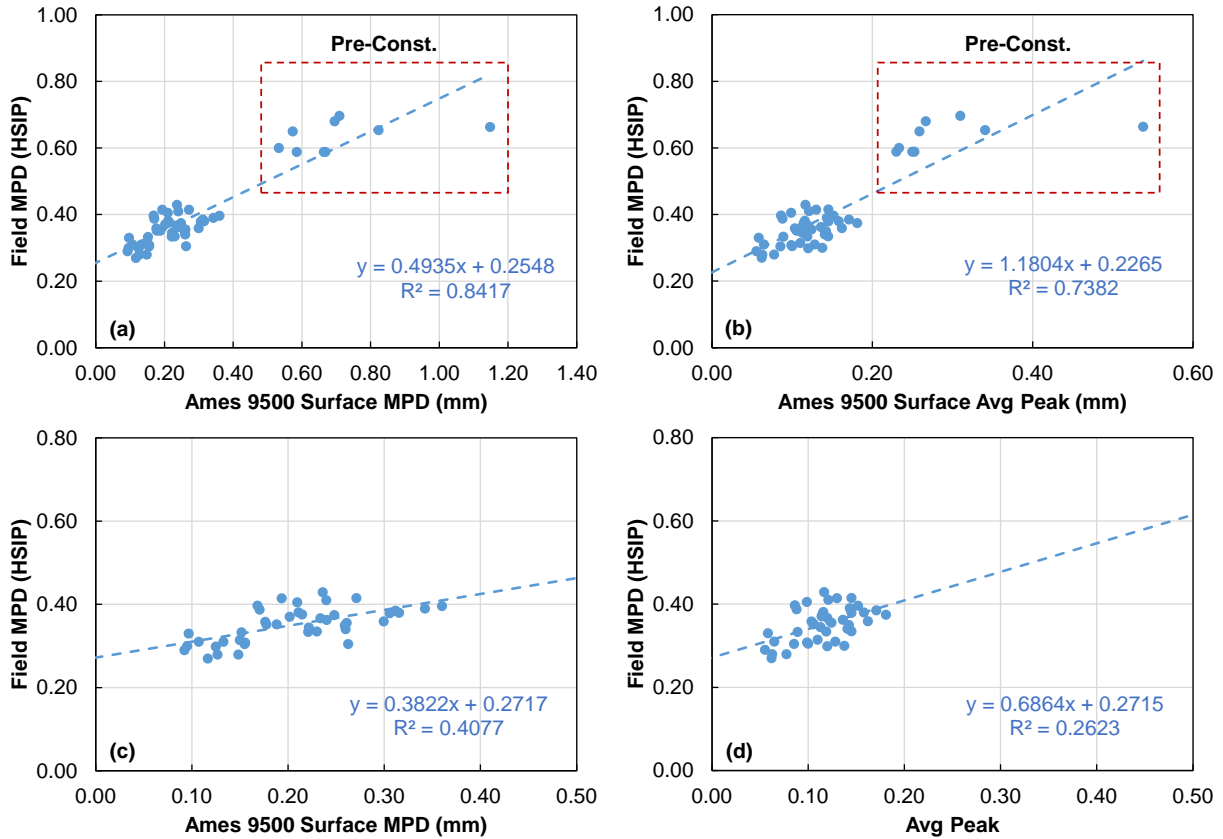


Figure F.8. Comparison of laboratory measurements with field MPD: (a) lab MPD, (b) average peak, (c) lab BPN without pre-construction observations, and (d) average peak without pre-construction observations.

Model to Predict Initial Texture and Friction in the Field using Laboratory Observations

After selecting the after-construction observations, a set of regression models were evaluated. The response variable in the prediction models was set either as the field friction ($Friction_{field}$) or the MPD in the field (MPD_{field}). The predictors are the mixture compositional factors presented in Table B.1 and the texture parameters extracted from the field cores, included in Table F.1. The correlation coefficient between the descriptors and the response was computed and it was found that the variables that positively correlates the most with $Friction_{field}$ and MPD_{field} are the MPD_{lab} , $EMTD$, $Peak$, $Valley$, D_{60} , and Cc ; similarly, the variables that negatively correlated the most with $Friction_{field}$ and MPD_{field} are $AC\%$, and P_{200} .

An iterative approach was then used wherein each variable was first used as the only explanatory parameter and then the most significant ones were included in a multilinear regression model. The R^2 of the model and the significance of each parameter were computed and used to select the best model fit. In addition, three more variables were ‘created’ by combining the descriptors with the highest positive correlation and the descriptors with the highest negative correlation; in this sense, variables were combined by adding them or by multiplying them. All the possible permutations were evaluated, see Table F.4 and Table F.5, and it was found that the best combination for the positive correlation was $Cc+Peak+Valley$, and the combination that best describe the negative correlation was $AC\% \times P_{200}$. These combined variables were treated as a separate predictor and

the resulting model was selected based on the significance of the parameters and prediction accuracy.

Table F.4. Coefficients of the *MPD* models derived with the ALL sites using the surface scanned with the AMES 9500 laser.

Mod	Inter.	<i>MPD</i> _{lab}	<i>EMTD</i>	<i>Peak</i>	<i>Valley</i>	<i>D</i> ₆₀	<i>Cc</i>	<i>AC</i> %	<i>P</i> ₂₀₀	Adj. <i>R</i> ²
1	0.27*	0.39*	-	-	-	-	-	-	-	0.38
2	0.23*	-	0.34*	-	-	-	-	-	-	0.32
3	0.27*	-	-	0.69*	-	-	-	-	-	0.24
4	0.28*	-	-	-	0.41*	-	-	-	-	0.25
5	0.25*	-	-	-	-	0.04***	-	-	-	0.19
6	0.32*	-	-	-	-	-	0.04*	-	-	0.04
7	0.63*	-	-	-	-	-	-	-0.05*	-	0.24
8	0.43*	-	-	-	-	-	-	-	0.01**	0.01
9	0.43*	0.31*	-	-	-	-	-	-0.02*	-	0.43
10	0.42**	-	-	0.20***	0.17***	0.01***	-	-0.02**	-	0.26

*Significant at 95% confidence level, **significant at 90% confidence level, ***not significant.

The proposed models to predict the mean *MPD*_{field} and friction in the field are presented in Equation (109) and (110). As presented, in both models the *AC*% negatively affects both the initial texture and friction. Moreover, in the case of friction the model of Equation (110) suggests that when the interaction of *AC*% and *P*₂₀₀ increases the initial friction reduces, this may be associated with the initial asphalt film that covers the aggregate that reduce the friction microtexture component. The verification plot of each model is included in Figure F.9.

Table F.5. Coefficients of the friction models derived with ALL sites using the surface scanned with the AMES 9500 laser.

Mod	Inter.	<i>MPD</i> ^a	<i>EMTD</i>	<i>Peak</i>	<i>Valley</i>	<i>D</i> ₆₀	<i>Cc</i>	<i>AC</i> %	<i>P</i> ₂₀₀	<i>Cc</i> + <i>Pk</i> + <i>Va</i>	<i>AC</i> % * <i>P</i> ₂₀₀	Adj. <i>R</i> ²
1	0.37*	0.98*	-	-	-	-	-	-	-	-	-	0.52
2	0.27*	-	0.86*	-	-	-	-	-	-	-	-	0.44
3	0.33*	-	-	2.13*	-	-	-	-	-	-	-	0.49
4	0.34*	-	-	-	1.39*	-	-	-	-	-	-	0.62
5	0.31*	-	-	-	-	0.1*	-	-	-	-	-	0.30
6	0.40*	-	-	-	-	-	0.2*	-	-	-	-	0.41
7	1.30*	-	-	-	-	-	-	0.12*	-	-	-	0.36
8	1.14*	-	-	-	-	-	-	-	0.09*	-	-	0.38
9	0.33*	-	-	-	-	-	-	-	-	0.22*	-	0.58
10	0.95*	-	-	-	-	-	-	-	-	-	0.01*	0.44
11	0.62*	-	-	-	-	-	-	-	-	0.17*	0.01*	0.74

*Significant at 95% confidence level, **significant at 90% confidence level, ***not significant, ^a*MPD*_{Lab}.

$$MPD_{field} = 0.433 + 0.310 \times MPD_{lab} - 0.025 \times AC\%; R^2 = 0.460 \quad (109)$$

where;

*MPD*_{field} = mean *MPD*, computed over a 500-ft window, measured in the field using a HSIP,

*MPD*_{lab} = *MPD* calculated in the lab using the surface measured with the AMES profiler, (mm),
and

AC% = binder content in %.

$$Friction_{field} = 0.619 + 0.172 \times (Cc + Peak + Valley) - 0.0060 \times (AC \times P_{200}); R^2 = 0.742 \quad (110)$$

where;

$Friction_{field}$ = mean friction, computed over a 500-ft window, measured in the field using a CFME,

Cc = coefficient of curvature,

$Peak$ = average peak height (positive texture elevation), in mm,

$Valley$ = average valley depth (negative texture elevation), in mm,

$AC\%$ = binder content in %, and

P_{200} = percent passing sieve No. 200.

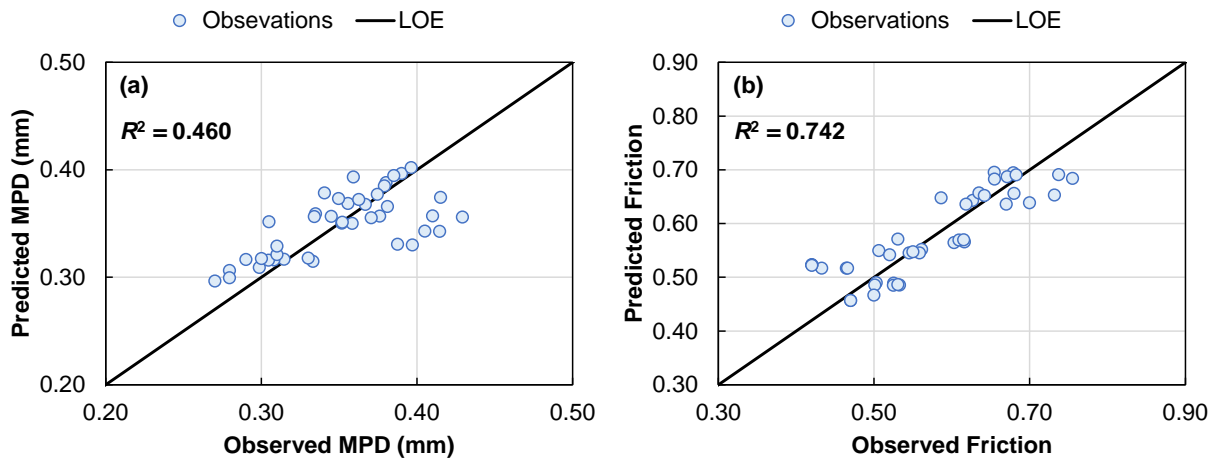


Figure F.9. Model prediction plot for: (a) texture and (b) friction

It is important to notice that the models derived with the field cores used ‘spot’ friction and texture values (average friction and texture values computed in a window of 500-ft around the core location) as the response variables. For this reason, the first set of models presented in the preceding section were developed. Those models predict the representative as-designed friction and texture based on the mixture volumetrics.

Conclusions

Based on the measurements collected, it was shown that the representative friction and texture in the field could be defined as the 2.5th and 50th percentile of the values grouped by 160 m (0.1-mile) increments. By using these quantities to represent the available friction and texture in the field it is possible to capture the spatial variability of both quantities and to remove any possible outlier captured during the measurement process.

The comparison of the laboratory and the field observations collected before and after the overlay has shown, at least in the case of North Carolina’s mixtures, there is strong evidence that texture reduces after an asphalt overlay. This reduction was 55% on average and observed to be as high as 73%. On the other hand, the effect of asphalt overlays on friction is not clear because half of the sites showed an average reduction of 17%, whereas the other half showed an increase of 19%.

Two sets of models were derived. The first set can be used to predict the average representative friction and texture in the field based on the as-designed mixture composition. It was found that the MPD can be estimated using the gradation coefficient of curvature and the voids filled with

asphalt (*VFA*). In the case of friction, the proposed model indicates that friction is affected by the skewness of the texture profile and the interaction of asphalt content (*AC%*) and the proportion of fines in the mix (*P₂₀₀*). The second set of models can be used to obtain ‘spot’ estimates of friction and texture in the field using laboratory measurements of texture combined with mixture compositional factors. A ‘spot’ is understood as the average value of each of these skid resistance properties in a window of 500 ft (150 m) around a field core location.

It was found friction values in the field can be approximated by using the gradation coefficient of curvature *C_c* and the surface irregularities quantified in the scanned surface of the field cores. In the case of texture, the *MPD* observed in the field correlates with the *MPD* calculated from the core scanned surface, although the resulting model encompasses a high amount of uncertainty as reflected by the *R²* of 0.46. Collectively, these models serve as a tool to quickly estimate the available friction and texture in the field by using a set of measurements collected in the laboratory. These results indicate that better friction predictions are obtained by incorporating ‘spot’ specific texture values extracted from the field cores.

All the measurements were conducted on a set of field cores extracted using the same methodology to obtain the samples for in-place density control. For this reason, the models and methodology presented here could set the basis for defining a process that allows the quality assurance and control of the surface skid resistance of newly constructed asphalt surfaces. The advantage of the proposed models is that the laboratory measurements can be conducted on the specimens collected during the regular quality control process without incurring extra cost or time.

Finally, the proposed models can set the basis for screening potential problematic mixture design to explicitly account for friction and texture performance in the field. These models provide a rough estimate of the expected friction and texture given the mixture composition. So, engineers and practitioners can use them to estimate the skid resistance that will be available given an asphalt job mix formula, versus the demand established based on the project and site-specific characteristics. More research is needed to improve the accuracy of the models and to properly account for the skid resistance demand during the mix design.

APPENDIX G. FRICTION AND TEXTURE PERFORMANCE MODEL TECHNICAL DETAILS

Methodology

Comparison of the CL and RWP Observations

The CL and RWP measurements were statistically compared to evaluate if there was evidence that the RWP deteriorates faster than the CL because of the higher traffic repetitions. The statistical comparison focused on the sites that have both the CL and RWP measurements collected. This comparison was made by traffic direction (approach), to keep the sample size as large as possible. Although sequential observations were collected in each site after the asphalt overlay, not all the traffic directions and wheel paths were tested on each measurement date. For example, Site 19 was tested on eight dates, but the SB direction was tested only on five of these dates and the NB direction was tested in all of them. Though the SB direction was tested five times, the CL was tested only four times. Likewise, despite the NB direction being tested eight times, the CL was tested only on seven of these dates. In other words, for Site 19 five and eight pairs of CL-RWP were available for comparison in the SB and NB direction, respectively.

Based on this discrepancy the total number of site observations with friction and texture in both CL and RWP was 251. For each of these sites, a two-sample t-test comparison was made to test the significance of the difference and whether the RWP records were higher or lower than the CL. To this end, the statistic T shown in Equation (111) was computed. This statistic has the degrees of freedoms (dof) indicated in Equation (112) and follows the distribution $T \sim t_{dof}$. At a significance level of 95% confidence, the difference between the two means will be significant if $T \geq t_{0.025,dof}$ or if $T \leq -t_{0.025,dof}$. Similarly, the RWP mean will be statistically significantly higher than the CL mean if $T \geq t_{0.05,dof}$ and statistically significantly lower if $T \leq -t_{0.05,dof}$.

$$T = \frac{(\bar{X}_{RWP} - \bar{X}_{CL}) - (\mu_{RWP} - \mu_{CL})}{\sqrt{\frac{S_{RWP}^2}{N_{RWP}} + \frac{S_{CL}^2}{N_{CL}}}} \quad (111)$$

$$dof = \frac{\left(\frac{S_{RWP}^2}{N_{RWP}} + \frac{S_{CL}^2}{N_{CL}}\right)^2}{\frac{\left(\frac{S_{RWP}^2}{N_{RWP}}\right)^2}{N_{RWP}-1} + \frac{\left(\frac{S_{CL}^2}{N_{CL}}\right)^2}{N_{CL}-1}} \quad (112)$$

where;

\bar{X}_{RWP} = RWP representative friction or texture,

\bar{X}_{CL} = CL representative friction or texture,

S_{RWP} = RWP standard deviation, of the 2.5th friction percentile or the 50th texture percentile, computed on 0.1-mile increments, and

S_{CL} = CL standard deviation, of the 2.5th friction percentile or the 50th texture percentile, computed on 0.1-mile increments.

Modeling Seasonality

Based on a review of the literature (38), the sigmoidal model presented in Equation (113) was chosen as the basic form to describe the seasonal variation. To calibrate this model, only the observations collected in the CL were employed because it was assumed that the CL has minimal traffic exposure in comparison to the RWP, and therefore the variation in the CL values can be attributed to seasonality. For the seasonal effects analysis, only observations from sites with at least three observations after the overlay were included, i.e., a total of 33 sites.

$$SF = \frac{Obs_{Seasonal}}{Obs_{Mean}} = a_0 + a_1 \times \sin\left(\frac{2\pi \times DoY}{365} + a_2\right) + a_3 \times Temp + a_4 \times DD \quad (113)$$

where;

- SF = seasonal factor,
- $Obs_{seasonal}$ = observed value at any given day of the year,
- Obs_{Mean} = mean value of friction or texture without seasonal effect,
- a_0 to a_4 = coefficients to be calibrated,
- DoY = Julian calendar days,
- $Temp$ = average 7-day mean temperature, Celsius degrees, and
- DD = number of dry days.

Friction Performance

For Group-2 sites, the percent change between the first and second friction measurements with respect to the first observation was calculated using Equation (114). The sites that were rehabilitated or that exhibited an accelerated texture deterioration process were identified and excluded from the analysis. The *MPD %Change* is defined in the next section and computed with Equation (118), those sites with an absolute *MPD %Change* greater than 20% or with a rehabilitation action reported sometime between year 2020 and 2022 were excluded from the analysis. The proposed functional form for the friction performance model is depicted in Equation (115) and Figure G.1. This functional form was selected based on the friction variation described in the previous project FHWA/NC 2020-11.

The first phase of the performance curve is modeled as a second order polynomial and the second phase is modeled using exponential decay. The boundary between the two models is expressed by T_{max} , which represents the cumulative traffic required to reach the maximum friction (F_{max}). The general mathematical representation of this model is presented in Equation (115). As shown, both phases are modeled using a mixed random effect structure, where the intercept of each model has a random effect introduced by each site, and the random effect in the friction rate of change (b and B for Phase 1 and 2, respectively) is controlled by each site and the family defined in Table 4, respectively.

$$Friction \%Change = \frac{(Friction_{2022} - Friction_{2020})}{Friction_{2020}} \times 100 \quad (114)$$

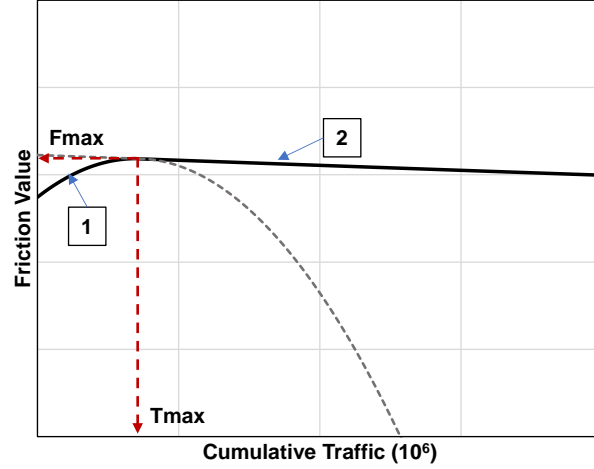


Figure G.1. Proposed friction performance curve.

$$F(T) = \begin{cases} (a + \Delta a_{site}) + (b + \Delta b_{site}) \cdot T + c \cdot T^2 \rightarrow T \leq T_{max} \\ (A + \Delta A_{site}) \cdot \exp\left[(B + \Delta b_{family}) \cdot T\right] \rightarrow T > T_{max} \end{cases} \quad (115)$$

where;

- a = fixed effect of Phase-1 *Friction* intercept,
- Δa_{site} = random effect of Phase-1 *Friction* intercept, one value per site,
- b = fixed effect of Phase-1 *Friction* rate of change,
- Δb_{site} = random effect of Phase-1 *Friction* rate of change, one value per site,
- c = fixed effect of the second order curvature,
- A = fixed effect of Phase-2 *Friction* intercept,
- ΔA_{site} = random effect of Phase-2 *Friction* intercept, one value per site,
- B = fixed effect of Phase-2 *Friction* rate of change,
- ΔB_{family} = random effect of Phase-2 *Friction* rate of change, one value per family, and
- T = cumulative traffic (or truck traffic).

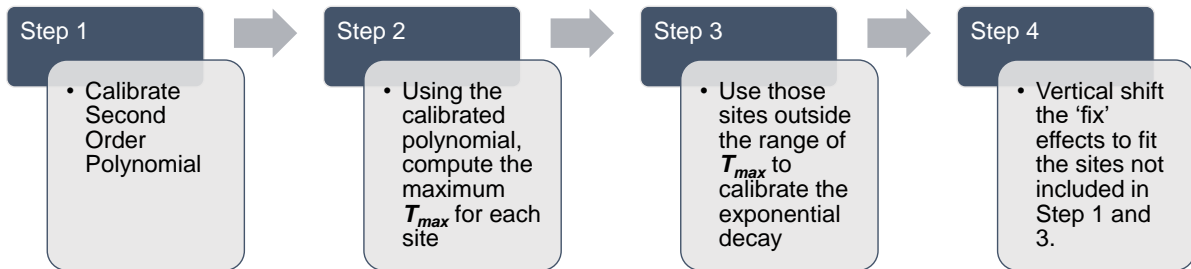


Figure G.2. Friction performance model calibration procedure.

Given the number of parameters to be calibrated, a step-by-step procedure for the model calibration was defined that is described in Figure G.2. As indicated, Step 1 consisted of calibrating Phase 1 of the friction performance. For this purpose, Group-1 sites with at least three observations were used together with those Group-2 sites that have an age lower than or equal to two years at the moment of the first measurement, i.e., that were rehabilitated either in 2018 or 2019. A total of 18 sites met these criteria. In Step 2, the second order polynomial calibrated in Step 1 was used to estimate T_{max} and F_{max} using Equation (116) and (117), respectively. This approach means that a

total of 18 T_{max} were estimated, one per site. The range of these estimated values was used to define the transition range.

$$T_{max} = \frac{-b}{2c} \quad (116)$$

$$F_{max} = a - \frac{b^2}{2c} + \frac{b^2}{4 \cdot c} \quad (117)$$

In Step 3, those Group-2 sites with a cumulative traffic greater than the maximum T_{max} computed in Step 2 were used for calibration of Phase 2. Then, in Step 4, those Group-2 sites with a cumulative traffic less than T_{max} were fitted using the fix effect model estimated in Step 1 but shifted vertically to match the observed deterioration. This means that in the second order polynomial component of Equation (115), parameters b and c are set as the fixed effect coefficients, whereas parameter a varied for each site. This task was performed by minimizing the sum of square errors by changing a .

Texture Performance

For the 117 Group-2 sites, the percent change of the last measurement (the one collected in 2022) with respect the first measurement (the one collected in 2020) was computed using Equation (118). For this calculation, ten sites with a surface different than asphalt were excluded. A reduction in MPD results in a negative value in Equation (118), while an increase in MPD corresponds to a positive value.

$$MPD \% Change = \frac{(MPD_{2022} - MPD_{2020})}{MPD_{2020}} \times 100 \quad (118)$$

The $MPD \% Change$ was used to flag sites that may have been rehabilitated or deteriorated excessively between the first and second measurement. Individual assessment of the flagged sites was conducted to determine if the site should be kept for model calibration or if it should be removed. A site was removed if the absolute value of the $MPD \% Change$ was higher than 20% or if a rehabilitation action was reported sometime between year 2020 and 2020. After this filtering process, Equation (119) was used to model texture performance. Equation (119) is a mixed effect power model that accounts for heterogeneity in the intercept and the rate of change. The random effects in the intercept are set to be a function of the site, while the random effects in the rate of change are set to be a function of the family, i.e., it depends on the climate and the surface type. Equation (119) is proposed based on the findings presented in FHWA/NC 2020-11, where it was observed that the MPD after an asphalt overlay can be described using a power function. The main update from the model proposed in the previous report is the inclusion of the random effects terms and the use of traffic instead of time as the independent variable.

$$MPD = (a + \Delta a_{site}) \cdot T^{(b + \Delta b_{family})} \quad (119)$$

where;

- a = fixed effect of MPD intercept,
- Δa_{site} = random effect of MPD intercept, one value per site,
- T = cumulative traffic (or truck traffic),
- b = fixed effect of the MPD rate of change, and
- Δb_{family} = random effect of MPD rate of change, one value per family.

Results

Analysis of seasonal variation of friction and texture is shown first. Then, the early friction and texture evolution behaviors are described. Next, the long-term performance is modeled and discussed.

Evaluation of the Statistical Differences between CL and RWP Observations

Friction CL – RWP Comparison

After conducting the statistical evaluation, 226 out of the 251 comparisons indicated the difference between the CL and RWP are statically significant, i.e., 90% of the cases. Of these 226 sites, 175 indicated that the mean 2.5th friction percentile in the RWP was lower than the mean 2.5th friction percentile in the CL (70% of the cases) and 51 indicated that the mean 2.5th friction percentile RWP was higher than the mean 2.5th friction percentile in the CL (20% of the cases). The remaining 25 cases (10% of the cases) showed similar results between the CL and RWP, i.e., the Welch t-test failed to reject the null hypothesis that the two means were equal.

Texture CL – RWP Comparison

In the case of *MPD*, 238 comparisons between CL and RWP were made. Of these, 211 out of the 238 comparisons indicated the difference between the CL and RWP is statically significant, i.e., 89% of the cases. Of these 211, 104 indicated that the RWP mean was lower than the CL mean (44% of the cases) and 107 indicated that the RWP mean was higher than the CL mean (45% of the cases). The remaining 27 cases (11% of the total cases) suggested that the RWP and CL texture values were statistically similar.

Friction and Texture Seasonality

The analysis started by plotting the friction and texture observations as a function of the day of the year when the measurement was collected. An example of such analysis for friction and texture in Site 17 is shown in Figure G.3 and Figure G.4, respectively. In each figure, part (a) and (b) presents the measurements recorded in the CL and the RWP, respectively; also, measurements were made in both traffic directions, denoted Direction 1 (Dir 1) and Direction 2 (Dir 2).

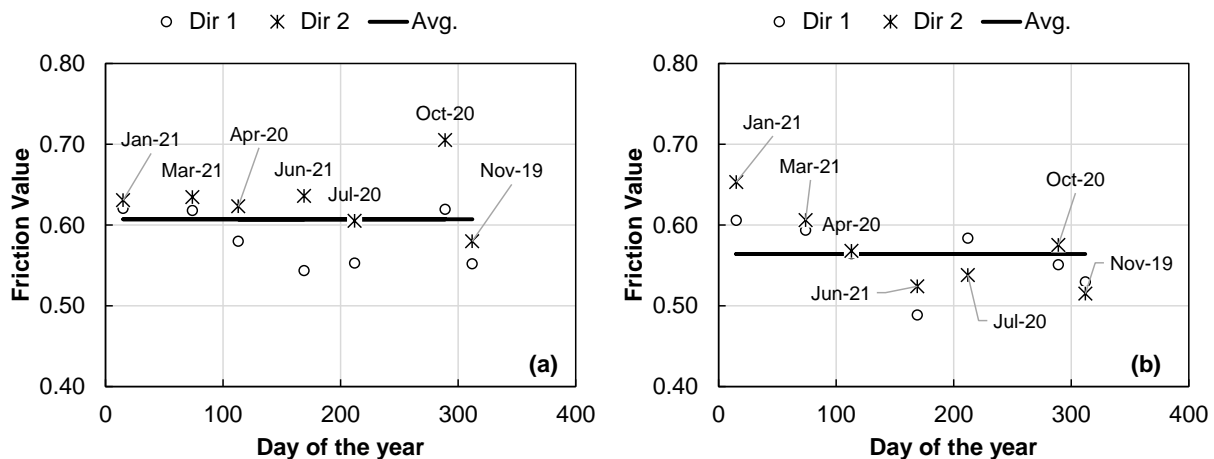


Figure G.3. Friction values variation by the day of the year for measurements in the: (a) CL and (b) RWP.

As stated before, the main hypothesis for the seasonal analysis is that the CL is only impacted by seasonal effects. This hypothesis was evaluated by comparing trends in friction and texture evolution in the CL versus the RWP. If they differ, it supports the hypothesis that the CL is less impacted by traffic than the RWP. However, if the CL and the RWP are statistically similar then it indicates that seasonality and traffic effects cannot be isolated. As observed in Figure G.3 (b), the RWP friction observations are lower than those observed in Figure G.3 (a) for the CL. Individual t-test were conducted between these observations as discussed in previous section.

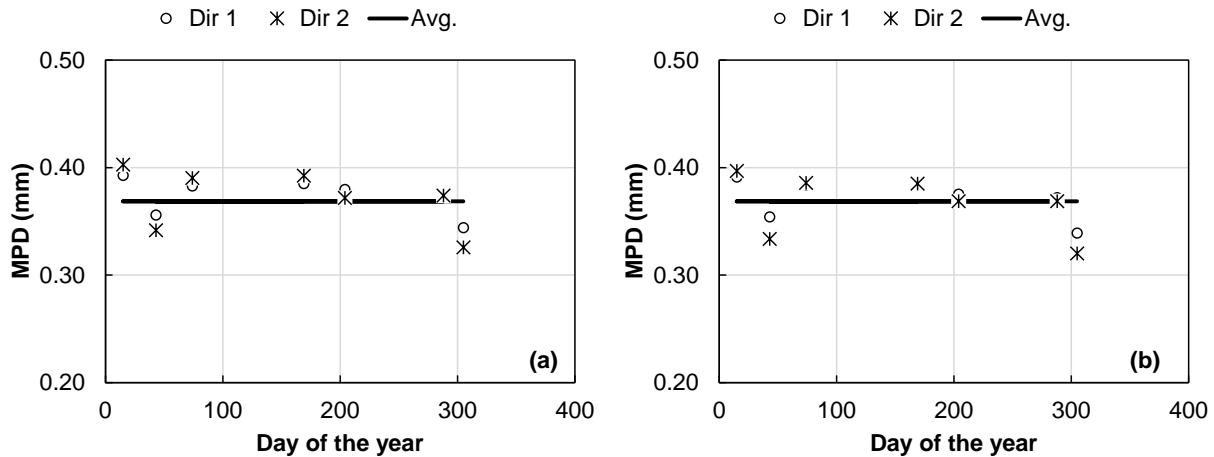


Figure G.4. Texture *MPD* values variation with the day of the year for measurements in the: (a) CL and (b) RWP.

However, when conducting a similar analysis for texture observations, shown in Figure G.4, there was no qualitative or statistical evidence suggesting the *MPD* observations from the RWP are lower than the CL, because the individual t-test comparison indicated that in half of the comparisons texture was lower in the RWP, but the other half showed that texture was higher in the RWP than in the CL. This situation was observed in all sites and for this reason the seasonal model shown in Equation (113) was calibrated only for the friction observations.

All the climate predictors to calibrate the model shown in Equation (113) were extracted from the MERRA-2 database (100). Values at the nearest grid point were identified for each test site. On average, the nearest grid point was 40 km away (25 mi) from the test site. The response for the model was set as the ratio of the friction values observed at the day of the measurement to the average friction of the measurement set collected at the site. This was possible because the measurements were evenly distributed, as much as possible, through the different seasons. Of the 33 sites with at least three observations, 29 are dense mixes and the remaining are two UTBWC and two OGFC mixes. The model coefficients are presented in Table G.1. For comparison purposes, the expressions calibrated in the previous project are included in the last two rows of Table G.1.

As shown, four models were calibrated, one for dense mixes only, another for high friction courses (UTBWC + OGFC), one for the long-term sites (those sites selected from Group-2 sites to evaluate the long-term seasonal effect), and one combining all sites. The model calibrated for the long-term sites was selected as the expression that describe the seasonal variation, because the sites used for its calibration provided friction observations for ‘old’ pavement surfaces, i.e., a minimum of 3 years passed since construction for the first observation. This expression is presented in Equation (121). The prediction accuracy of the model for the calibration set was verified by predicting the

$Friction_{Seasonal}$ in terms of the overall $Friction_{Mean}$ using Equation (120). The comparison between observed and predicted friction is shown in Figure G.5.

Equation (121) is an updated version of the model presented in the previous research project, FHWA/NC 2020-11. Two separate expressions were also provided in the FHWA/NC 2020-11, one for dense-graded surfaces and another for high-friction courses (UTWBC), with a special note on the limited sample used to generate the model for High Friction Course (HFC) surfaces.

$$Friction_{Seasonal} = Friction_{Mean} \times SF \quad (120)$$

$$\frac{Friction_{Seasonal}}{Friction_{Mean}} = 1.10 - 0.028 \times \sin\left(\frac{2\pi \times DoY}{365} + 1.59\right) - 0.0065 \times Temp - 0.0002 \times DD \quad (121)$$

Table G.1. Parameters of the seasonal model.

Mix Type	Parameter				
	a_0	a_1	a_2	a_3	a_4
Dense	1.00	0.059	1.34	0.0006	-0.0011
High Friction Course (HFC)	1.18	-0.110	1.46	-0.0133	0.0015
Long-Term Sites	1.10	-0.028	1.59	-0.0065	-0.0002
All	1.03	0.039	1.39	-0.0012	-0.0009
Dense (FHWA/NC 2020-11)	1.09	-0.046	1.32	-0.0058	-0.0033
HFC (FHWA/NC 2020-11)	0.82	0.858	0.98	0.0059	0.0440

The dataset available to calibrate the model was limited to only a few sections per climate region. Thus, Equation (121) is considered a preliminary model for friction seasonality in North Carolina; a broader data set is needed to enable more reliable predictions of seasonal effects. Individual prediction plots were created for each site. Examples are shown for Sites 111.3, 134.1, and 142 in Figure G.6 to Figure G.8, respectively. As shown in these figures, the model calibrated only for the long-term sites produces predictions similar to the ones made with the model calibrated with all sites combined.

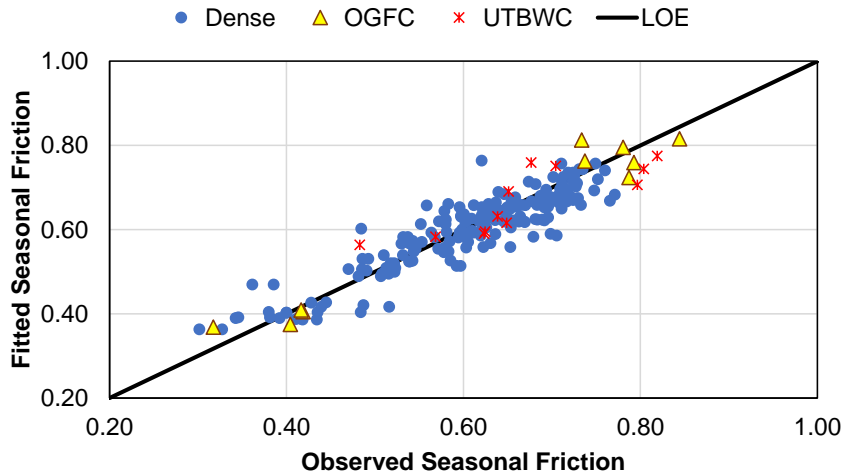


Figure G.5. Prediction checks of the seasonal friction model.

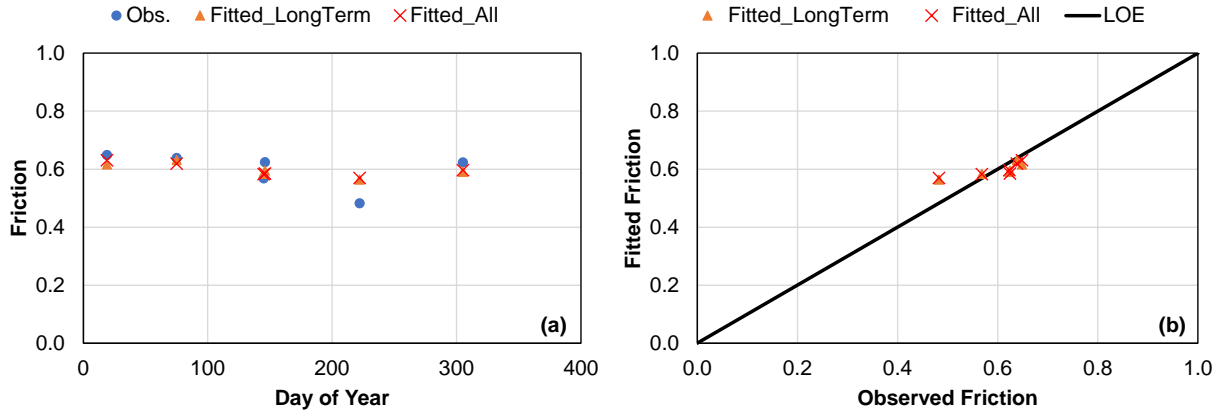


Figure G.6. Prediction check for Site 111.3 (UTBWC): (a) model fit and (b) fitted values along line of equality.

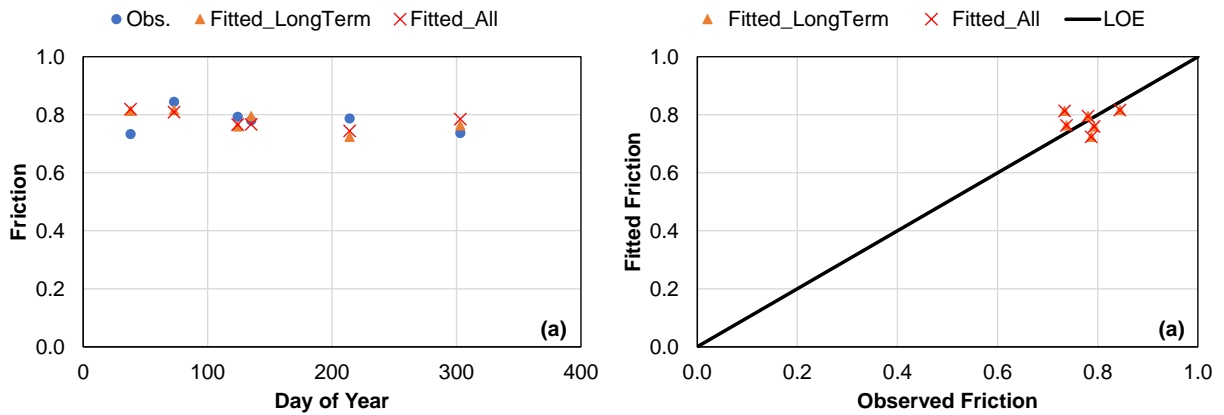


Figure G.7. Prediction check for Site 134.1 (OGFC): (a) model fit and (b) fitted values along line of equality.

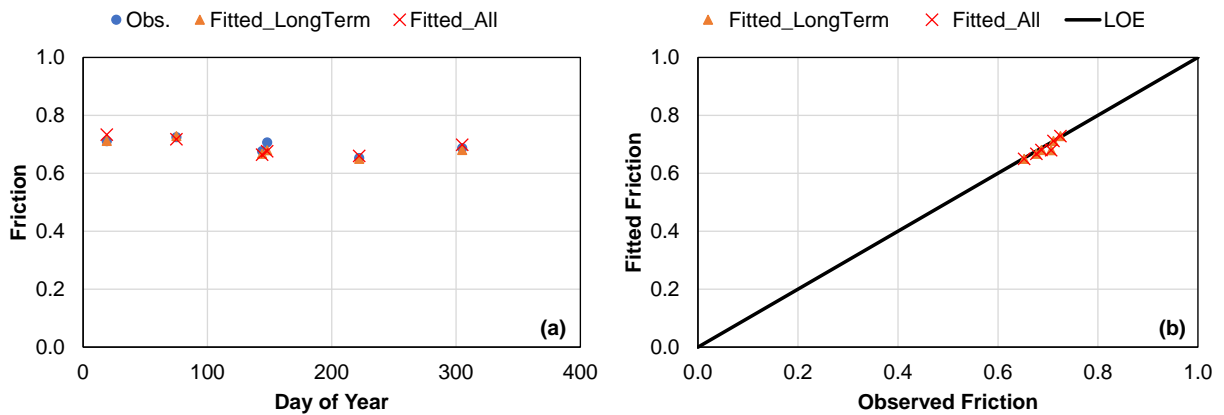


Figure G.8. Prediction check for Site 142 (Dense Mix): (a) model fit and (b) fitted values along line of equality.

Modeling Friction Performance

Friction values were plotted as a function of the cumulative traffic and the cumulative truck traffic, as depicted in Figure G.9. A summary of the percent change values across surface types are presented in Table G.2. It should be noted that there were 102 sites with friction observations whereas texture observations were made in 107 sites. This discrepancy occurred because even though both surface properties were measured in all sites, some of the friction measurements were not collected either at the desired speed (close to 60-mph) or were not collected in the desired wheel path (RWP) and therefore were omitted.

As summarized in Table G.2, 64% of the sites showed a reduction in friction and 36% showed an increase in friction, with an average reduction of 5.7%, 11.4%, and 8.8% for dense mixes, OGFC, and UTBWC, respectively. In the case of the eight rehabilitated surfaces, three showed an average reduction of 7%, whereas five showed an increase with an average increase of 16.2%. The average increase in the dense mixes, OGFC, and UTBWC was 5.1%, 5.3%, and 8.3%, respectively.

No further filtering was applied to the dataset because there was no other consideration that highlighted a feasible reason to exclude a site, like a very distinct jump in texture, or a significant change in traffic. This means that even though a site has a high cumulative traffic and showed a friction increase, the site was still used to calibrate the model. In other words, the friction variation showed in Figure G.9 is considered as a normal fluctuation of a consecutive measurement on a given site. The plots included in Figure G.9 reaffirm the conclusions presented by Goenaga et al. (28) and FHWA/NC 2020-11, i.e., initially friction increases due to the action of traffic repetitions, reaches a maximum, and then decays.

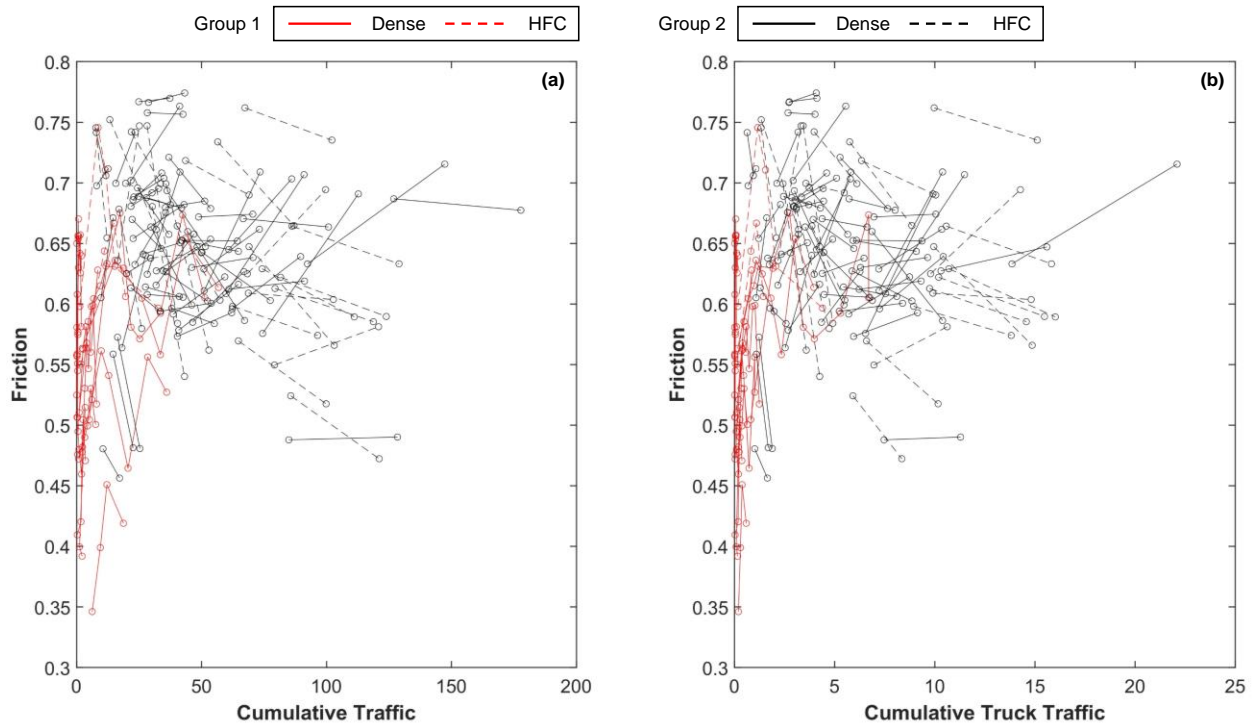


Figure G.9. Friction variation with respect to: (a) cumulative traffic and (b) cumulative truck traffic.

Table G.2. Friction percent changes on Group-2 sites.

Surface	Number of sites	Sites with a reduction	Average %Reduction	Sites with an increase	Average %Increase
Dense	61	36	-5.7	25	5.1
OGFC	16	12	-11.4	4	5.3
UTBWC	17	14	-8.8	3	8.3
Rehabilitated	8	3	-7.0	5	16.2
Total	102	65	-	37	-

As discussed above, friction observations are affected by seasonality. Hence, to observe the influence of traffic volumes on friction, the raw measurements in the RWP were first corrected using Equation (121) and (120). Then, Equation (115) was calibrated using the MATLAB ‘fitglm’ function. Figure G.2 depicts the calibration process.

Step 1

First, the Group-1 sites with at least three observations and the Group-2 sites rehabilitated either in 2018 or 2019 were used to calibrate Phase-1 of the friction performance model. Table G.3 summarizes the ANOVA for the Phase-1 model. As presented, the initial friction intercept (Parameter *a*) is 0.54 and its random effect has a standard deviation of 0.08. Similarly, the mean initial friction rate of change (Parameter *b*) has a mean of 0.0051 friction-units/million-traffic and the random effect of this parameter has a standard deviation of 4.9×10^{-4} . The curvature coefficient (Parameter *c*) has an estimated value of -7.3×10^{-5} . All the parameters of the model are significant at a 95% confidence level with an R^2 around the line of equality of 0.76.

Table G.3. ANOVA table for Phase-1 friction model.

Parameter	Estimate	SE	t-statistic	DF	p-Value	Lower*	Upper*	Std Δa_{site}	Std Δb_{site}
<i>a</i>	0.54	0.02	25.30	88	0.00	0.50	0.58		
<i>b</i>	0.0051	0.00	3.58	88	0.00	0.00	0.01	0.08	4.9×10^{-4}
<i>c</i>	-7.3×10^{-5}	0.00	-2.65	88	0.01	-1.3×10^{-4}	-2.0×10^{-5}		

*95% confidence interval

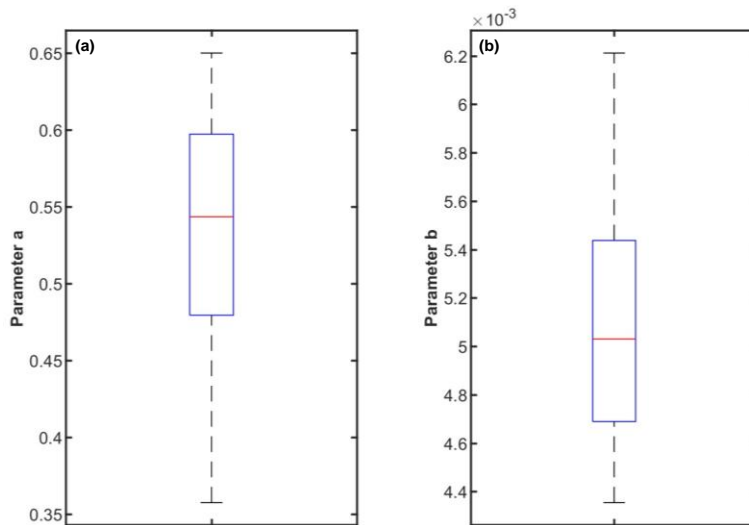


Figure G.10. Histogram of the site-specific parameters; (a) parameter *a* and (b) parameter *b*.

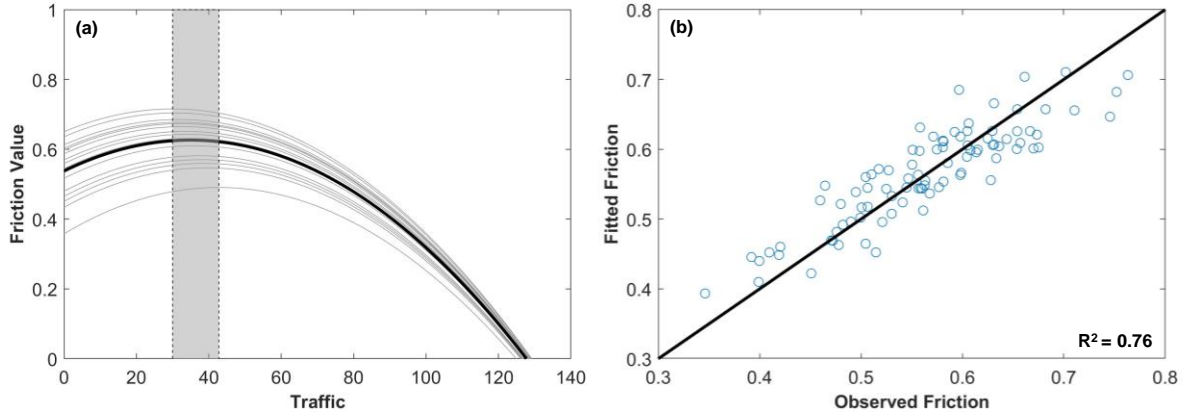


Figure G.11. Friction model evaluation: (a) individual Phase 1 friction performance curves and (b) prediction check.

Based on the resultant model, individual performance curves can be obtained by calculating site specific coefficients, where the intercept is defined as $a + \Delta a_{site}$ and the initial rate of change is $b + \Delta b_{site}$. The histogram of the site-specific parameters is included in Figure G.10. As depicted, the initial friction ranged from 0.37 to 0.65, whereas the initial rate of change ranged from 0.0044 to 0.0062 friction-units/million-traffic. The resulting curves are plotted in Figure G.11 (a) and the prediction check is included in Figure G.11 (b). Also, it was verified that the random effect terms followed a normal distribution.

Step 2

Both T_{max} and F_{max} were computed using Equation (116) and (117), respectively. The vertical boundaries of the grey region in Figure G.11 (a) represent the lowest and the highest T_{max} computed among the different sites. This range was 30.0 to 42.8 million-traffic repetitions. The maximum friction, F_{max} , values spanned 0.50 to 0.72. The average values $\overline{T_{max}}$ and $\overline{F_{max}}$ were computed using the fixed effects, resulting in 34.9 million-traffic repetitions and 0.63, respectively.

Step 3

Next, 81 Group-2 sites that were not used in Step 1 remained for analysis. From these 81 sites, 51 have a cumulative traffic greater than the maximum T_{max} registered in the previous step (i.e., 42.8 million-traffic repetitions) and were used to calibrate Phase 2 of the friction performance model, represented by the exponential decay in Equation (122). The other 30 have a cumulative traffic lower than 42.8 million-traffic, these were used in the next step of the analysis. As shown, random effects were included in the intercept and the rate of change; however, after a first calibration it was observed the random effect on the rate of change was not significant. For this reason, the Phase 2 model was simplified to Equation (122).

$$F(T) = F = (A + \Delta A_{site}) \cdot \exp[B \cdot T] \rightarrow T > T_{max} \quad (122)$$

Table G.4. ANOVA table for Phase-2 friction model.

Parameter	Estimate	SE	t-statistic	DF	p-Value	Lower*	Upper*
A	-0.44	0.02	-19.91	104	0.000	-0.48	-0.39
B	-0.00037	0.00	-1.30	104	0.196**	0.00	0.00

*95% confidence interval ** not significant

To calibrate Equation (122), a logarithmic transform was used to allow linear estimation of the model coefficients. Hence, Parameter A is equal to $Exp(-0.44) = 0.65$, while Parameter B is equal to -0.00037 friction-units/million-traffic repetitions. It should be noted that Parameter B is not significant and given its low value, the model is essentially a one-way random effect, i.e., a model with different means but no slope. Even though Parameter B was not found to be statistically significant, it was decided to use this functional form to express the deterioration process because this is the expression most widely used in literature. Figure G.12 shows the model prediction accuracy, displaying the R^2 of 0.63.

As shown, a small bias is induced in the predictions because friction increases in some sites during Phase 2, leading to under prediction of the observed values. As mentioned before, it was decided to use a single model and treat all the sites as if the friction was reducing, because there is no evidence or causative factor that explains the observed friction increment. Friction can increase due to numerous reasons, such as raveling that exposes new particles with high microtexture. Severe raveling is generally accompanied by an increase in macrotexture, but this was not the case in these sites because abrupt texture changes were not recorded.

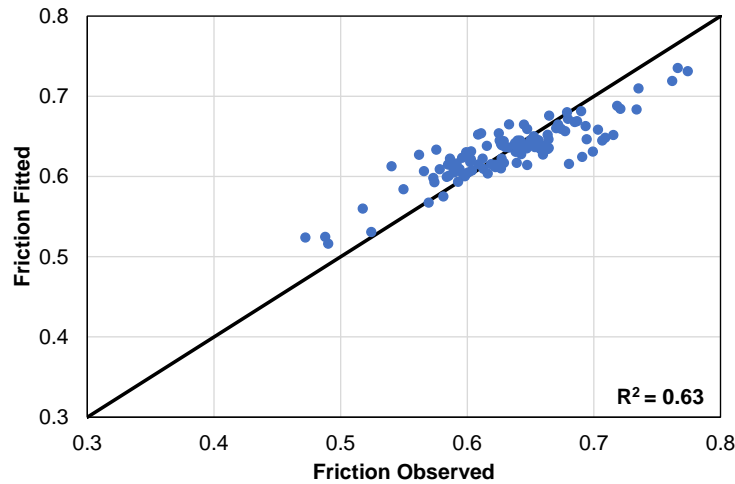


Figure G.12. Prediction plot for Phase 2 model.

Step 4

The final step in calibrating the friction performance model consisted of using the fixed effect models of Phase 1 to fit the 30 sites that were not used during the calibration process of Phase 2 conducted in Step 3, i.e., those sites with a cumulative traffic lower than 42.8 million-traffic repetitions. This was done because the second order polynomial is used when the cumulative traffic is lower than T_{max} . These 30 sites were not included in Step 1 because they were rehabilitated earlier than 2018, and in Step 1 only Group-2 sites rehabilitated either in 2018 or 2019 were used to calibrate Phase 1. The fixed effect of the second order polynomial that describes Phase 1 was shifted vertically for each of these 30 sites. This process means that parameters b and c take the value of 0.0051 and -7.3×10^{-5} , as indicated in Table G.3, and the random effect of Parameter a is estimated by vertically shifting the model in order to best match the deterioration trend of each site. This process was carried out in MATLAB by minimizing the sum of square errors, the specific function used was ‘fmincon’.

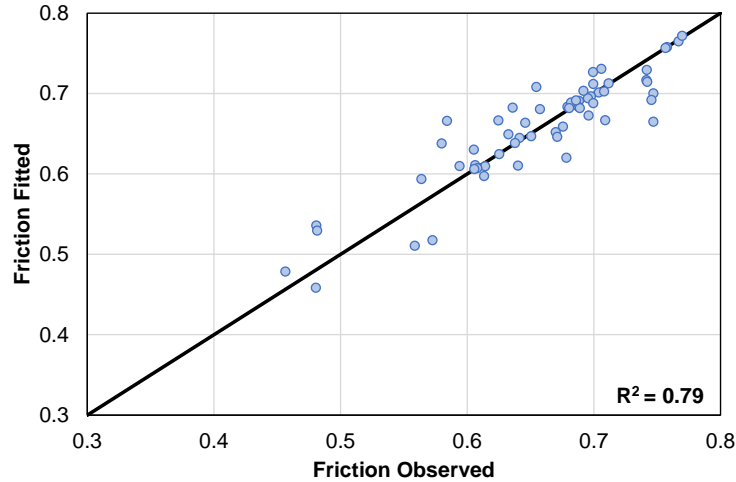


Figure G.13. Prediction plot for Group-2 sites in Phase 1 of friction performance.

After this process, the prediction check was plotted in Figure G.13. To conclude the calibration process, Phase 1 models and Phase 2 models are intersected and plotted together, for example the plot obtained after intersecting the Phase 1 models of Step 1 with the fixed effect model of Step 3 is presented in Figure G.14.

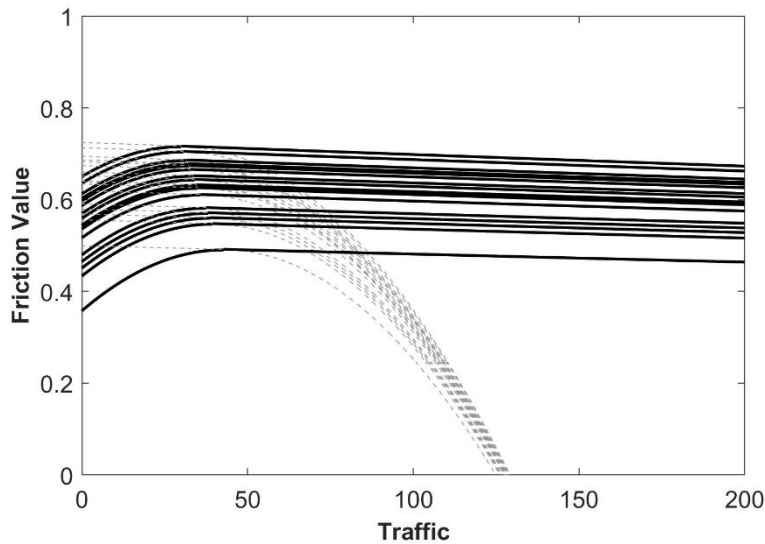


Figure G.14. Example of entire friction performance model for sites used in Phase 1 calibration.

Friction Predictions on New Sites

As illustrated with the examples presented in Figure 12, the inclusion of the random effects improves the prediction accuracy. If these random effect terms are not available, then the best representation of the performance curve is the fixed effects. The procedure to predict friction involved a few steps. First, the functional form described in Equation (13) consists of two separate models, the second order polynomial and the exponential decay. Equation (14) is used to estimate the time to maximum friction, T_{max} , based on the second order polynomial model. T_{max} defines whether one should use the Phase-1 or Phase-2 of the performance model.

Depending on the information that is at hand, there are three different situations when one wants to make friction predictions on a new pavement using the model of Equation (13). Here the term ‘new pavement’ refers to a pavement that has not been monitored for friction before, either an in-service pavement that is monitored for the first time or a recently constructed surface, or a pavement that is being designed. The three situations are:

- Situation 1: Only the surface type is known,
- Situation 2: The mixture composition is known, and a measure of the texture profile is available.
- Situation 3: One or more friction observations are at hand. The surface type and surface composition may or may not be known.

Situation 1

The model of Equation (13) was calibrated using dense mixes (S9.5B, S9.5C, and S9.5D) and high-friction courses (OGFC and UTBWC). Although the final form of the friction model did not include a random effect representing the family, pavements can be group by surface type and is possible to obtain the average values of the random effects by surface type and in this way estimate the average performance curve by each surface type as indicated in Table G.5. Hence, if the surface type is known, the coefficients of Table G.5 can be replaced in Equation (17), with Δa_{site} , Δb_{site} , and ΔA_{site} equal to zero and forecast friction performance. Situation 1 applies for in-service pavements where the only information available is the surface type, which can be found in the NCDOT PMS database, or during the design stage when a quick estimate of the average expected texture is needed.

Table G.5. Average values of the parameters of the friction model for the different mix types.

Surface Type	Parameters					
	<i>a</i>	<i>b</i>	<i>c</i>	T_{max}	<i>A</i>	<i>B</i>
S9.5B	0.54	0.0051	-7.27×10^{-5}	34.84	0.64	-3.70×10^{-4}
S9.5C	0.56	0.0051	-7.27×10^{-5}	35.13	0.64	-3.70×10^{-4}
S9.5D	0.56	0.0050	-7.27×10^{-5}	34.58	0.65	-3.70×10^{-4}
UTBWC	0.56	0.0050	-7.27×10^{-5}	34.61	0.66	-3.70×10^{-4}
OGFC	0.57	0.0050	-7.27×10^{-5}	34.46	0.67	-3.70×10^{-4}

Situation 2

If the mixture composition is known and the surface profile has been collected, it is possible to use Equation (8) to get an estimate of the initial friction. Equation (8) was calibrated using observations collected as early as one week after construction and as far as one month after construction. Hence, it is safe to assume the predictions make with Equation (8) estimate the representative friction 1-month after construction. If that is the case, Equation (17) can be solved and rewritten as shown in Equation (123) to estimate the value of Δa_{site} if Δb_{site} is equal to zero.

$$\Delta a_{\text{site}} = FN(T = T_{1\text{-month}}) - 0.0051 \cdot T_{1\text{-month}} + 7.3 \times 10^{-5} \cdot T_{1\text{-month}} - a \quad (123)$$

where;

$T_{1\text{-month}}$ = cumulative traffic in 1-month, and

$FN(T = T_{1\text{-month}})$ = friction prediction using Equation (17).

Next, T_{max} is estimated using Equation (14) and the second order polynomial and the exponential decay will intersect at $T = T_{\text{max}}$. Hence, the value of ΔA_{site} can be estimated with Equation (124).

After estimating Δa_{site} and ΔA_{site} , the values are replaced in Equation (17) and friction predictions are obtained as a function of the cumulative traffic.

$$\Delta A_{\text{site}} = \left[(0.54 + \Delta a_{\text{site}}) + 0.0051 \cdot T_{\text{max}} - 7.3 \times 10^{-5} \cdot T_{\text{max}} \right] / \exp(-3.7 \times 10^{-4} \cdot T_{\text{max}}) \quad (124)$$

Because the texture profile is needed to estimate the skewness (Rsk), Situation 2 applies for recently overlay pavements where a first high-speed texture measurement was collected and the mixture composition is known, or it also applies for existing pavements where these inputs are available.

Situation 3

Situation 1 and 2 describes the process to predict friction on a new surface when no friction records are available, and the best estimates are obtained using the fixed effects alone or by including the mixture composition parameters to estimate the initial friction. When friction records are at hand, it is possible to constrain the predictions in such a way that the model passes by the observed records. The process described here applies for Situation 1 or 2 when friction observations become available after the initial predictions.

To illustrate this case, refer to the example shown in Figure 12 (b) for Site 14. In this figure, the blue dashed line and the red dotted line represent the fix effects, either after using the values of Table G.5 in Situation 1 or after applying Equation (123) and (124) in Situation 2. Because the two lines do not pass through the observed records, the curves need to be vertically shifted to minimize the sum of square errors shown in Equation (125). The shifting is vertically only, therefore a shift factor (α) is applied to Parameter a in Equation (17). In other words, $a_{\text{site}} = a + [\Delta a_{\text{site}} + \alpha]$. This updated value is replaced in Equation (124) to update the value of ΔA_{site} .

$$\sum_{k=1}^N \varepsilon_k = \sum_{k=1}^N [y_k(T) - y_{k,p}(T)]^2 \quad (125)$$

where;

ε_k^2 = square error for observation k ,

$y_k(T)$ = k^{th} friction observation corresponding to cumulative traffic T , and

$y_{k,p}(T)$ = friction prediction corresponding to a cumulative traffic T .

Model Validation with New Sites

To validate the model for new sites, (i.e., sites where none of their observations were part of the calibration set), the pavements summarized in Table G.6 were used. In these cases, the performance curves were adjusted to the observed values. These sites followed Situation 2, i.e., the mixture composition and the texture profile skewness were available. Hence, Equations (123) and (124) were used to estimate the random effects and then Equation (17) was used to make the predictions. Then, the predictions on these sites were grouped together with the other sites, i.e., the sites used only for calibration, the ones used for calibration and validation, and the ones only used for validation. The resulting prediction check is depicted in Figure G.15, which shows the proposed model produced a good representation of all the data used for calibration and validation.

Table G.6. New sites used for friction model validation.

Site	Surface	Cc	%AC	VFA	New Observations
43	OGFC	1.23	6.2	39.7	A-1, A-2
44	UTBWC	0.67	5.4	74.5	A-2
37	S9.5C	0.48	6.9	77	A-1, A-2

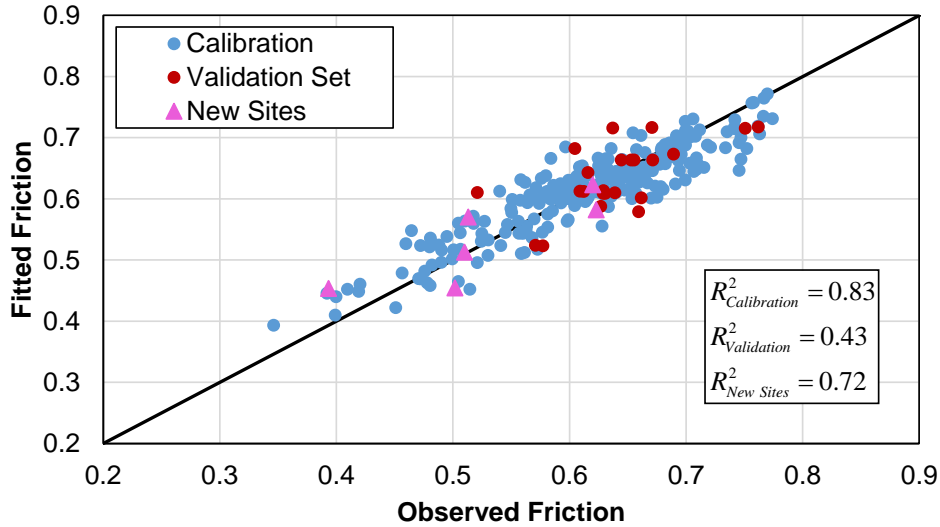


Figure G.15. Friction prediction checks for all data sets.

Table G.7. Summary of the root mean square errors on the completely new sites for friction model validation.

Site	RMSE	
	Calibration	Validation
43	-	0.046
44	-	0.058
37	-	0.054

Modeling Texture Performance

Steps Taken for Model Development

The *MPD* results for both group of sites were plotted with respect to the cumulative traffic and with respect the cumulative truck traffic, as indicated in Figure G.16. As depicted in Figure G.16, some Group-2 sites showed a reduction in the second observation, but most of sites presented an increase in *MPD*. Table G.8 also shows that 13% of the 107 sites yielded a *MPD* reduction, whereas 87% showed an increase. Also, those sites that were treated between the first and second measurement have been flagged and are reported in Table G.8 in the rehabilitated category. As indicated, of the nine sites that were rehabilitated, six showed an average reduction in *MPD* of 83% and three presented an average increase of 46%. These nine sites were not used for further analysis. Additionally, two more sites were removed from the database because they were older than 10 years, reflecting a deteriorated condition that did not match the rest of the sites.

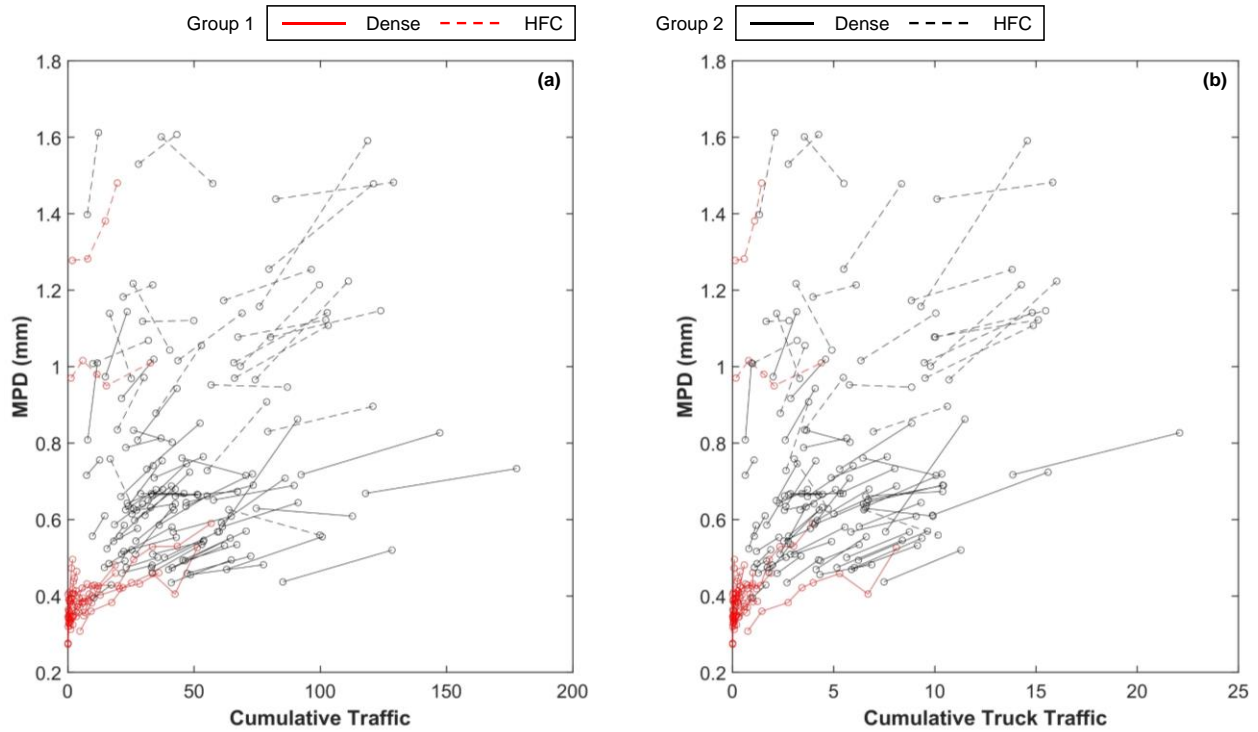


Figure G.16. *MPD* variation with respect to: (a) cumulative traffic and (b) cumulative truck traffic.

Table G.8. *MPD* percent changes on Group-2 sites.

Surface	Number of sites	Sites with a reduction	Average %Reduction	Sites with an increase	Average %Increase
Dense	63	2	-6.0	61	10.9
OGFC	17	2	-9.7	15	12.9
UTBWC	18	4	-7.7	14	10.9
Rehabilitated	9	6	-82.5	3	45.9
Total	107	14	-	93	-

After this sorting and filtering process, a total of 96 Group-2 sites remained for further analysis. These sites were then combined with Group-1 sites to develop a comprehensive texture model shown in Equation (119). The model coefficients were calibrated using the MATLAB ‘fitglm’ function. To facilitate the estimation process, a logarithmic transform was used to conduct a linear estimation. The traffic was modeled using both the cumulative mixed traffic and the cumulative truck traffic and the resultant models were quite similar, so the cumulative mixed traffic was selected as the independent variable in the models.

The ANOVA analysis for the texture model is presented in Table G.9. As shown in the table, all the parameters in the model are significant at a 95% confidence level. The fixed effect of the model is $Exp(-0.74) = 0.48$ for the intercept (Parameter *a*) and 0.13 for the rate of change (Parameter *b*), which means that on average *MPD* values change 0.13 mm per each million-traffic repetitions. Also, Table G.9 includes the standard deviation of the random effect models. The standard deviations are equal to 0.24 mm for the intercept and 0.06 mm/million-traffic for the rate of change.

Table G.9. ANOVA table for texture model.

Parameter	Estimate	SE	t-statistic	DF	p-Value	Lower*	Upper*	Std Δa_{site}	Std Δb_{family}
<i>a</i>	-0.74	0.04	-20.6	264	0.0	-0.81	-0.67	0.24	0.06
<i>b</i>	0.13	0.03	4.7	264	0.0	0.08	0.18		

*95% confidence interval

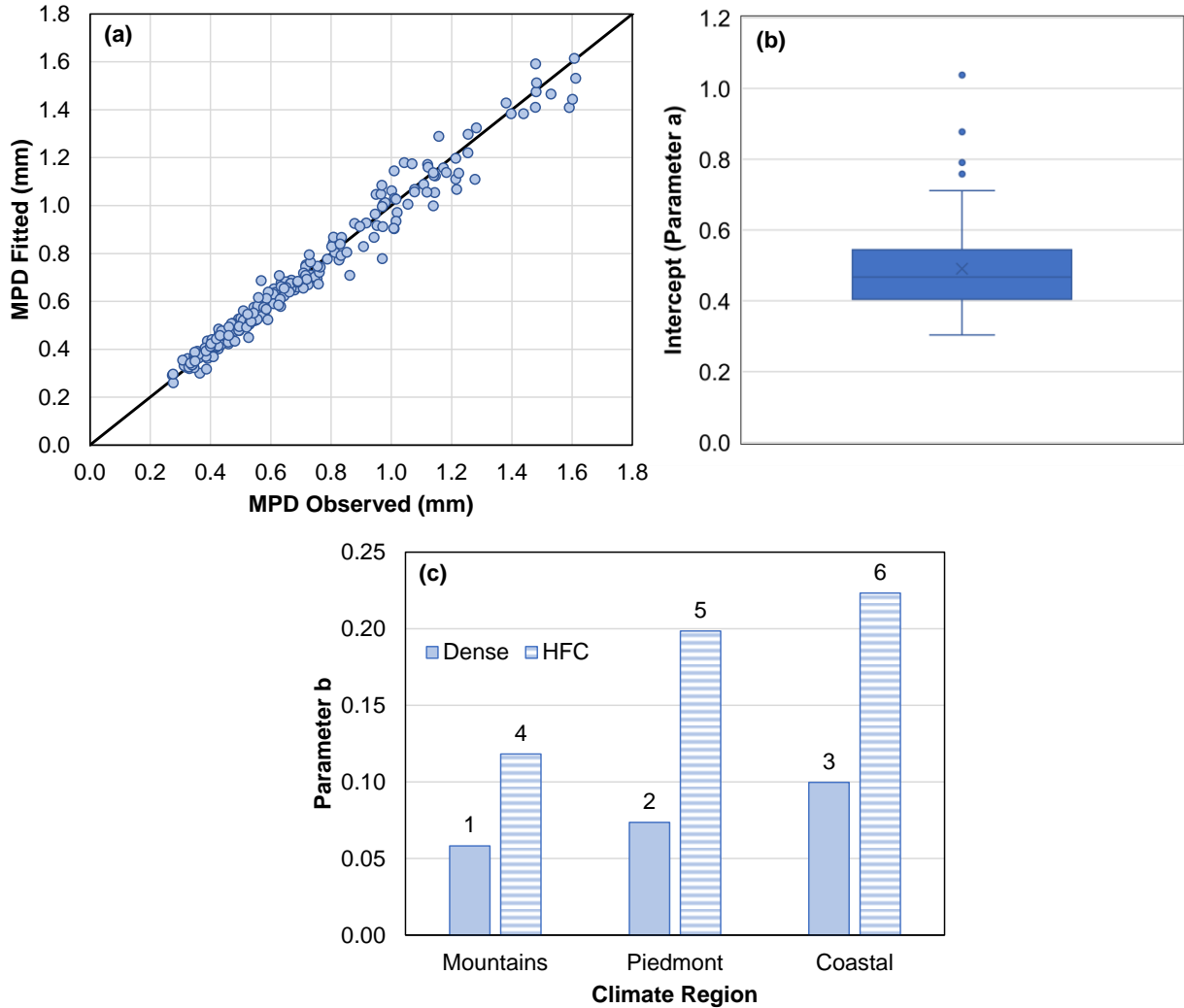


Figure G.17. MPD model assessment: (a) prediction check, (b) initial MPD variation across sites (Parameter *a*), and (c) MPD rate of change across families (Parameter *b*).

Figure G.17 conveys the texture model prediction accuracy for the sites used to calibrate the model, the variation of the initial *MPD* (i.e., the intercept of the model), and the rate of change computed for each family. As depicted in Figure G.17 (a), the model has a good prediction accuracy and fits the data without any noticeable bias. The R^2 of the model is 0.98. Furthermore, the intercept parameter varies from 0.30 mm to 1.04 mm. The normality of the distribution was checked and indicated that the model can capture the whole spectrum of texture surfaces in the database. Finally, as indicated in Equation (119), a random effect was induced for each family in the texture rate of change. The model coefficients computed as $b + \Delta b_{family}$, are plotted in Figure G.17 (c). As illustrated, the lowest rate of change is registered in the Blue Ridge climate region for both surface

types, with a rate of change of 0.06 mm/million-traffic and 0.12 mm/million-traffic for the dense mixes and HFC, respectively. In contrast, the highest rate of change is observed in the Coastal area, with a rate of change equal to 0.10 mm/million-traffic and 0.22 mm/million-traffic for the dense mixes and HFC, respectively.

Texture predictions on New Sites

Like in the friction case, for a new site, i.e., a pavement not included in the calibration process, one will face one of the following three possible situations:

- Situation 1: Only the surface type is known,
- Situation 2: The mixture composition is known, and a measure of the texture profile is available.
- Situation 3: One or more friction observations are at hand. The surface type and surface composition may or may not be known.

Situation 1

If only the surface type is known, Table G.10 can be used to get an estimate of the random effect in the intercept, Δa_{site} . Then, given the surface type and the location of the site Table 8 is used to get the value of Δb_{family} . Afterwards Equation (18) is used to make predictions.

Table G.10. Average value Δa_{site} of the texture model for the different mix types.

Surface Type	Δa_{site}
S9.5B	-0.15
S9.5C	-0.18
S9.5D	-0.12
OGFC	0.22
UTBWC	0.32

Situation 2

If the mixture composition is known, it is possible to use Equation (10) to get an estimate of the initial *MPD*. Equation (10) was calibrated using observations collected as early as one week after construction and as far as one month after construction. Hence, it is safe to assume the predictions make with Equation (10) predicts the representative *MPD* 1-month after construction. If that is the case, Equation (18) can be solved and rewritten as shown in Equation (126) to estimate the value of Δa_{site} .

$$\Delta a_{site} = MPD(T = T_{1-month}) / (T_{1-month})^{0.13 + \Delta b_{family}} - 0.48 \quad (126)$$

where;

$T_{1-month}$ = cumulative traffic in 1-month, and

$MPD(T = T_{1-month})$ = *MPD* prediction using Equation (10).

After estimating Δa_{site} and obtaining Δb_{family} from Table 8 the values are replaced in Equation (18) and *MPD* predictions are obtained as a function of the cumulative traffic.

Situation 3

Situation 1 and 2 describes the process to predict *MPD* on a new surface when no *MPD* records are available, and the best estimates are obtained using the fixed effects alone or by including the mixture composition parameters to estimate the initial *MPD*. When *MPD* records are at hand, it is possible to constrain the predictions in such a way that the model passes by the observed records.

The process described here applies for Situation 1 or 2 when *MPD* observations become available after the initial predictions.

To illustrate this case refer to the example shown in Figure 15. In this figure, the blue dashed line represent the fixed effect, either after using the values of Table G.10 in Situation 1 or after applying Equation (126) in Situation 2. Because the predicted curve do not pass through the observed records, the curve need to be vertically shifted to minimize the sum of square errors shown in Equation (127). The shifting is vertically only, therefore a shift factor (α) is applied to Parameter a in Equation (18). In other words, $a_{site} = a + [\Delta a_{site} + \alpha]$.

$$\sum_{k=1}^N \varepsilon_k = \sum_{k=1}^N [y_k(T) - y_{k,p}(T)]^2 \quad (127)$$

where;

ε_k^2 = square error for observation k ,

$y_k(T)$ = k^{th} *MPD* observation corresponding to cumulative traffic T , and

$y_{k,p}(T)$ = *MPD* prediction corresponding to a cumulative traffic T .

Situation 2 is applied on the three validation sites shown in Table G.6. Equation (10) is used to predict the *MPD* 1-month after construction, then Equation (126) is used to predict the random effect in the intercept Δa_{site} . Afterwards, Table 8 is used to obtain the value of Δb_{family} . All these values are replaced in Equation (18) to obtain the *MPD* predictions. Then, the predictions for these sites were grouped together with the other sites, i.e., the sites used only for calibration, the ones used for calibration and validation, and the ones only used for validation. The resulting predictions are depicted in Figure G.18, which shows that the proposed model produced a good representation of all the data used for calibration and validation. The RMSE for these sites is also summarized in Table G.11.

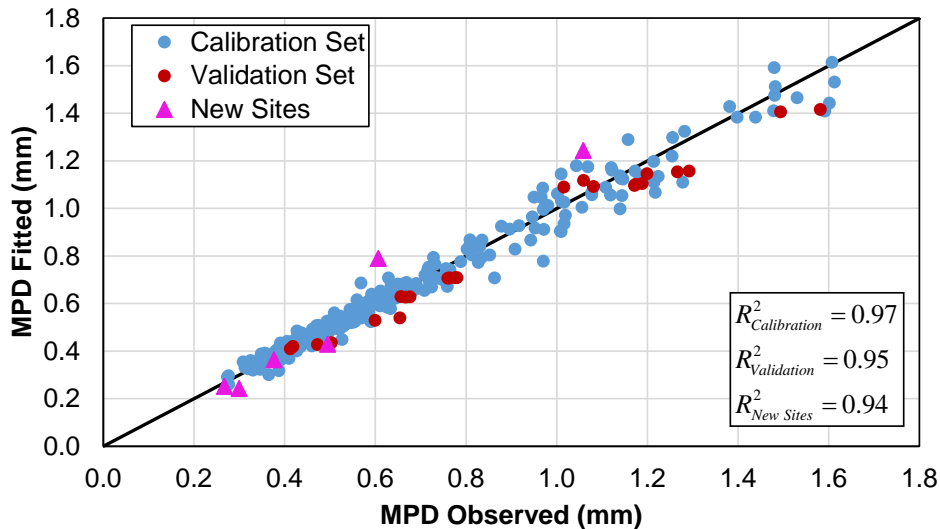


Figure G.18. *MPD* prediction checks for all data sets.

Table G.11. Summary of the root mean square errors on the completely new sites for *MPD* model validation.

Site	RMSE	
	Calibration	Validation
43	-	0.184
44	-	0.047
37	-	0.041

Temporal Texture Variation

The texture performance model shown in Equation (119) has as independent variable the cumulative traffic (T). Therefore, to predict the surface *MPD* it is necessary to know the AADT in addition to the pavement family and surface type. The distribution of AADT values across the sites used in the calibration procedure is depicted in Figure G.19. As shown, 25% of the sites have an AADT lower than or equal to 18,000 vpd, whereas 75% of the sites have an AADT lower than or equal to 46,250 vpd. The average and median AADT is equal to 34,278 and 32,000 vpd, respectively.

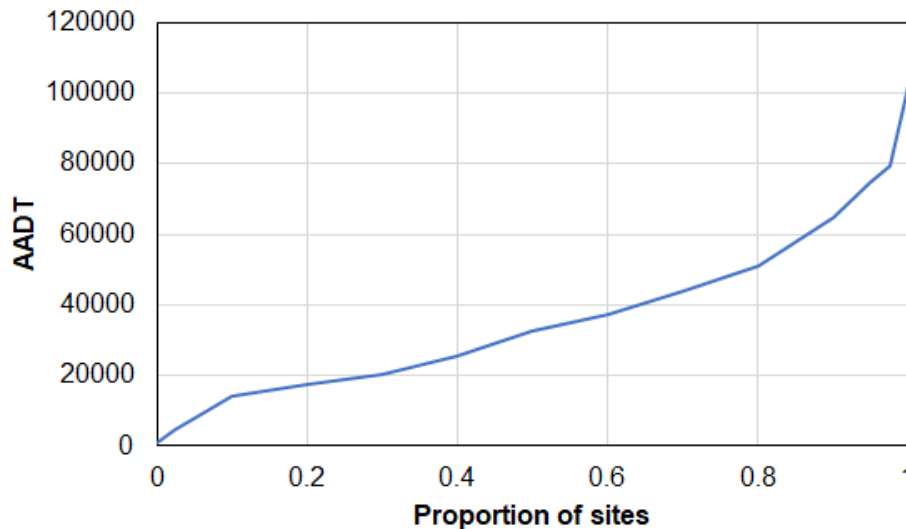


Figure G.19. AADT distribution across the texture performance model calibration set.

As indicated in Table 4 of Chapter 3, there are six different families, three for dense mixes and three for HFC. As indicated in Equation (119) the texture performance model has two parameters, Parameter a that represents the initial *MPD* and Parameter b that represents the deterioration rate. Depending on the information at hand, one can use either of the three situations described in Section 3.4.2 of Chapter 3. However, in order to provide an average performance curve for dense, OGFC, and UTBWC surfaces, Situation 3 will be used.

If t represents the number of days after construction, based on the observations made in Group-1 sites, see Chapter 2 for further details, the average *MPD* one month after construction for the three surface types is as shown in Table G.12.

Table G.12. Average *MPD* values one month after construction for each surface type.

Surface type	Surface type		
	Dense	OGFC	UTBWC
	0.35	1.08	0.98

Equation (119) can be rewritten as indicated in Equation (128). Given that the model predictions at $t = 30$ days must be equal to the values of Table G.12, Parameter a in Equation (128) is adjusted as shown in Equation (129). The values of Parameter b are obtained in Table 7 (fix effect) and Table 8 (Δb_{family}), as shown three possible values are possible for dense mixes and another three for HFC mixes (OGFC and UTBWC). Hence, if one uses the median AADT, 32,000 vpd, the predictions for the three surface types and the different deterioration rates Table G.13 is obtained. If one takes the average of these predictions by surface type Table G.14 is obtained.

$$MPD = a \times \left(\frac{AADT \times t}{1000000} \right)^b \quad (128)$$

$$a_{site} = MPD(t = 30 \text{ days}) / \left(T_{t=30 \text{ days}} \right)^b \quad (129)$$

Table G.13. Prediction of the expected MPD at different number of days after construction.

Surface Type	Parameter		Number of days after construction (t)								
	a	b	5	30	60	90	180	365	548	730	3,650
Dense	0.351	0.058	0.32	0.35	0.36	0.37	0.39	0.40	0.41	0.42	0.46
	0.351	0.074	0.31	0.35	0.37	0.38	0.40	0.42	0.43	0.44	0.50
	0.351	0.100	0.29	0.35	0.38	0.39	0.42	0.45	0.47	0.48	0.56
OGFC	1.085	0.118	0.87	1.08	1.17	1.23	1.33	1.45	1.52	1.57	1.90
	1.089	0.199	0.76	1.08	1.24	1.34	1.54	1.77	1.92	2.04	2.80
	1.090	0.223	0.72	1.08	1.26	1.38	1.61	1.89	2.07	2.20	3.15
UTBWC	0.985	0.118	0.79	0.98	1.06	1.12	1.21	1.32	1.38	1.43	1.73
	0.988	0.199	0.69	0.98	1.12	1.22	1.40	1.61	1.74	1.85	2.54
	0.989	0.223	0.66	0.98	1.14	1.25	1.46	1.71	1.87	2.00	2.86

Table G.14. Average MPD values at different number of days after construction.

Surface Type	MPD (mm)						
	0-month	1-month	3-month	6-month	12-month	18-month	10-yrs
Dense	0.3	0.35	0.38	0.40	0.42	0.44	0.51
UTBWC	0.8	1.08	1.32	1.50	1.70	1.84	2.62
OGFC	0.7	0.98	1.20	1.36	1.55	1.67	2.38

APPENDIX H. EVALUATION OF THE EFFECT OF ASPHALT OVERLAYS ON HIGHWAY SAFETY

Introduction

According to Hauer (76, 101, 102), the safety of a facility should not be equated with the fluctuating accident counts; rather, one should define safety as an underlying stable property defined by averaging over a sufficiently long-time span. Consequently, Hauer defines safety as follows: “the number of accidents (crashes) per unit of time by kind and severity, expected to occur on a facility during a specific period.” Based on this definition, safety is an expected accident frequency.

Crash events are influenced by various factors like road geometry, driver response, vehicle characteristics, and pavement condition. Before-after studies are conducted to assess the effect of changing one factor while keeping others constant. These studies involve collecting data before implementing safety improvements (e.g., asphalt overlay or signalization changes) and comparing it to data after the intervention. The objective is to determine if the safety measures successfully reduced accidents, injuries, and fatalities.

Before-after studies can be grouped into three types: the simple (naïve) before-after study; the before-after study with control groups; and the before-after study using the Empirical-Bayes (EB) technique (also using a control group) (77). According to Hauer (76), the traditional before-after study (no matter which type is used) can be accomplished through two tasks. The first task consists of predicting the expected number of target crashes for a specific entity (i.e., intersection, segment) or series of entities in the “after” period had the safety treatment not been implemented, π . The second task consists of estimating the number of target crashes for the specific entity (or group of entities) in the “after” period with the treatment in place, λ .

Background

The term “after” means the time after the implementation of a treatment; correspondingly, the term “before” refers to the time before the implementation of the treatment. In most practical cases, either π or λ , can be applied to a composite series of entities where a similar treatment was implemented at each entity. The effect of the treatment on safety is judged by comparing π and λ after defining the following difference and ratio terms; 1) $\delta = \pi - \lambda$ is the reduction in the ‘after’ period of the expected number of target crashes, and 2) $\theta = \lambda/\pi$ is the ratio of what safety was with the treatment to what it would have been without the treatment. When $\theta < 1$, the treatment is effective at improving safety whereas cases where $\theta > 1$ indicate the treatment had a detrimental effect on safety. Also, $100 \times (1 - \theta)$ is the percent reduction in the expected accident frequency. As indicated above, π and λ are expected values. Expected values are never known, but can be estimated from observed data; the estimates are termed π_e and λ_e . The difference between the many variants of before-after studies resides in the methods used to obtain π_e and λ_e .

Before-After Studies for a Single Entity

The sequence of steps used to conduct a before-after study for a single entity (individual road segment or intersection) are the followings:

1. **Estimate λ and predict π .** λ can be estimated from the counts of ‘after’ crashes. The prediction of π will depend on the statistical method chosen (naïve, methods of moments, EB, or non-parametric).

2. **Estimate $Var(\pi_e)$ and $Var(\lambda_e)$.** The variance estimates will depend on the method chosen to obtain the estimate and prediction of λ and π , respectively. Typically, it is assumed that the count of accidents is Poisson distributed and the counts in the ‘before’ and ‘after’ period are mutually independent (76, 102). Therefore, $Var(\lambda_e) = \lambda_e$ and $Var(\pi_e) = \pi_e$.
3. **Estimate δ_e and θ_e using Equation (130) and (88), respectively.**

$$\delta_e = \pi_e - \lambda_e \quad (130)$$

$$\theta_e = \frac{\lambda_e}{\pi_e} \cdot \left[\frac{1}{1 + \frac{VAR(\pi_e)}{(\pi_e)^2}} \right] \quad (131)$$

4. **Estimate the variance of δ_e and θ_e using Equation (132) and (90), respectively.**

$$VAR(\delta_e) = VAR(\pi_e) + VAR(\lambda_e) \quad (132)$$

$$VAR(\theta_e) = (\theta_e)^2 \left[\frac{\left(\frac{VAR(\lambda_e)}{(\lambda_e)^2} \right) + \left(\frac{VAR(\pi_e)}{(\pi_e)^2} \right)}{\left(1 + \frac{VAR(\pi_e)}{(\pi_e)^2} \right)^2} \right] \quad (133)$$

Before-After Studies for a Group of Entities

Usually, the effect of a treatment on safety is estimated after the treatment has been applied to a set of entities. If these are numbered as $j = 1, 2, \dots, n$, then for each entity j , estimates of $(\pi_e)_j$ and $(\lambda_e)_j$ are obtained. See Step 1 of the previous section. Similarly, the variance in the expected number of crashes for each entity is estimated according to Step 2 of previous section to yield $Var((\pi_e)_j)$ and $Var((\lambda_e)_j)$. To draw overall conclusions, the following sums are tabulated:

$$\pi = \sum_{j=1}^n (\pi_e)_j \quad \text{and} \quad (134)$$

$$\lambda = \sum_{j=1}^n (\lambda_e)_j. \quad (135)$$

And the variance for each quantity is obtained as follows:

$$VAR(\pi_e) = \sum_{j=1}^n VAR((\pi_e)_j) \quad \text{and} \quad (136)$$

$$VAR(\lambda_e) = \sum_{j=1}^n VAR((\lambda_e)_j). \quad (137)$$

Objective

The objectives of this appendix is;

- Conduct a before-after study to evaluate the effect of an asphalt overlay on highway safety.

Data

This study used data from asphalt concrete surfaced pavements in the North Carolina Department of Transportation (NCDOT) highway network. The pavements were selected to monitor the evolution of surface skid resistance as part of two research projects: FHWA/NC/2020-11, focused on the evolution of pavement friction and macrotexture after an asphalt overlay, and FHWA/NC/2022-05, focused on the development of pavement friction and texture performance models. The selection criteria for the pavements included the speed limit (preferably above 55-mph, but some lower speed limit roads were included), road geometry (preferably access control, but some undivided facilities were included), spatial distribution (evenly spread across the state), and surface type (dense-graded mixtures, Open-Graded-Friction-Courses - OGFC, and Ultrathin-Bounded-Wearing-Courses - UTBWC) used by NCDOT.

Information about the primary road network's rehabilitation activities, construction history, and surface type was extracted from the NCDOT Pavement Management System (PMS). The annual average daily traffic volume (AADT) data was obtained from the NCDOT annual traffic survey, and basic geometry information was extracted from the NCDOT Road Characteristics layer, including road type, divided or undivided layout, and posted speed limit.

A total of 153 pavements were identified for friction and texture testing based on the criteria mentioned above, but the analysis in this paper focused on 100 pavements that were rehabilitated after 2013. These 100 pavement sections are referred to as "sites" throughout the document and their characteristics are visually summarized in Figure H.1, Figure H.2, and Figure H.3. As shown, 84 of them are divided facilities, 64% of the sites have a speed limit of 60-mph or greater, the median AADT is 27,279 vehicles per day, with a 95% confidence interval of 4,220 to 71,410 vpd. The surface type distribution is 73% with a dense-graded mix surface, while 13% and 14% have an OGFC or UTBWC surface, respectively.

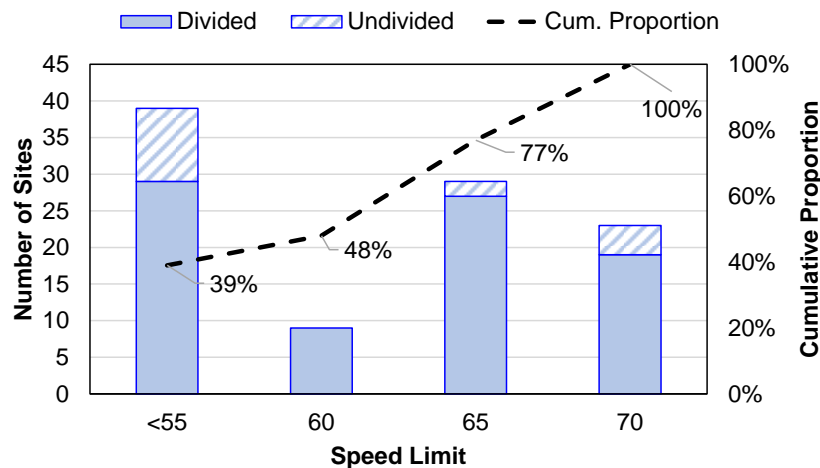


Figure H.1. Geometry and speed limit distribution across the study sites.

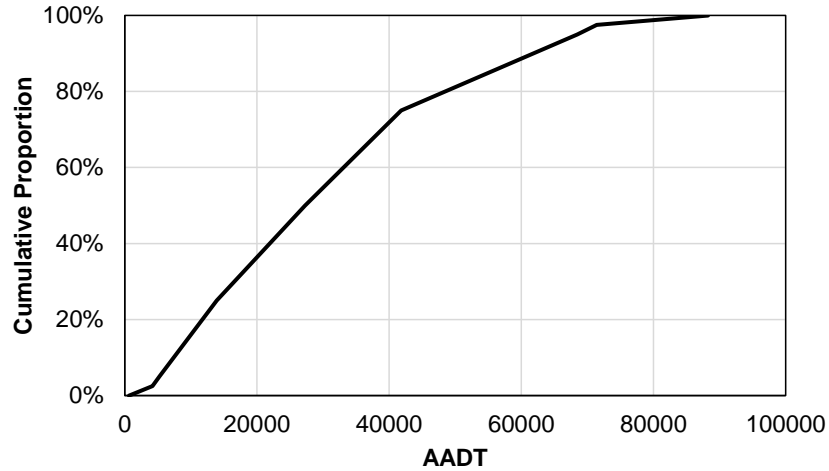


Figure H.2. AADT distribution across the study sites.

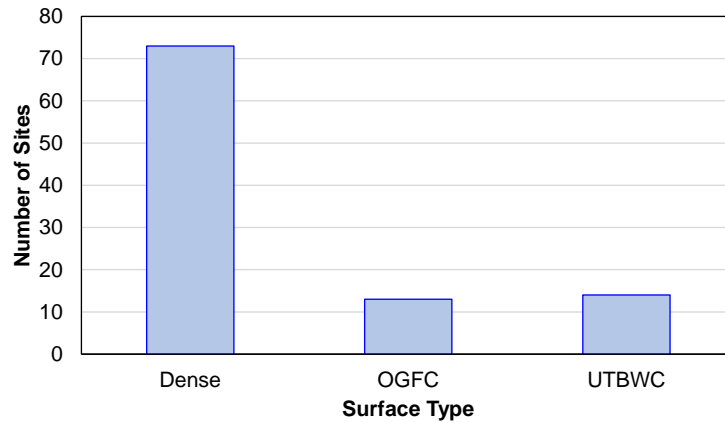


Figure H.3. Surface type distribution across the study sites.

The crash history data was extracted from the NCDOT Traffic Safety Systems (TSS), covering January 1, 2010, to April 30, 2023. Each crash event in the NCDOT-TSS is documented using a collision report form, which includes information about the crash severity, weather conditions, and causal factors. Crashes are classified into four severity levels: K (fatal), A (serious), B (evident), and PDO (property damage only). For this analysis, all crashes were considered together, without segregating them by severity. The study evaluated four crash types: total, total wet, lane departure, and lane departure wet crashes.

Methodology

Crash records were totaled by month; therefore, each site has a total of 160 months (m_i) of information, where $i = 1, 2, \dots, 160$ and $m_{i=0}$ is January 2010 and $m_{i=160}$ is April 2023. The delineation of the ‘before’ (N_B) and ‘after’ (N_A) periods is made based on the overlay date, i.e., for each site the month at which the overlay was performed was identified and a 13-month period centered in this month was defined in all sites as the duration of the rehabilitation activities. In this sense, the ‘before’ period ends seven months earlier than the overlay month, and the ‘after’ period begins seven months after the overlay is applied.

For example, the variation in the number of crashes/mile in Site R1 is depicted in Figure H.4 where the asphalt overlay was applied in October of 2019 ($m_{i=118}$). Hence, the ‘before’ period ends at

$m_{i=111}$ (March 2019) and the ‘after’ period starts at and $m_{i=125}$ (May 2020), respectively. As a result, considering there are 160 months of crashes for the analysis, $N_B = 111$ months and $N_A = 36$ months.

Figure H.5 summarizes the number of months in the ‘before’ and ‘after’ period, N_B and N_A , respectively, for the 100 sites analyzed. The blue data series represents the number of months in the ‘before’ period, for 10% of the sites this period was as short as 35 months. On the other hand, 4% of the sites have up to 140 months of information in the ‘before’ period. Those sites with the shortest ‘before’ period have the longest ‘after’ period with more than 100 months of observation. Equivalently, those sites with the longest ‘before’ period have the shortest ‘after’ period with only a few months of crash records. It is important to note that the ‘overlay’ period was set as 13-months in all sites.

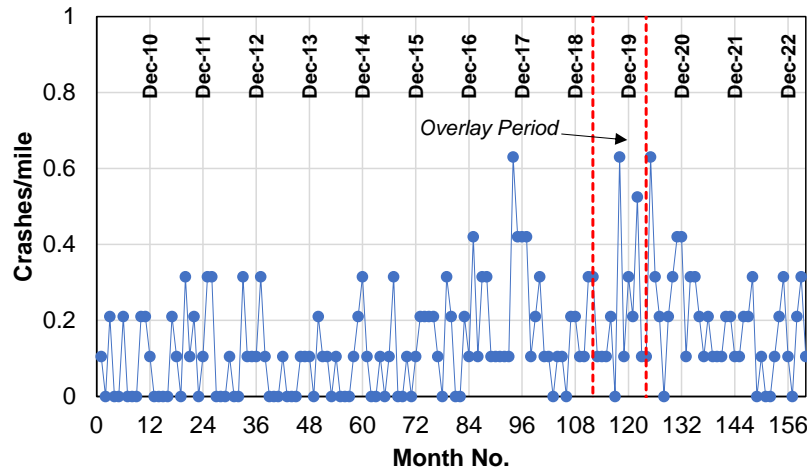


Figure H.4. Monthly variation in the number of crashes for Site R1.

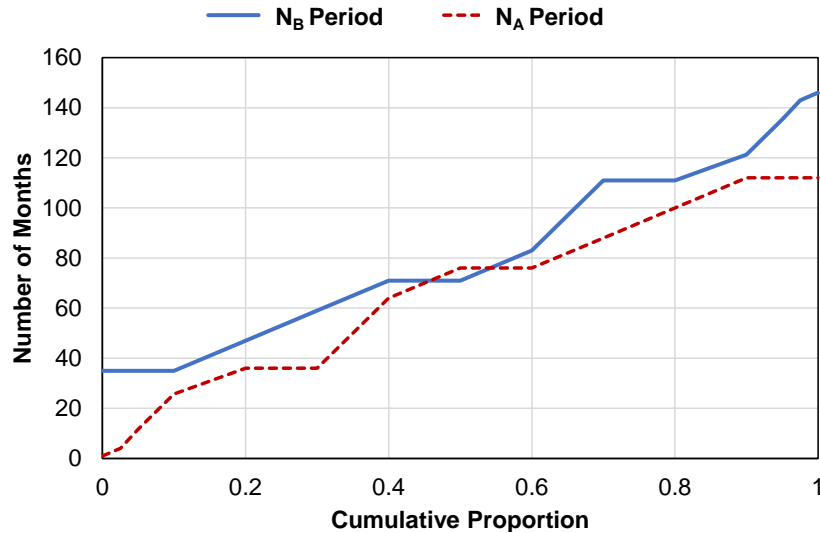


Figure H.5. Distribution of site for ‘before’ and ‘after’ periods.

To characterize the long-term variation in crash frequencies, a rolling average of different base lengths was used. This method was adopted to evaluate temporal fluctuations and to identify the minimum rolling average unit that can be used to capture long-term trends in each site. Three different rolling average periods were evaluated: 7, 13, and 19 months, with each centered around

the month of interest. For example, if the month of interest is m_i , a 7-month rolling average will include the observations from m_{i-3} to m_{i+3} . In contrast, a 19-month rolling average will include observations from m_{i-9} to m_{i+9} . In general, if the number of crashes in month m_i is denoted by Y_i , the following equations are used for the rolling average computation:

$$Y_{i,7M} = \frac{Y_{i-3} + Y_{i-2} + \dots + Y_{i+2} + Y_{i+3}}{7} \quad (138)$$

$$Y_{i,13M} = \frac{Y_{i-6} + Y_{i-5} + \dots + Y_{i+5} + Y_{i+6}}{13} \quad (139)$$

$$Y_{i,19M} = \frac{Y_{i-9} + Y_{i-8} + \dots + Y_{i+8} + Y_{i+9}}{19} \quad (140)$$

where;

$Y_{i,7M}$ = average number of crashes/mile in month m_i , using a 7-month rolling average,

$Y_{i,13M}$ = average number of crashes/mile in month m_i , using a 13-month rolling average, and

$Y_{i,19M}$ = average number of crashes/mile in month m_i , using a 19-month rolling average,

To determine the moving average base length, only total crashes were considered. The need for a rolling average is demonstrated by examining the crash totals for Site R1. Figure H.6 shows that the month-by-month crash numbers can vary greatly because crashes are (statistically speaking) “rare events”. Using monthly crash numbers directly would result in widely varying crash frequencies, making it challenging to identify trends and make informed decisions. In crash analysis, this process typically involves aggregating crash numbers over a period of 3-5 years (76). However, in the case of the analysis here on the effects of pavement friction and texture changes following an overlay, crashes must be aggregated over shorter time periods. Goenaga et al. (28) showed friction and texture tend to vary after an asphalt overlay due to traffic repetitions, requiring shorter-term aggregation to account for surface condition variations.

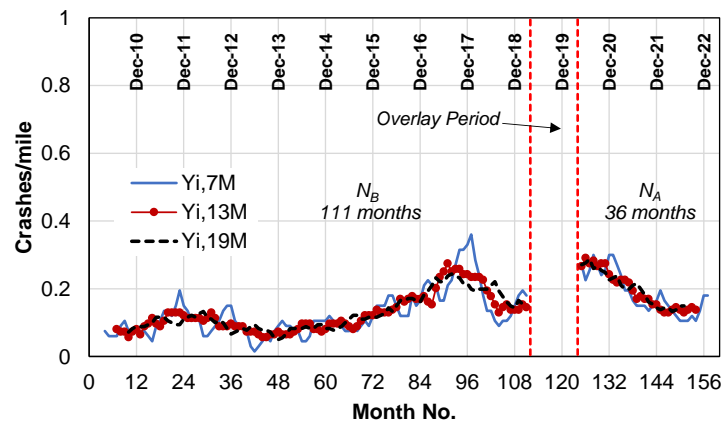


Figure H.6. Rolling average for the total number of crashes in Site R1.

Three aggregation periods were evaluated to find the minimum number of aggregated months needed to smooth out random variations and make accurate observations. Figure H.6 presents the rolling average of total crashes at Site R1 using three different windows: 7, 13, and 19 months. If there are 160 months of crash data, using a 7-month rolling average (excluding the 13-month

overlay period) results in 141 observations, a 13-month rolling average results in 135 observations, and a 19-month rolling average results in 129 observations.

To compare the performance of the different rolling average windows, Figure H.7 presents the monthly variation in the average crash numbers in four different sites, ordered from low to high traffic volumes. Figure H.7 shows that the 7-month rolling average yields greater variation from month-to-month (noise) in the analysis results. This outcome is undesirable and might be an indication that the data included in the moving window is insufficient. This variation reduces with the 13-month window case. Furthermore, if one computes the standard deviation in the ‘raw’ crash profile (without moving average), and then computes this statistic for the crash numbers after each rolling average filter, it is observed that in general the 13-month and 19-month numbers produce similar values, and both are half the value of this statistic. Therefore, the 13-month window was selected.

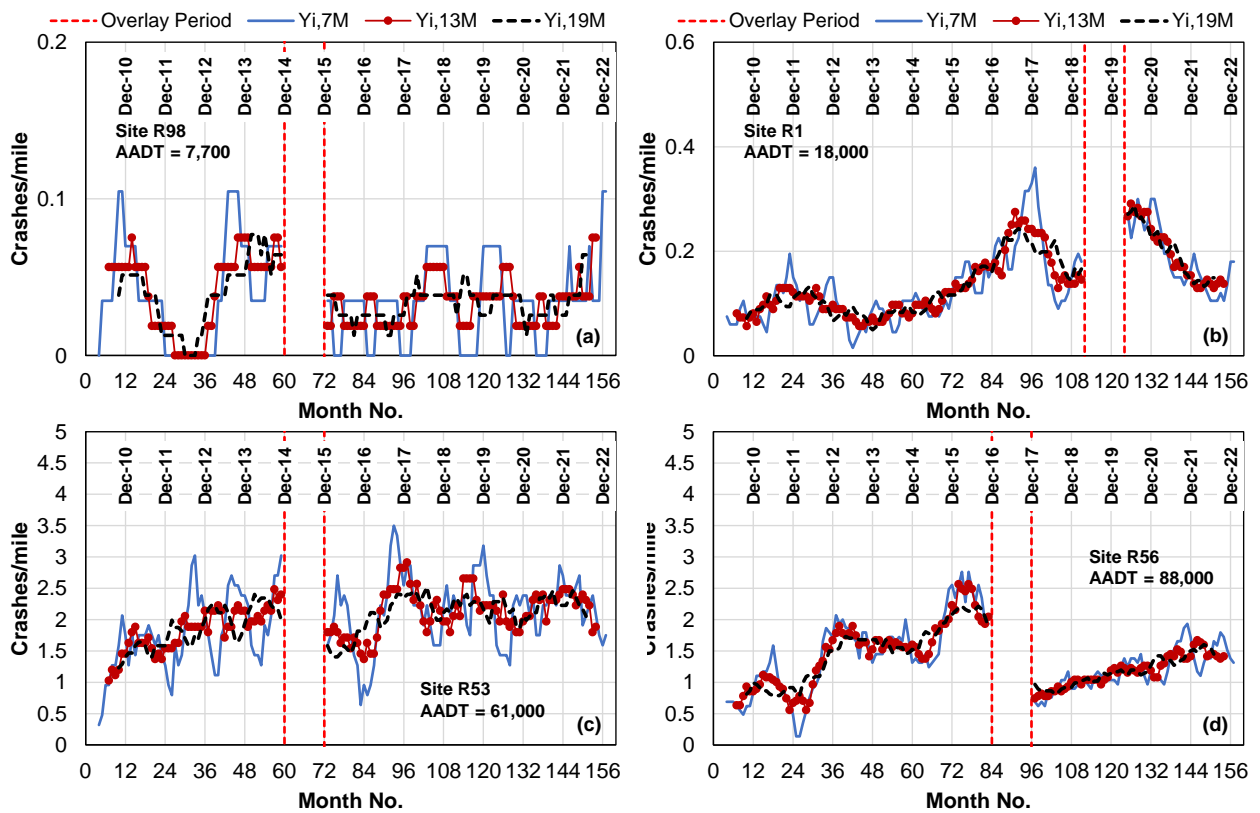


Figure H.7. Rolling average for sites with different traffic levels.

Finally, in the cases where the ‘before’ and ‘after’ period durations differ, a correction factor is estimated using Equation (141) to normalize the estimate of the average crash numbers in the ‘before’ period to the same time window of the ‘after’ period through Equation (142). For example, if a 13-month moving average is used for Site R98 in Figure H.7, then $N_B = 53$ and $N_A = 82$, whereas $N_B = 105$ and $N_A = 30$ for Site R1. In the former case $r_d = 82/53 = 1.55$ and in the latter case is $r_d = 30/105 = 0.29$. Hence, Equations (142) and (143) are used to calculate π and λ .

$$r_d = \frac{\# \text{time-units in the 'after' period}}{\# \text{time-units in the 'before' period}} \quad (141)$$

$$\pi = r_d \times \frac{1}{N_B} \sum_{i=1}^{N_B} Y_{i,13M} \quad (142)$$

$$\lambda = \frac{1}{N_A} \sum_{i=1}^{N_A} Y_{i,13M} \quad (143)$$

One of the factors that affects the results of a before-after study is the definition of the ‘before’ and ‘after’ periods. Because asphalt overlays were placed at different dates on each site, it was decided to define a set of scenarios of specific ‘before’ and ‘after’ periods. In this way, the effect of the asphalt overlay is assessed using the same ‘before’ and ‘after’ periods for each site. Two lengths for the ‘before’ period was evaluated: 30 and 60 months. For each ‘before’ period length, three ‘after’ period windows were analyzed: 13, 26, and 60 months. The combination of a ‘before’ and ‘after’ period length defines a scenario; in this sense, a total of six scenarios were defined:

- Scenario 1: Before = 30 months and After = 13 months.
- Scenario 2: Before = 30 months and After = 26 months.
- Scenario 3: Before = 30 months and After = 60 months.
- Scenario 4: Before = 60 months and After = 13 months.
- Scenario 5: Before = 60 months and After = 26 months.
- Scenario 6: Before = 60 months and After = 60 months.

Given the available ‘before’ and ‘after’ windows, the number of sites that were considered in each scenario are shown in Figure H.8. A site can be evaluated in multiple scenarios, depending on N_B and N_A . For example, Site R33 has $N_B = 83$ and $N_A = 64$, hence this site can be analyzed in all six scenarios because the two ‘before’ periods of 30 and 60 months can be defined and the three ‘after’ periods can be created from the available N_A . In contrast, Site R1 can only be included in Scenarios 1, 2, 4, and 5 because $N_B = 111$ and $N_A = 36$ for this site.

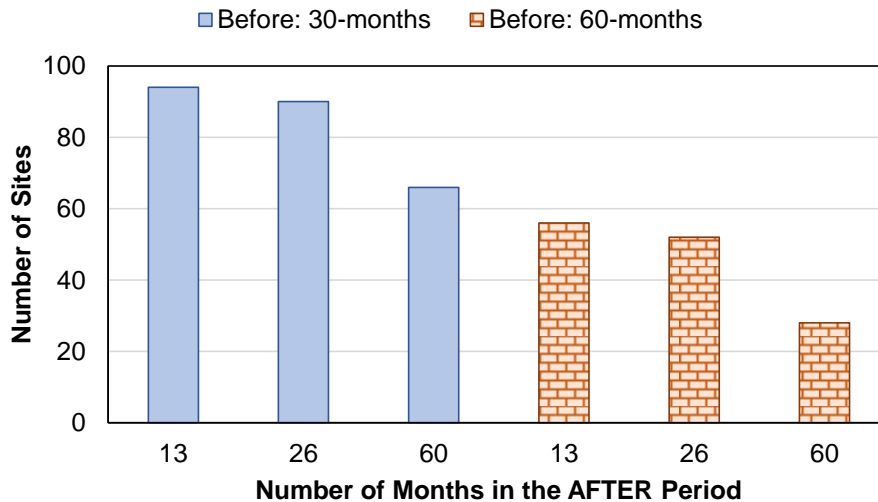


Figure H.8. Combinations of ‘before’ and ‘after’ periods.

These scenarios permit an evaluation of the effect of doubling the ‘before’ period duration, from 30 to 60 months, and permit evaluating the effect of increasing the ‘after’ period. However, it must be noted that the results between scenarios are not totally independent. The number of sites per scenario is not the same and not all the sites are included in all the scenarios. Evaluating the effect

of the ‘after’ period duration is particularly important because as stated above there is evidence that after an overlay skid resistance varies over time, so by using different ‘after’ period durations it will be possible to assess what is the ‘after’ period duration needed to capture a difference in the ‘before’ and ‘after’ periods.

Once the six before-after scenarios were defined, a naïve before-after study was conducted on all the sites that are part of each scenario. It is important to note that a 13-month moving average was applied to crash numbers prior to any analysis.

As indicated in Figure H.1 and Figure H.3, some sites are undivided or divided facilities, some of them have a dense surface mix while others have either a UTBWC or an OGFC. It is assumed here that the surface type, geometry, and speed limit did not change during the analysis period, i.e., if the surface type placed in the overlay reported in the NCDOT PMS is an OGFC, it is assumed that the previous surface was also an OGFC. This assumption regarding the surface type was made because the surface that was prior the overlay is not reported in the NCDOT PMS. The results are organized according to surface type, geometry, and speed limit.

Results

Two different ‘before’ periods were evaluated, 30 and 60 months, and three ‘after’ periods were defined, 13, 26, and 60 months. To illustrate the analysis process, the crash record of Site R34 will be used.

The total length of Site R34 is 2.3-miles. Site R34 is a divided facility and crash records were evaluated in both traffic directions. Hence, the total number of miles associated with the number of crashes is 4.6-miles. For this site, in Scenario 1 the correction factor is $r_d = 13/30 = 0.43$, the estimated mean total number of crashes ‘before’ and ‘after’ the overlay was $\pi_e = 44$ crashes/month/4.54-miles $\times 0.43 = 4.20$ crashes/month/mile and $\lambda_e = 21$ crashes/month/4.54-miles $= 4.63$ crashes/month/mile, respectively. The variance of both quantities is equal to the estimated mean in each period. Equation (130) and Equation (88) are used to estimate the crash reduction (δ_e) and ratio of safety levels (θ_e). Equation (132) and (90) provide estimates for $Var(\delta_e)$ and $Var(\theta_e)$, respectively. For this scenario, $\delta_e = -0.46$ crashes/mile and $\theta_e = 1.0$, respectively.

In this analysis, special attention is given to θ_e , wherein a site has been flagged if $\theta_e \geq 0.8$ by considering this a sign that crash levels have increased in the ‘after’ period. As mentioned above, practitioners used values of $\theta_e > 1$ as an indication that λ_e/π_e , however the value of 0.8 was used as a conservative method to include sites that might get closer to the threshold of $\theta_e = 1$.

A similar procedure is followed for all crash types and all the scenarios. As mentioned, depending on N_B and N_A each site may be evaluated in different scenarios. For example, Site R34 has $N_B = 71$ -months and $N_A = 76$ -months, so this site was evaluated in all six scenarios.

Based on the results, the number of sites with $\theta_e > 0.8$ are tabulated. It is important to note that an undefined crash ratio is obtained when the number of crashes in the ‘before’ period is equal to zero (i.e., $\pi_e = 0$). This situation was observed for some sites and crash types. Consequently, the results were summarized as either the site having $\theta_e > 0.8$, $\theta_e \leq 0.8$, or θ_e is undefined.

To illustrate this calculation, the θ_e values for the sites in Scenario 1 are summarized in Figure H.9. In this plot, the dots represent θ_e , blue for dense-graded mixtures and orange for UTBWC/OGFC surfaces, whereas the error bars illustrate the standard deviation, $\sigma = \sqrt{Var(\theta_e)}$,

associated with each θ_e . Also, the limit of $\theta_e = 0.8$ is indicated by the red line. The error bars convey an interval centered at the mean with width 2σ . Thus, this interval roughly represents the 68% confidence interval. As presented in Figure H.9, the 68% confidence interval for some of these sites includes the 0.8 value, so for these sites $\theta_e = 0.8$ is no distinct from other values in the 68% interval and is plausible that θ_e takes values greater than 0.8 but also lower than that.

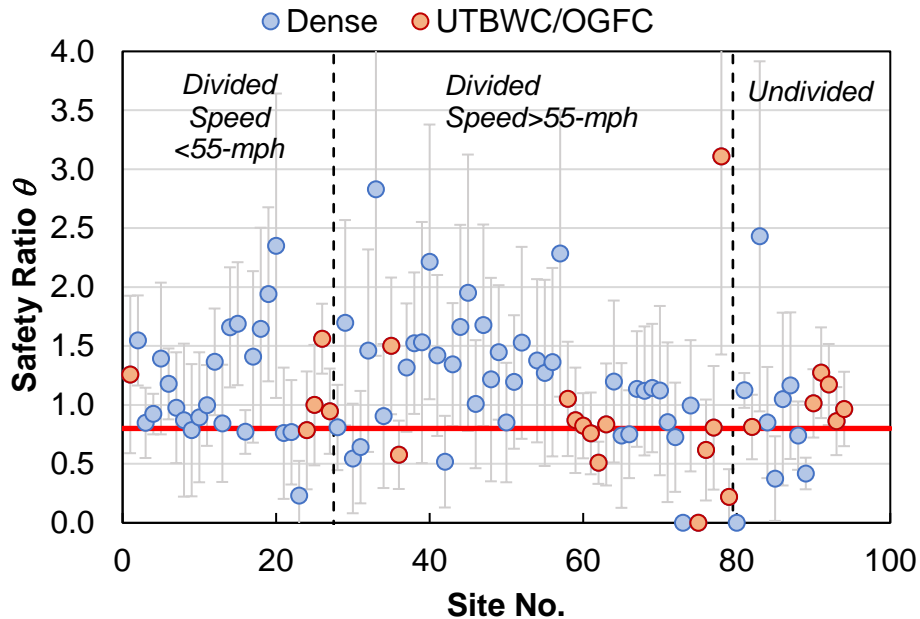


Figure H.9. Ratio of total crashes, θ_e , for each site in Scenario 1.

Scenario 1 was evaluated for a total of 94 sites in terms of total crashes, wherein 70 sites have a $\theta_e > 0.8$, 23 have $\theta_e \leq 0.8$, and θ_e is undefined for one site (it has zero crashes in the ‘before’ period). Based on these numbers, one can say 75% (70/93) of the sites showed $\theta_e > 0.8$. If one groups the sites by the surface type in the after period of analysis (excluding the one where θ_e was undefined), it is observed that 77% of the dense-graded mixture sites and 70% of the UTBWC/OGFC sites resulted in $\theta_e > 0.8$. However, if lane-wet departure crashes are used in this scenario, 44 sites have $\theta_e > 0.8$, 42 sites have $\theta_e \leq 0.8$, and θ_e is undefined for 8 sites. Hence, 51% (44/86) of the sites showed $\theta_e > 0.8$. Grouped by surface type, 63% of the dense-graded mixture have $\theta_e > 0.8$, whereas only for 21% of the UTWBC/OGFC $\theta_e > 0.8$.

The analysis described above was replicated for all scenarios and crash types and the results are summarized in Table H.1. In this table, the sites are grouped based on two criteria. First, they are grouped by the facility type, i.e., Divided vs. Undivided. Next, they are grouped by surface type, i.e., dense-graded mixtures vs. UTBWC/OGFC. The total number of sites evaluated listed in Table H.1 includes only sites where θ_e was defined. Figure H.10 and Figure H.11 provide graphical depictions of the results for dense-graded and UTBWC/OGFC mixtures, respectively.

Two main trends are observed. The divided highways have a higher proportion of sites with $\theta_e > 0.8$, this is particularly true for the crashes in wet condition as shown in Figure H.10. Additionally, Figure H.11 shows that under wet conditions the UTBWC/OGFC has the lowest proportion of sites with $\theta_e > 0.8$, especially for wet lane departure crashes. If crashes are used without filtering by wet conditions, there is no appreciable difference between the proportion of

sites where $\theta_e > 0.8$ for UTBWC/OGFC and dense-graded mixtures. For this reason, in order to identify differences in the safety performance obtained with different surface types, wet lane departure crashes are the ones that better capture differences in safety levels associated with different surface types.

It is speculated that the divided facilities exhibit higher crash risk in comparison to undivided facilities because in general the speed limit of the divided facilities is higher than undivided facilities. The finding in the dense-graded mixture surfaces matches with the results reported by others (2), but it is important to note the number of sites with a dense-graded mixture is almost three times higher than the number of sites with a UTBWC/OGFC surface (see Figure H.3).

Table H.1. Summary of results based on the parametric method.

Scenario	Crash Type	No. Sites	Divided		Dense	UTBWC/OGFC
			Undivided			
S1	Total	Where $\theta > 0.8$	76%	73%	77%	71%
		Total Evaluated	78	15	69	24
	Total-Wet	Where $\theta > 0.8$	58%	23%	65%	21%
		Total Evaluated	76	13	65	24
	LD	Where $\theta > 0.8$	68%	43%	70%	46%
		Total Evaluated	77	14	67	24
	LD-Wet	Where $\theta > 0.8$	58%	8%	63%	21%
		Total Evaluated	74	12	62	24
S2	Total	Where $\theta > 0.8$	80%	73%	80%	75%
		Total Evaluated	74	15	65	24
	Total-Wet	Where $\theta > 0.8$	64%	8%	66%	29%
		Total Evaluated	72	13	61	24
	LD	Where $\theta > 0.8$	74%	36%	70%	63%
		Total Evaluated	73	14	63	24
	LD-Wet	Where $\theta > 0.8$	60%	0%	64%	21%
		Total Evaluated	70	12	58	24
S3	Total	Where $\theta > 0.8$	86%	88%	86%	86%
		Total Evaluated	57	8	43	22
	Total-Wet	Where $\theta > 0.8$	69%	25%	80%	82%
		Total Evaluated	55	8	41	22
	LD	Where $\theta > 0.8$	79%	88%	79%	82%
		Total Evaluated	56	8	42	22
	LD-Wet	Where $\theta > 0.8$	61%	13%	70%	27%
		Total Evaluated	54	8	40	22
S4	Total	Where $\theta > 0.8$	87%	70%	84%	82%
		Total Evaluated	46	10	45	11
	Total-Wet	Where $\theta > 0.8$	70%	25%	70%	36%
		Total Evaluated	46	8	43	11
	LD	Where $\theta > 0.8$	85%	56%	80%	82%
		Total Evaluated	46	9	44	11
	LD-Wet	Where $\theta > 0.8$	60%	14%	59%	36%
		Total Evaluated	45	7	41	11
S5	Total	Where $\theta > 0.8$	90%	70%	85%	91%
		Total Evaluated	42	10	41	11

Scenario	Crash Type	No. Sites	Divided	Undivided	Dense	UTBWC/ OGFC
			Where $\theta > 0.8$	Where $\theta > 0.8$	Where $\theta > 0.8$	Where $\theta > 0.8$
S6	Total-Wet	Where $\theta > 0.8$	74%	25%	72%	45%
		Total Evaluated	42	8	39	11
	LD	Where $\theta > 0.8$	74%	22%	75%	91%
		Total Evaluated	42	9	40	11
	LD-Wet	Where $\theta > 0.8$	71%	14%	70%	36%
		Total Evaluated	41	7	37	11
S6	Total	Where $\theta > 0.8$	92%	67%	89%	89%
		Total Evaluated	25	3	19	9
	Total-Wet	Where $\theta > 0.8$	64%	0%	68%	33%
		Total Evaluated	25	3	19	9
	LD	Where $\theta > 0.8$	92%	67%	89%	89%
		Total Evaluated	25	3	19	9
	LD-Wet	Where $\theta > 0.8$	64%	0%	74%	22%
		Total Evaluated	25	3	19	9

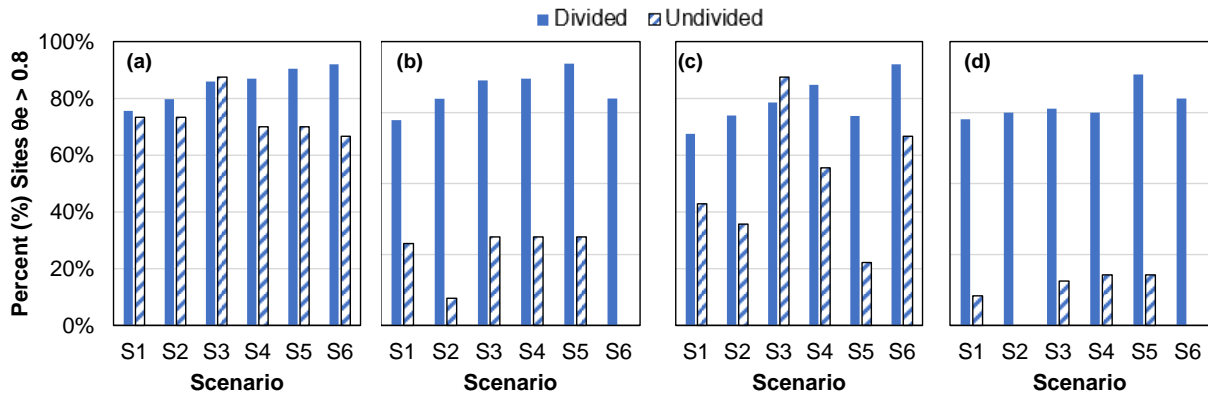


Figure H.10. Proportion of divided and undivided sites, for each crash type, where $\theta_e > 0.8$. (a) Total crashes, (b) Total wet crashes, (c) Lane departure crashes, and (d) Lane departure wet crashes.

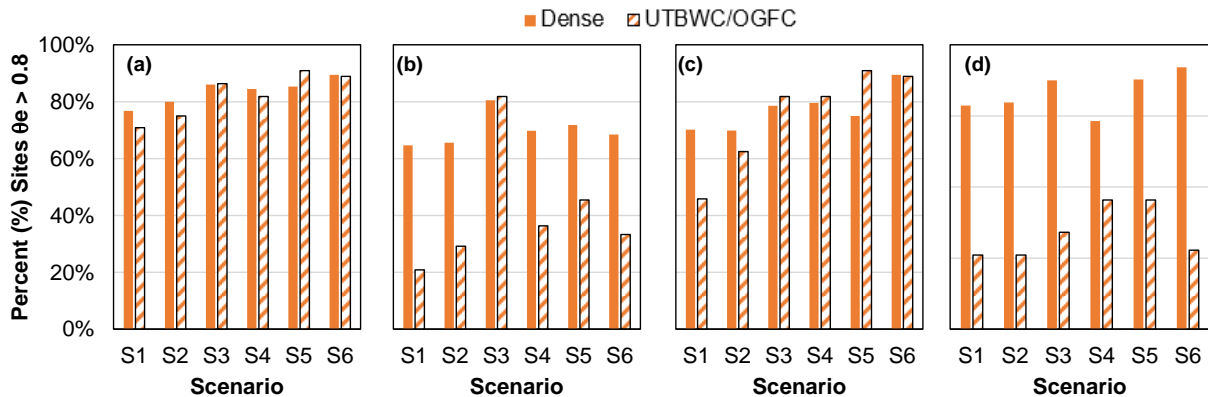


Figure H.11. Proportion of sites with a dense-mix and UTWBC/OGFC surface, for each crash type, where $\theta_e > 0.8$. (a) Total crashes, (b) Total wet crashes, (c) Lane departure crashes, and (d) Lane departure wet crashes.

It is important to remember that the main assumption for this analysis is that crashes follow a Poisson distribution, this assumption might affect the outcome and interpretation of the results. This issue has been discussed in detail by Hauer (76), who indicated the following: “to reliably detect a change in safety of only a few percentage points requires such a large number of accidents, that the conduct of such a study is rarely practical.” In the same work, Hauer also stated as a good rule of thumb, “the standard deviation of the estimate has to be 2-3 times smaller than the effect which one expects to detect.” Looking into the results, only a few sites met this requirement. Therefore, analyzing the data at hand in using non-parametric methods may more accurately quantify the effect of overlays on safety.

Conclusions

The main conclusions derived from the analysis are;

- To identify differences in the safety performance obtained with different surface types, wet lane departure crashes are the ones that better capture differences in safety levels associated with different surface types.
- The divided highways have a higher proportion of sites with $\theta_e > 0.8$, this is particularly true for the crashes in wet condition.
- In all the scenarios evaluated, the OGFC/UTBWC have a lower proportion of sites with $\theta_e > 0.8$ than dense mixes.
- Doubling the ‘before’ period length, N_B , accentuates the difference between the expected number of crashes in the ‘before’ and ‘after’ period. In other words, if one wants to assess the effect of asphalt overlays it is more beneficial to increase the ‘before’ period length than increasing the ‘after’ period.
- A time window of 13-months provides a stable safety representation, without noise, and it can be used to track temporal variations in safety levels.

APPENDIX I. INVESTIGATORY AND INTERVENTION THRESHOLDS

Texture

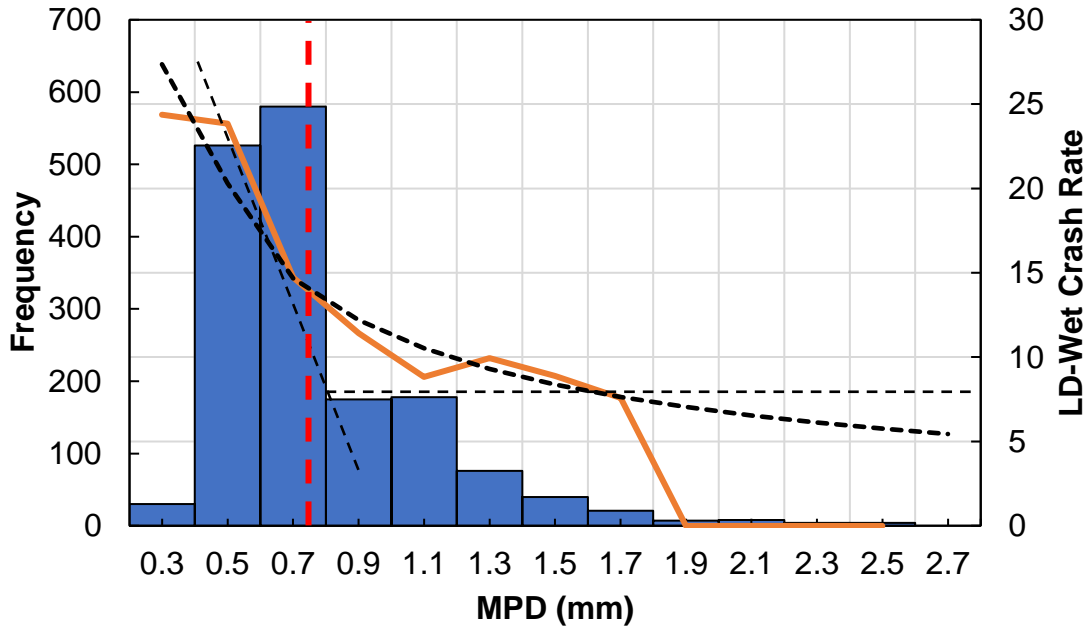


Figure I.1. Wet lane departure crash rate variation as a function of *MPD* for Category-1.

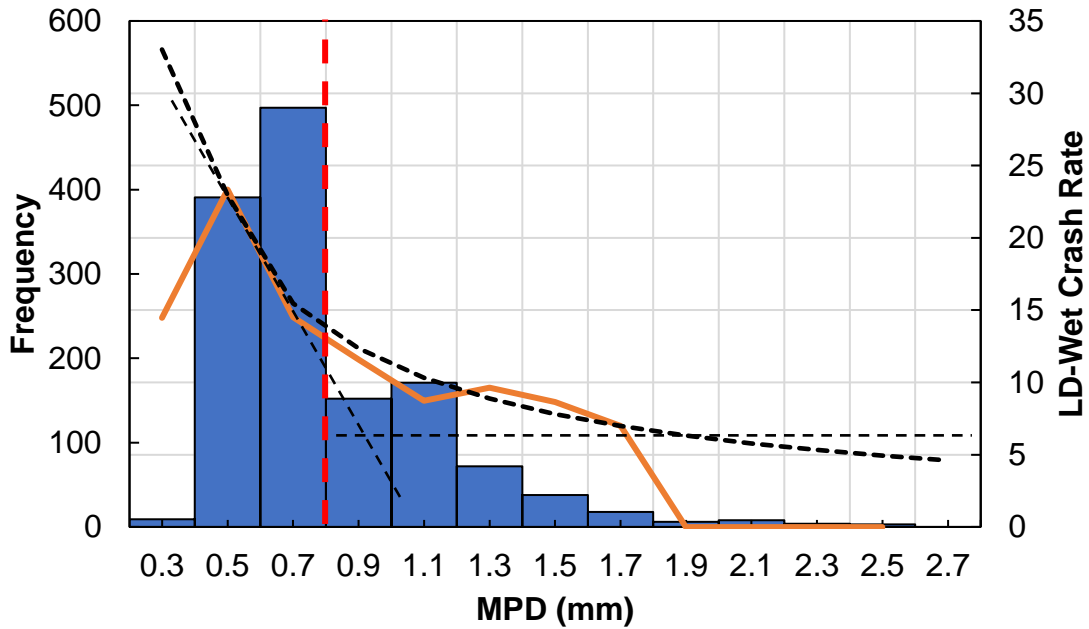


Figure I.2. Wet lane departure crash rate variation as a function of *MPD* for Category-1 at 65-70 mph.

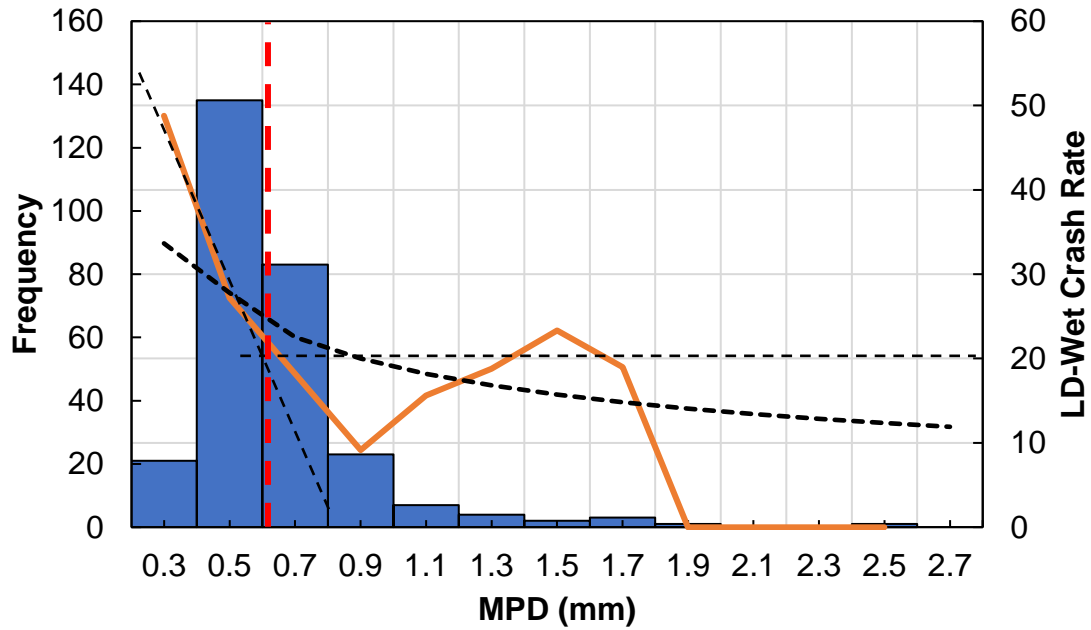


Figure I.3. Wet lane departure crash rate variation as a function of *MPD* for Category-1 at 55-60 mph.

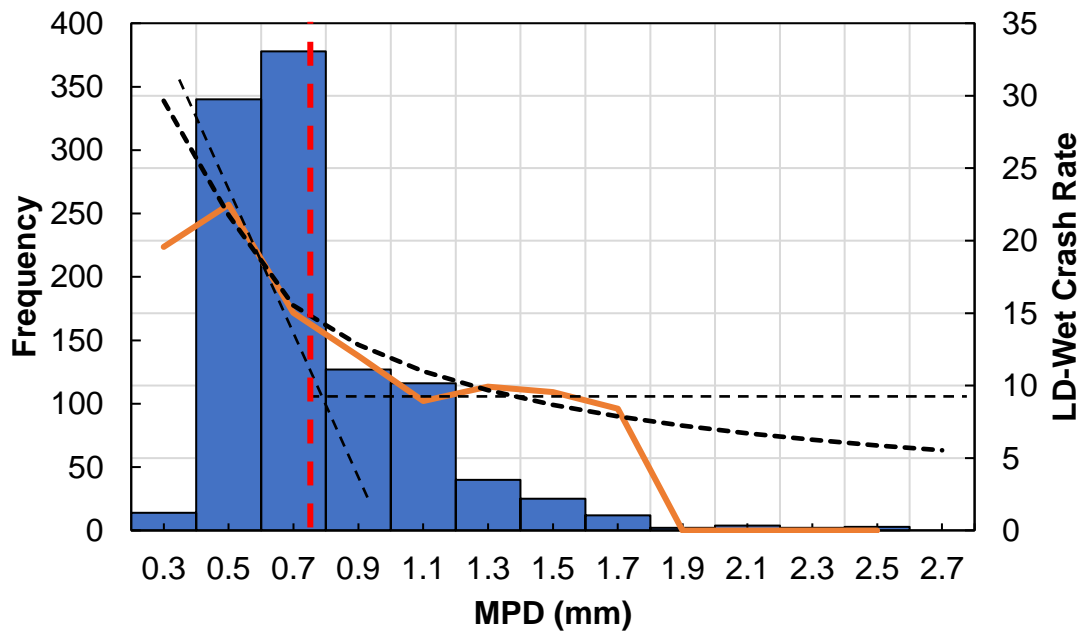


Figure I.4. Wet lane departure crash rate variation as a function of *MPD* for Category-2 (tangents).

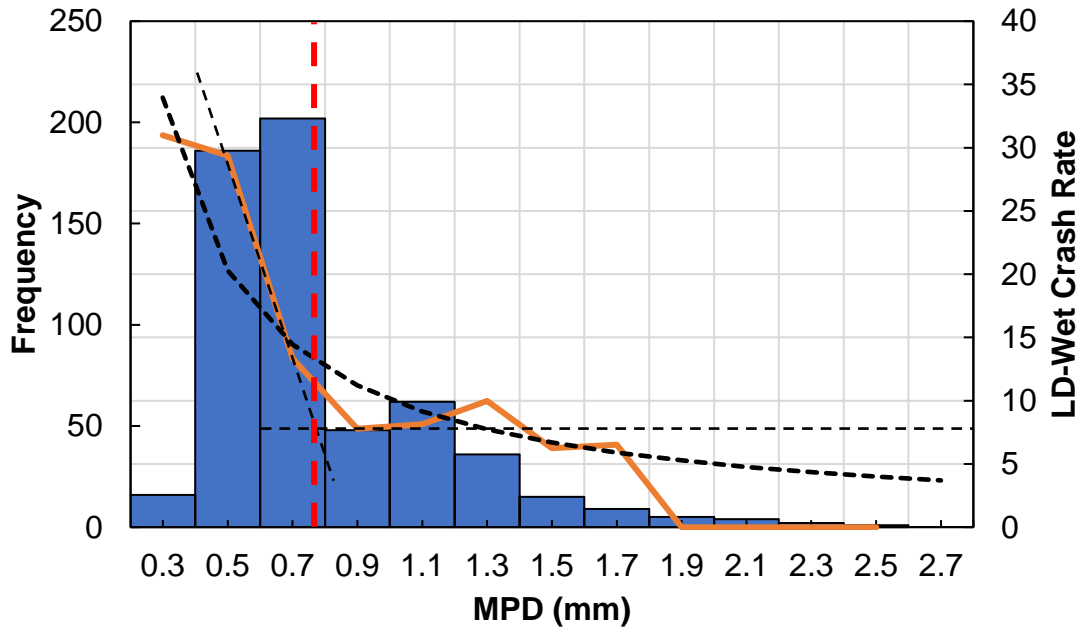


Figure I.5. Wet lane departure crash rate variation as a function of *MPD* for Category-3 (curves).

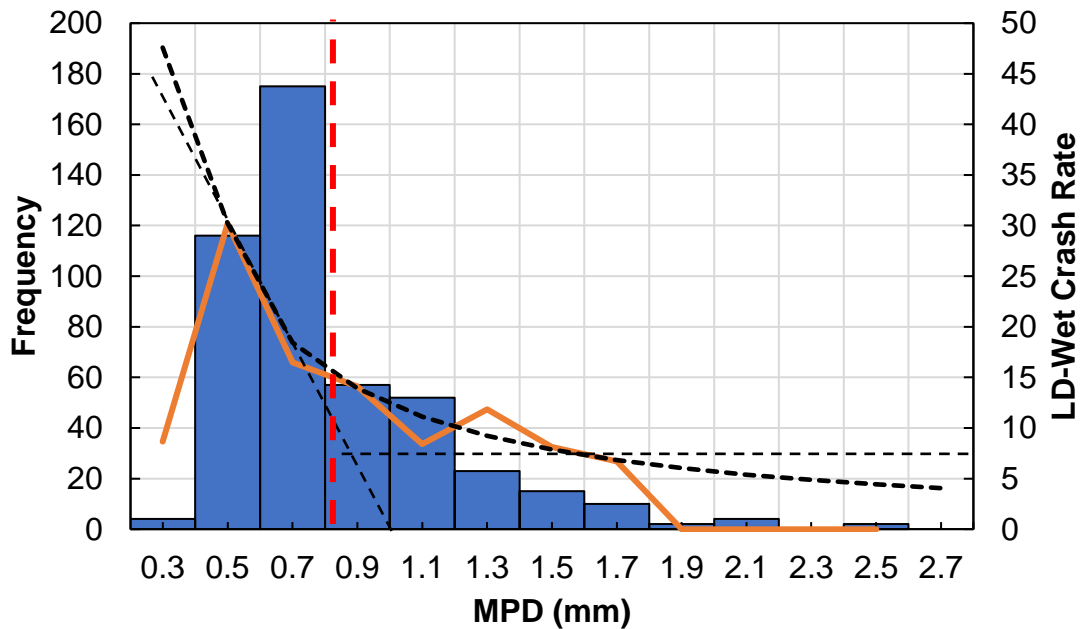


Figure I.6. Wet lane departure crash rate variation as a function of *MPD* for Category-4 (interchanges).

Friction

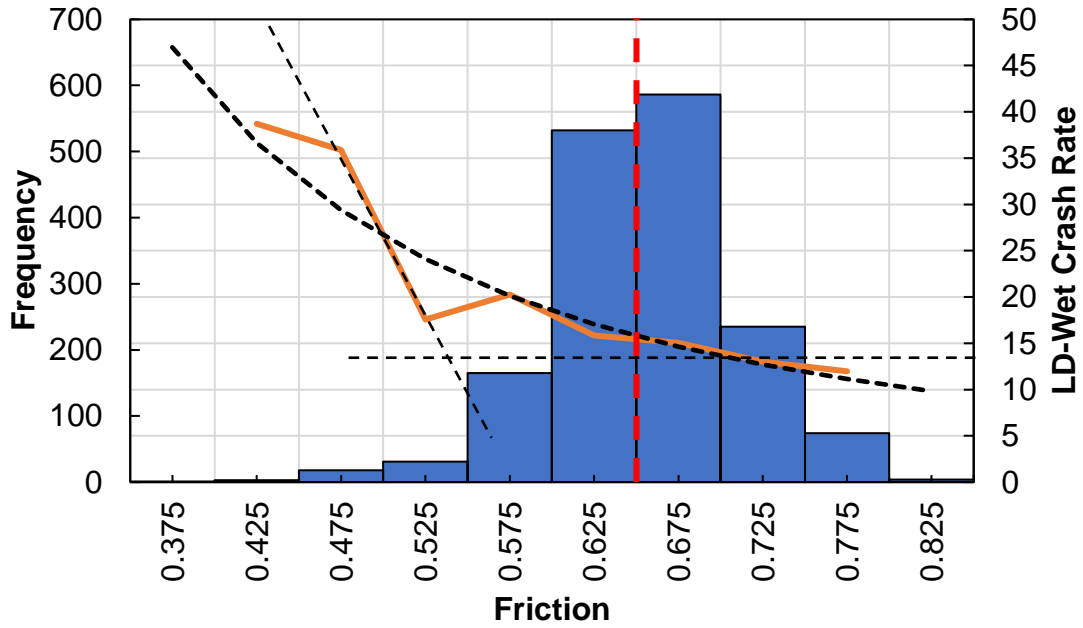


Figure I.7. Wet lane departure crash rate variation as a function of friction for Category-1.

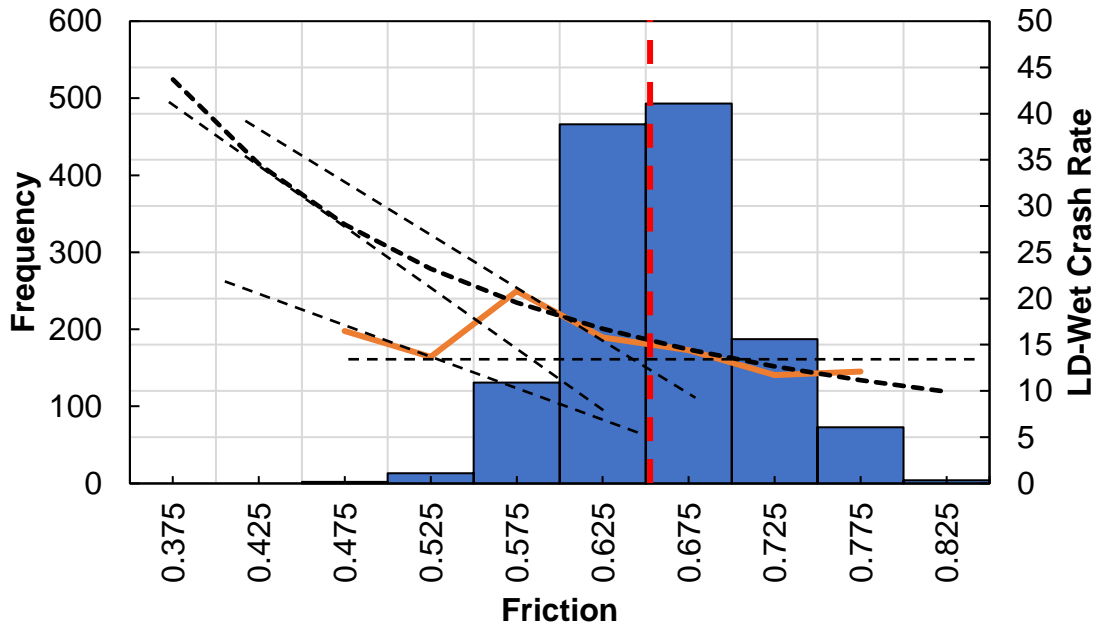


Figure I.8. Wet lane departure crash rate variation as a function of friction for Category-1 at 65-70 mph.

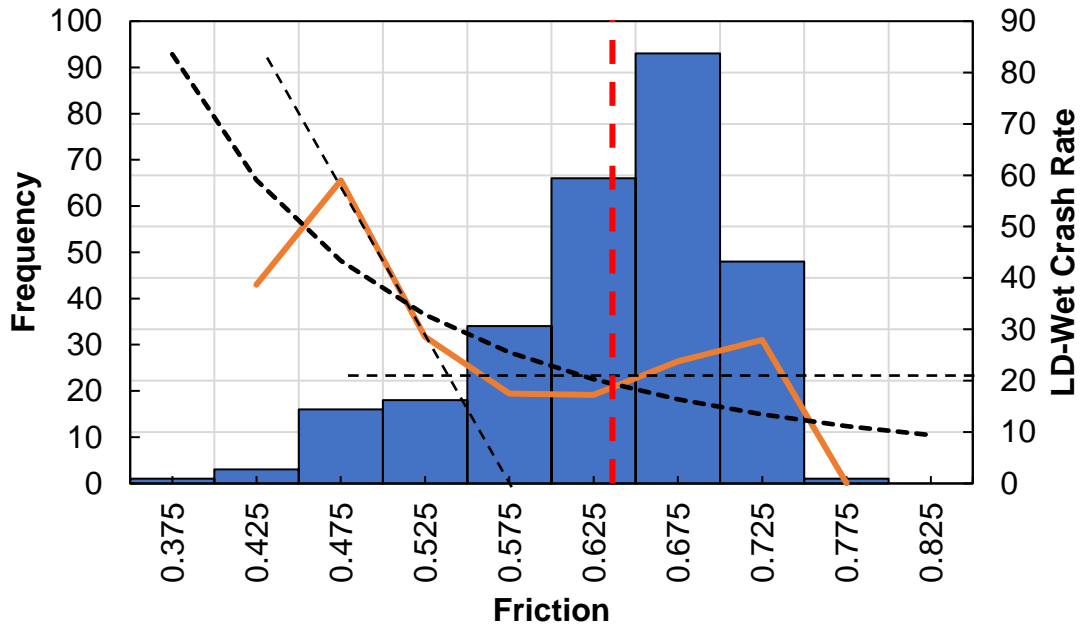


Figure I.9. Wet lane departure crash rate variation as a function of friction for Category-1 at 55-60 mph.

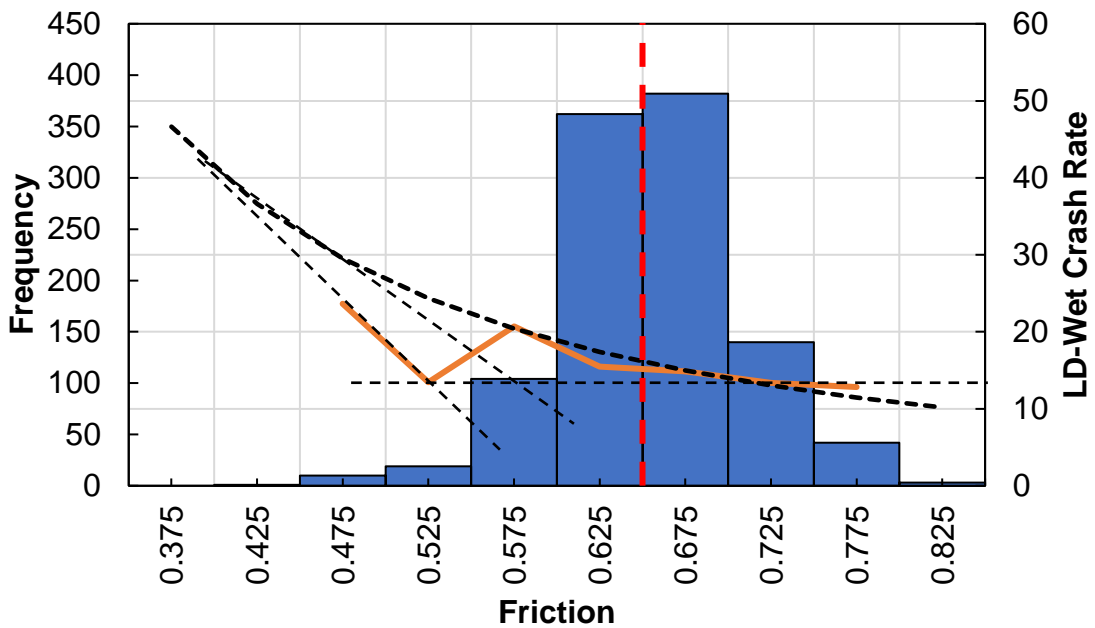


Figure I.10. Wet lane departure crash rate variation as a function of friction for Category-2 (tangents).

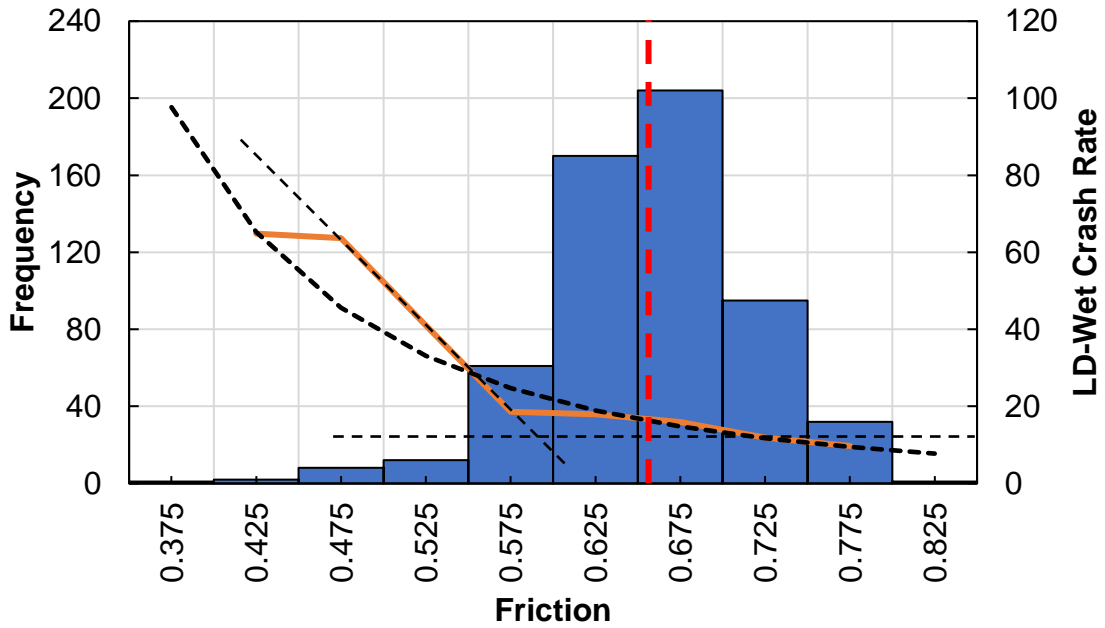


Figure I.11. Wet lane departure crash rate variation as a function of friction for Category-3 (curves).

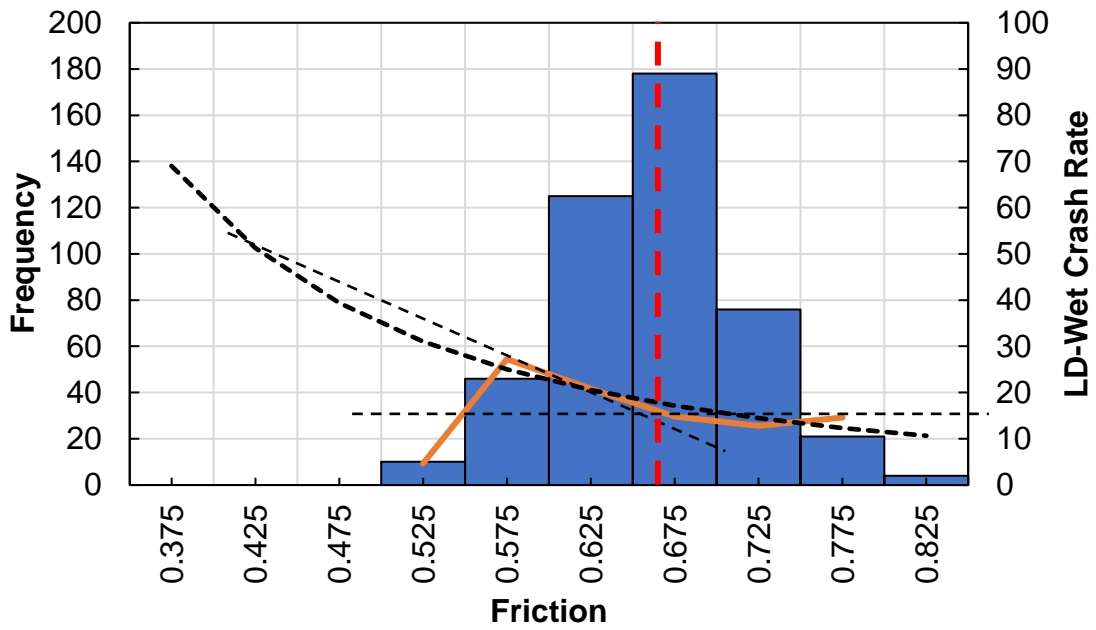


Figure I.12. Wet lane departure crash rate variation as a function of friction for Category-4 (interchanges).

APPENDIX J. COST-BENEFIT ANALYSIS

A case study is provided, in which the road network surveyed for friction and texture was co-located along with the climate regions defined during the friction and texture performance models calibration process. This overlap is illustrated in Figure J.1. The friction and texture dataset used for this analysis was collected by WDM, as requested by the NCDOT.

During September to November of 2022, WDM measured friction and texture using the SCRIM machine. A total of 4,715 miles were inventoried on the NCDOT primary road network. The data was collected in both traffic directions and the surface age and type was characterized by WDM personnel using the NCDOT PMS. Some sections of roads are not properly cataloged in terms of surface type or functional classification, others do not have accurate data on the latest rehabilitation action, which is needed to define the pavement age.

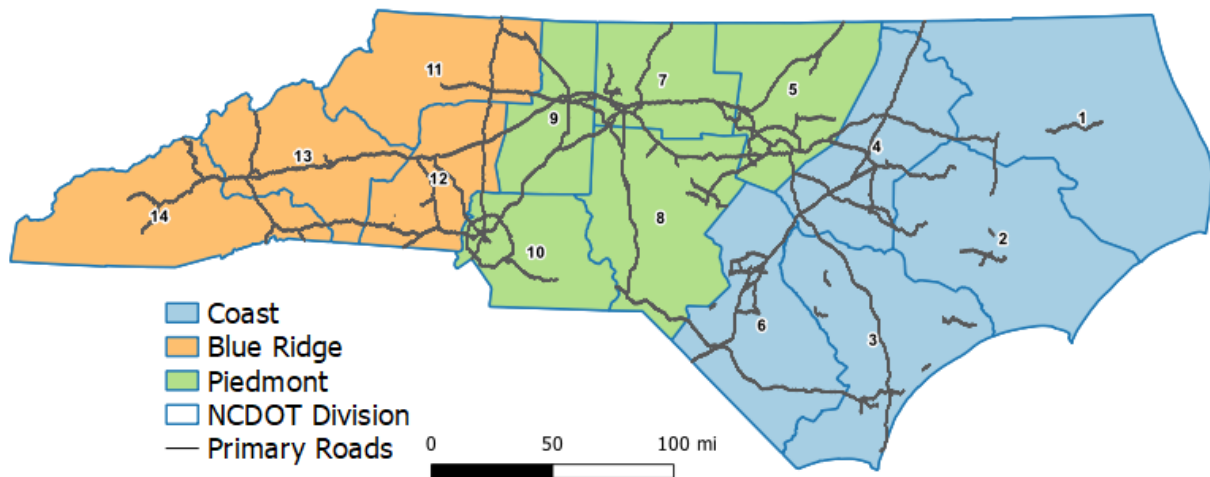


Figure J.1. North Carolina primary road network across the different climate regions.

On the other hand, for each route crash data is stored only on the inventory direction. Consequently, the analysis only included the friction and texture collected in the inventory direction to facilitate the alignment of the different datasets. In addition to the route inventory criteria, segments were filtered further based on five surface types: S9.5B, S9.5C, S9.5D, UTBWC, and OGFC. It was possible to focus only on the inventory direction because, as noted in previous quarterly reports, for the same paving contract, similar friction and texture values are obtained regardless the traffic direction, i.e., similar values in the inventory and non-inventory directions.

After this selection, a total of 1,132.2 road miles were used to represent North Carolina's primary network. This network is represented by a total of 11,322 0.1-mile segments. As presented in Figure J.2 (a), the largest proportion of these roads have a S9.5C mix type, nearly 55% (of this proportion, 71% was rehabilitated in or prior 2018), the second biggest proportion (22%) have a S9.5D, and the other three surface types are equally distributed with proportions close to 10% each.

In terms of age, the newest sections are either OGFC or UTBWC, and the oldest ones are the dense mixes, in particular the S9.5D surface type. The average age of the OGFC is 4 years, for the UTBWC it is 5 years, and the age is around 6 years for the dense mixes.

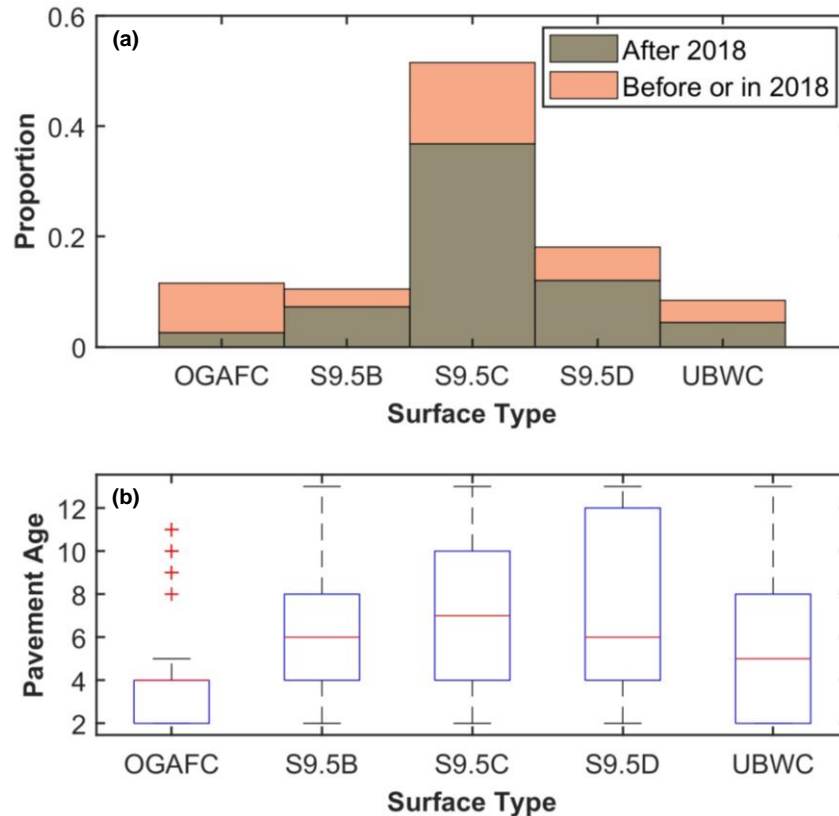


Figure J.2. (a) Proportion of the network in each surface type and (b) Distribution of pavement age for each surface type.

For most of this research, the CFME used was the Moventor Skiddometer BV-11. With this device, friction was measured in the RWP and the center of the lane (in some sites); similarly, the AMES HSTP collected texture in the RWP and center of the lane. In contrast, the SCRIM collected all the information in the left wheel path (LWP). Due to these circumstances, making a direct comparison of the measurements collected by the two devices is not a straightforward process.

An analysis was made in Appendix H, where the friction number (FN) measured with the BV-11 was compared against the SCRIM coefficient (SC) measured with the SCRIM machine, and the MPD measured with the AMES HSTP was compared against the MPD measured with the SCRIM (MPD_{SCRIM}). The result of that comparison showed the two friction devices do not produce similar results and there is not a direct relationship between the two friction indices. In contrast, the readings made by the two lasers produce values that follow a close relationship where the MPD_{SCRIM} is consistently higher than MPD by 0.2 mm.

Although there is not a relationship between FN and SC , it was observed the central tendency of their respective distribution is very close, in Appendix H it was shown the mean and median of both distributions were close to each other. For this reason, the SCRIM data was used to assess the methods and thresholds previously proposed, because on average similar results will be observed. Additionally, this analysis is made only to illustrate the application of the PFMP concepts. To this end, the following assumptions were made:

- Although the performance models developed were calibrated using RWP observations, these models can be used to describe the deterioration process of the SCRIM coefficient

(SC), which is measured in the left wheel path. To this end, the mean effect deterioration curve was shifted vertically to match the SC measured in 2022. Then, this adjusted curve was used to forecast SC over time. This same procedure was applied for the MPD, i.e., the models were shifted vertically to match the MPD observed in 2022 with the SCRIM machine.

- The thresholds proposed using the values measured with the Moventor Skiddometer and the HSTP can be used directly with the SCRIM values.

Both assumptions are used only to demonstrate the framework proposed for the implementation of the PFMP. Both hypotheses must be verified, and more research is needed to determine the relationship between the values measured with the different devices.

Current State of the Network Selected for Evaluation

The SCRIM observations collected in 2022 are distributed as indicated in Figure J.3. For the brevity of this discussion, only friction demand Category 1 was used. In other words, the same friction and texture threshold was used independently of the geometry or the speed limit of the facility. The candidate investigatory thresholds for friction and texture estimated with the GPF-Pivot method were 0.8-mm for texture and 0.53 for friction. Based on the results of Appendix I, the investigatory threshold for MPD_{SCRIM} is set as 1-mm, and the investigatory threshold for the SC is set equal to 0.53.

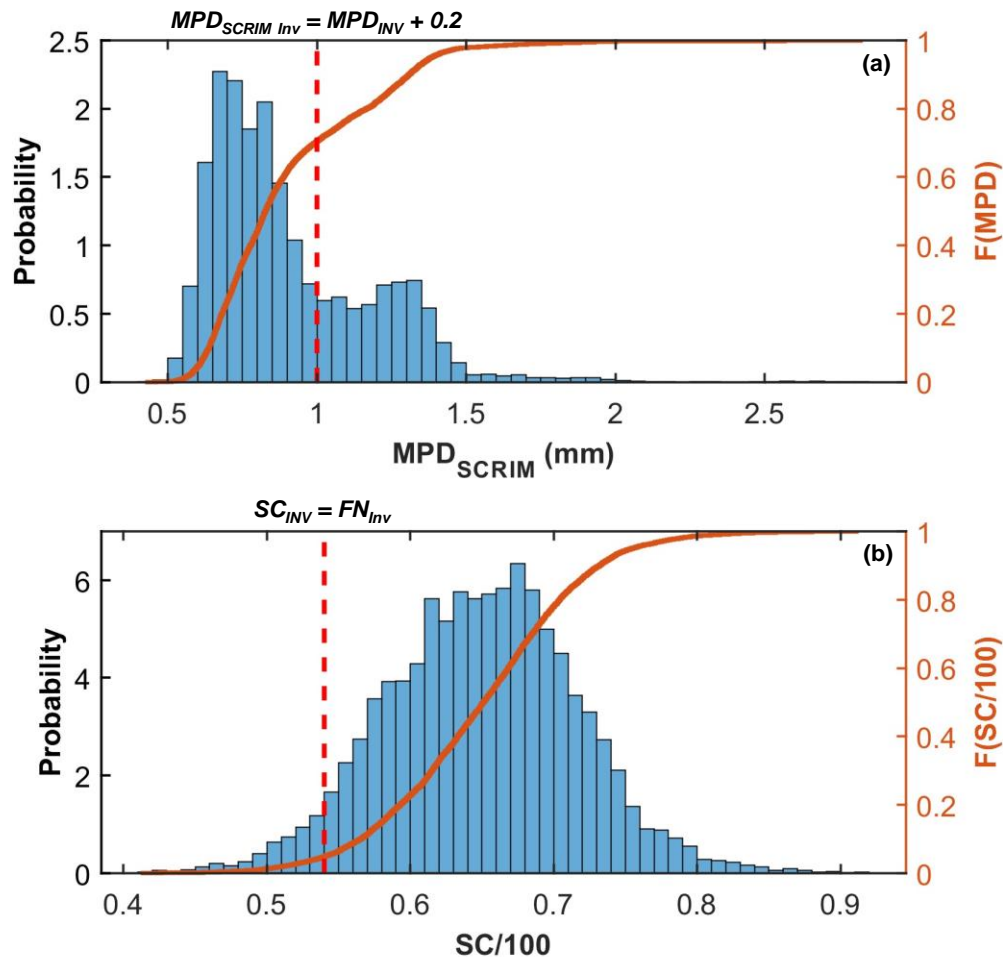


Figure J.3. Distribution of SCRIM measurements: (a) MPD_{SCRIM} and (b) SC.

The two histograms of Figure J.3 indicate that most of the network has a friction value above the investigatory level, in fact only 4.8% of the 0.1-mile segments have friction values below 0.53. In contrast, 70% of the network have MPD values lower than 1.0-mm. These values reaffirm the findings presented by Flintsch et al. (2017) (1), i.e., North Carolina's skid resistance issues (where they exist) are primarily due to texture. For the analysis presented here, three possible candidates of macrotexture intervention thresholds are evaluated, 0.5, 0.6, and 0.7-mm. In the case of friction, the intervention threshold has been set equal to the candidate investigatory threshold.

Analysis Scenarios

For this evaluation, a rehabilitation treatment is triggered by three possible cases:

- A treatment is applied after a predefined number of years, set based on the recommendations provided by the NCDOT Pavement Design Procedure (2019) (109), the performance trends observed in the PMS database, and recommendations from NCDOT personnel. The application of the treatment is not safety-related, because the treatment is triggered based on the pavement age.
- A treatment is applied because the pavement was flagged either by texture or friction. This outcome happens when one, or both, skid resistance parameters are below their respective intervention thresholds.
- A treatment is applied based on the concept of allowable risk. The risk is defined based on the probability of observing a crash rate less than or equal to 10 100-Mvmt₁₃, i.e., $P(R < 10)$.

The first scenario (S1) is named as the 'Business-as-Usual' scenario, where the network is maintained as usual with the current level of consideration for skid resistance. The second scenario (S2) is named 'Maintenance-With-Safety' wherein a treatment is triggered either because the section has reached the age to be treated or because either friction and/or texture are below their intervention threshold. The third scenario (S3) is referred as the 'Safety-Risk-Balance' and is based on the criteria of observing a given $P(R < 10)$.

The inputs used on each scenario are defined in Table J.1. To illustrate the approach of implementing a PFMP, evaluations can be made on potential safety benefits. Evaluating the costs linked to various types of crashes or the expenses necessary to mitigate the likelihood of crashes with a particular level of severity (such as injury or fatality) can entail a sophisticated assessment of diverse econometric studies (7). To this end, the maintenance actions, and the expected crash reductions due to these actions were estimated based on the crash analysis conducted in Chapter 4.

In summary, there are three scenarios evaluated (S1, S2, and S3), three maintenance alternatives for the OGFC (OG1, OG2, and OG3), and two maintenance alternatives for the UTBWC (UT1 and UT2), all of these options are detailed in Table J.1. The maintenance alternatives have been set based on NCDOT recommendations to represent the most extreme conditions, the premise is that if the evaluation indicates the safety treatments are economically viable under these conditions, then it will also be viable under real maintenance schedules.

Table J.1. Inputs defined on each scenario.

Input	Value
Pavement Age and Maintenance	<ul style="list-style-type: none"> • For a dense mix mill and replace every 12 years. • For OGFC there are three alternatives: <ul style="list-style-type: none"> ○ OG1 (Low Structural Damage): Every 5 years mill off the OGFC and replace. With every other treatment (i.e., every 10 years), mill off the underlying surface mix and replace in addition to the OGFC. ○ OG2 (High Structural Damage): Every 5 years mill off the OGFC and the underlying surface and replace both. ○ OG3 (Modified Structural Damage): Every 8 years mill off the OGFC layer and the underlying surface and replace both. • For UTBWC there are two alternatives: <ul style="list-style-type: none"> ○ UT1 (Low Structural Damage): Every 7 years mill off the UTBWC and replace. With every other treatment (i.e., every 14 years), mill off the underlying surface mix and replace in addition to the UTBWC. ○ UT2 (Modified Structural Damage): Every 10 years mill off the UTBWC layer and the underlying surface and replace both. • If the pavement reaches the maximum life, and there are no safety related issues, it has been assumed the new overlay will be the same surface type as the existing one.
Costs	<ul style="list-style-type: none"> • The cost of treatment per 0.1-mile-lane segment is: <ul style="list-style-type: none"> ○ \$7,500 for dense asphalt overlay ○ \$3,700 for OGFC ○ \$3,400 for UTBWC ○ \$2,100 for Skidabrader • It is assumed that before an OGFC or UTBWC is applied, an asphalt overlay is applied first.
Safety Treatments	<ul style="list-style-type: none"> • Divisions 11 to 14 (Western divisions) will receive an UTBWC. • Divisions 1 to 10 (Eastern divisions) will receive an OGFC. • Parameter <i>a</i> of Equation (145) for UTBWC is set equal to 1-mm, for an OGFC is 1.3-mm, for a fine dense mix is 0.35, and after a Skidabrader (or for a coarse dense mix) is 0.8-mm. • It is assumed that neither the Skidabrader, a dense mix, coarse mix, nor an OGFC affects the initial friction. For UTBWC it is assumed the initial friction is 0.8.
Discount rate	<ul style="list-style-type: none"> • 3, 5, and 7% • The typical discount rates are in the range of 3 to 5%, the 7% value was included to evaluate how variable are the results to this variable.
Analysis Period	<ul style="list-style-type: none"> • 40 years, starting at 2022.

For evaluation purposes, there is only one alternative for the dense mixes, dense + Skydabrader or Coarse dense mix, because these are modeled identically (i.e., assumed to produce the same safety benefit and have the same maintenance cost). As indicated in Table J.1, three discount rates were evaluated to establish an uncertainty band of the cost/benefit ratio. In this sense, a total of 18

evaluations needed to be done for each discount rate to evaluate all the possible combinations of maintenance strategies. Each of these evaluations is identified with a unique code as follows:

$$S\# - OG\# - UT\# \quad (144)$$

where;

- S# = code to identify the scenario (1 to 3),
- OG# = code to identify the OGFC maintenance alternative (1 to 3), and
- UT# = code to identify the UTWB maintenance alternative (1 to 2).

For example, the code S2-OG2-UT1 indicates Scenario S2 (Maintenance-With-Safety), with OGFC maintenance Alternative 2 (high-structural damage), and with UTBWC maintenance Alternative 1 (low-structural damage).

The Transportation Mobility and Safety Division periodically updates costs associated with traffic crashes for use by division personnel for cost analyses. Starting with the 2017 update, the division is now using the final recommendation from FHWA’s Crash Costs for Highway Safety Analysis. The comprehensive crash costs are based on the values provided in the FHWA report. These provided values have not been updated since the report’s initial release in January 2018. In addition to total statewide crashes, crash costs are also calculated for seven specific crash types: total crashes, frontal impact crashes, lane departure crashes, rear end crashes, pedestrian crashes, bicycle crashes, train crashes, and truck crashes. Since the FHWA cost values have not been updated in several years, the 2021 standardized crash cost estimates for North Carolina (compiled by the NCDOT) for the lane departure collisions have been used. These costs are summarized in Table J.2. In this table, it is shown that the average lane departure crash cost is \$218,000 USD. The treatment and maintenance costs are presented in Table J.2, these were provided by the NCDOT personnel.

Table J.2. Cost per crash – Lane Departure Crashes¹.

Crash Type	Cost per Crash (2021 Dollars)
Fatal crash	\$11,411,000
A Injury crash	\$624,000
B Injury crash	\$183,000
C Injury Crash	\$100,000
Property Damage Only Crash	\$12,600
Average Crash	\$218,000
Injury Crash (F+A+B+C)	\$633,000
Non-Fatal Injury Crash (A+B+C)	\$189,000
Severe Injury crash (F+A)	\$3,618,000
Moderate Injury crash (B+C)	\$137,000

¹ Run off road – straight, right, and left, fixed object, overturn/rollover, sideswipe opposite direction, parked motor vehicle, and head on crashes.

The friction and texture performance models, detailed in Chapter 3, are presented in Equation (145) and (146), respectively.

$$MPD = (a + \Delta a_{site}) \cdot T^{(b + \Delta b_{family})} \quad (145)$$

where;

- a = fixed effect of MPD intercept,

Δa_{site} = random effect of *MPD* intercept, one value per site,
 T = cumulative traffic (or truck traffic),
 b = fixed effect of the *MPD* rate of change, and
 Δb_{family} = random effect of *MPD* rate of change, one value per family.

$$F(T) = \begin{cases} (a + \Delta a_{site}) + (b + \Delta b_{site}) \cdot T + c \cdot T^2 \rightarrow T \leq T_{\max} \\ (A + \Delta A_{site}) \cdot \exp\left[(B + \Delta b_{family}) \cdot T\right] \rightarrow T > T_{\max} \end{cases} \quad (146)$$

where;

a = fixed effect of Phase-1 *Friction* intercept,
 Δa_{site} = random effect of Phase-1 *Friction* intercept, one value per site,
 b = fixed effect of Phase-1 *Friction* rate of change,
 Δb_{site} = random effect of Phase-1 *Friction* rate of change, one value per site,
 c = fixed effect of the second order curvature,
 A = fixed effect of Phase-2 *Friction* intercept,
 ΔA_{site} = random effect of Phase-2 *Friction* intercept, one value per site,
 B = fixed effect of Phase-2 *Friction* rate of change,
 ΔB_{family} = random effect of Phase-2 *Friction* rate of change, one value per family, and
 T = cumulative traffic (or truck traffic).

Equation (147), relates the wet lane departure crash rate as a function of texture and friction, respectively. That expression can be solved as indicated in Equation (148) to predict the number of crashes in a 12-month period (1 year).

$$R_{13} = a \cdot X^b = \frac{C_{13}}{VMT_{13}} \times 10^8 \quad (147)$$

$$C_{pred} = \frac{12}{13} \left(\frac{a \times VMT_{13}}{10^8} \right) \times (X)^b \quad (148)$$

where;

C_{pred} = predicted number of crashes in a 12-month period,
 VMT_{13} = number of vehicle miles traveled in a 13-month period,
 X = predictor, i.e., friction or *MPD*, and
 a and b = fitted coefficients.

Finally, based on information provided by NCDOT personnel on the use of OGFC and UTWBC, it was decided that the sites in Divisions 11 to 14 (i.e., the western side of the state) will be rehabilitated with an UTWBC, whereas those located in the eastern side, Divisions 1 to 10 will get an OGFC. Both treatments will only be placed on Interstates. Also, in Scenarios S2 and S3, if a site receives a dense mix, this will be a coarse-graded dense mix (termed coarse-dense herein), or a fine-graded dense mix that has been immediately treated with a Skidabrader treatment. Because the exact cost increment required to provide coarser gradations is not known, it is assumed that this cost increment is equal to the cost of applying a Skidabrader. In other words, the cost of a Skidabrader + fine-dense mix is equal to a coarse-dense mix.

Business-As-Usual Scenario (S1)

In this scenario, a surface is treated based on its age, i.e., if the age is greater than or equal to the rehabilitation limit the surface is treated. Under this scenario, the surface type after rehabilitation does not change. For example, if the original surface is an S9.5D mix, then the overlay mix will also be an S9.5D. All the current dense mixes are specified to have a fine gradation; therefore, after an overlay, the new surface will have an MPD_{SCRIM} of 0.35-mm.

An example of the MPD_{SCRIM} performance curve expected during this scenario is depicted in Figure J.4. This graph shows the performance curve under the evaluation S1-OG1-UT1, i.e., Scenario 1 with OGFC maintenance Alternative 1 and UTBWC maintenance Alternative 1. Part (a) shows the performance curve for an OGFC, which in year 2022 (first data point in the series) has an age of 10 years (year 0 of the analysis period) and an MPD_{SCRIM} of 1.54-mm. Because of the aforementioned age criterion (span of 5 years), this section is flagged to be treated, and then in year 2023 (year 1 of the analysis period) will have an age equal to zero. Parameter a of Equation (145) is equal to 1.3-mm, which ultimately results in an initial texture of 1.06-mm. According to the scheme selected (S1-OG1-UT1), this section will receive a total of seven rehabilitations over the 40-year analysis period. Three of these will include a full-depth milling (OGFC + underlaying asphalt layer) and the other four will consist of milling the top OGFC surface only.

Similarly, Part (b) shows the treatment plan corresponding to a S9.5D mix. This section has an age of 13 years at 2022 (year 0 of the analysis period), it is flagged for rehabilitation and in 2023 (year 1 of the analysis period) parameter a from Equation (145) is set equal to 0.35. Based on the expected life of 12 years, this section receives a total of four overlays over the 40-year analysis period. Although an example for an UTBWC has not been included, it follows the same pattern as the OGFC, with the difference that the expected service life is 7-years and parameter a of Equation (145) is set equal to 1.0-mm. For friction, the procedure is similar except that Equation (146) is used to make predictions, the performance curves for the same two sections are included in Figure J.5.

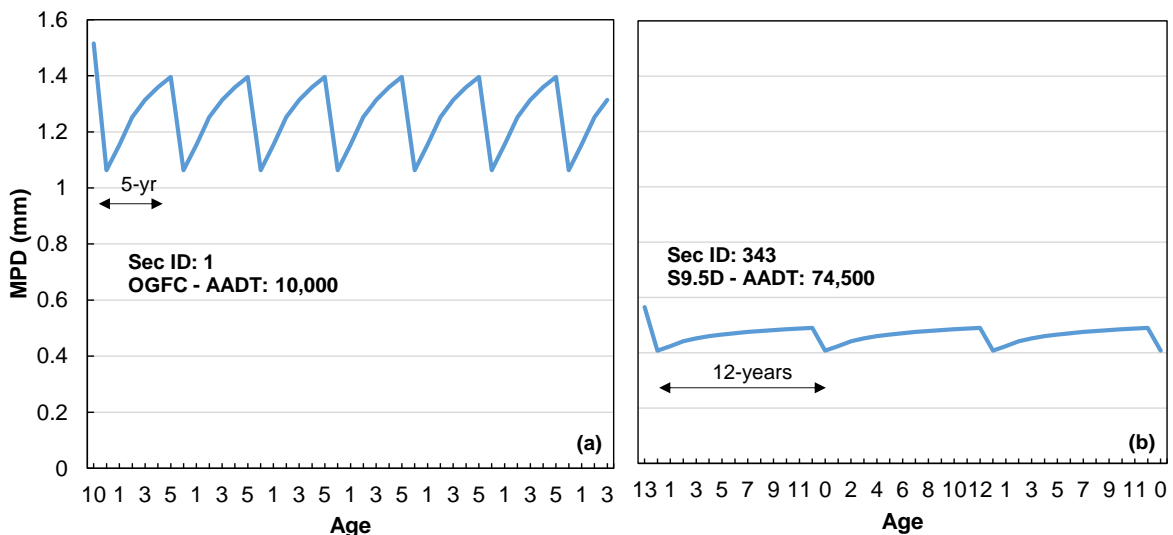


Figure J.4. Example of the MPD_{SCRIM} performance curve for Scenario 1: (a) Section ID: 1, and (b) Section ID: 343.

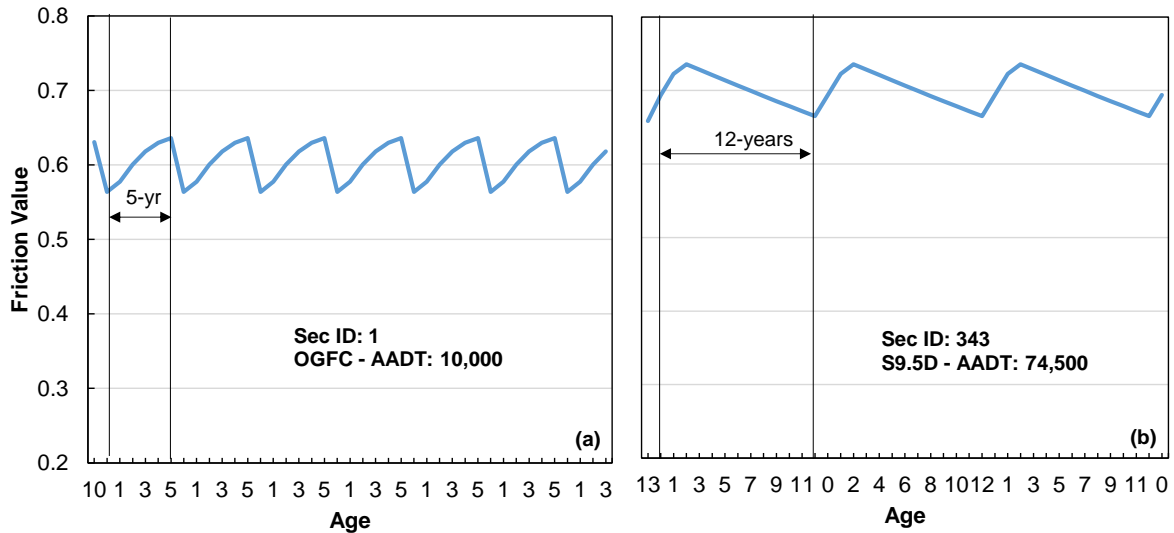


Figure J.5. Example of the friction performance curve for Scenario 1: (a) Section ID: 1, and (b) Section ID: 343.

The procedure described above was applied in all the 11,322 0.1-mile road segments from which friction and texture predictions were obtained for the 40-year analysis period. Afterwards, Equation (148) was used to predict the number of crashes associated with each friction and texture value. Individual predictions were made based on friction and texture, then these were averaged to get the total number of wet lane departure crashes in each year. Over the course of the 40-year simulation, a total of 28,912, 9,121, and 2,868 0.1-mile road segments with a dense, OGFC, and UTBWC surface were rehabilitated, respectively. During the same period, a total of 78,963 crashes (on average 1,926 crashes per year) were predicted across the network. A similar procedure was applied for all the other evaluation conditions (17 more).

Maintenance-With-Safety (S2)

For this scenario, a treatment is triggered by two possible situations; the surface reaches its expected life, or either the MPD_{SCRIM} or friction are below their respective intervention threshold. As mentioned earlier, the candidate investigatory MPD_{SCRIM} threshold is 1.0-mm, whereas for friction it is 0.54. Based on the histograms shown in Figure C.2 and Figure C.1, the friction intervention threshold was set equal to the investigatory threshold, because the portion of the network under evaluation does not have a friction problem, only 4.8% of the segments are below 0.54. For texture, three possible thresholds were evaluated in this scenario: 0.5, 0.6, and 0.7-mm.

The decision tree illustrated in Figure J.6 was used to determine whether a segment needed to be rehabilitated and to select the rehabilitation action that would be taken. As shown in the figure, the target for the safety improvement is the dense mixes. If a site with a dense mix is an Interstate and has a safety problem (texture or friction below their threshold), the site will receive an UTBWC or an OGFC independently of its age. But, for older sections that need to be rehabilitated (the age reaches the maximum allowed) the site will receive a coarse mixture (or an equivalent dense mix + Skidabrader treatment). If a segment with a dense mix is on a US-Route, this segment will be rehabilitated based only on its age and will receive a coarse dense mix. Independently of the road class classification, the current OGFCs and UTWBCs will be replaced for a surface of the same kind.

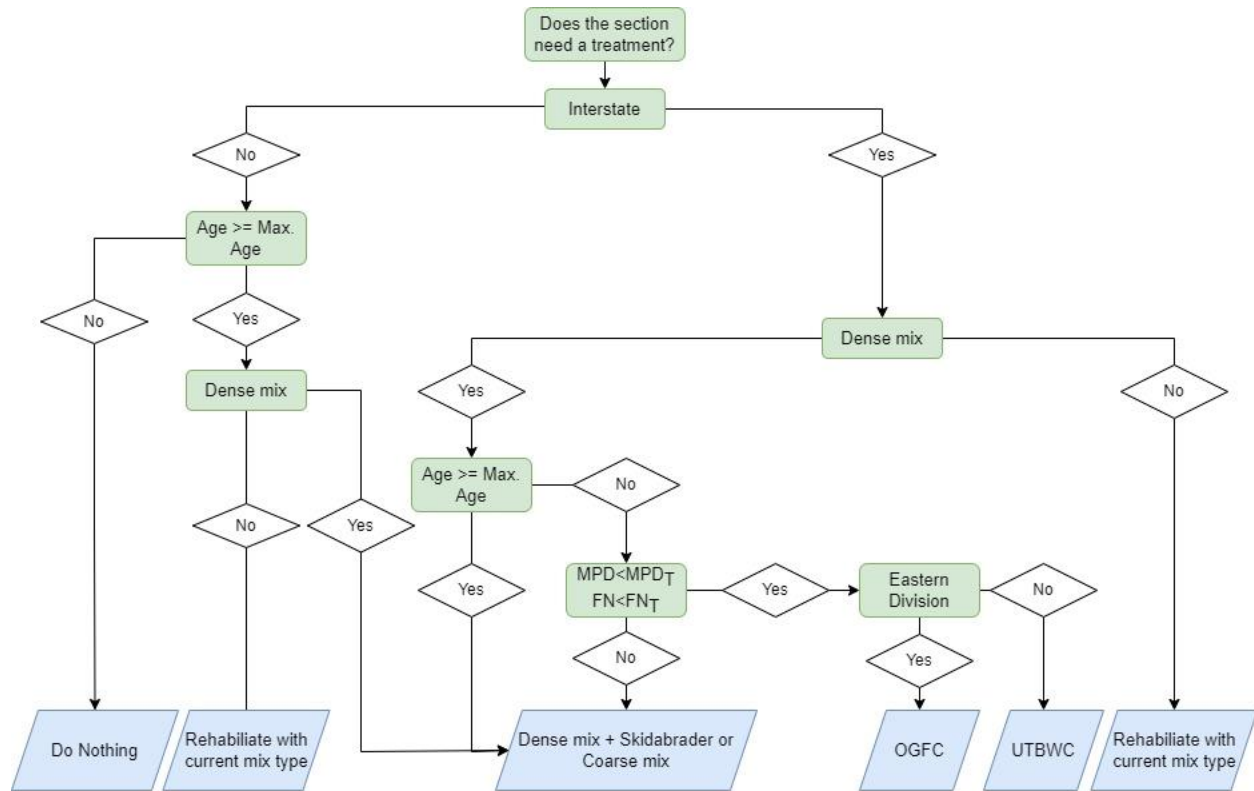


Figure J.6. Treatment selection decision tree for Scenario 2.

After conducting the analysis for the 40-year period assuming an MPD_{SCRIM} intervention level of 0.5-mm, a total of 28,386, 9,876, and 3,084 0.1-mile road segments with a dense, OGFC, and UTBWC surface were rehabilitated, respectively. During the same period, a total of 63,657 crashes (on average 1,553 crashes per year) were recorded on the network. This represents a reduction of 15,306 crashes in comparison to Scenario 1. If the MPD_{SCRIM} intervention level is increased to 0.6-mm and 0.7-mm the expected reduction in crashes, based on the number registered in Scenario 1, will be 15,410 and 16,488, respectively. As shown, almost the same crash reduction is expected at an intervention level of 0.5-mm and 0.6-mm. In the next section it will be discussed the cost associated with these treatments and the cost-benefit ratio for each of the scenarios analyzed.

Safety-Risk-Balance (S3)

The analysis on this third scenario is like that of Scenario 2, but instead of using friction and texture separately to flag a potential safety problem, they are used together to assess the risk. For this analysis, the Logit model proposed in Chapter 4 was used to compute the probability of observing a crash rate below 10 100-Mvmt13, i.e., $P(R < 10)$. This probability was selected to illustrate the process; however, other probabilities could also be used, e.g., $P(R < 30)$.

The distribution of these two probabilities across the segments of the network is depicted in Figure J.7. In this scenario, three probability levels that $P(R < 10)$ were evaluated: 45%, 55%, and 65%, as shown in Part (a) of Figure J.7. In the first case, 1.9% of the segments have a $P(R < 10) < 45\%$. Similarly, if the second and third risk level are selected, there are 35% and 74.7% of the road segments with a $P(R < 10)$ less than or equal to 55% and 65%, respectively.

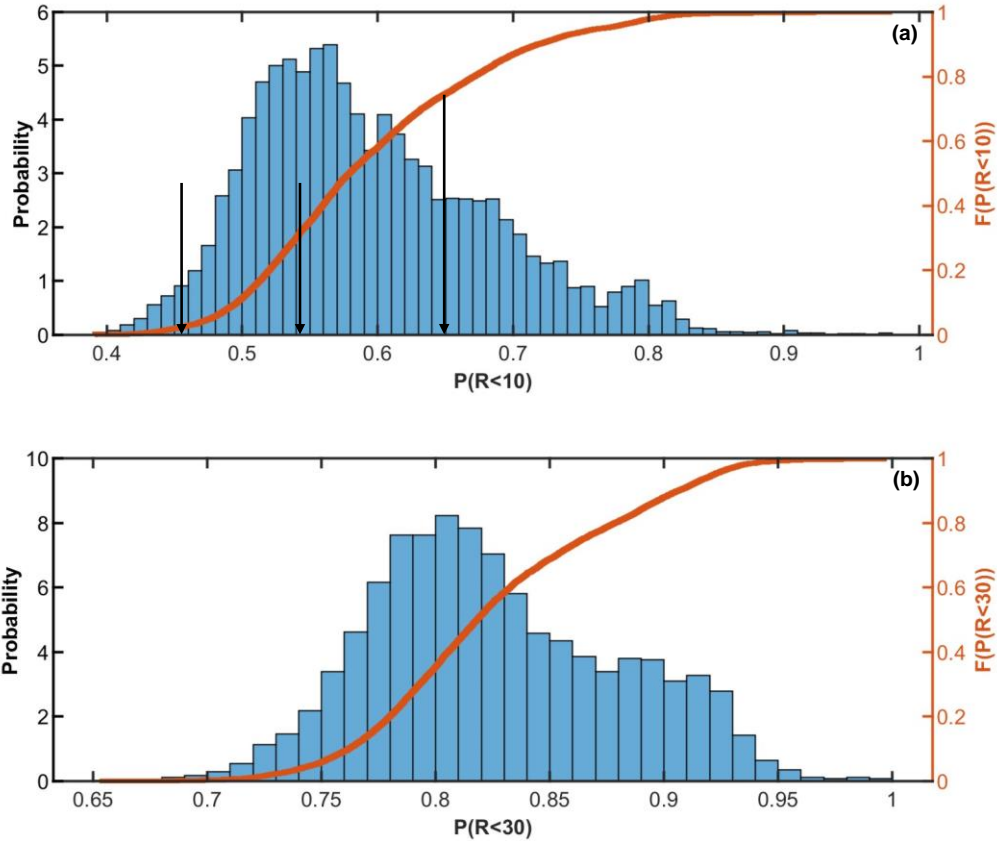


Figure J.7. Distribution of the probabilities (a) $P(R<10)$ and (b) $P(R<30)$ in year 2022.

The decision tree defined for this scenario is almost identical to the one established for Scenario 2, as shown in Figure J.8. In this figure, the red text indicates the difference between the two scenarios. After conducting the analysis for the 40-year period using a risk level set as 45% $P(R<10)$, a total of 28,682, 9,214, and 3,951 0.1-mile road segments with a dense, OGFC, and UTBWC surface were rehabilitated, respectively. During the same period, a total of 64,110 (on average 1,564 crashes per year) crashes were recorded in the network. This represents a reduction of 14,853 crashes in comparison to Scenario 1. Now, if the allowable risk is increased to 55% and 65% $P(R<10)$, then the expected crash reduction will be 19,447 and 21,891, respectively.

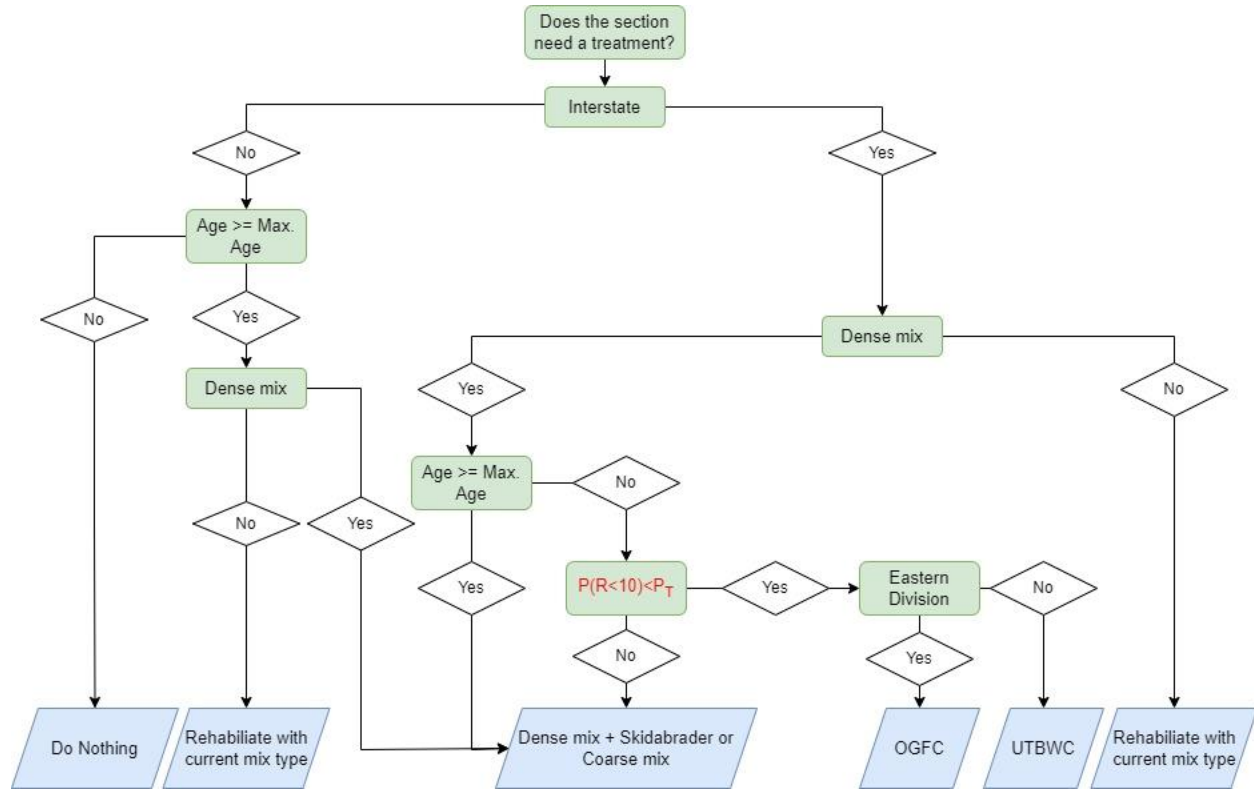


Figure J.8. Treatment selection decision tree for Scenario 3.

Cost-Benefit Analysis

After running each evaluation condition, the number of sections selected for treatment for each of the treatments available were used to estimate the cost associated with maintenance during the analysis period. Based on Table J.2, the average cost of a crash event (C_{cost}) is \$218,000. Hence, the Net Present Value (NPV) of the cost needed to be invested and the NPV of the cost expected on crashes is computed for each year in the analysis period.

The NPV was computed using discount rates of 3, 5, and 7%. Scenarios S2 and S3 were compared against the values of Scenario S1. The expected NPV of the crash cost reduction between scenarios is computed using Equation (149) and the NPV investment needed for that reduction is computed using Equation (150).

$$Crash\ Cost\ Reduction = (Crashes_{Scenario-1} - Crashes_{Scenario-i}) \times C_{cost} \quad (149)$$

$$Investment = Maintenance\ Cost_{Scenario-i} - Maintenance\ Cost_{Scenario-1} \quad (150)$$

The summary of these calculations is presented in tabular form in Table J.3 through Table J.5 for discount rates of 3%, 5%, and 7%, respectively. The results indicate that, in general terms, the higher the NPV investment, the higher the expected crash reduction during the period of analysis. All the evaluated conditions have a cost-benefit ratio above 4.5. This finding matches the cost-benefit ratio reported by (18) and (110). The highest B/C ratio is obtained with a discount rate of 3%, whereas the lowest ones are obtained with a discount rate of 7%.

The scenario that leads to the highest reduction in crashes is Scenario 3. However, this scenario also results in the highest investment costs. By comparing those evaluation cases where the

UTBWC was treated as indicated by the low structural damage alternative, i.e., UT1, it is observed that in all cases OG1 (OGFC with the low structural damage maintenance alternative) results in the lowest investment cost, followed by the OG3 (modified structural damage alternative), and the one with the highest investment cost is always the OG2 (high structural damage). Similarly, if one compares the result for the evaluation cases with the same OGFC maintenance alternative, suppose it is say OG1, the UTBWC low structural damage maintenance alternative (UT1) result to low investment than that observed with the UT2 maintenance alternative. Similar results were observed among the different evaluation cases.

It is important to note that there is a compensation effect in the cases evaluated. For example, with the UT2 and the OG3 maintenance alternatives, the rehabilitation period is 10 years and 8 years, respectively. These alternatives consider full depth milling and replacement at the end of the rehabilitation period, the longer the rehabilitation period is, the lower the number of crashes. This outcome occurs because the texture performance model suggests that the older the surface higher the MPD, and because friction is not a problem in the network, fewer crashes will be observed for the longer rehabilitation period. Therefore, the increase in the number of crashes is contrasted with the increment in maintenance costs compared to those observed with the UT1 and OG1 maintenance alternatives.

Limitations of the Analysis

There are some limitations in the analysis conducted here that should be acknowledged:

- First, the mobilization cost incurred to monitor those sites where either friction or texture is below their candidate investigatory threshold is not included.
- Second, it is assumed that once a surface is treated, the initial *MPD* is equal to the average value of that surface type, instead this should be modeled as a random variable.
- Third, the analysis here only evaluated primary economic effects, i.e., those directly related to the pavements. However, there are secondary and tertiary economic implications that may affect how well the calculated cost/benefit ratios would match real cost/benefits. Some of the other economic implications that were not included in the analysis are:
 - the budgetary implications of widespread implementation of the friction/texture thresholds and rehabilitation strategies and the agency operational adjustments that would be needed for such implementation;
 - the longer-term impact of shifting funding priorities on the maintenance, operations, and conditions of the entire transportation system in North Carolina to complete the activities resulting from the PFMP;
 - the time and cost required for contractors to get familiar and train their personnel to construct the different surface treatments to ensure that they perform well;
 - iv) the availability and possible impacts on the supply and cost of component materials required for these treatments; and
 - the impacts to sustainability and the costs/benefits from downstream effects (if any) of the use of these treatments (e.g., changes in the balance of waste materials at material suppliers, an imbalance in the amount of RAP generated versus what is used, impacts of increased construction times and lane closures over the life of the pavement that would be needed to construct and maintain these treatments, etc.).

The limitations noted above are considered substantial and should be addressed for before applying the findings here to make far reaching policy decisions. Had the analysis performed in this study not shown a cost/benefit ratio greater than one, then it would have been clear that the effort to better understand and quantify these secondary and tertiary effects was not worthwhile.

Conclusions

The results of this analysis indicate that it may be economically feasible to treat the network to maintain a minimum friction and texture levels. A minimum benefit-cost ratio of 4.5 was obtained and the maximum observed was 12.

The results also indicate that one possible alternative to increase texture at a network level might be placing coarse-graded dense mixes that provide a mean initial texture value of 0.8-mm and a minimum friction of 0.50 (measured with the AMES AccuTexture 100 and Moventor Skiddometer BV-11 at 60-mph, respectively). More research is needed to evaluate the implications of using coarser gradations in pavement performance.

Table J.3. Summary of the cost-benefit analysis (discount rate of 3%).

Scenario	Scenario	Investment (\$)	Benefit (\$)	B/C	No Crashes reduced
Business-as-Usual	S1-OG1-UT1	-	-	-	-
	S1-OG2-UT1	-	-	-	-
	S1-OG3-UT1	-	-	-	-
	S1-OG1-UT2	-	-	-	-
	S1-OG2-UT2	-	-	-	-
	S1-OG3-UT2	-	-	-	-
Maintenance-with-Safety	S2(MPD<0.5)-OG1-UT1	151,820,432	1,806,909,246	11.90	15,306
	S2(MPD<0.5)-OG2-UT1	157,284,399	1,806,909,246	11.49	15,306
	S2(MPD<0.5)-OG3-UT1	151,837,601	1,815,168,955	11.95	15,377
	S2(MPD<0.5)-OG1-UT2	152,206,299	1,807,807,346	11.88	15,311
	S2(MPD<0.5)-OG2-UT2	157,670,266	1,807,807,346	11.47	15,311
	S2(MPD<0.5)-OG3-UT2	152,223,468	1,808,900,618	11.88	15,320
	S2(MPD<0.6)-OG1-UT1	152,362,733	1,819,904,383	11.94	15,410
	S2(MPD<0.6)-OG2-UT1	158,053,200	1,819,904,383	11.51	15,410
	S2(MPD<0.6)-OG3-UT1	152,380,613	1,828,590,553	12.00	15,484
	S2(MPD<0.6)-OG1-UT2	152,935,410	1,820,802,482	11.91	15,415
	S2(MPD<0.6)-OG2-UT2	158,625,877	1,820,802,482	11.48	15,415
	S2(MPD<0.6)-OG3-UT2	152,953,290	1,821,655,803	11.91	15,422
	S2(MPD<0.7)-OG1-UT1	176,930,314	1,961,253,930	11.08	16,488
	S2(MPD<0.7)-OG2-UT1	194,337,488	1,961,253,930	10.09	16,488
	S2(MPD<0.7)-OG3-UT1	176,985,012	1,978,707,149	11.18	16,630
	S2(MPD<0.7)-OG1-UT2	180,147,091	1,962,152,030	10.89	16,493
S2(MPD<0.7)-OG2-UT2	197,554,265	1,962,152,030	9.93	16,493	
S2(MPD<0.7)-OG3-UT2	180,201,789	1,964,781,221	10.90	16,512	
Safety-Risk-Balance - 45%	S3(45)-OG1-UT1	145,433,474	1,754,577,239	12.06	14,853
	S3(45)-OG2-UT1	146,120,003	1,754,577,239	12.01	14,853
	S3(45)-OG3-UT1	145,435,632	1,755,169,574	12.07	14,858
	S3(45)-OG1-UT2	145,967,217	1,754,150,682	12.02	14,847
	S3(45)-OG2-UT2	146,653,746	1,754,150,682	11.96	14,847
	S3(45)-OG3-UT2	145,969,375	1,756,067,674	12.03	14,863
Safety-Risk-Balance - 55%	S3(55)-OG1-UT1	260,762,785	2,341,926,286	8.98	19,447
	S3(55)-OG2-UT1	331,538,288	2,341,926,286	7.06	19,447
	S3(55)-OG3-UT1	260,985,179	2,409,599,904	9.23	19,989
	S3(55)-OG1-UT2	268,624,317	2,281,653,377	8.49	18,959
	S3(55)-OG2-UT2	339,399,820	2,281,653,377	6.72	18,959
	S3(55)-OG3-UT2	268,846,711	2,349,326,995	8.74	19,501
Safety-Risk-Balance - 65%	S3(65)-OG1-UT1	330,519,707	2,653,661,032	8.03	21,891
	S3(65)-OG2-UT1	453,570,116	2,653,661,032	5.85	21,891
	S3(65)-OG3-UT1	330,915,227	2,767,902,838	8.36	22,777
	S3(65)-OG1-UT2	341,268,633	2,548,244,895	7.47	21,064
	S3(65)-OG2-UT2	464,319,042	2,548,244,895	5.49	21,064
	S3(65)-OG3-UT2	341,664,154	2,662,486,701	7.79	21,950

Table J.4. Summary of the cost-benefit analysis (discount rate of 5%).

Scenario	Scenario	Investment (\$)	Benefit (\$)	B/C	No Crashes reduced
Business-as-Usual	S1-OG1-UT1	-	-	-	-
	S1-OG2-UT1	-	-	-	-
	S1-OG3-UT1	-	-	-	-
	S1-OG1-UT2	-	-	-	-
	S1-OG2-UT2	-	-	-	-
	S1-OG3-UT2	-	-	-	-
Maintenance-with-Safety	S2(MPD<0.5)-OG1-UT1	114,561,639	1,276,601,273	11.14	15,306
	S2(MPD<0.5)-OG2-UT1	118,316,979	1,276,601,273	10.79	15,306
	S2(MPD<0.5)-OG3-UT1	114,565,051	1,282,410,783	11.19	15,377
	S2(MPD<0.5)-OG1-UT2	114,862,770	1,277,388,574	11.12	15,311
	S2(MPD<0.5)-OG2-UT2	118,618,110	1,277,388,574	10.77	15,311
	S2(MPD<0.5)-OG3-UT2	114,866,182	1,278,214,756	11.13	15,320
	S2(MPD<0.6)-OG1-UT1	115,055,702	1,286,204,408	11.18	15,410
	S2(MPD<0.6)-OG2-UT1	118,984,400	1,286,204,408	10.81	15,410
	S2(MPD<0.6)-OG3-UT1	115,059,271	1,292,335,139	11.23	15,484
	S2(MPD<0.6)-OG1-UT2	115,488,140	1,286,991,709	11.14	15,415
	S2(MPD<0.6)-OG2-UT2	119,416,838	1,286,991,709	10.78	15,415
	S2(MPD<0.6)-OG3-UT2	115,491,709	1,287,650,199	11.15	15,422
	S2(MPD<0.7)-OG1-UT1	136,600,952	1,394,068,419	10.21	16,488
	S2(MPD<0.7)-OG2-UT1	149,246,561	1,394,068,419	9.34	16,488
S2(MPD<0.7)-OG3-UT1	136,612,441	1,406,736,210	10.30	16,630	
S2(MPD<0.7)-OG1-UT2	138,890,421	1,394,855,720	10.04	16,493	
S2(MPD<0.7)-OG2-UT2	151,536,029	1,394,855,720	9.20	16,493	
S2(MPD<0.7)-OG3-UT2	138,901,910	1,396,871,725	10.06	16,512	
Safety-Risk-Balance - 45%	S3(45)-OG1-UT1	109,848,658	1,240,298,618	11.29	14,853
	S3(45)-OG2-UT1	110,335,175	1,240,298,618	11.24	14,853
	S3(45)-OG3-UT1	109,849,100	1,240,746,109	11.30	14,858
	S3(45)-OG1-UT2	110,223,820	1,240,145,154	11.25	14,847
	S3(45)-OG2-UT2	110,710,337	1,240,145,154	11.20	14,847
	S3(45)-OG3-UT2	110,224,262	1,241,533,410	11.26	14,863
Safety-Risk-Balance - 55%	S3(55)-OG1-UT1	204,861,335	1,680,815,756	8.20	19,447
	S3(55)-OG2-UT1	256,158,369	1,680,815,756	6.56	19,447
	S3(55)-OG3-UT1	204,907,940	1,730,181,804	8.44	19,989
	S3(55)-OG1-UT2	210,361,142	1,637,158,762	7.78	18,959
	S3(55)-OG2-UT2	261,658,175	1,637,158,762	6.26	18,959
	S3(55)-OG3-UT2	210,407,747	1,686,524,810	8.02	19,501
Safety-Risk-Balance - 65%	S3(65)-OG1-UT1	262,386,667	1,914,385,408	7.30	21,891
	S3(65)-OG2-UT1	353,439,387	1,914,385,408	5.42	21,891
	S3(65)-OG3-UT1	262,473,403	1,999,277,811	7.62	22,777
	S3(65)-OG1-UT2	270,072,806	1,836,603,775	6.80	21,064
	S3(65)-OG2-UT2	361,125,527	1,836,603,775	5.09	21,064
	S3(65)-OG3-UT2	270,159,543	1,921,496,178	7.11	21,950

Table J.5. Summary of the cost-benefit analysis (discount rate of 7%).

Scenario	Scenario	Investment (\$)	Benefit (\$)	B/C	No Crashes reduced
Business-as-Usual	S1-OG1-UT1	-	-	-	-
	S1-OG2-UT1	-	-	-	-
	S1-OG3-UT1	-	-	-	-
	S1-OG1-UT2	-	-	-	-
	S1-OG2-UT2	-	-	-	-
	S1-OG3-UT2	-	-	-	-
Maintenance-with-Safety	S2(MPD<0.5)-OG1-UT1	90,576,043	941,809,840	10.40	15,306
	S2(MPD<0.5)-OG2-UT1	93,271,093	941,809,840	10.10	15,306
	S2(MPD<0.5)-OG3-UT1	90,569,786	946,085,599	10.45	15,377
	S2(MPD<0.5)-OG1-UT2	90,805,493	942,502,022	10.38	15,311
	S2(MPD<0.5)-OG2-UT2	93,500,542	942,502,022	10.08	15,311
	S2(MPD<0.5)-OG3-UT2	90,799,235	943,156,475	10.39	15,320
	S2(MPD<0.6)-OG1-UT1	91,026,280	949,240,559	10.43	15,410
	S2(MPD<0.6)-OG2-UT1	93,857,957	949,240,559	10.11	15,410
	S2(MPD<0.6)-OG3-UT1	91,019,706	953,766,623	10.48	15,484
	S2(MPD<0.6)-OG1-UT2	91,351,163	949,932,741	10.40	15,415
	S2(MPD<0.6)-OG2-UT2	94,182,839	949,932,741	10.09	15,415
	S2(MPD<0.6)-OG3-UT2	91,344,588	950,465,947	10.41	15,422
	S2(MPD<0.7)-OG1-UT1	110,605,433	1,035,265,959	9.36	16,488
	S2(MPD<0.7)-OG2-UT1	120,151,854	1,035,265,959	8.62	16,488
S2(MPD<0.7)-OG3-UT1	110,583,268	1,044,843,884	9.45	16,630	
S2(MPD<0.7)-OG1-UT2	112,280,063	1,035,958,141	9.23	16,493	
S2(MPD<0.7)-OG2-UT2	121,826,484	1,035,958,141	8.50	16,493	
S2(MPD<0.7)-OG3-UT2	112,257,898	1,037,559,585	9.24	16,512	
Safety-Risk-Balance - 45%	S3(45)-OG1-UT1	86,974,628	915,578,362	10.53	14,853
	S3(45)-OG2-UT1	87,333,964	915,578,362	10.48	14,853
	S3(45)-OG3-UT1	86,973,793	915,937,275	10.53	14,858
	S3(45)-OG1-UT2	87,247,292	915,573,169	10.49	14,847
	S3(45)-OG2-UT2	87,606,628	915,573,169	10.45	14,847
	S3(45)-OG3-UT2	87,246,458	916,629,457	10.51	14,863
Safety-Risk-Balance - 55%	S3(55)-OG1-UT1	168,835,920	1,261,218,039	7.47	19,447
	S3(55)-OG2-UT1	207,436,528	1,261,218,039	6.08	19,447
	S3(55)-OG3-UT1	168,746,296	1,298,646,389	7.70	19,989
	S3(55)-OG1-UT2	172,815,592	1,228,348,204	7.11	18,959
	S3(55)-OG2-UT2	211,416,200	1,228,348,204	5.81	18,959
	S3(55)-OG3-UT2	172,725,968	1,265,776,553	7.33	19,501
Safety-Risk-Balance - 65%	S3(65)-OG1-UT1	218,845,183	1,444,382,120	6.60	21,891
	S3(65)-OG2-UT1	288,654,045	1,444,382,120	5.00	21,891
	S3(65)-OG3-UT1	218,684,937	1,509,799,643	6.90	22,777
	S3(65)-OG1-UT2	224,483,084	1,384,842,708	6.17	21,064
	S3(65)-OG2-UT2	294,291,947	1,384,842,708	4.71	21,064
	S3(65)-OG3-UT2	224,322,838	1,450,260,230	6.47	21,950